



Cardiff School of Pharmacy and Pharmaceutical Sciences

Cardiff University

Caveolin-1 is a modulator of clonogenicity in Renal Cell Carcinoma

A thesis submitted *in accordance with the conditions governing
candidates* for the degree of

Philosophiae Doctor in Cardiff University

Robert James Gutteridge

Supervisor: Prof. M. Gumbleton

Supervisor: Dr. D. F. R. Griffiths

Supervisor: Dr. C. J. Pepper

December 2015

Acknowledgements

I would like to thank my supervisor Professor Mark Gumbleton for his constant guidance, support and enthusiasm, always passionate for me to reach my full potential. A special thanks to my co-supervisors Dr David Griffiths and Dr Chris Pepper who dedicated several work hours (and more than a few after work hours) of their time to take me under their wing and share their respective expertise.

A heartfelt thanks to Muthanna, Jack, Chiara and Dan their friendship and support means more than they realise, I am better person for the ownership of it.

I thank my close friends outside of academia for helping me keep my sanity (and some semblance of a social life).

Mum and Dad needless to say I couldn't have done this without you, thank you does not seem quite enough.

I devote my deepest thanks and love to Valentina, whose love and support held my head up and kept me smiling, I treasure it always.

Abstract

Renal cell carcinoma (RCC) represents a group of aggressive tumours of the kidney. These tumours have a high propensity for metastasis and are extremely treatment refractive after disease relapse. Therefore, the identification of new therapeutic targets is of great importance. One such potential target for therapy are cancer stem cells (CSCs). CSCs are populations of cells imbued with a stem cell-like phenotype capable of driving tumour formation, metastasis and chemoresistance. As such, reliable methods for the identification of CSC populations and defining targets important to their functionality, in hopes of developing more potent therapeutics is of great importance. Previous work has found CAV1 to play a significant role in the malignant progression of RCC and also in the maintenance of adult stem cell populations.

As such, this work aimed to understand if common markers of CSC phenotype in combination with CAV1 can act indicators of poor prognostic outcome in clinically confined RCC. Furthermore, this work sought to identify CSC populations from RCC cell lines using a panel of surface markers common to embryonic, mesenchymal and cancer stem cells. Then, understand if CAV1 is responsible for driving the CSC phenotype in these CSC populations by regulating one of the major characteristics of CSC biology, self-renewal.

Co-expression of CD44 and CAV1 in RCC tumours indicated greatly reduced disease free survival in clinically confined RCC. Additionally, CD44/CAV1 was found to be the most significant covariate in predicting disease recurrence. *In vitro* analysis, using a panel of CSC related markers, was unable of identifying a putative CSC population. However, CAV1 expression in the VHL positive CAKI-1 cell line was important for the maintenance of clonogenicity. Incubation of CAV1 deficient CAKI-1 cells under hypoxic conditions was able to restore lost clonogenicity. Further

work revealed that CAV1 maintains clonogenicity in CAKI-1 through activation of STAT3 and β -catenin. This suggests an important role for CAV1 in the maintenance of clonogenicity through STAT3 activation in VHL competent RCC.

Contents

| | | |
|-------|---|----|
| 1 | General Introduction..... | 2 |
| 1.1 | Renal cell carcinoma | 2 |
| 1.1.1 | Epidemiology, etiology and pathology of renal cell carcinoma | 2 |
| 1.1.2 | Treatment of RCC | 5 |
| 1.2 | The 'Cancer Stem Cell' hypothesis | 8 |
| 1.2.1 | Tumour heterogeneity..... | 8 |
| 1.2.2 | Characteristics of cancer stem cells..... | 9 |
| 1.3 | Caveolin-1 | 14 |
| 1.3.1 | Caveolin-1 in cancer..... | 16 |
| 1.4 | General thesis aims..... | 21 |
| 2 | Cancer Stem Cell markers in combination with Caveolin-1 in predicting disease outcome in clinically confined renal cell carcinoma | 23 |
| 2.1 | Introduction..... | 23 |
| 2.1.1 | CAV1 as a prognostic marker | 23 |
| 2.1.2 | Markers of CSC phenotype and metabolic activity as prognostic tools 24 | |
| 2.1.3 | CD44 | 28 |
| 2.1.4 | CD105 | 29 |
| 2.1.5 | EpCAM..... | 31 |
| 2.1.6 | CD146 | 32 |
| 2.1.7 | Vimentin | 33 |
| 2.1.8 | MCT4 | 34 |
| 2.1.9 | Cavin-1 (PTRF) | 35 |

| | | |
|--------|--|-----|
| 2.1.10 | Aims | 36 |
| 2.2 | Materials and Methods | 37 |
| 2.2.1 | Patient cohort and RCC tissue microarrays | 37 |
| 2.2.2 | Immunohistochemistry of tissue microarrays and scoring | 38 |
| 2.2.3 | Statistical analysis | 41 |
| 2.3 | Results | 43 |
| 2.3.1 | CAV1 expression in RCC tumour samples predicts poor disease free survival which increases with increased CAV1 expression..... | 43 |
| 2.3.2 | CD44 expression in RCC tumours indicates poor disease free survival and identifies high risk patient groups, which is more pronounced in combination with CAV1 | 49 |
| 2.3.3 | CD105 in RCC tumours does not identify high risk patients alone or as a covariate with CAV1..... | 59 |
| 2.3.4 | EpCAM in RCC tumours does not identify high risk patients alone or as a covariate with CAV1 | 67 |
| 2.3.5 | CD146 in RCC tumours does not identify high risk patients alone or covariate with CAV1..... | 76 |
| 2.3.6 | Vimentin expression in RCC tumours does not identify high risk patients alone or covariate with CAV1..... | 83 |
| 2.3.7 | MCT4 expression in RCC tumours does not identify high risk patients alone or as a covariate with CAV1 | 90 |
| 2.3.8 | Cavin-1 expression in RCC tumours does not identify high risk patients as a univariate or covariate with CAV1 | 100 |

| | | |
|-------|--|-----|
| 2.3.9 | Regression modeling of all markers conducted as both simple covariate and composite covariates with CAV1 finds CD44+ve/CAV1+ve to be the strongest indicator of poor disease outcome | 106 |
| 2.4 | Discussion | 107 |
| 2.4.1 | CAV1 covariate..... | 107 |
| 2.4.2 | CSC marker covariates..... | 108 |
| 2.4.3 | CD44 covariate..... | 108 |
| 2.4.4 | MCT4 covariate | 110 |
| 2.4.5 | Vimentin covariate | 111 |
| 2.4.6 | CD105 covariate..... | 112 |
| 2.4.7 | Other markers | 113 |
| 3 | Identification and clonogenic evaluation of sub-populations of renal cell carcinoma cells dependant on the expression of cancer stem cell related markers | 116 |
| 3.1 | Introduction..... | 116 |
| 3.1.1 | Identification and isolation of cancer stem cell populations | 116 |
| 3.1.2 | Putative CSC surface marker panel..... | 118 |
| 3.1.3 | CD44..... | 118 |
| 3.1.4 | CD105..... | 119 |
| 3.1.5 | CD90..... | 120 |
| 3.1.6 | CD146..... | 121 |
| 3.1.7 | EpCAM..... | 122 |
| 3.1.8 | CD117..... | 123 |
| 3.1.9 | CD29 and CD73..... | 124 |

| | | |
|--------|--|-----|
| 3.1.10 | Aims | 124 |
| 3.2 | Materials and methods | 126 |
| 3.2.1 | Cell lines..... | 126 |
| 3.2.2 | Flow cytometry and sorting..... | 126 |
| 3.2.3 | Colony formation assay | 129 |
| 3.2.4 | Statistical analysis | 129 |
| 3.3 | Results | 130 |
| 3.3.1 | Identification of sub-populations within RCC cell lines | 130 |
| 3.3.2 | Subpopulation heterogeneity in RCC cell lines | 133 |
| 3.3.3 | Colony forming capacity of CD90/CD146 subpopulations from RCC cell lines..... | 143 |
| 3.4 | Discussion | 148 |
| 4 | Effect of CAV1 knockdown on the subpopulation distribution and clonogenicity of RCC cell lines | 154 |
| 4.1 | Introduction..... | 154 |
| 4.1.1 | CAV1 as a regulator of stem cell phenotype..... | 154 |
| 4.1.2 | Aims | 158 |
| 4.2 | Materials and Methods | 159 |
| 4.2.1 | Generation of CAV1 shRNA knockdown cell lines | 159 |
| 4.2.2 | Western Blot..... | 160 |
| 4.2.3 | Spheroid formation assays | 161 |
| 4.2.4 | Proliferation assays | 162 |
| 4.2.5 | Cell cycle analysis | 163 |

| | | |
|-------|---|-----|
| 4.2.6 | Statistical analysis | 163 |
| 4.3 | Results | 164 |
| 4.3.1 | CAV1 differentially affects the distribution of CD146/CD90 subpopulations between RCC cell lines and drives colony formation in CAKI-1 cells | 164 |
| 4.3.2 | CAV1 expression drives spheroid formation of CAKI-1 cells but not 786-O or A498 | 174 |
| 4.3.3 | CAV1 expression suppresses proliferation in adherent CAKI-1 cultures and appears to maintain CAKI-1 G2/M phase under non-adherent culture conditions..... | 176 |
| 4.3.4 | Activation of hypoxic signalling in CAKI-1 cells helps restore clonogenicity in the absence of CAV1 | 180 |
| 4.4 | Discussion | 184 |
| 5 | Down-regulation of CAV1 alters various oncogenic signalling pathways in CAKI-1 under clonogenic and hypoxic conditions. | 191 |
| 5.1 | Introduction..... | 191 |
| 5.1.1 | Wnt/ β -catenin signalling in the CSC phenotype and RCC..... | 191 |
| 5.1.2 | STAT3 signalling in the CSC phenotype and RCC | 194 |
| 5.1.3 | Aims | 196 |
| 5.2 | Materials and Methods | 197 |
| 5.2.1 | Proteomic microarrays..... | 197 |
| 5.2.2 | Inhibitor studies | 198 |
| 5.2.3 | Statistical analysis | 198 |
| 5.3 | Results | 199 |

| | | |
|-------|---|-----|
| 5.3.1 | Effect of CAV1 knockdown on regulation of phospho-kinase regulated cell signalling under different culture conditions | 199 |
| 5.3.2 | Effect of CAV1 knockdown on cancer related cell signalling under different culture conditions | 205 |
| 5.3.3 | Effect of CAV1 knockdown on the expression of pluripotent stem cell markers under different culture conditions..... | 213 |
| 5.3.4 | Down-regulation of CAV1 causes the downregulation of both STAT3 phosphorylation and β -catenin expression but only STAT3 inhibition affects clonogenicity. | 216 |
| 5.4 | Discussion | 219 |
| 6 | Concluding discussion | 227 |
| 7 | References | 232 |
| 8 | Appendix..... | 267 |

Table of Figures

| | |
|--|----|
| Figure 1.1 Graphical representation of the clonal evolution of carcinogenesis and tumour maintenance..... | 9 |
| Figure 1.2 Graphical representation of CSC driven tumourigenicity | 10 |
| Figure 1.3 Graphical representation of CSC driven metastasis..... | 11 |
| Figure 1.4 Graphical representation of CSC driven disease relapse..... | 13 |
| Figure 1.5 Schematic of CAV1 localisation and structure..... | 16 |
| Figure 1.6 Model for the interaction of CAV1 with signalling mechanisms in both normal and cancerous tissue..... | 18 |
| Figure 2.1 Example of a wide field image of full TMA section stained with isotypic rabbit serum..... | 38 |
| Figure 2.2 Positive staining of endothelial structures in normal kidney serves as a positive control for specificity of the CAV1 antibody used.. .. | 44 |
| Figure 2.3 Immunohistochemical staining of RCC TMAs for CAV1 expression.. .. | 45 |
| Figure 2.4 Kaplan-Meier survival curves for CAV1 expression..... | 46 |
| Figure 2.5 Negative staining in normal kidney tubules (A) and positive staining of infiltrating lymphocytes in RCC tumour samples (B-D) serve as specificity controls for the CD44 antibody used..... | 51 |
| Figure 2.6 Immunohistochemical staining of RCC TMAs for CD44 expression..... | 52 |
| Figure 2.7 Kaplan-Meier survival curves for CD44 expression..... | 53 |
| Figure 2.8 Correlation of CD44 with CAV1 expression and impact on disease free survival..... | 56 |
| Figure 2.9 Immunohistochemical staining of CD105 in endothelial structures of normal kidney tissue serves as a positive control for the CD105 antibody..... | 60 |
| Figure 2.10 Immunohistochemical staining of RCC TMAs for CD105 expression.. | 61 |
| Figure 2.11 Kaplan-Meier survival curves for CD105 expression..... | 62 |

| | |
|---|----|
| Figure 2.12 Correlation of CD105 with CAV1 expression and Kaplan-Meier survival analysis.. | 64 |
| Figure 2.13 Immunohistochemical staining of EpCAM in epithelial tubule structures in normal kidney tissue is a positive control for specificity of the EpCAM antibody used..... | 69 |
| Figure 2.14 Immunohistochemical staining of RCC TMAs for EpCAM expression.. | 70 |
| Figure 2.15 Kaplan-Meier survival curves for EpCAM expression. | 71 |
| Figure 2.16 Correlation of EpCAM with CAV1 expression and Kaplan-Meier survival analysis. | 73 |
| Figure 2.17 Immunohistochemical staining of CD146 in endothelial structures in normal kidney tissue acts as a positive control for the specificity of the CD146 antibody used.. | 77 |
| Figure 2.18 Immunohistochemical staining of RCC TMAs for CD146 expression... | 78 |
| Figure 2.19 Kaplan-Meier DFS curves for CD146.. | 79 |
| Figure 2.20 Correlation of CD146 with CAV1 expression and Kaplan-Meier survival analysis. | 81 |
| Figure 2.21 Immunohistochemical staining of vimentin in endothelial structures in normal kidney tissue acts as a positive control for specificity of the vimentin antibody used..... | 84 |
| Figure 2.22 Immunohistochemical staining of RCC TMAs for vimentin expression and Kaplan-Meier DFS analysis..... | 85 |
| Figure 2.23 Correlation of vimentin with CAV1 expression and Kaplan-Meier DFS analysis. | 88 |
| Figure 2.24 Immunohistochemical staining of MCT4 in the epithelial tubule cells in normal kidney acts as a specificity control for the MCT4 antibody selected. | 92 |

| | |
|---|-----|
| Figure 2.25 Immunohistochemical staining of RCC TMAs for MCT4 expression.... | 93 |
| | |
| Figure 2.26 Kaplan-Meier DFS curves for MCT4 expression..... | 94 |
| Figure 2.27 Correlation of MCT4 with CAV1 expression and Kaplan-Meier DFS analysis.. | 97 |
| | |
| Figure 2.28 Immunohistochemical staining of cavin-1 in endothelial structures in the normal kidney acts as a positive control for the specificity of the cavin-1 antibody used..... | 101 |
| Figure 2.29 Immunohistochemical staining of RCC TMAs for Cavin-1 expression and Kaplan-Meier DFS analysis..... | 102 |
| Figure 2.30 Correlation of Cavin-1 with CAV1 expression and impact on disease free survival.. | 104 |
| | |
| Figure 2.31 Putative model for CD44/CAV1 driven invasion.. | 110 |
| Figure 3.1 Spectral overview of fluorophores selected for flow cytometry analysis. (A) Shows fluorophores excited by the 408nm laser and their subsequent emission range (B) shows the same for the 488nm laser..... | 127 |
| Figure 3.2 Spectral overview for fluorophores excited by the 635nm laser selected for flow cytometry analysis..... | 128 |
| Figure 3.3 Single marker histograms of cell surface CSC markers CD90, CD146, CD44 and CD105.. | 131 |
| Figure 3.4 Single marker histograms of cell surface CSC markers EpCAM, CD117, CD29 and CD73. | 132 |
| Figure 3.5 Gating hierarchy used for sorting of subpopulations from all three RCC cell lines..... | 134 |
| Figure 3.6 Identification of CD90/CD146 subpopulations in 786-O WT cells by flow cytometry..... | 136 |
| Figure 3.7 Identification of CD90/CD146 subpopulations in A498 WT cells by flow cytometry..... | 137 |

| | |
|---|-----|
| Figure 3.8 Identification of CD90/CD146 subpopulations in CAKI-1 WT cells by flow cytometry,..... | 142 |
| Figure 3.9 Colony formation assays for CD146/CD90 subpopulations in 786-O cells. | 145 |
| Figure 3.10 Colony formation assays for CD146/CD90 subpopulations in A498 cells | 146 |
| Figure 3.11 Colony formation assays for CD146/CD90 subpopulations in CAKI-1 cells. | 147 |
| Figure 4.1 Downregulation of CAV1 in 786-O, A498 and CAKI-1 cells by SureSilencing shRNA plasmid. | 165 |
| Figure 4.2 Gating hierarchies for both scrambled shRNA control cells and CAV1 shRNA transfected 786-O cells using the 8 marker putative CSC panel.. | 166 |
| Figure 4.3 Gating hierarchies for both scrambled shRNA control cells and CAV1 shRNA transfected A498 cells using the 8 marker putative CSC panel..... | 167 |
| Figure 4.4 Gating hierarchies for both scrambled shRNA control cells and CAV1 shRNA transfected CAKI-1 cells using the 8 marker putative CSC panel..... | 168 |
| Figure 4.5 Effect of CAV1 knockdown on the mean percentage distribution of CD146/CD90 subpopulations in 786-O (A), A498 (B) and CAKI-1 (C)..... | 169 |
| Figure 4.6 Effect of CAV1 downregulation on colony formation of 786-O CD146/CD90 populations. | 171 |
| Figure 4.7 Effect of CAV1 downregulation on colony formation of A498 CD146/CD90 populations. | 172 |
| Figure 4.8 Effect of CAV1 downregulation on colony formation of CAKI-1 CD146/CD90 populations | 173 |
| Figure 4.9 Spheroid formation assays of 786-O (A), A498 (B) and CAKI-1 (C) cells bearing scrambled shRNA control or CAV1 shRNA knockdown.. | 175 |
| Figure 4.10 Down regulation of CAV1 induces proliferation in CAKI-1 cells. | 178 |

| | |
|---|-----|
| Figure 4.11 Cell cycle analysis of CAKI-1 cells under monolayer adherent conditions and non-adherent spheroid forming conditions in the CAKI-1 Scrambled shRNA control and CAV1 shRNA knockdown cell lines.. | 179 |
| Figure 4.12 Cell cycle analysis of CAKI-1 scrambled shRNA control and CAV1 shRNA cells grown in adherent monolayer and non-adherent spheroid forming conditions now showing both S phase and G2/M phase.. | 180 |
| Figure 4.13 Hypoxia drives clonogenicity in the absence of CAV1 in VHL positive CAKI-1..... | 182 |
| Figure 4.14 Western blots showing activation of hypoxic signalling by expression of HIF-2 α and the effect of hypoxia on CAV1 expression..... | 183 |
| Figure 4.15 The hypoxic response is able to restore clonogenicity in CAKI-1 cells in the absence of CAV1 expression..... | 188 |
| Figure 5.1 Human phospho-kinase array data of CAKI-1 Scrambled shRNA control and CAV1 shRNA knockdown cells grown as an adherent monolayer under normoxic conditions..... | 201 |
| Figure 5.2 Human phospho-kinase array data of CAKI-1 Scrambled shRNA control and CAV1 shRNA knockdown cells grown as spheroids in non-adherent normoxic conditions..... | 202 |
| Figure 5.3 Human phospho-kinase array data of CAKI-1 Scrambled shRNA control and CAV1 shRNA knockdown cells grown as spheroids in non-adherent hypoxic conditions..... | 203 |
| Figure 5.4 Human oncology array data of CAKI-1 Scrambled shRNA control and CAV1 shRNA knockdown cells grown as an adherent monolayer under normoxic conditions..... | 208 |
| Figure 5.5 Human oncology array data of CAKI-1 Scrambled shRNA control and CAV1 shRNA knockdown cells grown as non-adherent spheroids under normoxic conditions..... | 209 |

| | |
|--|-----|
| Figure 5.6 Human oncology array data of CAKI-1 Scrambled shRNA control and CAV1 shRNA knockdown cells grown as non-adherent spheroids under hypoxic conditions.. | 210 |
| Figure 5.7 Human pluripotent stem cell array data of CAKI-1 Scrambled shRNA control and CAV1 shRNA knockdown cells grown as an adherent monolayer under normoxic conditions.. | 214 |
| Figure 5.8 Human pluripotent stem cell array data of CAKI-1 Scrambled shRNA control and CAV1 shRNA knockdown cells grown as an non-adherent spheroids under normoxic conditions. | 214 |
| Figure 5.9 Human pluripotent stem cell array data of CAKI-1 Scrambled shRNA control and CAV1 shRNA knockdown cells grown as an non-adherent spheroids under hypoxic conditions. | 215 |
| Figure 5.10 CAV1 dependant downregulation of STAT3 and b-catenin in CAKI-1 cells | 217 |
| Figure 5.11 Inhibition of STAT3 phosphorylation by WP1066 (A) and β -catenin by IWP-2 (B)..... | 217 |
| Figure 5.12 Colony formation of CAKI-1 scrambled shRNA control and CAV1 shRNA knockdown cells after small molecule inhibition of STAT3 phosphorylation by WP1066 and Wnt signalling by IWP-2..... | 218 |
| Figure 5.13 Schematic overview of CAV1 regulation of clonogenicity in CAKI-1 cells. | 223 |
| Figure 6.1 Schematic illustrating the role of CAV1 in the VHL +/+ PTEN +/+ CAKI-1 cell line (A) and the VHL-/- PTEN -/- 786-O cell line..... | 230 |

Table of Tables

| | |
|---|----|
| Table 2.1 Table of markers selected for clinical studies..... | 26 |
| Table 2.2 Table of markers not selected for clinical studies..... | 27 |
| Table 2.3 Antibodies used in the immunohistochemical staining of RCC TMAs..... | 41 |
| Table 2.4 Crosstabulation of CAV1 with histopathological characteristics of RCC... | 47 |
| Table 2.5 Cox regression analysis of CAV1 with histopathological characteristics of RCC..... | 48 |
| Table 2.6 Crosstabulation of CD44 with histopathological characteristics of RCC... | 54 |
| Table 2.7 Cox regression analysis of CD44 with histopathological characteristics of RCC cohort..... | 55 |
| Table 2.8 Crosstabulation of All other tumours and CD44 +ve/CAV1 +ve with histopathological characteristics of RCC..... | 57 |
| Table 2.9 Cox regression analysis of combined CD44 and CAV1 expression with histopathological characteristics of RCC..... | 58 |
| Table 2.10 Crosstabulation of CD105 with histopathological characteristics of RCC. | 63 |
| Table 2.11 Cox regression analysis of CD105 expression with histopathological characteristics of RCC..... | 63 |
| Table 2.12 Crosstabulation of All other tumours and CD105 +ve/CAV1 +ve with histopathological characteristics of RCC..... | 65 |
| Table 2.13 Cox regression analysis of combined CD105 and CAV1 expression with histopathological characteristics of RCC..... | 66 |
| Table 2.14 Crosstabulation of EpCAM with histopathological characteristics of RCC. | 72 |

| | |
|---|----|
| Table 2.15 Cox regression analysis of EpCAM expression with histopathological characteristics of RCC. | 72 |
| Table 2.16 Crosstabulation of EpCAM and CAV1 with histopathological characteristics of RCC. | 74 |
| Table 2.17 Cox regression analysis of combined EpCAM and CAV1 expression with histopathological characteristics of RCC. | 75 |
| Table 2.18 Crosstabulation of CD146 with histopathological characteristics of RCC. | 80 |
| Table 2.19 Cox regression analysis of CD146 expression with histopathological characteristics of RCC. | 80 |
| Table 2.20 Crosstabulation of CD146 and CAV1 with histopathological characteristics of RCC. | 82 |
| Table 2.21 Cox regression analysis of CD146 and CAV1 expression with histopathological characteristics of RCC. | 82 |
| Table 2.22 Crosstabulation of vimentin with histopathological characteristics of RCC. | 86 |
| Table 2.23 Cox regression analysis of vimentin expression with histopathological characteristics of RCC. | 87 |
| Table 2.24 Crosstabulation of vimentin and CAV1 with histopathological characteristics of RCC. | 89 |
| Table 2.25 Cox regression analysis of vimentin and CAV1 expression with histopathological characteristics of RCC. | 89 |
| Table 2.26 Crosstabulation of MCT4 with histopathological characteristics of RCC. | 95 |
| Table 2.27 Cox regression analysis of combined MCT4 expression with histopathological characteristics of RCC. | 96 |
| Table 2.28 Crosstabulation of MCT4 and CAV1 expression with histopathological characteristics of RCC. | 98 |

| | |
|--|-----|
| Table 2.29 Cox regression analysis of MCT4 and CAV1 expression with histopathological characteristics of RCC..... | 99 |
| Table 2.30 Crosstabulation of Cavin-1 expression with histopathological characteristics of RCC..... | 103 |
| Table 2.31 Cox regression analysis of Cavin-1 expression with histopathological characteristics of RCC. | 103 |
| Table 2.32 Crosstabulation of Cavin-1 and CAV1 expression with histopathological characteristics of RCC. | 105 |
| Table 2.33 Cox regression analysis of Cavin-1 and CAV1 expression with histopathological characteristics of RCC..... | 105 |
| Table 2.34 Cox proportional hazard model of time to disease recurrence using the forward selection function. | 106 |
| Table 3.1 Fluorophore conjugated antibody panel corresponding to markers selected for flow cytometry analysis..... | 129 |
| Table 3.2 The frequency of detectable subpopulations in 786-O based on the expression of CSC marker panel. | 135 |
| Table 3.3 The frequency of detectable subpopulations in A498 based on the expression of CSC marker panel. | 135 |
| Table 3.4 The frequency of detectable subpopulations in CAKI-1 based on the expression of CSC marker panel. | 140 |
| Table 3.5 The frequency of detectable subpopulations in CAKI-1 based on the expression of CSC marker panel. | 141 |
| Table 3.6 Characterisation summary of CSC surface markers used in RCC cell lines | 151 |
| Table 4.1 Proportions of CD90/CD146 subpopulations in the cell lines 786-O, A498 and CAKI-1 in scrambled shRNA control and CAV1 shRNA knockdown cells. | 170 |
| Table 5.1 Heat-map showing the fold changes in phosphorylation induced by CAV1 down-regulation in adherent, spheroid and hypoxic spheroid cells..... | 204 |

| | |
|--|-----|
| Table 5.2 Heat-map showing the fold changes in proteins identified by the oncology array induced by CAV1 down-regulation in adherent, spheroid and hypoxic spheroid cells. | 211 |
| Table 5.3 Heat-map showing the fold changes in proteins identified by the oncology array induced by CAV1 down-regulation in adherent, spheroid and hypoxic spheroid cells. | 212 |
| Table 5.4 Heat-map showing the fold changes in proteins identified by the pluripotent stem cell array induced by CAV1 down-regulation under all three conditions. | 215 |

Chapter 1 – General Introduction

1 General Introduction

1.1 Renal cell carcinoma

Tumours originating in the kidney can be placed into two generalised groupings. Those which are derived from and develop in the cortex and medulla of the kidney, termed renal cell carcinomas (RCCs) and those which are derived from the urothelium of the renal pelvis termed transitional cell carcinoma (TCC). RCCs account for the vast majority of kidney cancers at around 80%, the remainder being comprised of TCCs. As such RCC has been the malignancy investigated in this work.

1.1.1 Epidemiology, etiology and pathology of renal cell carcinoma

RCC represents the ninth most common cancer worldwide with 337,860 cases diagnosed in 2012[1]. In 2013, of the 65,150 patients diagnosed with RCC in the United States 13,680 succumbed to the disease[1]. Cases of RCC are more common in men than women, being the seventh most common cancer in men and the ninth most in women[2]. Over the last few decades the incidence of RCC increased year by year with a concomitant increase in mortality rate[3]. The reason for the increase is not fully understood however this increased incidence is thought to be partially due to the increased efficacy of diagnostic methodologies and the more routine use of abdominal imaging techniques resulting in an improvement in early diagnosis [4].

RCC is characterised as a highly metastatic disease with 20-30% of patients diagnosed with RCC presenting with metastatic tumours and 20% of patients diagnosed with localised disease will progress to metastatic disease[5]. Indeed many of the symptoms associated with RCC that are present at diagnosis are indicative of late stage tumours. Despite major advances in treatment options, such as the molecular inhibition of cell signalling pathways important for oncogenesis,

metastatic RCC has remained remarkably treatment refractive. Median overall survival times for RCC treated with molecular targeted therapy are around 11-26 months depending on the treatment modalities used[6]–[8]. This represents a drastic improvement from the classical non-specific interleukin-2 (IL-2) and interferon- α (IFN- α) based treatment of RCC in which only 30% of patients were responsive with a durable response only observable in 7% lasting to around 4 to 6 months[9], [10]. Thus, there is a requirement to further develop and discover novel strategies for the treatment of metastatic RCC.

Numerous factors have been implicated in the etiology and increased risk of RCC such as: active and passive cigarette smoking[11], obesity[12] and hypertension[13], [14]. Patients with end-stage renal failure, tuberous sclerosis and renal cystic disease appear to be more vulnerable to the development of RCC[15], [16]. However with most patients, risk factors are extremely difficult to identify, as the mechanisms of pathogenesis for each risk factor remains unclear.

Inheritance of autosomal dominant syndromes accounts for 2-3% of all RCC cases, the most notable of these being von Hippel-Lindau syndrome (1 birth in 36,000)[17]. The disease is characterised by the formation of highly vascularised tumours such as: ccRCC, pheochromocytoma and haemangioblastomas of the central nervous system[18]. The syndrome arises from loss of function mutations in the *VHL* gene (chromosome 3p25.3), which encodes the von Hippel-Lindau tumour suppressor (VHL), a critical modulator of the cellular response to hypoxia. Loss of functional VHL results in tumourigenesis in the affected organ. Loss of functional VHL activity by heterozygous deletion of chromosome 3p[19] is identified in around 80% of RCCs[20].

Renal cell carcinoma does not present as a single disease but a grouping of histologically distinct tumours, the classification guidelines for which are generated

by the world health organisation (WHO) (with the latest being generated in 2016)[21]. Each of these subtypes are formed from a different portion of the nephron, meaning each type displays different histological features, gene expression and observable phenotypes[1], [22]. Of these sub-types, clear cell renal cell carcinoma (ccRCC), arising from the epithelium of the proximal convoluted tubule, is the most commonly observed constituting 70-80% of RCC patients. ccRCCs are characterised by a tendency for inactivation of functional VHL by either genetic mutation, promoter hypermethylation or chromosome 3p deletions as well as high concentrations of cytoplasmic lipid and a clear cytoplasm upon histological preparation[1], [23]. The second most common sub-type, papillary renal carcinoma, accounts for 10-15% of cases and is divided into two sub-types. Type 1 characterised by tumour cells with low grade nuclei. Type 2 papillary carcinomas are the more aggressive form and are characterised by intense eosinophilic cytoplasmic staining[23]. Other subtypes include collecting duct, chromophobe and medullary. Some tumours display sarcomatoid differentiation; a spindle-like morphology with pronounced mesenchymal differentiation. While this does not define a distinct physiological sub-type of RCC, as it is a phenotype that has been identified in all histological sub-types, such observations indicate a more aggressive tumour and poor prognosis[24].

The established way of assessing prognosis of RCC patients is by accessing the stage and grade of tumours. Staging is determined by scoring patient tumours according to the size and extent of the tumour (T), the presence of invasion to lymph nodes (N) and presence of distant metastasis. Depending on the scores of each of these criteria a composite value of stage from I to IV is given[21]. While stage is a good indicator of disease outcome, its effectiveness relies on the accurate detection of invasive and metastatic events. Fuhrman grade, on the other hand, is a powerful instrument in identifying ccRCC patients with a poor prognostic

outcome[25] and requires only the assessment of tumour cell nuclei. The larger and more irregular in shape the nuclei are, the higher the grade score will be on a scale of I to IV.

For most of the disease course RCC remains virtually asymptomatic. When patients eventually present with symptoms such as haematuria, flank pain or a palpable abdominal mass (symptoms which are not universal to all patients) it is usually an indication of advanced disease[26]. Diagnosis can be further confused by the myriad of systemic and paraneoplastic symptoms produced by the tumour and its subsequent metastasis such as: secretion of renin causing hypertension and erythropoietin causing erythrocytosis and fever[27].

1.1.2 Treatment of RCC

First line treatment for RCC remains excision of the tumour mass and a portion of surrounding tissue or complete nephrectomy of the afflicted kidney. As such a radical surgery can have a large impact on a patient's future quality of life, clinicians must make informed decision, based on the size stage and anatomical location of the tumour, as to which surgical approach is the most appropriate for therapy while keeping the highest possible kidney function.[28]. Despite such considerations surgery only proves to be successful in 40 to 60% of patients[29][30]. For patients whose RCC has formed metastatic lesions treatment traditionally involved the use of IL-2 and IFN- α . Such therapies have now largely been replaced with the more efficacious molecularly targeted therapies (though IL-2 treatment does still remain viable for patients with favourable response to surgery and no pre-existing conditions that would exacerbate toxicity). These are treatments which target specific pathways identified as important for the pathogenesis and maintenance of malignant activity. Two major pathways so far have been identified in ccRCC as being the aberrantly activated, the VEGF/HIF and mTOR/Akt signalling pathways.

VHL is often downregulated in RCC. In solid tumours, areas of low oxygen concentration can develop very rapidly, as uncontrolled proliferation results in consumption of oxygen faster than it can be supplied[31]. VHL is the molecular gatekeeper in response to these conditions. Under normal oxygen conditions VHL forms an E3 ubiquitin ligase complex with Cullins and elongins B and C[32], this complex polyubiquitinates hypoxia inducible factors (HIFs), targeting them for degradation by the proteasome[33]. HIFs are a group of transcription factors capable of mediating the expression of a wide variety of genes involved in processes such as angiogenesis, mitogenesis and invasion[33]. These include a number of growth factors and their receptors: platelet derived growth factor (PDGF), epithelial growth factor receptor (EGFR) and vascular endothelial growth factor (VEGF), as well as adhesion molecules important for invasion such as Mucin 1 (MUC1)[34]. Due to the lack of functional VHL in most ccRCC tumours there is constitutive expression of HIF induced genes. Sunitinib (Pfizer) is the first in a series of small molecule inhibitors developed to disrupt the constitutive activation of HIF signalling by targeting receptor tyrosine kinases (RTK) of VEGF and PDGF[35]. Clinical studies comparing the efficacy of Sunitinib treatment compared to interferon- α found a median overall survival rate of 26.4 months in the sunitinib patient group and 21.8 months in the interferon- α group[36]. This has led to the development of a series of various RTK inhibitors for use in RCC such as sorafenib[37] and the anti-VEGF antibody bevacizumab (avastin)[38].

Mammalian target of rapamycin (mTOR) and protein kinase B (Akt) form a signalling nexus that can regulate a wide variety of processes essential for tumourigenesis and disease progression. Together the Akt/mTOR signalling network can regulate proliferation, protein synthesis, inhibition of apoptosis and also angiogenesis. It has been demonstrated that expression of Akt, mTOR and the downstream activator of S6 p70S6K is higher in malignant RCC tissue than normal adjacent tissue[39].

Furthermore increased staining of p-Akt in RCC tissue samples was indicative of lower patient survival[40]. The release and autocrine activity of soluble growth factors such as VEGF and PDGF through their cognate receptor tyrosine kinase induces the activity of phosphoinositide-3-kinase (PI3K) leading to increased proliferation and resistance to apoptotic signalling. Intervention of the activity of the Akt/mTOR pathway has also proven somewhat successful in the treatment of RCC. Drugs such as temsirolimus (an analogue of rapamycin) prevent the activation of the S6/4E binding protein-1 (4E-BP1)/eukaryotic initiating factor 4 subunit E (EIF4E) pathways, activation of which facilitates the transcription of a number of proliferative regulators, transcription factors and HIFs[41]. Temsirolimus prevents the activation of mTORC1 by forming a complex with FK-506 binding protein[42]. Patients treated with temsirolimus had a 3.6 month increase in survival compared to treatment with interferon[43].

Though these therapeutic approaches and improved diagnostic techniques have greatly improved the prognostic outlook for RCC patients, achieving durable and consistent treatment remains elusive. Over the last decade a great deal of research has been invested into cancer cells found within tumours endowed with properties similar to that of normal stem cells. The cancer stem cell (CSC) theory of cancer progression may offer potential explanations for carcinogenesis, resistance to chemo and radiotherapy and drive recurrence of disease after apparent remission. As such the search for CSC populations, understanding the molecular mechanisms behind their activity and targeting of them by specific therapeutic agents is well underway.

1.2 The 'Cancer Stem Cell' hypothesis

1.2.1 Tumour heterogeneity

Tumours are not a homogenous population of cancer cells but composed of heterogeneous subpopulations of cells[44]. This has led to two distinct, but most likely overlapping, schools of thought in how tumours are initiated, maintained and progress to advanced metastatic disease.

The classical view of tumour progression[45], states that tumours arise from a single or small number of cells that gain an advantageous mutation, most likely in proliferative capacity. This mutation offers the cell, or group of cells, a substantial growth advantage over other cells. This process repeats as subclones of cells gain genetic advantages which allow them to out compete other subclones (Figure 1.1). Thus the process of malignant transformation is thought to be driven in a microevolutionary manner. This theory has offered explanations as to how cancers are able to acquire the hallmarks of cancer[46], display intratumoural heterogeneity and develop resistance to therapy. However, clonal evolution alone fails to explain some more recent observations namely the ability for groups of cells to generate and maintain tumour heterogeneity[47], [48]. Such findings have been demonstrated as evidence for the presence of CSC populations.

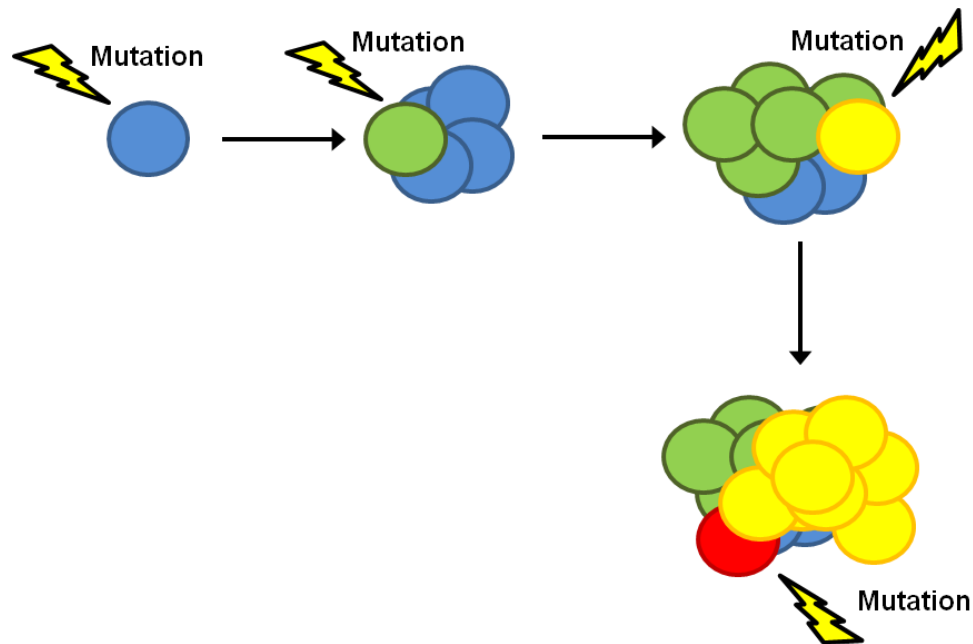


Figure 1.1 Graphical representation of the clonal evolution of carcinogenesis and tumour maintenance. Successive advantageous mutations give rise to more aggressive subclones of cancer cells (represented by the different coloured groups of cells) which can out-compete others. This is thought to be a continuous process as genetic mutations accumulate within the tumour.

1.2.2 Characteristics of cancer stem cells

Cancer stem cells were first identified in acute myeloid leukemia (AML) as a population of cancer cells identified by expression of surface marker combination $CD34^+/CD38^-$. These cells were found to be capable of recapitulating AML in severe combined immunodeficient (SCID) mice[49], [50]. This approach was then applied to breast cancer tumours by Al-Hajj et al.[51]. Using the surface marker combination $CD44^+/CD24^-$ they were able to isolate a subpopulation of cells capable of generating a solid tumour in SCID mice. Following these early studies CSCs have now been identified in a multitude of cancers such as: brain[52], [53], colon[54], [55], lung[56], [57], prostate[58] and pancreatic[59], [60]. Such populations of CSCs have been identified by a number of different surface marker expression profiles. Generally, the markers selected are similar to those of normal embryonic or mesenchymal stem cells. CSCs can also be distinguished by the functional

characteristics of stem cells (a more detailed discussion found in chapter 2). CSC populations have also been identified in RCC by surface marker expression of CD105[61] and much more recently by CXCR4[62]. Putative RCC CSC populations have also been isolated by Hoechst dye exclusion[63] and non-adherent tumour spheroid formation[64].

Similar to their name sake, CSCs are thought to be a distinct population of cancer cells within tumours endowed with functions similar to that of normal stem cells. Namely, the unlimited capacity for differentiation to drive tumour formation and self-renewal to preserve the pool of CSCs (Figure 1.2) but also the ability to drive tumour formation after therapeutic intervention by an increased resistance to chemo and radiotherapeutics (Figure 1.4).

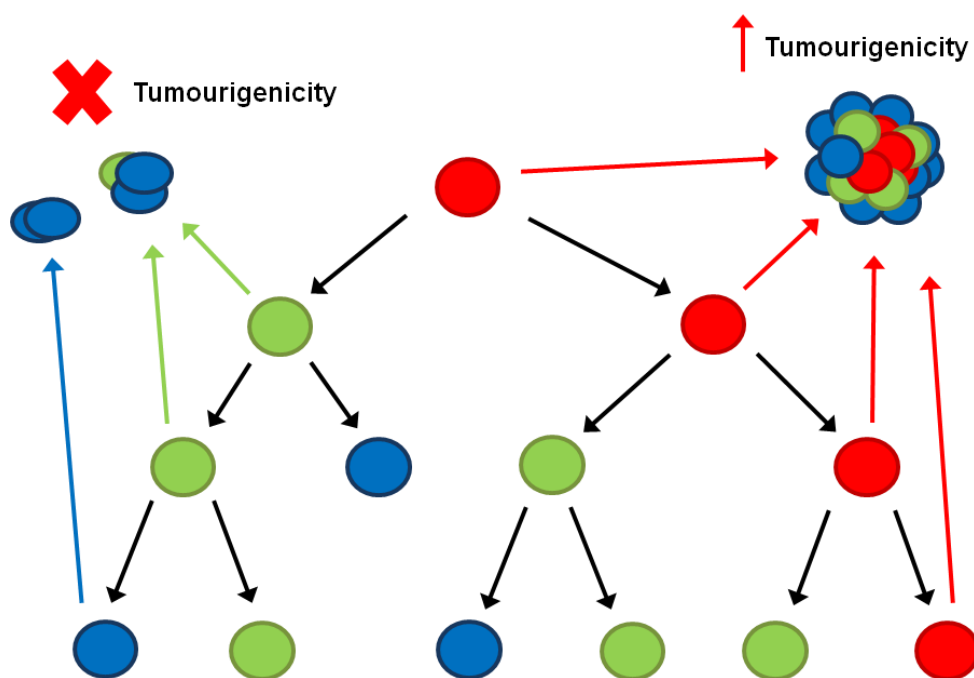


Figure 1.2 Graphical representation of CSC driven tumourigenicity. Red circles represent CSCs which are endowed with tumourigenic ability with green and blue circles representing more differentiated daughter cells which are incapable of tumourigenicity.

The CSC model suggests that a single CSC has the ability to drive primary tumour growth, but also enable metastatic tumour growth by their ability to self-renew and differentiate. Through asymmetric division a single CSC can divide into a more

differentiated cell and retain CSC functionality. This more differentiated cell may go on to further proliferate and generate more differentiated cells or undergo terminal differentiation. The CSC is then able to undergo another round of self-renewal and differentiation and thereby produce the tumour bulk (Figure 1.2). Thus the self-renewal and differentiation capacity of CSCs is vital for the generation and maintenance of tumours.

The CSC model also helps address the issue of heterogeneity of metastatic tumours similar to that of primary tumour, an issue which cannot be easily explained by the clonal evolutionary model. Genetic hybridisation analysis of primary and metastatic tumours found them to be extremely similar[65] as is also the case with gene expression profiles[66], [67]. When viewed solely from a clonal evolutionary perspective, metastasis should generate tumours that are much more genetically divergent to the primary tumours by virtue of the mutation events required for a circulating tumour cell to generate a successful metastatic lesion. When taking into account the CSC model of tumourigenesis, a single CSC should have the capacity to generate a metastatic lesion which mirrors the heterogeneity of the primary tumour (Figure 1.3).

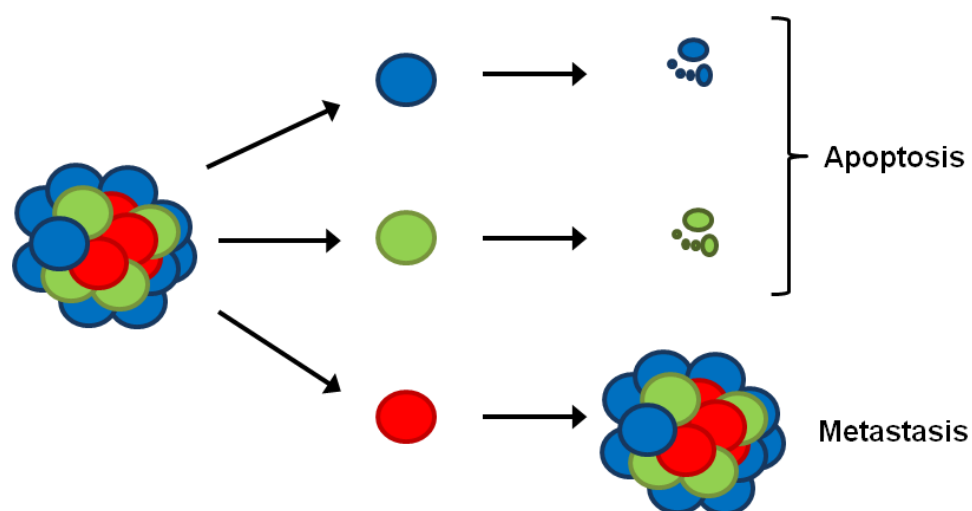


Figure 1.3 Graphical representation of CSC driven metastasis. Only CSC populations (in red) are capable of producing a metastatic tumour resembling the heterogeneity of the primary tumour.

Relapse of disease after what appears to be complete treatment response remains one of the most challenging issues in treating cancer. This phenomenon has been termed minimum residual disease (MRD). It has been speculated that if CSCs truly do exhibit a stem cell-like phenotype then they may offer an explanation to MRD. Normal stem cells are well known to have more robust mechanisms of DNA damage repair[68], [69] and higher expression of multidrug efflux pumps[70]. Such protective mechanisms are thought to be also present in CSC populations. By this increased inherent resistance, CSCs are thought to evade destruction by non-specific treatments such as radio and chemotherapy while the rest of the tumour is driven back or 'de-bulked', these MRD CSCs then go on to drive tumour formation and relapse (Figure 1.4). This characteristic has been directly observed in glioma CSCs. Glioma cells treated with radiation caused an enrichment of cells expressing the glioma CSC marker CD133⁺, these cells survived treatment in a greater proportion than CD133⁻ cells by virtue of an upregulated DNA damage response[71]. In order to overcome MRD specific targeting of CSC populations it appears necessary to target either the self-renewal capacity or specific resistance mechanisms of CSC (Figure 1.4). Indeed targeting of the self-renewal and differentiation CSCs is already starting to show promise. Inhibiting the activation of interleukin-4 (IL-4) signalling in colon CSCs by using an anti-IL-4 antibody induced greater sensitivity to chemotherapy both *in vitro* and *in vivo*[72]. Such an approach has also been employed in RCC where treatment of CD105⁺ RCC CSCs with interleukin-15 induced differentiation to an epithelial phenotype, resulting in reduced tumourigenic capacity and increased sensitivity to cytotoxic compounds[73].

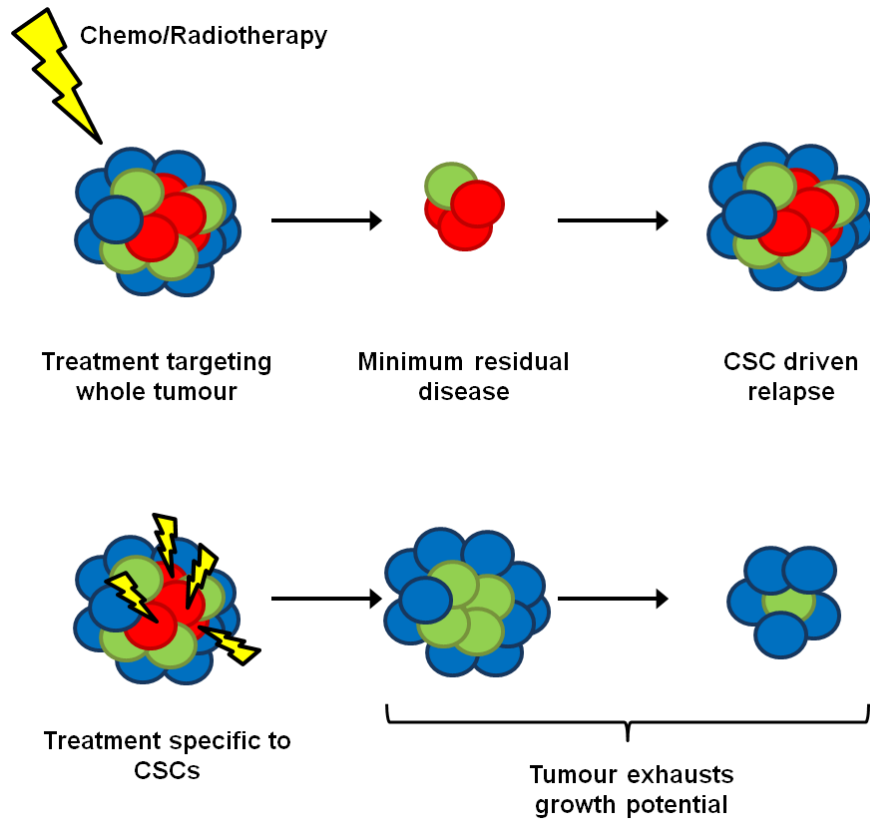


Figure 1.4 Graphical representation of CSC driven disease relapse. The inherent resistance of CSC populations allows them to drive disease relapse after apparent curative therapy. Treatment of CSC populations would disrupt the ability of CSCs to reform tumours by removing the drivers of growth. Red circles represent CSCs, blue and green circles represent differentiated cancer cells.

1.3 Caveolin-1

Caveolin-1 is a 22 kDa scaffolding protein essential for the formation of cholesterol rich plasma membrane invaginations termed caveolae[74]. Caveolae perform clathrin-independent endocytosis, cholesterol efflux and lipid and protein sorting in the plasma membrane (the membrane trafficking functions of caveolin and caveolae reviewed here[75]). The caveolin family consists of caveolin-1, -2 and -3. Caveolin-1 (CAV1) and Caveolin-2 (CAV2) are expressed in a wide variety of cell types, with particularly strong expression in adipocytes, fibroblasts and endothelial cells[76], with Cav-3 being expressed in smooth muscle[77]. CAV1 is the most widely studied of the Caveolins, due to the requirement for CAV1 expression in order for CAV2 to be trafficked from the Golgi complex to the plasma membrane[78].

Caveolins mainly reside in the inner leaflet of the plasma membrane with a hairpin conformation which allows both the N and C termini to be exposed to the cytosol[79] (Figure 1.5). Additionally, depending on cell type, CAV1 can also be found as a soluble cytoplasmic protein associated with cholesterol[80], or can be secreted as a result of serine 80 phosphorylation[81]. CAV1 forms either homo or hetero (with other Caveolin molecules) dimers within caveolae domains. This is thought to be facilitated through interaction of palmitoylations at C terminal cysteines of Caveolins[82].

Interactions of CAV1 with cell surface receptors and soluble proteins takes place at a short aromatic amino acid dense sequence (residues 82-101) known as the caveolin scaffolding domain (CSD)[83]. Through this region CAV1 is able to bind and cause either positive or negative regulation of the bound signalling molecule. Such regulatory activity has been found with various types of signalling molecules such as: receptor tyrosine kinases (RTKs)[84], integrins[85] and G-protein coupled receptors[86]. Such a diverse array of binding partners is reflected in a diverse array of signalling activity for CAV1. Binding of Src tyrosine kinases to CAV1 inhibits their

activity reducing auto-activation of Src[87]. Whereas binding of PTEN to CAV1 increases the localisation of PTEN to the membrane and inhibits Akt activation[88]. Conversely, overexpression of CAV1 has been found to maintain increased activation of Akt signalling by interaction and inhibition of the serine/threonine phosphatases PP1 and PP2A[89]. CAV1 can also regulate cell surface receptor activity through endocytosis. For example, CAV1 specific siRNA treatment was sufficient to reduce the activation of IGF1R signalling in Ewing sarcoma[90]. Interaction of CAV1 with epithelial growth factor receptor (EGFR) has been shown to maintain activation of EGFR in the absence of epithelial growth factor (EGF) by facilitating homodimeric activation of EGFR[84]. Such a wide array of molecular interactions may underpin why CAV1 is found to be tumour suppressing in some tumours while oncogenic in others.

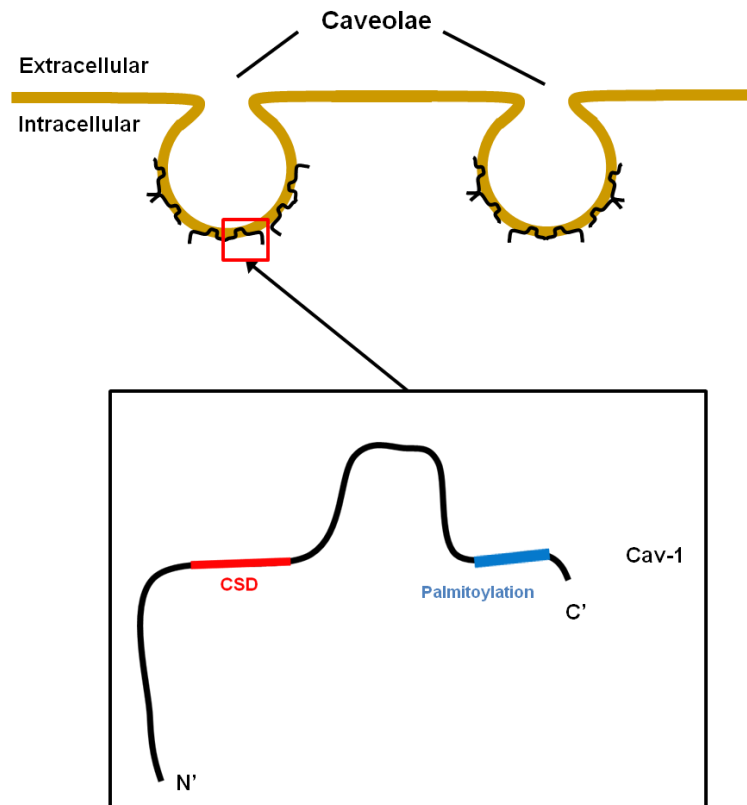


Figure 1.5 Schematic of CAV1 localisation and structure. Caveolin-1 is localised to caveolae in the plasma membrane. Caveolin-1 contains a hairpin structure, allowing both the C and N terminal to protrude into the cytoplasm from the plasma membrane, as well as a scaffolding domain (CSD shown in red) capable of binding and modulating cell surface receptor activity.

1.3.1 Caveolin-1 in cancer

CAV1 has been identified as both oncogenic and tumour suppressing depending on tumour type. In cancers of the lung[91], breast[92], colon[93], ovaries[94] as well as stromal cells in breast tumours[95] loss of CAV1 expression was associated with progression to malignant disease. In the case of breast[92], colon[93] and ovarian[94] cancer overexpression of CAV1 partially reversed the malignant phenotype. Downregulation of CAV1 has been demonstrated as sufficient for malignant transformation. In the non-cancerous NIH 3T3 cell line knockdown of CAV1 induced tumourigenicity by increased activity of the mitogen activated protein kinase cascade, which upregulation of CAV1 ablated[96]. *In vivo* reduction of CAV1

expression has been found to sensitise tissues to carcinogenesis. CAV1 (-/-) knockout mice had a drastically increased incidence of epidermal hyperplasia and tumour formation when treated with the carcinogen 7,12-dimethylbenzanthracene (DMBA)[97].

In contrast to these studies, CAV1 expression has been identified as oncogenic in a number of malignancies. Upregulation of CAV1 expression has been associated with carcinogenesis of both prostate and breast cancer[98]. In the normal kidney, cells of the proximal convoluted tubule are negative for the expression of CAV1; however upregulation of CAV1 is detected in RCC and indicates poor disease outcome[99]. Other clinicopathological studies of CAV1 overexpression have also found it to be indicative of poor prognosis. Such cancers include: oesophageal[100], pancreatic[101] and prostate cancers[102] (a more detailed discussion of the prognostic significance of CAV1 expression is found in chapter 2). This paradox of a protein having both tumour suppressing and oncogenic effects can be rationalised viewing CAV1 not as the direct activator of these signalling events but as a scaffold or signalling platform for these pathways[103] (Figure 1.6).

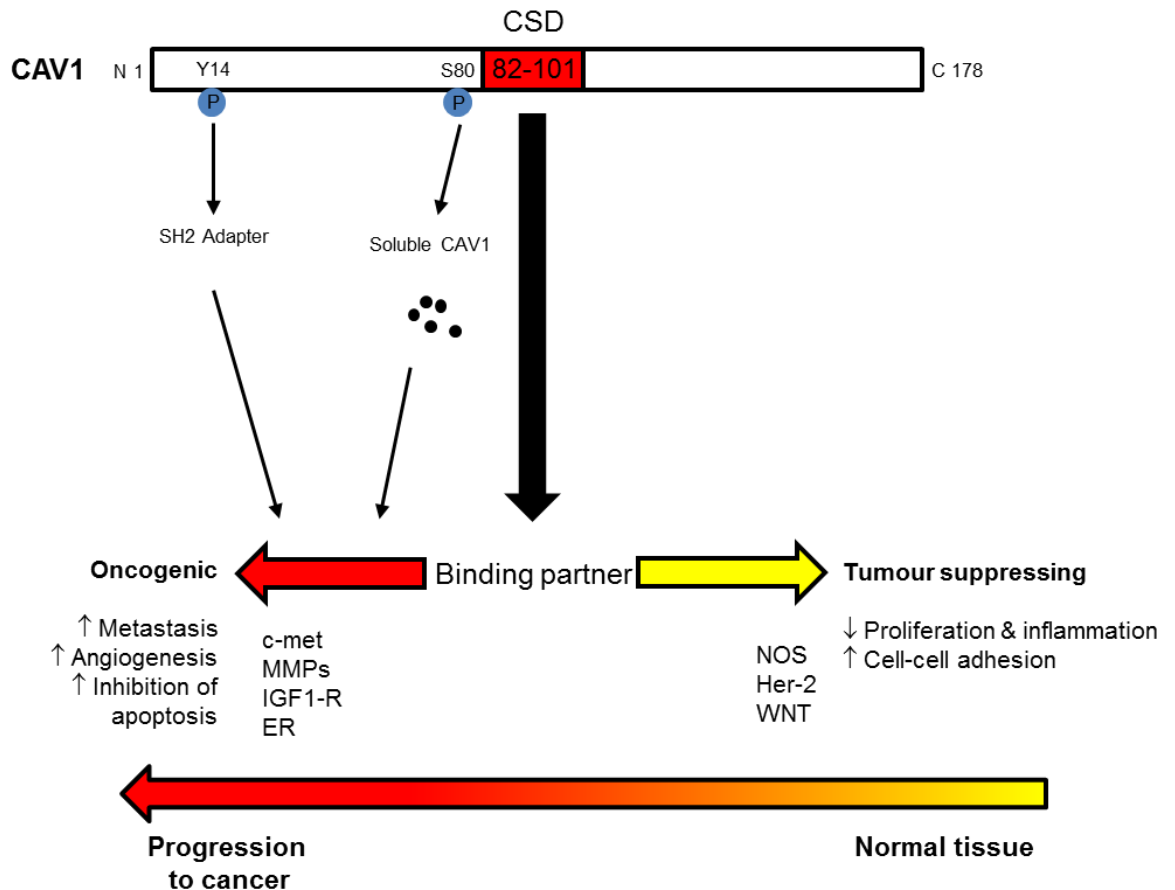


Figure 1.6 Model for the interaction of CAV1 with signalling mechanisms in both normal and cancerous tissue. CAV1 is capable of modulating signalling activity through the interaction of the CSD with either oncogenic or tumour suppressing binding partners.

CAV1 has been demonstrated to regulate a number of characteristics key to the progression of malignant disease such as invasive/migratory potential, resistance to apoptotic cell death and increased growth capacity. In multidrug-resistant colon cancer cells inherent overexpression of CAV1 dramatically suppressed proliferative capacity but such cells displayed higher resistance to chemotherapeutics[104]. CAV1 mediated chemoresistance is also observed in gastric cancer cells. In this study, CAV1 expression was required for β -catenin dependent transcription of WNT6, this resulted in increased resistance to epirubicin induced apoptosis[105]. In colon cancer, CAV1 has been demonstrated to upregulate survival by binding to

Ku70 and inhibiting the chemotherapeutic induced release of pro-apoptotic Bax[106].

CAV1 has also been shown to upregulate survival under irradiation. Intestinal crypt stem cells of CAV1 knockout mice exhibited a higher degree of proliferation with increased activity of the Wnt/ β -catenin signalling pathway. When irradiated these CAV1 negative crypt stem cells were more prone to apoptosis[107]. Similarly, siRNA mediated knockdown of CAV1 in pancreatic cancer cell lines induced pronounced apoptosis in response to radiation[108]. However, in this study downregulation of CAV1 attenuated proliferation, thought to be mediated by CAV1/focal adhesion kinase (FAK) potentiation of Akt signalling. In breast and colon cancer, upregulation of CAV1 has been associated with increase multidrug resistance, thought to be due to the association of drug efflux pumps such as P-glycoprotein (P-gp) with CAV1 and caveolae domains[109]. Further to this, siRNA knockdown of CAV1 in MDCK cells resulted in the reduced activity of the drug efflux pump BCRP increasing sensitivity to cytotoxic compounds. The activity of BCRP being important to the maintenance of the stem cell populations by resisting cytotoxic death[110]. In RCC, CAV1 knockdown in metastasis derived SN12CPM6 cells caused sensitisation to doxorubicin induced apoptosis. Injection of CAV1 knockdown SN12CPM6 cells in combination with doxorubicin into SCID mice resulted in significantly lower incidences of lung metastasis[111]. The ability for CAV1 to upregulate resistance to potential chemotherapeutics hints at the possibility for a role in regulating such resistant mechanisms in CSC populations.

Metastatic spread and increased vascular density by angiogenesis are characteristics key to the progression of all solid tumours. Effective cellular motility is a property integral for the occurrence of both these events, of which CAV1 and caveolae may pay an important role. Polarization of CAV1 and Caveolae has been observed in normal endothelial cells during two and three dimensional migration.

CAV1 was found to dissociate from caveolae and relocalise to the migratory cell front dependant on phosphorylation of CAV1[112]. Furthermore, induction of cell migration in normal endothelial cells caused the relocation of caveolae to the trailing edge of the cell with a concomitant localisation of Ca^{2+} wave initiation[113]. These caveolae contained signalling machinery required for ATP-stimulated Ca^{2+} release from the endoplasmic reticulum[113]. Rho signalling induced by Rho kinase (ROCK) is important to the polarisation and motility of both stem cells[114] and cancer cells[115]. Previously, tyrosine phosphorylation of CAV1 has been shown to maintain Rho/ROCK signalling which regulates the turnover of FAK complexes and increasing migratory potential[116]. In RCC, siRNA mediated downregulation of CAV1 resulted in decreased invasive ability of RCC cell lines[117].

CAV1 has been shown to regulate cell signalling pathways important to the maintenance of self-renewal and differentiation of stem cells. Stem cell related pathways that CAV1 has been found to regulate are: Wnt/ β -catenin[107], Notch[118], hedgehog[119] and STAT3[120]. Furthermore, CAV1 and caveolae have been implicated in directing self-renewal and differentiation capacity of mesenchymal and embryonic stem cells (discussed in detail in chapter 4).

It is clear to see that CAV1 has a wide remit of functional activity in terms of cancer progression. It is clear that many of these characteristics such as stimulation of proliferation, chemotherapeutic resistance and cell motility are also important for acquisition and maintenance of the CSC phenotype. When taken together with CAV1's pro-oncogenic role in RCC, it seems that CAV1 may act as a regulator of CSC activity in RCC.

1.4 General thesis aims

The main aims of this thesis are as follows:

- To understand if a selection of common markers for embryonic, mesenchymal and cancer stem cell phenotype in various organs, tumour types and tissues can act as prognostic indicators of disease outcome in RCC alone and in combination with CAV1.
- Identify CSC populations from RCC cell lines using a panel of markers previously used to identify and purify CSC populations in both RCC and other tumour types.
- Examine the effect of CAV1 downregulation on self-renewal and clonogenicity in these populations.
- Investigate the mechanistic basis for any observable effect of CAV1 activity on the self-renewal and clonogenicity by probing cell signalling pathways relevant to these activities.

Chapter 2 - Cancer Stem Cell markers in combination with Caveolin-1 in predicting disease outcome in clinically confined renal cell carcinoma

2 Cancer Stem Cell markers in combination with Caveolin-1 in predicting disease outcome in clinically confined renal cell carcinoma

2.1 Introduction

The prevalence of relapse in patients with seemingly localised RCCs following nephrectomy indicates the existence of undetected micrometastasis occurring before or at the time of surgery, challenging the assessment of disease outcome[121]. The inability to successfully identify patient outcome in primary tumours sharing similar grade and histological stage[122] indicates that the potential mechanisms for relapse and micrometastasis are due to significant molecular heterogeneity of these tumours. This has necessitated the need for robust clinically prognostic biomarkers to use in combination with post-operative surveillance strategies and early intervention with molecularly targeted therapies.

2.1.1 CAV1 as a prognostic marker

CAV1 has been identified as both oncogenic and tumour suppressing in a number of different malignancies, in an apparent context dependant manner. Deregulation of CAV1 has been implicated in numerous cell physiological processes from invasion to chemoresistance (discussed in detail in Chapter 1). The context dependant functionality of CAV1 is further reflected in clinicopathological studies of the prognostic importance of CAV1. Upregulation of CAV1 has been found to be strongly associated to poor prognosis and presence of metastasis in cancers of the bladder[123] and prostate[124]. CAV1 upregulation in colon carcinomas has been linked with disease progression[125], [126], but also demonstrated to inhibit tumourgenicity, in mouse models using colon carcinoma cell lines[93]. In non-small

cell lung carcinomas, CAV1 expression correlated strongly with stage and presence of lymph node metastases[127] and indicated poor prognosis in patients with squamous cell carcinoma of the lung[128].

Although not present in the normal epithelial cells of the proximal convoluted tubules, clinicopathological studies found upregulation of CAV1 in RCC[99], , predicting poor disease outcome. These findings have been further strengthened in other RCC cohorts. Horiguchi et al.[129] found no difference in disease free survival based only on CAV1 positivity, however in patients without metastasis to distant sites or lymph nodes, CAV1 positivity in the primary tumour was associated with a significantly shorter disease free survival than primary tumour negative for CAV1. Joo et al.[130] found CAV1 in RCC to correlate with increased microvessel density, metastasis and indicative of a poor disease free survival.

Further clinicopathological studies carried out by our group sought to understand the prognostic impact of activated Erk and Akt; common targets of molecule specific therapies. Such studies[131] found activation of these pathways to be prognostically poor for RCC patients and found significant synergy with CAV1. Patients whose tumours were identified as co-expressing CAV1 and pErk were at much higher risk of relapse irrespective of tumour grade, i.e. either high or low grade. The same was true for tumours with both increased CAV1 and activated Akt/mTOR signalling. Specifically, CAV1 co-expression with pAkt improved the prognostic ability, with pAkt on its own lacking prognostic significance[132]. Altogether, these studies indicate CAV1 to be a key driving factor in the progression and metastasis of RCC.

2.1.2 Markers of CSC phenotype and metabolic activity as prognostic tools

With the discovery of stem cell-like populations harboured by tumours of various types has come a wealth of cell surface and functional markers with which to

identify them and access their activity[133] (a more detailed discussion on this topic is found in Chapter 3). Identification of such markers has naturally led to the possibility of unearthing new powerfully prognostic markers, which are capable of identifying more aggressive tumours by virtue of an enhanced stem-like phenotype. Growing consensus has linked the CSC phenotype with deregulation of normal energy metabolism in the form of the Warburg effect (the metabolic switch from aerobic respiration to anaerobic respiration which tumours have been widely observed to undergo, this has been considered important to generation of malignant disease [134]. As such, this chapter will investigate the prognostic importance of the expression of a series of CSC and metabolic activity markers, alone and in co-expression with CAV1 (summaries of the markers selected for study are included in Table 2.1 and Table 2.2).

Table 2.1 Table of markers selected for clinical studies.

| Markers selected | | | |
|-------------------------|------------------|--|---|
| Protein name | Gene name | General biological/stemness features | Reasons for inclusion |
| CD105/Endoglin | <i>ENG</i> | TGF- β binding protein. Involved in regulation of angiogenesis. MSC marker | Identified as a CSC marker in RCC primary samples[61]. |
| CD44 | <i>CD44</i> | Receptor for hyaluronic acid. Mediator of cell-cell and cell-matrix interactions. Maintenance of embryonic stem cell phenotype. | Used to identify CSC populations in multiple tumour types[135]–[138]. |
| CD146/MCAM | <i>MCAM</i> | Plays a role in cell adhesion and cohesion. Interacts with endothelial environment. Marker of MSCs | Implicated in the poor prognosis of multiple tumour types[139]. |
| EpCAM | <i>EpCAM</i> | Homotypic calcium-independent cell junction molecule. Important for cell adhesion in epithelial cells. Role in ESC proliferation and differentiation. | Used to identify CSCs in multiple tumour types[140]. |
| Vimentin | <i>Vim</i> | Intermediate filament protein, expressed in cells with a mesenchymal lineage. Organiser for critical molecular elements of cell attachment and migration | Association with stem cell phenotype[141]. May have strong prognostic relationship with CAV1. |
| MCT4 | <i>SLC16A4</i> | Proton-linked monocarboxyate transporter. Rapid transmembrane transport of lactate. | To account for the importance of metabolic shift in cancer and CSC activity[142], [143]. |
| Cavin-1 | <i>PTRF</i> | Important role in the formation and organisation of caveolae. Regulation of rRNA transcription. | Investigate synergistic effects with CAV1 and possible CSC markers[144]. |

Table 2.2 Table of markers not selected for clinical studies.

| Markers not selected | | | |
|-----------------------------|------------------|--|---|
| Protein name | Gene name | General biological/stemness features | Reasons for exclusion |
| CD133/Prominin 1 | <i>PROM1</i> | Transmembrane glycoprotein. Expressed in adult stem cell populations, thought to suppress differentiation | High variability of glycosylation[145], [146]. Previous studies found no clinical relevance of CD133[147]. |
| CD24 | <i>CD24</i> | Glycosyl phosphatidylinositol linked membrane sialoglycoprotein. Modulator of B-cell activation response. | Used to identify CSC populations, but in most cases CD24 negative populations which have a CSC phenotype[148], [149]. |
| CD117/c-kit | <i>KIT</i> | Cell surface receptor tyrosine kinase. Regulates proliferation, haematopoiesis, stem cell and gametogenesis. | Little evidence to suggest CD117 has a strong potential for prognostic significance in solid malignancies. |
| CD166 | <i>ALCAM</i> | Immunoglobulin receptor. Binds to CD6 to regulate T-cell activation. Some involvement in chemoresistance and metastasis. | Only shows CSC related presence in colorectal cancer[136]. |
| CD47 | <i>CD47</i> | Interaction with various integrins. Has roles in innate immunity. | Little direct involvement in CSC phenotype[150]. |
| ALDH1 | <i>ALDH1A1</i> | Belongs to the aldehyde dehydrogenase family. Important for chemoresistance. | No real direct involvement in clonogenicity[150]. |

2.1.3 CD44

CD44 defines a large family of transmembrane glycoprotein isoforms encoded by a single gene found on human chromosome 11 [151]. CD44 acts as a receptor for a wide array of extracellular matrix (ECM) ligands and microenvironmental components such as osteopontin, fibronectin, laminin heparin-binding epidermal growth factor (HB-EGF), collagens and matrix metalloproteinases (MMPs)[152]. However, the main physiological ligand for CD44 is hyaluronic acid (HA), a linear polysaccharide glycosaminoglycan, found universally in the ECM of vertebrate tissues where it helps to regulate cell migration, proliferation and adhesion[153]. CD44 is capable of transducing signals intracellularly by virtue of modification of growth factor receptors and hence their downstream functionality. Moreover, this marker has a more direct role through interaction of its C-terminal domain, which is able to form complexes with a variety of intracellular signalling molecules such as Src kinases and Rho-GTPases, as well as having a direct impact on the mechanical physiology of the cell through complexes formed with cytoskeletal proteins[154]. CD44 also undergoes a number of post-translational N- and O-glycosylations as well as homo-dimerisation, further expanding its role as a multifunctional signalling platform[155].

Such a wide array of interactions has led to significant investigation into CD44 expression in malignant pathologies[156]. Studies have shown CD44 to have a substantial role in invasion and migration[157], epithelial mesenchymal transition (EMT)[158], up-regulation of anti-apoptotic signalling[159], as well as upregulation of resistance to both oxidative stress[160] and chemotherapeutics[161]. These activities are orchestrated through interactions with HA and numerous other cell surface binding partners to regulate many cell signalling pathways such as G-protein coupled receptor (GPCR) signalling, MAPK/PI3K and β -catenin (reviewed here[162], [163]).

In colon cancer different CD44 isoforms, such as CD44 variant 6 (CD44-v6) are expressed during different stages of disease progression, with expression of the CD44-v6 isoform appearing to be an early event in malignant transformation[164]. CD44 in breast tumours is correlated to tumour invasion, metastasis and pathological grade[165]. Positive expression of CD44 in pancreatic cancer is correlated with occurrence of distant metastasis and also acts as an independent prognosticator for poor disease outcome[166].

Clinicopathological studies in the expression of CD44 in RCC have been previously conducted with CD44 expression correlating with a number of histopathological variables indicative of poor disease free survival to the extent that CD44 has been reported to act as an independent prognostic indicator in relatively small patient cohorts[167], [168]. Similar results were obtained in a larger (110 patient cohort) study by Byung et al.[169]. Given the apparent prognostic significance of CD44 in RCC progression and its tendency to be regulated in lipid rafts[170], [171], the combinatorial study of CD44 in relation to CAV1 expression in a large RCC patient cohorts appears to be warranted.

2.1.4 CD105

CD105, also known as endoglin, is a 180kDa homodimeric disulphide-linked transmembrane glycoprotein identified as an accessory receptor to transforming growth factor beta (TGF- β) and localised to the TGF- β receptor complex[172]. Primarily expressed in low levels in resting endothelial cells, CD105 undergoes a marked up-regulation in actively proliferating endothelia of tumour and tumour associated endothelial cells[173]. As such, this has made CD105 an attractive target for the development of anti-angiogenic therapeutics, imaging of tumour microvasculature and as a prognostic indicator[174], [175]. Such CD105 imaging has been used to identify the tumour microvasculature in *ex vivo* analysis of RCCs. CD105 was found to be expressed at the site of tumour endothelia where it was

able to reveal localised, undiagnosed kidney masses [176]. Elevated serum CD105 levels have been associated with metastatic disease in both breast and colorectal carcinomas[177], [178].

Expression of CD105 in a number of tumours has been associated with poor prognosis. In colorectal cancer CD105 expression has been significantly correlated with liver metastasis and angiolymphatic invasion[179]. A large scale study of CD105 expression in breast carcinomas involving 929 patients found CD105 positive expression to be indicative of poor disease outcome and to correlate with invasive characteristics and act as an independent marker of poor prognosis[180]. Similar studies have been carried out in endometrial carcinoma[181], non-small cell lung cancer[182], oesophageal adenocarcinoma[183] and high grade paediatric glioma[184], all of which found consistent positive correlations between CD105 expression and poor prognosis and the degree of both angiogenic and metastatic invasion.

Other studies have looked into the effects of tumour expression of CD105 in the disease progression of RCC with results being contradictory. An initial study by Sandlund et al.[185] found CD105 to be expressed in 75% of a 210 patient cohort study and with expression inversely correlated with Tumour-Node-Metastasis (TNM) stage and nuclear grade and associated with an overall better prognosis. This is contrary to the findings of Dubinski et al.[186]; who demonstrated positive correlations of CD105 with tumour stage and grade, poor disease outcome and the ability to act as an independent factor of poor prognosis. These findings were further confirmed by Saroufim et al[187], who found that CD105 positivity to correlate with grade and stage and acted as an independent predictor of poor disease outcome. CSC populations in RCC have previously been identified by a small population of CD105^{High} cells[61], it thus appears appropriate that this molecule is further characterised with respect to its prognostic ability in primary RCC tissue. Further to

this, CAV1 has been found to co-localise to and support the activation of TGF- β complexes[188], therefore the combinatorial investigation of CD105 and CAV1 may be of prognostic significance.

2.1.5 EpCAM

Epithelial cell adhesion molecule (EpCAM) is a 30 to 40 kDa type I transmembrane glycoprotein whose expression is restricted to epithelial cells in normal tissue, where it takes part in homotypic cell-cell adhesion[189]. EpCAM expression is also observed in nearly all adenocarcinomas and seems to indicate both positive and negative prognosis depending on tumour type[190]. The first study to uncover a potential oncogenic role for EpCAM in cancer cells was conducted in breast cancer. Osta et al.[191] found EpCAM to be overexpressed in both primary and metastatic tissue by 100-1000 fold. In siRNA knockdown in-vitro studies of EpCAM a decrease in breast cancer proliferation and significant down-regulation of both cell migration and invasion was seen. Subsequently, EpCAM has seen widespread use as a stem cell marker[192] and particularly in colorectal carcinomas[136], [193] (discussed in further detail in Chapter 3).

The overexpression of EpCAM in carcinomas seems to provide a context dependant prognosis depending on the tissue of origin and, in some cases, providing diverging prognosis in the same tumour type. In breast cancer EpCAM is associated with poor prognosis and node-positive breast cancer that was predictive of sensitivity to cytotoxic or hormonal adjuvant therapy[194]. Positivity of EpCAM in ovarian carcinomas is associated with a decrease in overall patient survival, particularly in patients classified as stage III or IV; the marker was also capable of acting as an independent prognostic variable[195]. A study of EpCAM expression in human oesophageal cancer found EpCAM positivity to associate with improved

patient survival, with high serum EpCAM levels appearing to indicate better overall prognosis[196].

Similarly, EpCAM expression in RCC is associated with improved patient outcome. A study by Went et al[197]. found EpCAM expression in 18% of clear cell RCC samples analysed and being to discriminate oncocytoma and chromophobe subtypes with Cox regression analysis showing a trend towards better patient outcome. Similar positive prognostic outcomes of EpCAM in RCC were also found by Eichelberg et al.[198] and Spizzo et al[199].

Study of the expression of EpCAM in RCC would therefore clarify the positive prognostic significance and examine how co-expression with CAV1 may further stratify patients into groups with intermediary outcomes.

2.1.6 CD146

CD146 is an 113kDa integral transmembrane glycoprotein and member of the immunoglobulin superfamily (IgSF). Another common alias for CD146 is melanoma cell adhesion molecule (MCAM), a name resulting from its preferential expression in melanoma tissue and absence in healthy surrounding tissue[200]. Interestingly, CD146 expression is present in the endothelia of blood vessels, infiltrating both primary and metastatic melanoma and indicating a possible role for CD146 in supporting both angiogenesis and metastasis of melanomas[201]. These findings have sparked interesting implications of CD146 expression in tumours from the stomach[202], breast[203], prostate[204] and lung[205]. Such experiments found CD146 expression to generally indicate poor prognosis, increased risk of metastasis and association with increased EMT related markers and morphology.

Investigation of CD146 expression in RCC and its relationship to patient outcome is so far very limited, with only one study carried out to date. Feng et al.[206] found

that upregulation of CD146 mRNA in clear cell RCC patients significantly correlated with metastatic disease, with patients displaying high expression of CD146 having a significantly higher probability of disease recurrence. As such this marker merits further study as to its prognostic significance at the protein level.

2.1.7 Vimentin

Vimentin is a type III component of the intermediate filament family of proteins, which together with varying amounts of tubulin and actin microfilaments, contributes to the cytoskeleton[207]. As such, vimentin plays a role in the anchoring, support and positioning of organelles within the cytoplasm[208] and also in cellular mechanical stability[209]. High levels of vimentin expression have been detected in cells of a mesenchymal origin, leading to the widespread use of vimentin as a marker for EMT, a key feature in the metastatic progression of tumours[210].

Analysis of vimentin expression in various tumours is correlated with features of poor disease outcome. Vimentin overexpression in prostate cancer identifies poorly differentiated tumours and correlates with tumour metastases to bone[211], [212]. In gastric cancer vimentin expression is linked to advanced disease stage, lymph node metastasis, lymphatic invasion and serving as a negative characteristic for patient prognosis[213]. Similar increases in vimentin expression is associated with lymph node metastasis found in oesophageal squamous cell carcinoma[214]. Expression of vimentin in breast cancers has been extensively documented [215] and implicated as crucial to EMT[216]. Vimentin expression in clinical breast cancer tissue is reported to have a strong correlation with a subset of oestrogen receptor low ductal carcinomas of high grade[217] with potential prognostic use in an ER-independent manner.

In RCC, the absence of vimentin expression in the chromophobe and oncocytoma histological types has been observed as useful in delineating these tumour types

from other more aggressive subtypes[218]–[221]. Vimentin-positive tumours were found to be associated with unfavourable prognosis and positively correlate with tumour grade and stage. However, in RCC vimentin may not act as an independent prognostic indicator[222]. Similarly vimentin does associate with patients at a greater risk of metastasis[223], and cannot independently identify poor disease outcome[224]. As such exploration is warranted on how the combination of vimentin/CAV1 may impact upon prognostication and metastatic progression.

2.1.8 MCT4

Monocarboxylate transporter 4 (MCT4) is a member of the proton-linked family of plasma membrane transporters capable of carrying monocarboxylates such as pyruvate and lactate[225]. MCT4 is strongly expressed in tissues with a tendency for increased glycolytic activity such as skeletal muscle white fibres, astrocytes, leucocytes and chondrocytes[226]–[229]. The efflux of lactate is suggested to be important in the maintenance of pH and progression through cellular respiratory metabolism, in tissues more reliant on glycolysis. It has long been understood that tumours exhibit a fundamental switch in glucose metabolism from the oxidative breakdown of pyruvate to non-oxidative glycolysis[230]. As such the MCT family is an attractive target for new therapeutic agents and for prognostication markers. Indeed, knockdown of MCTs in glioblastoma cells with either siRNA or the small molecule inhibitor α -cyano-4-hydroxy-cinnamate (CHC) has been shown to disrupt the migration, proliferation and survival of these cells[231], [232]. Moreover, a phase I clinical trial targeting MCT1 with AZD3965 is underway in diffuse large B cell lymphoma, prostate and gastric cancer patients [233].

Upregulation of MCT4 in relation to disease outcome has been investigated in several malignancies. MCT4 expression in cervical carcinoma is significantly associated with progression to an invasive disease phenotype[234]. Similarly, MCT4

expression in prostate cancer appears to increase with disease course and correlate with indicators of poor prognosis[235].

Genome-wide RNA interference analysis of RCC samples found MCT4 to be upregulated in eight RCC cell lines and was the seventh most overexpressed marker, the downregulation of which caused cell cycle arrest and apoptosis[236]. Epigenetic studies into the regulation of MCT4 expression in clinical RCC samples found increased methylation of CpG sites to be associated with prolonged survival[237]. A more recent study has focussed on further understanding the prognostic role of MCT4 in combination with family member MCT1 and the chaperone molecule CD147, all of which were linked to poor progression free survival. The study also found only MCT1 and CD147 to correlate with the poor prognostic factors of high grade and tumour necrosis. Moreover, MCT1 was seen to act alone as a prognostic indicator of poor disease outcome but not MCT4[238]. However, another study has demonstrated expression of MCT4 and methylation of the MCT4 gene to be a more informative marker of poor disease outcome than CD147[239]. As such, we have sought to further clarify the role of MCT4 in the prognosis of RCC and, when taking into account the ability of CAV1 to support glycolysis[240], [241], investigate whether markers of elevated metabolic activity, MCT4/CAV1 combination, can identify patients at greater risk of disease recurrence.

2.1.9 Cavin-1 (PTRF)

Until recently, CAV1 was thought to be the major structural component required for the formation and maintenance of caveolae[242]. Recently, this paradigm has been shifted with the discovery of an additional family of proteins named cavins. Knockdown of Cavin-1 expression in cells with abundant caveolae resulted in reduction in the number of caveolae formed and delocalisation of CAV1 into the plasma membrane, where it is internalised and degraded via the lysosome[243]. It appears that the major role for Cavin-1 in the formation of caveolae takes place in

the final steps, with Cavin-1/CAV1 interactions only taking place in the nascent caveolae but not in other sites in the cell where CAV1 is found such as the Golgi apparatus[244].

Such findings, especially the Cavin-1/CAV1 interaction, have led to studies into of the role of cavins in the pathology and progression of cancer. This relationship may further aid in the understanding of CAV1 regulation. For example, expression analysis of Cavin-1 and 2 in breast cancer cells found them to be generally downregulated through promoter methylation and proposed this as a possible reason for the loss of CAV1's downstream tumour suppressing functionality by loss of functional caveolae[245]. In the PC3 prostate cancer cell line, which highly expresses CAV1 but not Cavin-1, overexpression of Cavin-1 led to a reduction in migration of cells by reduced production of MMP9[246]. Analysis of the expression of Cavin-1 in pancreatic cancer has helped to explain the fluctuating patterns of oncogenic CAV1 expression in the disease, by stabilisation and prevention of lysosomal degradation, with the combination of both markers associated with an improved disease outcome[144].

To date, no studies have been conducted examining the expression of Cavin-1 in RCC, therefore we sought here to understand the prognostic implications of Cavin-1 expression in RCC and whether the combination with CAV1 is capable of providing a powerful marker combination in identifying patients at high risk of metastatic disease and relapse.

2.1.10 Aims

This chapter aims to understand the prognostic capability of the aforementioned stemness related markers using immunohistochemical analysis and subsequent statistical analysis of 174 RCC patient cohort. This analysis was carried out for each

of the markers alone and in combination with CAV1 to identify patients at higher risk of disease recurrence.

2.2 Materials and Methods

2.2.1 Patient cohort and RCC tissue microarrays

The patient cohort consisted of 174 RCC tumour cores taken from either radical nephrectomy or biopsy samples. The cohort consisted of 119 male patients and 55 females, the median age was 64 with an age range of 34 to 86 years old, and contained 144 clear cell, 23 papillary, 5 chromophobe and 2 collecting duct carcinomas. Ethical approval for this clinical study was obtained from the Research Ethics Committee for Wales, reference number 11/MRE09/3 Complete histopathological assessment was performed by pathologist Dr. David Griffiths who also extracted information regarding sex, date of birth, date of surgery, date of which first metastasis or recurrent disease was observed and date and cause of death from patient notes. Samples were gathered from two different hospitals: University Hospital Wales (cores split among two slides termed UHW 1 and 2) and the Royal Glamorgan Hospital (RGH).

Construction of tissue microarrays (TMAs) were performed by technical staff in the histopathology department of the University Hospital Wales and performed as follows: single 0.6mm diameter cores were punched from viable tumour tissue near the periphery of formalin fixed renal tumours; as controls normal renal parenchyma and liver were then embedded into predetermined array positions on a recipient paraffin block. This array block was then cut into 4µm thick sections and mounted into adhesive glass slides (Superforst Plus™) (Figure 2.1).

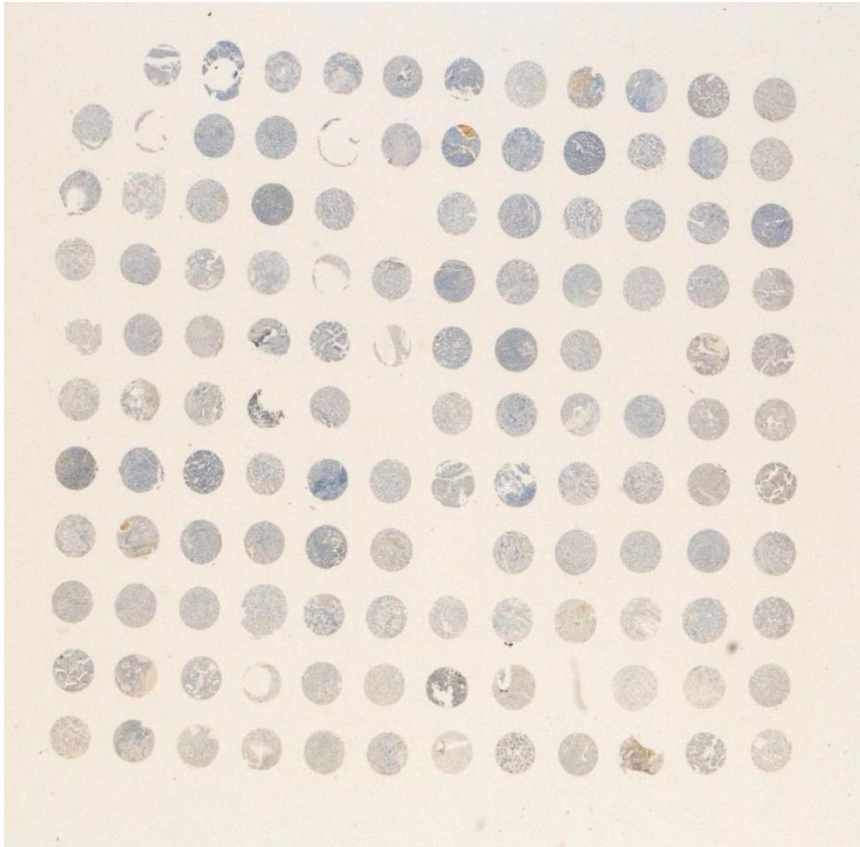


Figure 2.1: Example of a wide field image of full TMA section stained with isotypic rabbit serum.

2.2.2 Immunohistochemistry of tissue microarrays and scoring

Tissue microarray slides were first deparaffinised by submersion in two changes of 100% xylene (Fisher Scientific) for three minutes each. Slides were then gradually rehydrated by use of an ethanol gradient starting with incubation in a 1:1 solution of 100% ethanol and xylene, then two changes of 100% ethanol (Reagent grade obtained from Fisher Scientific), one change of 95% ethanol, one change of 70% ethanol, one change of 50% ethanol and finally 100% water (each incubation lasting three minutes). Following rehydration endogenous peroxidase activity was quenched by incubation in 3% hydrogen peroxide (Fisher Scientific) v/v with 100% methanol for 15 minutes and washed for another 5 minutes in running water. Antigen retrieval was carried out by boiling TMA slides in 10mM sodium citrate buffered to pH 6 after 20 minutes of incubation slides were allowed to gradually cool

using running water. Slides were washed once in 1x Optimax™ washing buffer (Biogenix) and then allowed to equilibrate for 15 minutes. Serum (isotype) control (Figure 2.1), primary and secondary antibodies were all diluted in Optimax™ buffer containing 0.6% bovine serum albumin (BSA) with concentrations for each antibody found in (Table 2.3). In addition to slides probed with primary antibody, each experiment also contained an isotypic control containing either rabbit or mouse serum (Dako), diluted to the concentration of the highest respective antibody used in that experiment as well as an omission control containing only 0.6% BSA in optimax solution. Following equilibration, slides were incubated with either primary antibody solutions, isotypic or omission control for 15 hours at 4°C in a humidified chamber. After incubation, excess antibody or control solution was aspirated and slides washed for 1 minute in 4 changes of Optimax™ wash buffer. Slides were then incubated with a 1:100 solution of horseradish peroxidase conjugated (HRP) anti-rabbit IgG (Dako) for 1 hour at room temperature. Slides were then washed for 1 minute in 4 changes of Optimax™ wash buffer. Immunoreactive staining was then carried out by submerging slides in a 5mg/mL solution of diaminobenzidine dihydrochloride (DAB) (Fisher Scientific) with 500µL of hydrogen peroxide for 10 minutes. Slides were then counter stained with the nuclear counterstain haematoxylin and washed with running water. Slides were then mounted by first dehydration by going through the ethanol gradient in reverse, followed by two changes of xylene and finally a coverslip was applied with a coating of DPX mounting medium and allowed to set for 24 hours.

To ensure immunohistochemical staining at an intensity that would be specific, with low background, but still provide sufficient signal so that staining intensities of cores could be distinguished, TMAs were first stained with each antibody in a dilution range to determine the optimal dilution for staining (Table 2.3). In order to further verify the specificity of a given antibody, it is possible to assay the antibody for its

ability to identify its target protein by western blot; such information is provided in some form by the manufacturer of the antibody. However, while this method does show that the antibody does bind to the target it was raised against, it does not demonstrate the ability to do so against either the fully folded protein or in whole protein expressed in tissue sections[247]. Additionally, it is entirely possible that an antibody that performs well in western blot validation assays may perform poorly in tissue sections. This is due to the fixation step required for processing of tissue sections, which may possibly distort the epitope that the antibody recognises[248]. To help prove the specificity of an antibody in the tissue of study some investigators provide absorption controls. This control involves the incubation of the antibody with either the peptide or whole protein the antibody was raised against. This complex is then added to TMA sections in the primary antibody incubation step of the staining procedure, this should ablate the presence of tissue staining patterns. Unfortunately, this control suffers from the same issues as providing a western blot as a positive control, in that it only demonstrates that the antibody is specific for the target it has been raised against[249]. As such, the gold standard for controlling/validating antibody specificity in immunohistochemical studies is the demonstration of positive or negative staining in a tissue or sub-type of cells where expression of the target in question has already been assessed[247], this was the approach adopted in these studies. Such controls gain further validity when they are demonstrated internally, either present in normal tissue or in normal tissue structures in tumour samples. Further to this antibody selection and verification of specific antibody staining was aided by the use of the Human Protein Atlas[250], a tissue based map of the human proteasome.

Table 2.3 Antibodies used in the immunohistochemical staining of RCC TMAs. All antibodies used for these markers were of rabbit origin and of isotype IgG. The CD44 antibody selected targeted the standard form of CD44.

| Marker | Company | Dilution Range | Working Dilution | Clonality | Product Code |
|----------|-----------------------------|----------------|------------------|------------|--------------|
| Cav-1 | Cell Signalling | 1:20-1:100 | 1:20 | Polyclonal | 3238 |
| CD44 | Abcam | 1:90-1:250 | 1:90 | Monoclonal | Ab51037 |
| CD105 | Abcam | 1:40-1:500 | 1:40 | Polyclonal | Ab107595 |
| EpCAM | Novus | 1:50-1:100 | 1:100 | Monoclonal | NB110-56958 |
| CD146 | Sigma | 1:200-1:500 | 1:200 | Polyclonal | HPA008848 |
| Vimentin | Cell Signalling | 1:35-1:100 | 1:35 | Monoclonal | 5741 |
| MCT4 | Santa Cruz Biotechnology | 1:50-1:200 | 1:100 | Polyclonal | Sc-50329 |
| Cavin | Proteintech | 1:20-1:200 | 1:200 | Polyclonal | 18892-1-AP |

Semi-quantitative scoring of stained TMAs was carried out by pathologist David F. Griffiths with the assistance of Robert Gutteridge and Dr. Mark Gumbleton using a multiheaded microscope without knowledge of either clinical outcome or histopathological parameters. Scoring criteria was determined in a customised manner for each of the markers used in this study. Each criterion is described in the respective results section for each marker within the results section.

2.2.3 Statistical analysis

Disease free survival (DFS) of patients dependant on scoring of selected CSC related markers was calculated by Kaplan-Meier survival analysis with the log-rank test. Using this method, time to event was considered first appearance of metastasis with data censored when the patient was last seen alive without metastasis or had died due to other causes. Original data were converted to a binary simple covariate dependant according to the most informative grouping after disease free survival, survival plots and the log-rank test were examined. To investigate synergy between CAV1 and CSC biomarker expression, composite covariates of the scoring were achieved by combining the two variables and reclassifying as appropriate.

Crosstabulation analysis was carried out in order to understand the association of each CSC marker with CAV1 and each CSC marker with histopathological characteristics of RCC, which was then repeated for the CSC marker/CAV1 composite covariate. In all cases of statistical analysis grade was pooled at grades 1 and 2 and grades 3 and 4. Significance of crosstabulation correlations was performed using either a chi-squared test or Fisher's exact test as relevant (groups containing less than five events were assessed by fisher's exact).

Multivariate Cox regression analysis was used to assess the prognostic value of each marker alone and in combination with CAV1 using both the enter and forward stepwise (likelihood ratio) functions with all covariates considered categorical. Time to event was defined as first appearance of metastasis. Compound covariates of CSC markers/CAV1 were regrouped to give the simple covariate CSC marker positive/CAV1 positive. Covariates of CSC marker and CSC marker/CAV1, grade, size, vascular invasion, capsular invasion and micronecrosis were all entered into the model. The forward stepwise function hazard ratios are provided at first step and entry into the analysis was set at a probability of 0.10 and rejected at 0.15. An independent multivariate analysis was carried out by Dr. Robert Hill to determine which of all the single marker, composite marker/CAV1 and histopathological covariate was the most influential contributor to disease outcome. This analysis was conducted using a Cox proportional hazards model with forward selection with calculation of a partial Wilk's statistic which reflects the each variables contribution to the model and determines entry into the model.

A *P* value of <0.050 was considered significant in all cases of statistical analysis. All data were analysed using the statistical package SPSS statistics 20 (IBM) multivariate analysis of all covariates was carried out using the statistical package SAS.

2.3 Results

2.3.1 CAV1 expression in RCC tumour samples predicts poor disease free survival which increases with increased CAV1 expression

To verify the specificity of the CAV1 antibody used, immune-staining localised to the endothelial structures was considered a positive control in both tumour and normal kidney[74]. Expression of CAV1 was found in the endothelia of both tumour (Figure 2.3 A) and normal kidney samples (Figure 2.3). Positive staining for a tumour core was defined as cell membrane associated staining of any visible tumour cells (Figure 2.3 B-D). Under this scoring criterion CAV1 was detectable in 109 of 174 tumour cores with the remaining 65 being CAV1 negative. Analysis of CAV1 scoring by Kaplan-Meier survival curves showed that CAV1 positivity resulted in a decrease in mean disease free survival (DFS) to 8.2 years from the overall survival time of 11, whereas CAV1 negative tumours were associated with a mean DFS of 15.5 years ($P < 0.001$) (Figure 2.4 A). Among CAV1 positive tumours it was clear that scoring of CAV1 positivity could be stratified into three different distinct scoring criteria: weak membrane staining (CAV1 score 1) (Figure 2.3 B), medium membrane staining (CAV1 score 2) (Figure 2.3 C) and strong membrane staining (CAV1 score 3) (Figure 2.3 D). Kaplan-Meier analysis of scoring stratified this way showed a decrease in mean DFS as CAV1 staining intensity increased resulting in a mean disease free survival for CAV1 score 1 of 8.7, CAV1 score 2 of 6.3 and CAV1 score 3 of 5.2 years, respectively (Figure 2.4 B).

Crosstabulation of CAV1 scoring (scoring criteria of Figure 2.4 A is used) with histopathological characteristics of RCC found statistically significant correlation of CAV1 expression with presence of vascular invasion ($P < 0.001$), microcapsular invasion ($P = 0.007$) and micronecrosis ($P = 0.016$). Correlations were also found between CAV1 and tumour grade ($P = 0.028$). CAV1 expression also correlated with clear cell histotype ($P = 0.001$) and with non-papillary carcinomas ($P = 0.003$) but not

with the papillary histotype (Table 2.4). No correlation was found between increased tumour size and CAV1 expression ($P=0.175$) (Table 2.4).

The multivariate Cox regression model (using the enter function), containing the histopathological variables together with variable of CAV1 expression, found a hazard ratio for CAV1 positive expression of 2.2 ($P=0.054$) (Table 2.5 A). When using forward step-wise (likelihood ratio function), with vascular invasion being rejected by the model as not influential in the analysis the hazard ratio of CAV1 positive tumours was reported as 2.3 and proved to be statistically significant ($P=0.036$) (Table 2.5 B).

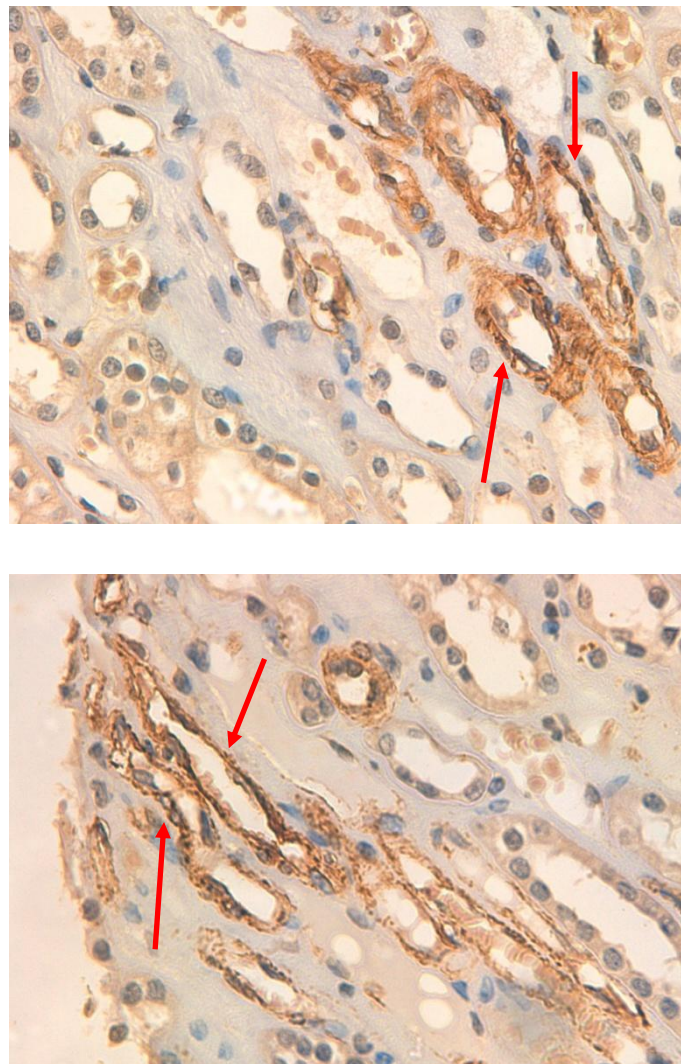


Figure 2.2 Positive staining of endothelial structures in normal kidney serves as a positive control for specificity of the CAV1 antibody used. Red arrows indicate areas where endothelial staining is observed images captured at x25 magnification.

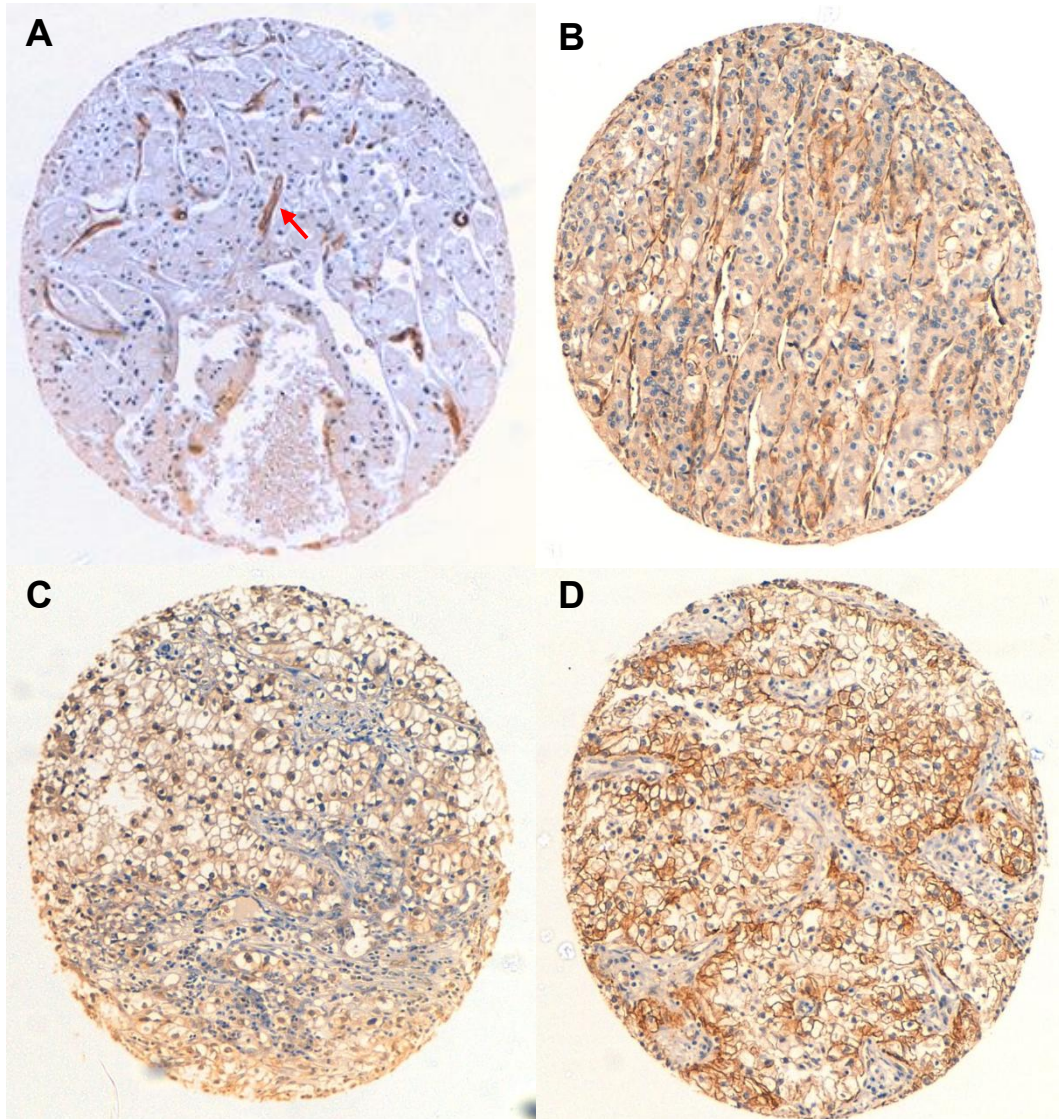


Figure 2.3 Immunohistochemical staining of RCC TMAs for CAV1 expression. Tumour cores shown are examples of each score shown at x10 magnification. The red arrow (A) indicating the presence of endothelial staining in a tumour sample considered CAV1 negative. Representative tumours of CAV1 scoring criteria (A) CAV1 score 0, (B) CAV1 score 1, (C) CAV1 score 2 and (D) CAV1 score 3.

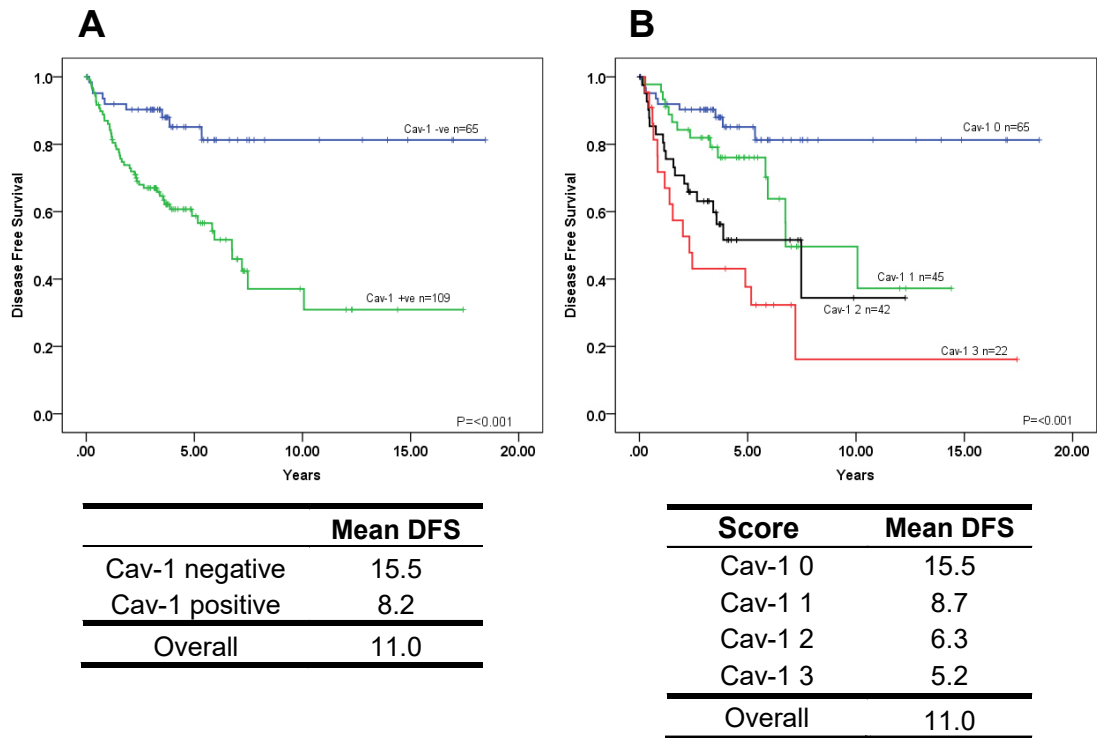


Figure 2.4 Kaplan-Meier survival curves for CAV1 expression. (A) Kaplan-Meier DFS survival curves for CAV1 negative tumours (tumours scored as 0 n=65) and CAV1 positive tumours (tumours scored between 1 to 3 n=109) P=<0.001 as determined by Log-rank comparison. (B) Kaplan-Meier DFS curves showing how increased intensity of CAV1 staining can indicate patients are high risk of disease relapse (CAV1 score 0 n=65, CAV1 score 1 n=45, CAV1 score 2 n=42 and CAV1 score 3 n=22) P=<0.001.

Table 2.4 Crosstabulation of CAV1 with histopathological characteristics of RCC. Significance calculated by Chi-squared or Fisher's exact test as relevant

| | Cav-1 negative | Cav-1 positive |
|-----------------------------------|-----------------------|-----------------------|
| Grade 1 and 2 | 52 | 70 |
| Grade 3 and 4 | 13 | 39 |
| | | P=0.028 |
| Tumour size <7cm | 42 | 59 |
| Tumour size >7cm | 23 | 50 |
| | | P=0.175 |
| Vascular invasion -ve | 51 | 55 |
| Vascular invasion +ve | 14 | 54 |
| | | P=<0.001 |
| Microcapsular invasion -ve | 60 | 83 |
| Microcapsular invasion +ve | 5 | 26 |
| | | P=0.007 |
| Micronecrosis -ve | 40 | 47 |
| Micronecrosis +ve | 24 | 61 |
| | | P=0.016 |
| Non-clear cell carcinoma | 19 | 11 |
| Clear cell carcinoma | 46 | 98 |
| | | P=0.001 |
| Non-Papillary | 50 | 101 |
| Papillary | 15 | 8 |
| | | P=0.003 |

Table 2.5 Cox regression analysis of CAV1 with histopathological characteristics of RCC. (A) Analysis performed using the 'Enter' function. (B) Analysis performed using the 'Forward Stepwise' (Likelihood ratio) function. Vascular invasion rejected by the model as not influential. 95% CI=95% Confidence interval

A

| Prognostic indicator | Hazard ratios | 95% CI | P value |
|-----------------------------|----------------------|---------------|----------------|
| Cav-1 negative | 1 | | |
| Cav-1 positive | 2.2 | 0.986-4.772 | 0.054 |
| Grade 1 and 2 | 1 | | |
| Grade 3 and 4 | 2.1 | 1.167-3.690 | 0.013 |
| Size <7cm | 1 | | |
| Size >7cm | 2.3 | 1.287-4.025 | 0.005 |
| Vascular invasion -ve | 1 | | |
| Vascular invasion +ve | 1.6 | 0.874-2.978 | 0.127 |
| Capsular invasion -ve | 1 | | |
| Capsular invasion +ve | 1.7 | 0.953-3.177 | 0.071 |
| Micronecrosis -ve | 1 | | |
| Micronecrosis +ve | 2.8 | 1.464-5.430 | 0.002 |

B

| Prognostic indicator | Hazard ratios | 95% CI | P value |
|-----------------------------|----------------------|---------------|----------------|
| Cav-1 negative | 1 | | |
| Cav-1 positive | 2.3 | 1.054-5.085 | 0.036 |
| Grade 1 and 2 | 1 | | |
| Grade 3 and 4 | 2.3 | 1.330-4.104 | 0.003 |
| Size <7cm | 1 | | |
| Size >7cm | 2.5 | 1.425-4.374 | 0.001 |
| Capsular invasion -ve | 1 | | |
| Capsular invasion +ve | 1.9 | 1.031-3.396 | 0.039 |
| Micronecrosis -ve | 1 | | |
| Micronecrosis +ve | 2.8 | 1.455-5.426 | 0.002 |

2.3.2 CD44 expression in RCC tumours indicates poor disease free survival and identifies high risk patient groups, which is more pronounced in combination with CAV1

The antibody selected for CD44 immunohistochemical analysis was raised against an immunogen present in all CD44 isoforms excluding isoform 2 and 19. Specific staining for CD44 was controlled by negative staining in normal kidney tissue as previously reported[251] and positive staining in the infiltrating lymphocytes of RCC tumour cores[252]–[254] (Figure 2.5).

CD44 positivity was defined as any detectible staining in the cell membrane of tumour cells. The scoring of CD44 expression was as follows: negative CD44 staining CD44 score 0 (Figure 2.6 A), weak positive membrane staining CD44 score 1 (Figure 2.6 B), medium positive membrane staining CD44 score 2 (Figure 2.6 C) and strong membrane staining CD44 score 3 (Figure 2.6 D). With the use of this scoring criteria, 13 tumours were scored CD44 score 1, 24 were scored CD44 score 2 and 25 were scored CD44 score 3. The remaining 112 showed no presence of CD44 associated staining. Kaplan-Meier DFS analysis of CD44 scoring revealed a mean DFS of 3.1 years in the most strongly expressing CD44 score 3 group ($P < 0.001$) (Figure 2.7 A). Tumours that were CD44 0, CD44 1, or CD44 2 showed very little distinction in terms of mean disease free survival with means of 11.8, 9.8 and 8.7 respectively with nearly complete overlap in DFS survival plots (Figure 2.7 A). As such, in subsequent analyses, CD44 expression was converted into the simple binary covariate, the groups CD44 score 0, CD44 score 1 and CD44 score 2 reclassified as CD44 negative and CD44 score 3 reclassified as CD44 positive (Figure 2.7 B).

Crosstabulation of CD44 with histopathological features of RCC correlated CD44 expression with grade ($P = 0.002$), vascular invasion ($P = 0.021$) and micronecrosis ($P = 0.015$) but not microcapsular invasion ($P = 0.555$). CD44 expression did not

appear to correlate strongly with either a clear cell ($P=0.334$) or papillary subtype ($P=0.279$) (Table 2.6).

Multivariate Cox regression analysis of CD44 expression using the enter function found CD44 positive tumours to have an associated hazard ratio of 2.8 ($P=0.001$) (Table 2.7 A). Using the forward stepwise (likelihood ratio) function vascular invasion was rejected as not influential in the analysis and resulted in a hazard ratio for CD44 positivity of 2.9 ($P=0.001$) (Table 2.7 B). Indicating CD44 to be a powerful independent variable of disease recurrence.

To understand if CAV1 and CD44 are simultaneously expressed in RCCs, and could thereby be used as a reliable covariate for further analysis, scoring data of CD44 and CAV1 were crosstabulated. Cross tabulation showed a significant correlation between CAV1 positivity and CD44 positivity ($P<0.001$ by Fisher's exact test), identifying 20 tumours co-expressing CAV1 and CD44, whereas and only five CD44 positive tumours were not expressing CAV1 (Figure 2.8 A). Kaplan-Meier DFS analysis of this covariate found that tumours both CD44 positive and CAV1 positive demonstrated significantly diminished mean disease free survival of 2.5 years compared to patients with tumours only positive for CAV1 expression with a mean disease free survival of 9.2 years ($P<0.001$) (Figure 2.8 B).

In order to perform subsequent crosstabulation and cox regression analysis, the CD44/CAV1 covariate was reduced to a binary form with CD44-ve/CAV1-ve, CD44+ve/CAV1-ve and CD44-ve/CAV1+ve pooled and reclassified "as all other tumours" and CD44+ve/CAV1+ve remaining the same. Crosstabulation of this covariate with histopathological characteristics of RCC found a significant correlation with high grade ($P<0.001$), vascular invasion ($P<0.001$) and micronecrosis ($P<0.001$) but not microcapsular invasion ($P=0.269$) or size ($P=0.769$). In histological subtypes, 55% of CD44+ve/CAV1+ve tumours were of

non-clear cell origin but no correlation was apparent in the papillary subtype with 85% non-papillary ($P=0.803$) (Table 2.8).

In the Cox regression, multivariate analysis of the CD44/CAV1 covariate (when using the enter method), CD44+ve/CAV1+ve carried an associated hazard ratio of 3.0 ($P<0.001$), (Table 2.9 A). When using the forward stepwise (likelihood ratio) function, CD44/CAV1 positivity resulted in a hazard ratio of 3.3 ($P=0.013$), higher than all other variables, though not distinguishable as greater due to the overlapping of confidence intervals (Table 2.9 B).

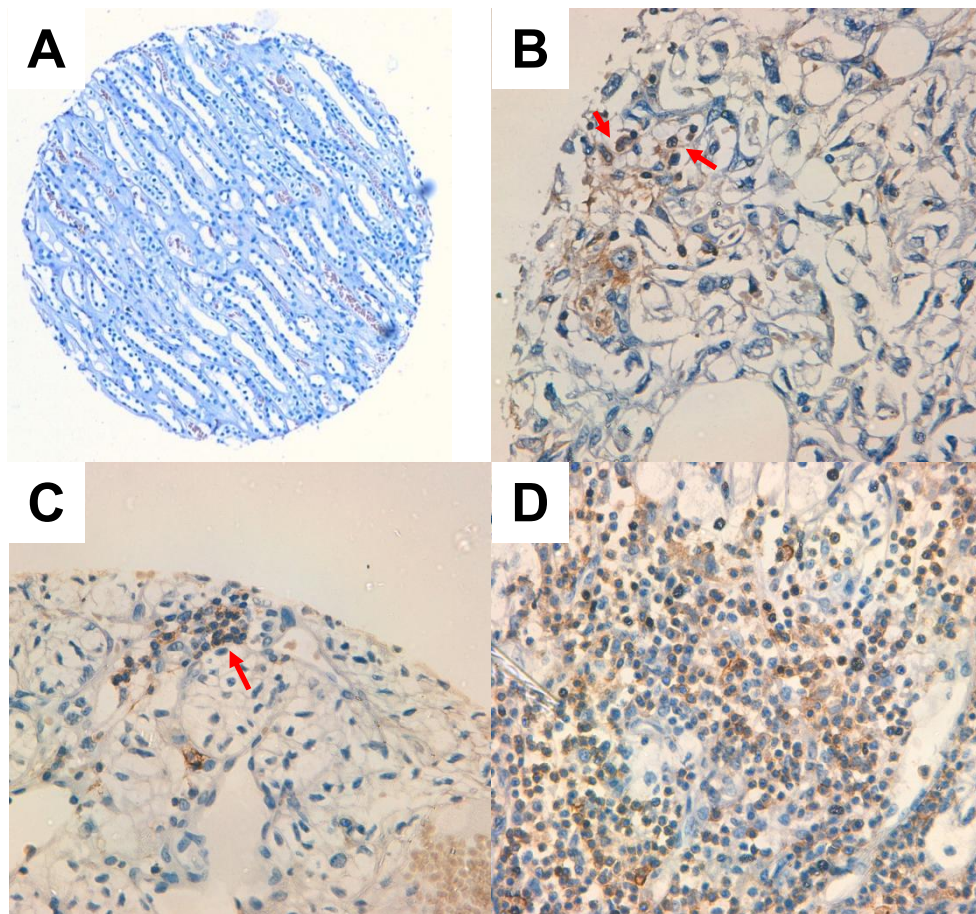


Figure 2.5 Negative staining in normal kidney tubules (**A**) and positive staining of infiltrating lymphocytes in RCC tumour samples (**B-D**) serve as specificity controls for the CD44 antibody used. (**A**) Normal kidney samples were negative for CD44 staining as previously demonstrated. In (**B**) and (**C**) red arrows indicate presence of infiltrating lymphocytes positive for CD44 staining. (**D**) Shows large scale infiltration of CD44 positive lymphocytes into RCC tumour tissue. (**A**) Image taken at x10 magnification. (**B-D**) Images taken at x25 magnification.

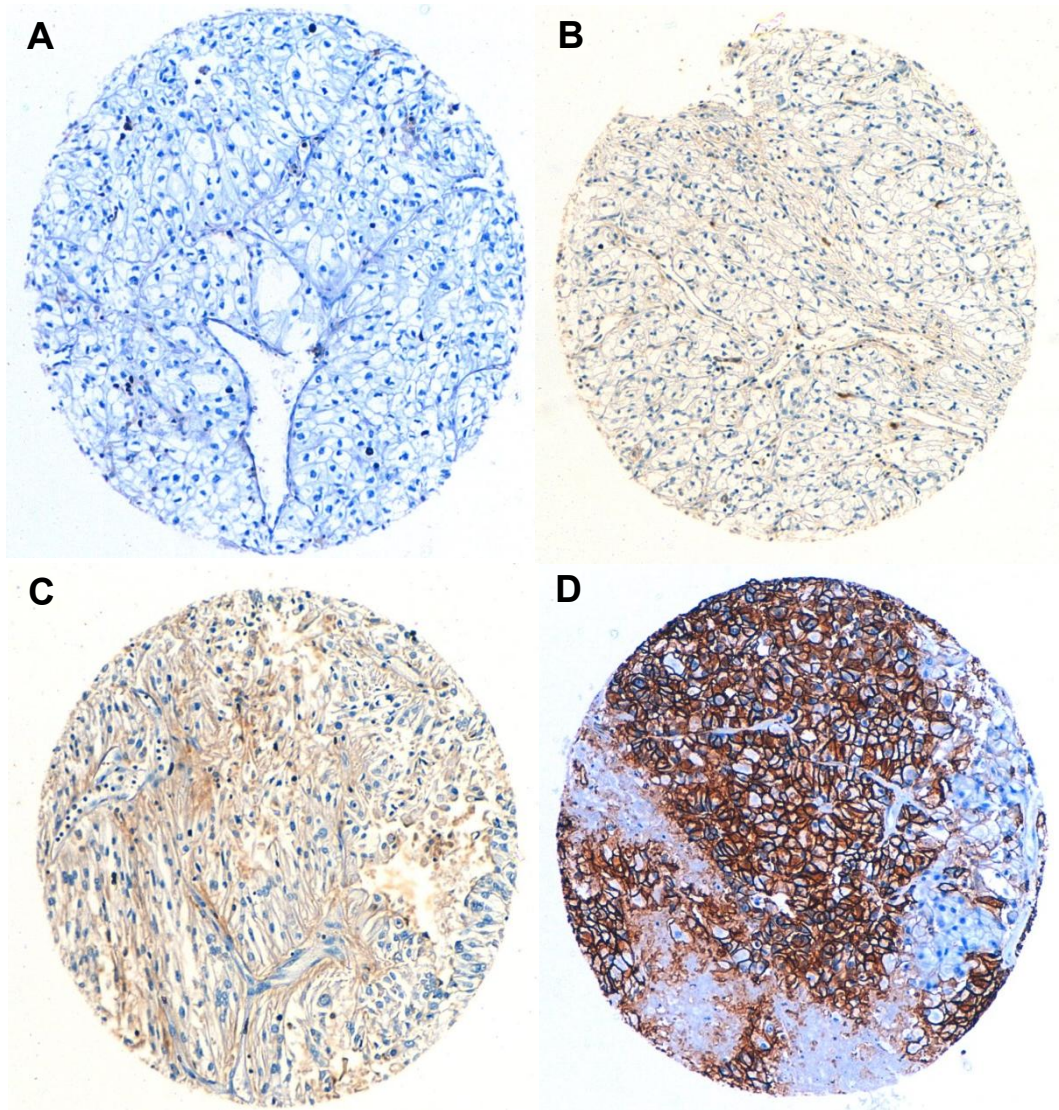


Figure 2.6 Immunohistochemical staining of RCC TMAs for CD44 expression captured at x10 magnification. Representative tumours of CD44 scoring criteria (A) CD44 score 0, (B) CD44 score 1, (C) CD44 score 2 and (D) CD44 score 3.

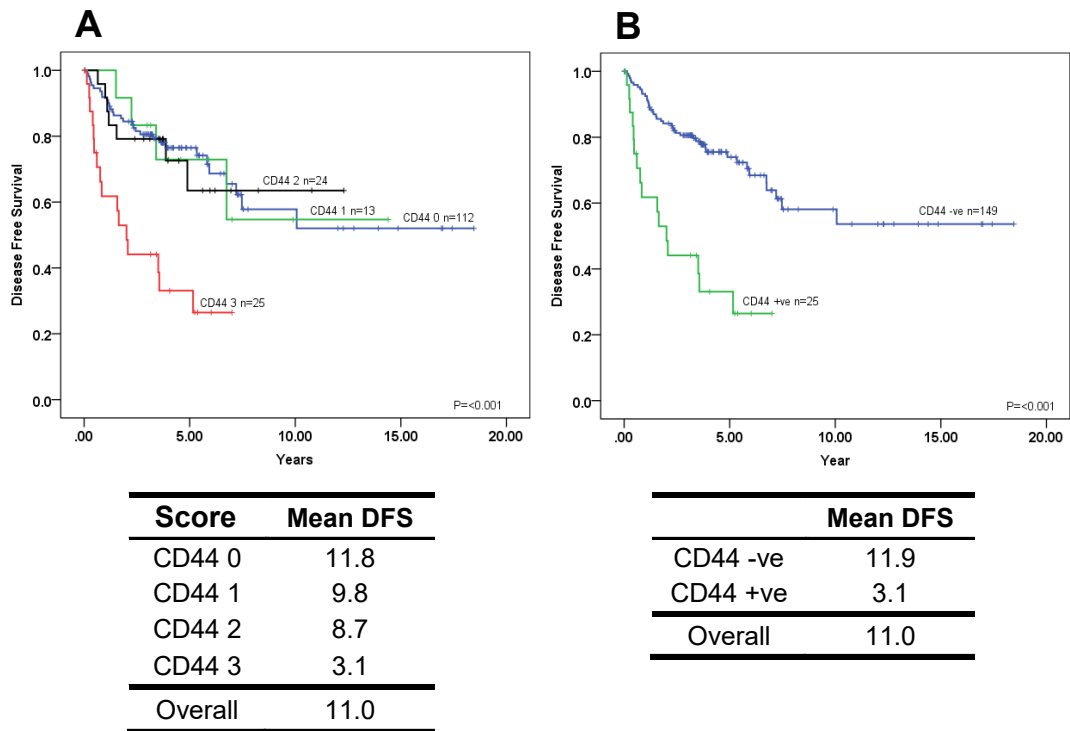


Figure 2.7 Kaplan-Meier survival curves for CD44 expression. (A) Kaplan-Meier DFS survival curves for scoring criteria of CD44 staining without recoding (CD44 score 0=112, CD44 score 1=13, CD44 score 2=24, CD44 score 3=25) with corresponding mean disease free survival shown below. P=<0.001 as determined by Log-rank comparison. (B) Kaplan-Meier DFS survival curves for CD44 staining re-plotted with scores from 0 to 2 pooled and recoded as CD44 negative (n=149) and scores of 3 recoded as CD44 positive (n=25). P=<0.001 as determined by Log-rank comparison.

Table 2.6 Crosstabulation of CD44 with histopathological characteristics of RCC. Significance calculated by Chi-squared or Fisher's exact test as relevant

| | CD44 negative | CD44 positive |
|-----------------------------------|----------------------|----------------------|
| Grade 1 and 2 | 111 | 11 |
| Grade 3 and 4 | 38 | 14 |
| | | P=0.002 |
| Tumour size <7cm | 88 | 13 |
| Tumour size >7cm | 61 | 12 |
| | | P=0.508 |
| Vascular invasion -ve | 96 | 10 |
| Vascular invasion +ve | 53 | 15 |
| | | P=0.021 |
| Microcapsular invasion -ve | 68 | 13 |
| Microcapsular invasion +ve | 81 | 12 |
| | | P=0.555 |
| Micronecrosis -ve | 80 | 7 |
| Micronecrosis +ve | 67 | 18 |
| | | P=0.015 |
| Non-clear cell carcinoma | 24 | 6 |
| Clear cell carcinoma | 125 | 19 |
| | | P=0.334 |
| Non-Papillary | 131 | 20 |
| Papillary | 18 | 5 |
| | | P=0.279 |

Table 2.7 Cox regression analysis of CD44 with histopathological characteristics of RCC cohort. (A) Analysis performed using the 'Enter' method. (B) Analysis performed using the 'Forward Stepwise' (Likelihood ratio) Vascular invasion rejected by the model as not influential. 95% CI=95% Confidence Interval.

A

| Prognostic indicator | Hazard ratios | 95% CI | P value |
|-----------------------------|----------------------|---------------|----------------|
| CD44 negative | 1 | | |
| CD44 positive | 2.8 | 1.516-5.257 | 0.001 |
| Grade 1 and 2 | 1 | | |
| Grade 3 and 4 | 1.9 | 1.092-3.465 | 0.024 |
| Size <7cm | 1 | | |
| Size >7cm | 2.2 | 1.225-3.798 | 0.008 |
| Vascular invasion -ve | 1 | | |
| Vascular invasion +ve | 1.7 | 0.909-3.067 | 0.098 |
| Capsular invasion -ve | 1 | | |
| Capsular invasion +ve | 2.4 | 1.281-4.416 | 0.006 |
| Micronecrosis -ve | 1 | | |
| Micronecrosis +ve | 2.6 | 1.362-5.136 | 0.004 |

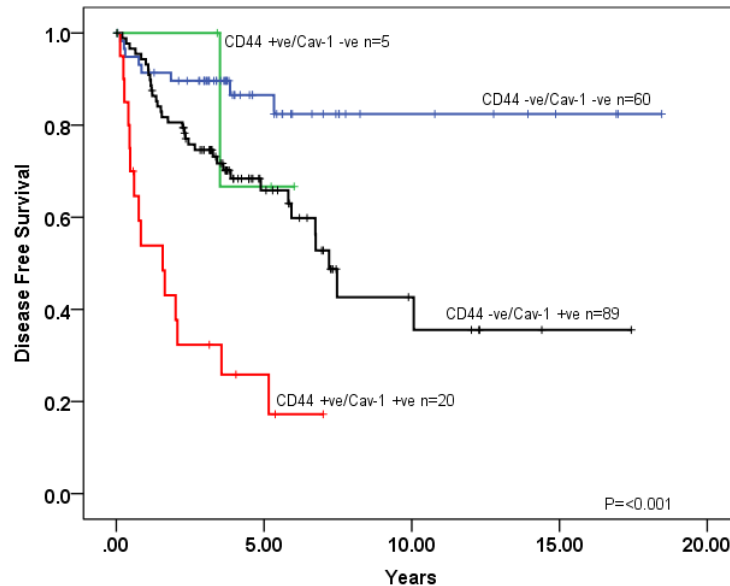
B

| Prognostic indicator | Hazard ratios | 95% CI | P value |
|-----------------------------|----------------------|---------------|----------------|
| CD44 negative | 1 | | |
| CD44 positive | 2.9 | 1.557-5.471 | 0.001 |
| Grade 1 and 2 | 1 | | |
| Grade 3 and 4 | 2.1 | 1.204-3.801 | 0.010 |
| Size <7cm | 1 | | |
| Size >7cm | 2.3 | 1.332-4.100 | 0.003 |
| Capsular invasion -ve | 1 | | |
| Capsular invasion +ve | 2.7 | 1.463-4.914 | 0.001 |
| Micronecrosis -ve | 1 | | |
| Micronecrosis +ve | 2.7 | 1.402-5.272 | 0.003 |

A

| | Cav-1 negative | Cav-1 positive |
|---------------|----------------|----------------|
| CD44 negative | 60 | 89 |
| CD44 positive | 5 | 20 |

P=0.040

B

| Score | Mean DFS |
|--------------------|----------|
| CD44 -ve/Cav-1 -ve | 15.7 |
| CD44 +ve/Cav-1 -ve | 5.2 |
| CD44 -ve/Cav-1 +ve | 9.2 |
| CD44 +ve/Cav-1 +ve | 2.5 |
| Overall | 11.0 |

Figure 2.8 Correlation of CD44 with CAV1 expression and impact on disease free survival. (A) Cross tabulation of CD44 and CAV1 expression in RCC tumour cores. Statistically significant correlation $P < 0.001$ as determined by chi-squared. (B) Kaplan-Meier DFS curves plotted for CD44 and CAV1 expressed as a composite variable (CD44-ve/CAV1-ve $n=61$, CD44+ve/CAV1-ve $n=4$, CD44-ve/CAV1+ve $n=89$, CD44+ve/CAV1+ve $n=20$) with corresponding mean disease free survival shown below. $P < 0.001$ as determined by Log-rank comparison.

Table 2.8 Crosstabulation of All other tumours and CD44 +ve/CAV1 +ve with histopathological characteristics of RCC. Significance calculated by Chi-squared or Fisher's exact test as relevant

| | All other tumours | CD44 +ve/Cav-1 +ve |
|-----------------------------------|--------------------------|---------------------------|
| Grade 1 and 2 | 115 | 7 |
| Grade 3 and 4 | 39 | 13 |
| | | P=<0.001 |
| Tumour size <7cm | 90 | 11 |
| Tumour size >7cm | 64 | 9 |
| | | P=0.769 |
| Vascular invasion -ve | 101 | 5 |
| Vascular invasion +ve | 53 | 15 |
| | | P=<0.001 |
| Microcapsular invasion -ve | 128 | 15 |
| Microcapsular invasion +ve | 26 | 5 |
| | | P=0.269 |
| Micronecrosis -ve | 84 | 3 |
| Micronecrosis +ve | 68 | 17 |
| | | P=<0.001 |
| Non-clear cell carcinoma | 26 | 4 |
| Clear cell carcinoma | 128 | 16 |
| | | P=0.728 |
| Non-Papillary | 134 | 17 |
| Papillary | 20 | 3 |
| | | P=0.512 |

Table 2.9 Cox regression analysis of combined CD44 and CAV1 expression with histopathological characteristics of RCC. (A) Analysis performed using the 'Enter' method. (B) Analysis performed using the 'Forward Stepwise' (Likelihood ratio) vascular invasion rejected by the model as not influential. 95% CI=95% Confidence Interval.

A

| Prognostic indicator | Hazard ratios | 95% CI | P value |
|-----------------------------|----------------------|---------------|----------------|
| CD44/Cav-1 negative | 1 | | |
| CD44/Cav-1 positive | 3.0 | 1.590-5.848 | <0.001 |
| Grade 1 and 2 | 1 | | |
| Grade 3 and 4 | 1.9 | 1.086-3.466 | 0.025 |
| Size <7cm | 1 | | |
| Size >7cm | 2.2 | 1.274-3.952 | 0.005 |
| Vascular invasion -ve | 1 | | |
| Vascular invasion +ve | 1.5 | 0.832-2.852 | 0.169 |
| Capsular invasion -ve | 1 | | |
| Capsular invasion +ve | 2.4 | 1.282-4.402 | 0.006 |
| Micronecrosis -ve | 1 | | |
| Micronecrosis +ve | 2.5 | 1.281-4.918 | 0.007 |

B

| Prognostic indicator | Hazard ratios | 95% CI | P value |
|-----------------------------|----------------------|---------------|----------------|
| CD44/Cav-1 negative | 1 | | |
| CD44/Cav-1 positive | 3.3 | 1.720-6.344 | 0.013 |
| Grade 1 and 2 | 1 | | |
| Grade 3 and 4 | 2.1 | 1.164-3.722 | 0.013 |
| Size <7cm | 1 | | |
| Size >7cm | 2.4 | 1.382-4.227 | 0.002 |
| Capsular invasion -ve | 1 | | |
| Capsular invasion +ve | 2.6 | 1.442-4.801 | 0.002 |
| Micronecrosis -ve | 1 | | |
| Micronecrosis +ve | 2.5 | 1.277-4.927 | 0.008 |

2.3.3 CD105 in RCC tumours does not identify high risk patients alone or as a covariate with CAV1

To ensure specificity of the CD105 antibody selected, positive staining in the endothelium of normal kidney control tissue was observed[187] (Figure 2.9). Immunohistochemical staining of RCC tumour cores with anti-CD105 revealed a scorable pattern of membrane staining (Figure 2.10). Tumours were given scores corresponding to the intensity of cell membrane staining of tumour cells with CD105 score 0, indicating no visible membrane staining (Figure 2.10 A), CD105 score 1, indicating light membrane staining (Figure 2.10 B), CD105 score 2, indicating medium membrane staining (Figure 2.10 C) and CD105 score 3, indicating strong membrane staining (Figure 2.10 D). This resulted in: 14 CD105 score 0 tumours, 29 CD105 score 1 tumours, 8 CD105 score 2 tumours and 63 CD105 score 3 tumours (Figure 2.11 A).

Kaplan-Meier DFS analysis of CD105 revealed no significant difference between any of the scoring intensity groups ($P=0.739$) (Figure 2.11 A). Recoding of CD105 score 0 with CD105 score 1 and CD105 score 2 as negative and CD105 score 3 as positive and repeating the Kaplan-Meier analysis provided a similar statistical outcome. Mean disease free survival for CD105 positive tumours was 9.6 years ($P=0.400$) (Figure 2.11 B).

Crosstabulation of CD105 (using the covariate in Figure 2.11 B) found CD105 positivity not to correlate with any of the histopathological characteristics of RCC (Table 2.10). Similarly, CD105 positivity did not prove significant in the multivariate Cox regression analysis (Table 2.11) and indicated a hazard ratio of 1.7 ($P=0.089$) (using the enter function) which lower than that of vascular invasion. Moreover, it was rejected, together with vascular invasion, by the forward stepwise (likelihood ratio) function.

Crosstabulation of CD105 and CAV1 identified substantial concordant expression in these tumours, despite no significant correlation between the two ($P=0.075$) (Table 2.11 A). Kaplan-Meier DFS analysis of the CD105/CAV1 covariate found that CD105+ve/CAV1+ve tumours had a decreased mean DFS of 5.7 years compared to that of only CD105-ve/CAV1+ve tumours, with a mean DFS of 9.7 years ($P<0.001$) (Figure 2.12 B). Both CD105+ve/CAV1-ve and CD105-ve/CAV1-ve tumours displayed a mean DFS of 14.9 and 14.7 years respectively higher than that of the overall average (Figure 2.12B).

Crosstabulation of the CD105/CAV1 covariate with histopathological characteristics of RCC found only a single correlation the presence of micronecrosis ($P=0.047$) (Table 2.12). Multivariate Cox regression analysis (using the enter function) of CD105+ve/CAV1+ve tumours indicated a statistically significant hazard ratio of 2.3 ($P=0.005$) when (Table 2.13 A). Using the forward stepwise function CD105+ve/CAV1 was also capable of entering generating a hazard ratio similar to that of size, vascular invasion and microcapsular invasion ($P=0.005$) (Table 2.13 B).

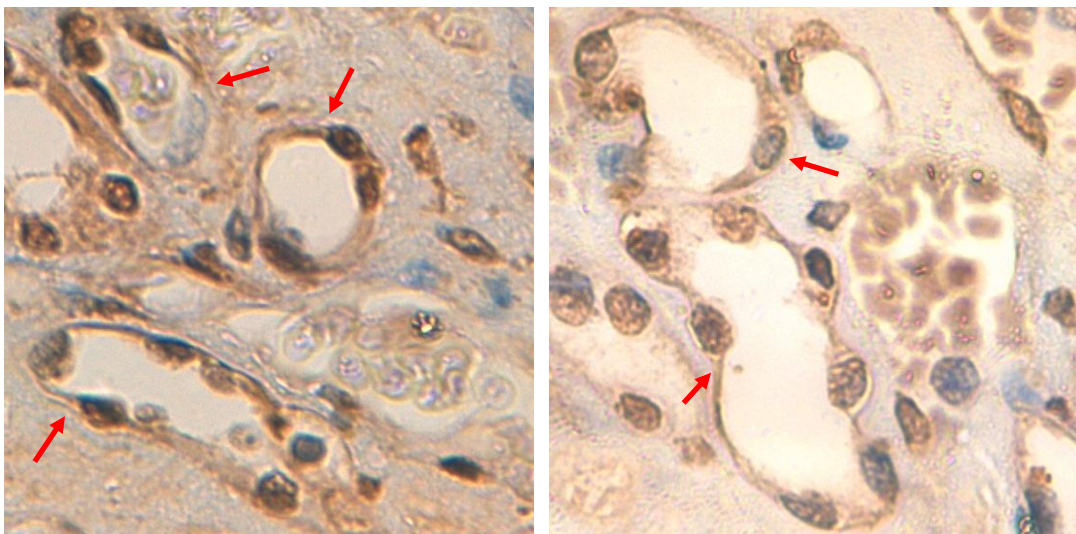


Figure 2.9 Immunohistochemical staining of CD105 in endothelial structures of normal kidney tissue serves as a positive control for the CD105 antibody. The red arrows indicate presence of endothelial CD105 staining.

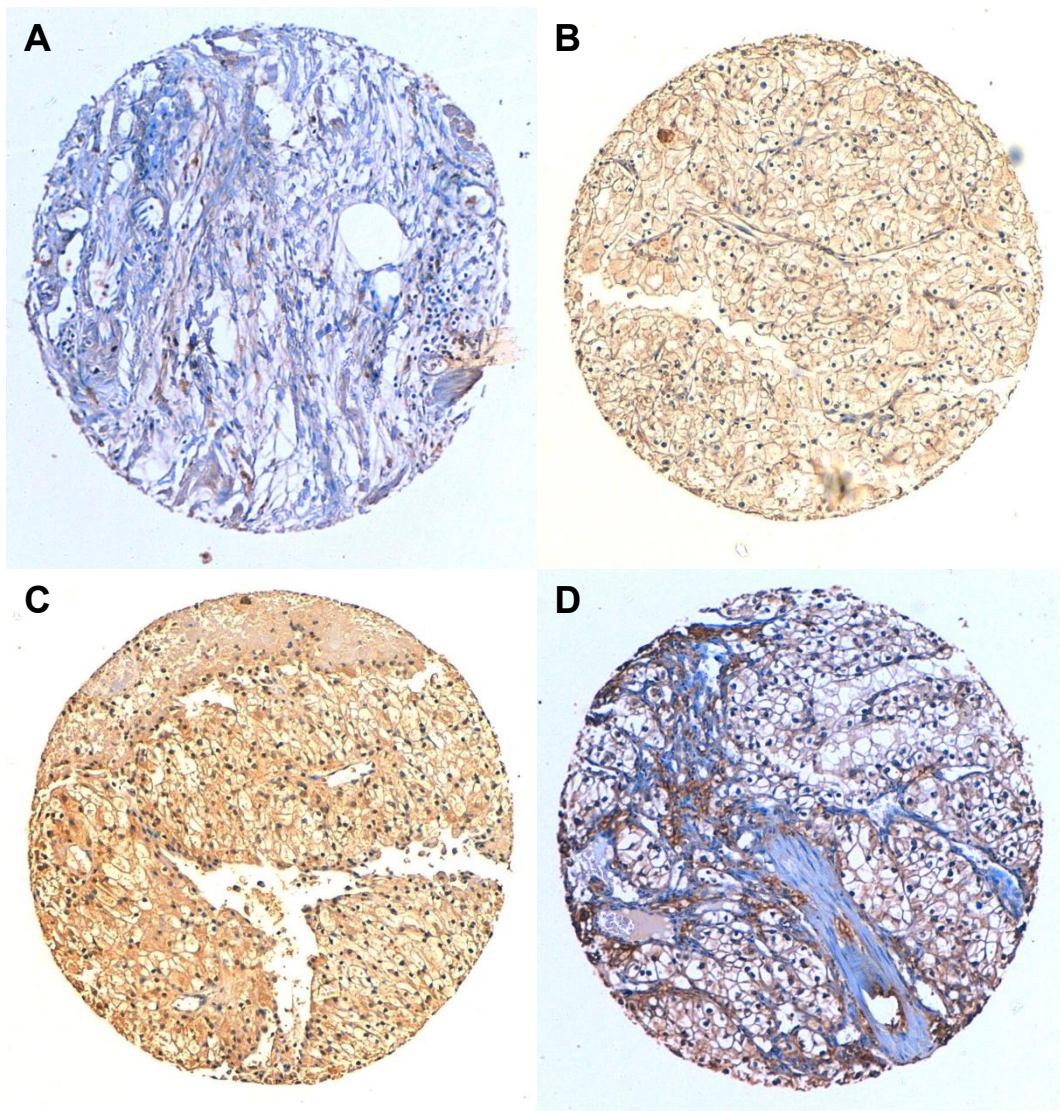


Figure 2.10 Immunohistochemical staining of RCC TMAs for CD105 expression captured at x10 magnification. Representative tumours of CD105 scoring criteria (A) CD105 score 0, (B) CD105 score 1, (C) CD105 score 2 and (D) CD105 score 3.

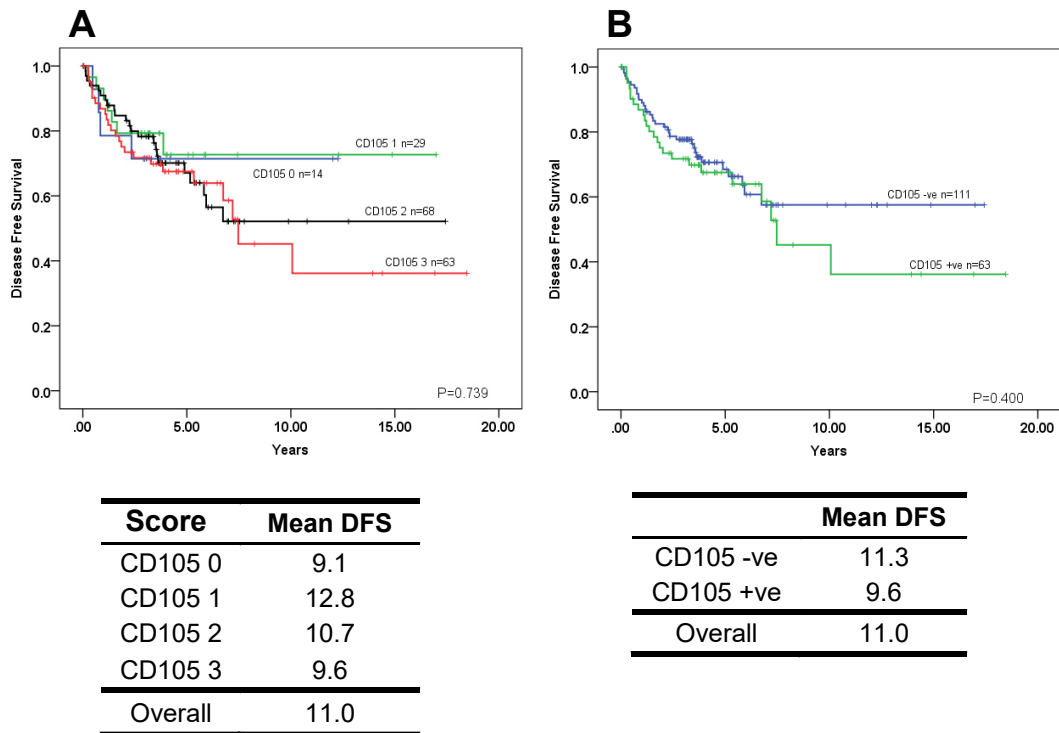


Figure 2.11 Kaplan-Meier survival curves for CD105 expression. (A) Kaplan-Meier DFS curves for CD105 plotted using the scoring criteria without recoding (CD105 0 n=14, CD105 1 n=29, CD105 2 n=68 and CD105 3 n=63) with corresponding mean disease free survival shown below. P=0.739 as determined by Log-rank comparison. (B) Kaplan-Meier DFS curves for CD105 staining re-plotted with scores from 0 to 2 pooled and recoded as CD105 negative (n=111) and scores of 3 classified as CD105 positive (n=63). P=0.400 as determined by Log-rank comparison.

Table 2.10 Crosstabulation of CD105 with histopathological characteristics of RCC. Significance calculated by Chi-squared or Fisher's exact test as relevant

| | CD105 negative | CD105 positive |
|-----------------------------------|----------------|----------------|
| Grade 1 and 2 | 77 | 45 |
| Grade 3 and 4 | 34 | 18 |
| | | P=0.776 |
| Tumour size <7cm | 66 | 35 |
| Tumour size >7cm | 45 | 28 |
| | | P=0.616 |
| Vascular invasion -ve | 63 | 43 |
| Vascular invasion +ve | 48 | 20 |
| | | P=0.135 |
| Microcapsular invasion -ve | 87 | 56 |
| Microcapsular invasion +ve | 24 | 7 |
| | | P=0.082 |
| Micronecrosis -ve | 59 | 28 |
| Micronecrosis +ve | 51 | 34 |
| | | P=0.286 |
| Non-clear cell carcinoma | 18 | 12 |
| Clear cell carcinoma | 93 | 51 |
| | | P=0.635 |
| Non-Papillary | 99 | 52 |
| Papillary | 12 | 11 |
| | | P=0.213 |

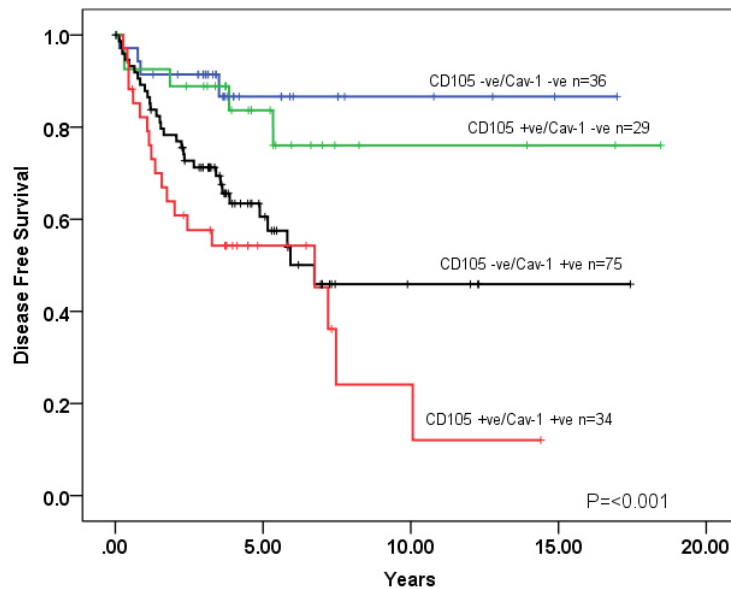
Table 2.11 Cox regression analysis of CD105 expression with histopathological characteristics of RCC. Analysis performed using the 'Enter' function. Both CD105 expression and vascular invasion rejected by the 'Forward Stepwise' (Likelihood ratio) model as not influential. 95% CI=95% Confidence Interval.

| Prognostic indicator | Hazard ratios | 95% CI | P value |
|-----------------------|---------------|-------------|---------|
| CD105 negative | 1 | | |
| CD105 positive | 1.7 | 0.926-2.945 | 0.089 |
| Grade 1 and 2 | 1 | | |
| Grade 3 and 4 | 2.3 | 1.263-4.083 | 0.006 |
| Size <7cm | 1 | | |
| Size >7cm | 2.1 | 1.210-3.794 | 0.009 |
| Vascular invasion -ve | 1 | | |
| Vascular invasion +ve | 1.9 | 1.001-3.557 | 0.050 |
| Capsular invasion -ve | 1 | | |
| Capsular invasion +ve | 2.2 | 1.215-4.027 | 0.009 |
| Micronecrosis -ve | 1 | | |
| Micronecrosis +ve | 2.9 | 1.500-5.518 | 0.001 |

A

| | Cav-1 negative | Cav-1 positive |
|----------------|----------------|----------------|
| CD105 negative | 36 | 75 |
| CD105 positive | 29 | 34 |

P=0.075

B

| | Mean DFS |
|---------------------|----------|
| CD105 -ve/Cav-1 -ve | 14.9 |
| CD105 +ve/Cav-1 -ve | 14.7 |
| CD105 -ve/Cav-1 +ve | 9.7 |
| CD105 +ve/Cav-1 +ve | 5.7 |
| Overall | 11.0 |

Figure 2.12 Correlation of CD105 with CAV1 expression and Kaplan-Meier survival analysis. (A) Cross tabulation of CD105 and CAV1 expression in RCC tumour cores. No significant correlation $P=0.075$ as determined by chi-squared. (B) Kaplan-Meier DFS curves plotted for CD105 and CAV1 expressed as a composite variable (CD105-ve/CAV1-ve $n=36$, CD105+ve/CAV1-ve $n=29$, CD105-ve/CAV1+ve $n=75$, CD105 +ve/CAV1 +ve $n=34$) with corresponding mean disease free survival shown below. $P < 0.001$ as determined by Log-rank comparison.

Table 2.12 Crosstabulation of All other tumours and CD105 +ve/CAV1 +ve with histopathological characteristics of RCC. Significance calculated by Chi-squared or Fisher's exact test as relevant

| | All other tumours | CD105 +ve/CAV1 +ve |
|-----------------------------------|--------------------------|---------------------------|
| Grade 1 and 2 | 99 | 23 |
| Grade 3 and 4 | 41 | 11 |
| | | P=0.726 |
| Tumour size <7cm | 83 | 18 |
| Tumour size >7cm | 57 | 16 |
| | | P=0.501 |
| Vascular invasion -ve | 85 | 21 |
| Vascular invasion +ve | 55 | 13 |
| | | P=0.910 |
| Microcapsular invasion -ve | 114 | 29 |
| Microcapsular invasion +ve | 26 | 5 |
| | | P=0.597 |
| Micronecrosis -ve | 75 | 12 |
| Micronecrosis +ve | 63 | 22 |
| | | P=0.047 |
| Non-clear cell carcinoma | 27 | 3 |
| Clear cell carcinoma | 113 | 31 |
| | | P=0.147 |
| Non-Papillary | 120 | 31 |
| Papillary | 20 | 3 |
| | | P=0.299 |

Table 2.13 Cox regression analysis of combined CD105 and CAV1 expression with histopathological characteristics of RCC. (A) Analysis performed using the 'Enter' method. (B) Analysis performed using the 'Forward Stepwise' (Likelihood ratio) all variables selected entered the model at the first step. 95% CI=95% Confidence Interval

| A | | | |
|-----------------------------|----------------------|---------------|----------------|
| Prognostic indicator | Hazard ratios | 95% CI | P value |
| CD105/Cav-1 negative | 1 | | |
| CD105/Cav-1 positive | 2.3 | 1.292-4.217 | 0.005 |
| Grade 1 and 2 | 1 | | |
| Grade 3 and 4 | 2.4 | 1.324-4.248 | 0.004 |
| Size <7cm | 1 | | |
| Size >7cm | 2.0 | 1.119-3.512 | 0.019 |
| Vascular invasion -ve | 1 | | |
| Vascular invasion +ve | 1.9 | 1.033-3.603 | 0.039 |
| Capsular invasion -ve | 1 | | |
| Capsular invasion +ve | 2.2 | 1.216-3.924 | 0.009 |
| Micronecrosis -ve | 1 | | |
| Micronecrosis +ve | 2.7 | 1.408-5.187 | 0.003 |

| B | | | |
|-----------------------------|----------------------|---------------|----------------|
| Prognostic indicator | Hazard ratios | 95% CI | P value |
| CD105/Cav-1 negative | 1 | | |
| CD105/Cav-1 positive | 2.3 | 1.292-4.217 | 0.005 |
| Grade 1 and 2 | 1 | | |
| Grade 3 and 4 | 2.4 | 1.324-4.248 | 0.004 |
| Size <7cm | 1 | | |
| Size >7cm | 2.0 | 1.119-3.512 | 0.019 |
| Vascular invasion -ve | 1 | | |
| Vascular invasion +ve | 1.9 | 1.003-3.603 | 0.039 |
| Capsular invasion -ve | 1 | | |
| Capsular invasion +ve | 2.2 | 1.216-3.924 | 0.009 |
| Micronecrosis -ve | 1 | | |
| Micronecrosis +ve | 2.7 | 1.408-5.187 | 0.003 |

2.3.4 EpCAM in RCC tumours does not identify high risk patients alone or as a covariate with CAV1

To control for specificity of immunohistochemical staining with the EpCAM antibody selected. Positive staining localised to renal epithelial cells in normal kidney tissue was used as a positive control[199] (Figure 2.13). EpCAM staining was identifiable by positive staining was localised to the cell membrane in both normal kidney epithelia and in RCC tumours (Figure 2.14). Scoring criteria for EpCAM was defined as: EpCAM score 0 for absent membrane staining (Figure 2.14 A), EpCAM score 1 for weak membrane staining (Figure 2.14 B), EpCAM score 2 for medium membrane staining (Figure 2.14 C) and EpCAM score 3 for strong membrane staining (Figure 2.14 D). This resulted in 9 EpCAM score 0 tumours, 34 EpCAM score 1 tumours, 63 EpCAM score 2 tumours and 68 EpCAM score 3 tumours.

Kaplan-Meier DFS curves of EpCAM scoring found no significant difference in mean disease free survival between any of the scoring intensity groups ($P=0.236$). Though, surprisingly, it did appear that the weakest EpCAM expressing group showed the lowest mean disease free survival of 7.6 years and tumours in the small EpCAM negative group showed a mean DFS of 15.2 years (Figure 2.15 A). To analyse the potential difference between EpCAM negative and EpCAM positive tumours, the EpCAM positive scores EpCAM score 1, EpCAM score 2 and EpCAM score 3 were pooled and recoded as EpCAM positive. Repeating the Kaplan-Meier analysis however proved no significant difference between these two groups ($P=0.144$) (Figure 2.15 B).

Crosstabulation of EpCAM with histopathological characteristics of RCC found no significant correlation among any of these features (Table 2.14). In multivariate Cox regression analysis using the enter function, EpCAM proved non-significant ($P=0.223$) and was rejected when using the forward stepwise (likelihood ratio) function (Table 2.15).

Crosstabulation of EpCAM and CAV1 showed no significant correlation between the two markers ($P=0.549$) (Figure 2.16 A). In order to carry out a Kaplan-Meier analysis with this covariate that would be in agreement to the requirements of the analysis data was pool such that tumours falling in the groups of EpCAM-ve/CAV1-ve, EpCAM+ve/CAV1-ve and EpCAM-ve/CAV1+ve were grouped as “all other tumours” with EpCAM+ve/CAV1+ve remaining the same. Kaplan-Meier analysis of this covariate found a mean disease free survival for EpCAM+ve/CAV1+ve tumours of 7.6 years with all other tumours showing a mean DFS of 15.8 years ($P=<0.001$) (Figure 2.16 B).

Crosstabulation of the EpCAM/CAV1 covariate found correlations with high grade ($P=0.015$), vascular invasion ($P=0.006$), microcapsular invasion ($P=0.002$) and micronecrosis ($P=0.003$). In histological subtyping EpCAM/CAV1 correlated with clear cell carcinoma ($P=0.002$) and negatively correlate with papillary ($P=0.003$) (Table 2.16). In multivariate Cox regression analysis using the enter function EpCAM+ve/CAV1+ve indicated a statistically significant hazard ratio of 2.9 ($P=0.009$) (Table 2.17 A) and was included in the forward stepwise (likelihood ratio) function as significant ($P=0.008$) with the highest associated hazard ($HR=2.9$) (Table 2.17 B).

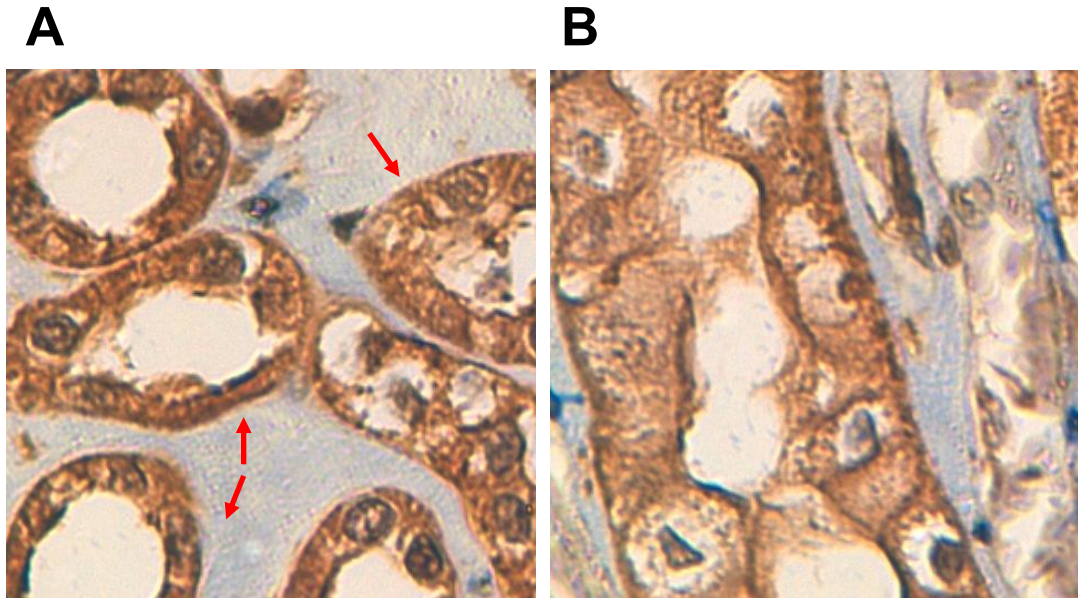


Figure 2.13 Immunohistochemical staining of EpCAM in epithelial tubule structures in normal kidney tissue is a positive control for specificity of the EpCAM antibody used. **(A)** Shows EpCAM staining in transverse sections of epithelial tubules (indicated by the red arrows). **(B)** Shows a longitudinal section through a EpCAM positive renal tubule.

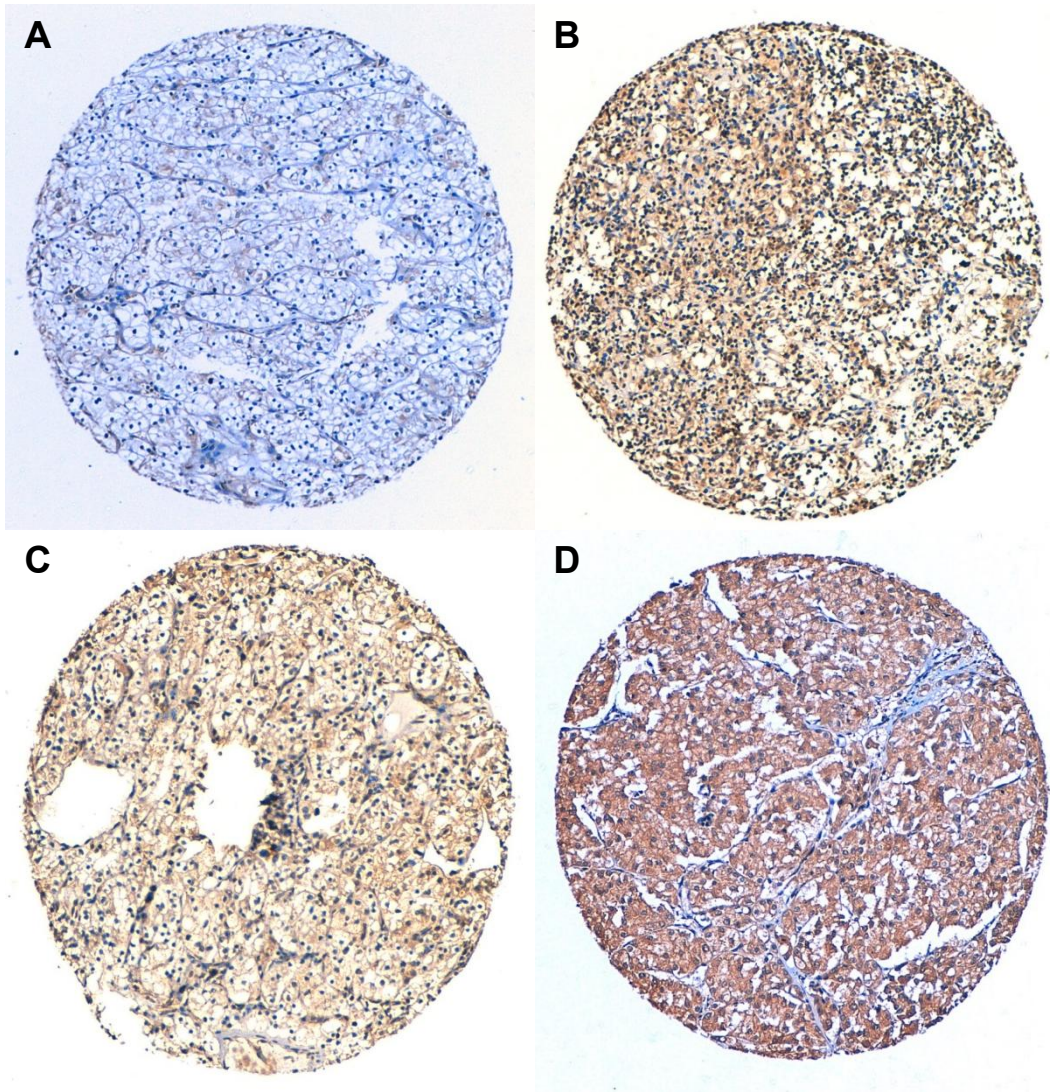


Figure 2.14 Immunohistochemical staining of RCC TMAs for EpCAM expression captured at x10 magnification. Representative tumours of EpCAM scoring criteria (A) EpCAM score 0, (B) EpCAM score 1, (C) EpCAM score 2 and (D) EpCAM score 3.

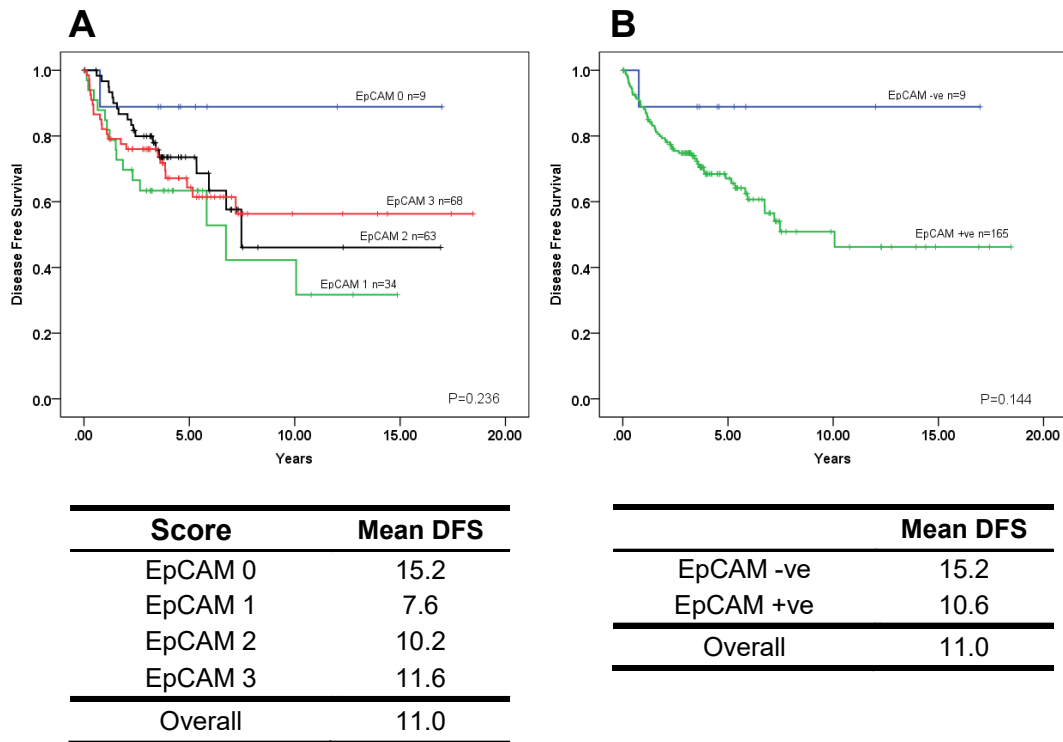


Figure 2.15 Kaplan-Meier survival curves for EpCAM expression. (A) Kaplan-Meier DFS curves for EpCAM plotted using the scoring criteria without recoding (EpCAM 0 n=9, EpCAM 1 n=34, EpCAM 2 n=63 and EpCAM 3 n=34) with corresponding mean disease free survival shown below. P=0.236 as determined by Log-rank comparison. (B) Kaplan-Meier DFS curves for EpCAM staining re-plotted with a score of 0 recoded as EpCAM negative n=9 and scores 1 to 3 pooled and recoded as EpCAM positive n=165. P=0.144 as determined by Log-rank comparison.

Table 2.14 Crosstabulation of EpCAM with histopathological characteristics of RCC. Significance calculated by Chi-squared or Fisher's exact test as relevant

| | EpCAM negative | EpCAM positive | |
|-----------------------------------|----------------|----------------|---------|
| Grade 1 and 2 | 8 | 114 | |
| Grade 3 and 4 | 1 | 51 | |
| | | | P=0.191 |
| Tumour size <7cm | 6 | 95 | |
| Tumour size >7cm | 3 | 70 | |
| | | | P=0.431 |
| Vascular invasion -ve | 3 | 103 | |
| Vascular invasion +ve | 6 | 62 | |
| | | | P=0.084 |
| Microcapsular invasion -ve | 8 | 135 | |
| Microcapsular invasion +ve | 1 | 30 | |
| | | | P=0.501 |
| Micronecrosis -ve | 5 | 82 | |
| Micronecrosis +ve | 4 | 81 | |
| | | | P=0.515 |
| Non-clear cell carcinoma | 1 | 29 | |
| Clear cell carcinoma | 8 | 136 | |
| | | | P=0.520 |
| Non-Papillary | 8 | 143 | |
| Papillary | 1 | 22 | |
| | | | P=0.661 |

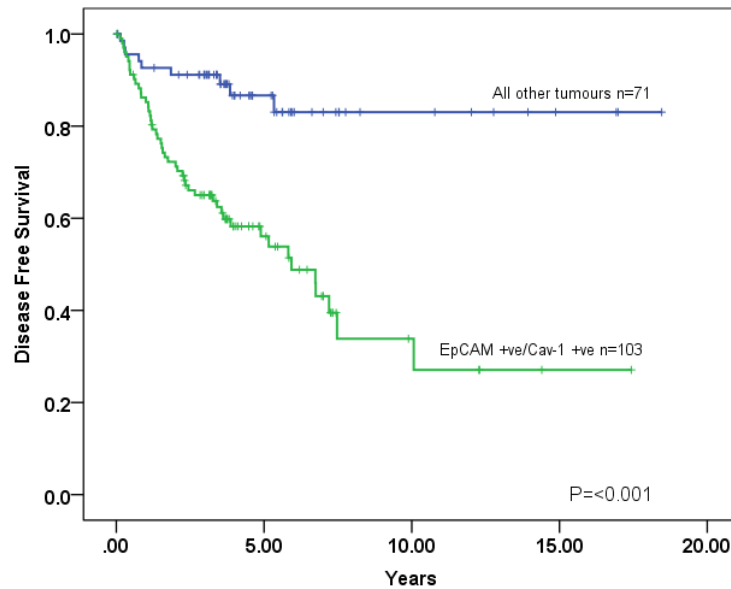
Table 2.15 Cox regression analysis of EpCAM expression with histopathological characteristics of RCC. Analysis performed using the 'Enter' method. Both EpCAM expression and vascular invasion rejected by 'Forward Stepwise' (Likelihood ratio) model as not influential. 95% CI=95% Confidence Interval.

| Prognostic indicator | Hazard ratios | 95% CI | P value |
|-----------------------|---------------|--------------|---------|
| EpCAM negative | 1 | | |
| EpCAM positive | 3.5 | 0.470-25.434 | 0.223 |
| Grade 1 and 2 | 1 | | |
| Grade 3 and 4 | 2.1 | 1.154-3.645 | 0.014 |
| Size <7cm | 1 | | |
| Size >7cm | 2.3 | 1.302-4.076 | 0.004 |
| Vascular invasion -ve | 1 | | |
| Vascular invasion +ve | 1.9 | 0.993-3.472 | 0.053 |
| Capsular invasion -ve | 1 | | |
| Capsular invasion +ve | 1.9 | 1.023-3.379 | 0.042 |
| Micronecrosis -ve | 1 | | |
| Micronecrosis +ve | 3.1 | 1.618-5.928 | <0.001 |

A

| | Cav-1 negative | Cav-1 positive |
|----------------|----------------|----------------|
| EpCAM negative | 3 | 6 |
| EpCAM positive | 62 | 103 |

P=0.549

B

| | Mean DFS |
|---------------------|----------|
| All other tumours | 15.8 |
| EpCAM +ve/Cav-1 +ve | 7.6 |
| Overall | 11.0 |

Figure 2.16 Correlation of EpCAM with CAV1 expression and Kaplan-Meier survival analysis. (A) Cross tabulation of EpCAM and CAV1 expression in RCC tumour cores. No significant correlation $P=0.549$ as determined by Fisher's exact test. (B) Kaplan-Meier DFS curves plotted for EpCAM and CAV1 expressed as a composite variable with double positive EpCAM+ve/CAV1+ve $n=71$ and all other combinations pooled and recoded as 'All other tumours' $n=103$ with corresponding mean DFS in years shown below. $P < 0.001$ as determined by Log-rank comparison.

Table 2.16 Crosstabulation of EpCAM and CAV1 with histopathological characteristics of RCC. Significance calculated by Chi-squared or Fisher's exact test as relevant.

| | All other tumours | EpCAM +ve/Cav-1 +ve |
|-----------------------------------|--------------------------|----------------------------|
| Grade 1 and 2 | 57 | 65 |
| Grade 3 and 4 | 14 | 38 |
| | | P=0.015 |
| Tumour size <7cm | 45 | 56 |
| Tumour size >7cm | 26 | 47 |
| | | P=0.236 |
| Vascular invasion -ve | 52 | 54 |
| Vascular invasion +ve | 19 | 49 |
| | | P=0.006 |
| Microcapsular invasion -ve | 66 | 77 |
| Microcapsular invasion +ve | 5 | 26 |
| | | P=0.002 |
| Micronecrosis -ve | 45 | 42 |
| Micronecrosis +ve | 25 | 60 |
| | | P=0.003 |
| Non-clear cell carcinoma | 20 | 10 |
| Clear cell carcinoma | 51 | 93 |
| | | P=0.002 |
| Non-Papillary | 55 | 96 |
| Papillary | 16 | 7 |
| | | P=0.003 |

Table 2.17 Cox regression analysis of combined EpCAM and CAV1 expression with histopathological characteristics of RCC. (A) Analysis performed using the 'Enter' method. (B) Analysis performed using the 'Forward Stepwise' (Likelihood ratio) method. Vascular invasion was rejected by the model as not influential. 95% CI=95% Confidence Interval.

A

| Prognostic indicator | Hazard ratios | 95% CI | P value |
|-----------------------------|----------------------|---------------|----------------|
| EpCAM/Cav-1 negative | 1 | | |
| EpCAM/Cav-1 positive | 2.9 | 1.294-6.281 | 0.009 |
| Grade 1 and 2 | 1 | | |
| Grade 3 and 4 | 2.1 | 1.190-3.769 | 0.011 |
| Size <7cm | 1 | | |
| Size >7cm | 2.4 | 1.341-4.214 | 0.003 |
| Vascular invasion -ve | 1 | | |
| Vascular invasion +ve | 1.7 | 0.919-3.093 | 0.092 |
| Capsular invasion -ve | 1 | | |
| Capsular invasion +ve | 1.5 | 0.838-2.858 | 0.163 |
| Micronecrosis -ve | 1 | | |
| Micronecrosis +ve | 2.7 | 1.396-5.168 | 0.003 |

B

| Prognostic indicator | Hazard ratios | 95% CI | P value |
|-----------------------------|----------------------|---------------|----------------|
| EpCAM/Cav-1 negative | 1 | | |
| EpCAM/Cav-1 positive | 2.9 | 1.319-6.404 | 0.008 |
| Grade 1 and 2 | 1 | | |
| Grade 3 and 4 | 2.4 | 1.367-4.234 | 0.002 |
| Size <7cm | 1 | | |
| Size >7cm | 2.6 | 1.487-4.601 | 0.001 |
| Capsular invasion -ve | 1 | | |
| Capsular invasion +ve | 1.7 | 0.927-3.107 | 0.086 |
| Micronecrosis -ve | 1 | | |
| Micronecrosis +ve | 2.7 | 1.404-5.226 | 0.003 |

2.3.5 CD146 in RCC tumours does not identify high risk patients alone or covariate with CAV1

To control for positive staining of CD146 in the antibody selected, staining of the endothelium, CD146 a widely expressed marker of endothelial cells[255] of normal kidney was identified as a positive control (Figure 2.17). Assessment of CD146 was complicated due to the strong amount of cytoplasmic staining present. However, it was possible to make a distinction between negative (Figure 2.18 C) and positive (Figure 2.18 D) membrane staining. As such the scoring criteria were determined as: no visible membrane coded as CD146-ve presence of membrane staining coded as CD146 +ve. This resulted in 72 tumours identified as CD146-ve and 102 tumours identified as CD146+ve. In Kaplan-Meier DFS analysis, CD146 positivity did not identify patients at higher risk of disease relapse, with mean DFS of CD146-ve tumours being 11.2 years and CD146+ve tumours being 10.3 years (P=0.535) (Figure 2.19).

Crosstabulation of CD146 with histopathological characteristics of RCC found CD146 to correlate with low grade (P=0.029) and absence of micronecrosis (P=0.032) but not size, vascular invasion or microcapsular invasion. Positive CD146 staining correlated strongly with a clear cell histology (P=<0.001) and decreased in papillary carcinomas (P=<0.001) (Table 2.18). Multivariate Cox regression analysis using the enter function found CD146 to have no ability to predict poor patient outcome with a hazard ratio of 1.3 (P=0.357), carrying less risk than vascular invasion (Table 2.19). Using the forward stepwise (likelihood ratio) function CD146 together with vascular invasion was rejected as uninformative on the analysis.

Crosstabulation of CD146 with CAV1 expression showed a positive correlation between CD146 and CAV1 (P=0.01) (Figure 2.20 A). Kaplan-Meier DFS analysis of this covariate found a mean DFS of 15.2 years for CD146-ve/CAV1-ve and a mean DFS of 14.6 years for CD146+ve/CAV1-ve, while CD146-ve/CAV1+ve tumours had

a mean DFS of 6.7 years and CD146+ve/CAV1+ve tumours had a mean DFS of 7.4 years ($P < 0.001$) (Figure 2.20 B).

Crosstabulation of the CD146/CAV1 covariate with the histopathological characteristics of RCC found only a correlation with vascular invasion ($P = 0.048$) but not grade, size, microcapsular invasion or micronecrosis. A correlation with the clear cell subtype ($P < 0.001$) appeared in the histological subtypes and absence in the papillary subtype ($P = 0.002$) (Table 2.20). Multivariate Cox regression analysis of CD146+ve/CAV1+ve using the enter function did not indicate patients at greater risk of disease relapse with a hazard ratio of 1.4 ($P = 0.210$). Using the forward stepwise (likelihood ratio) CD146/CAV1 was rejected together with vascular invasion as uninfluential on the analysis.

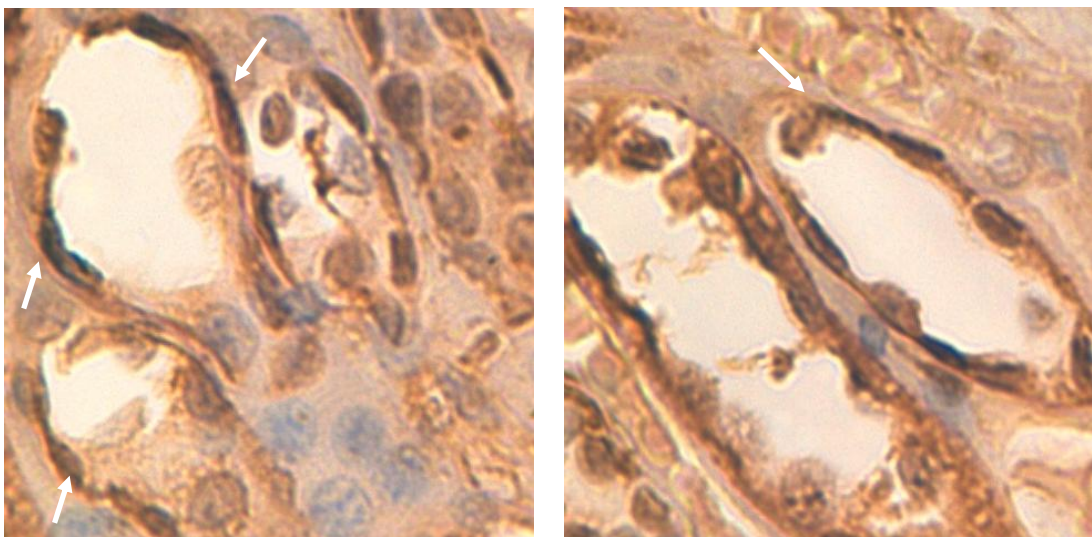


Figure 2.17 Immunohistochemical staining of CD146 in endothelial structures in normal kidney tissue acts as a positive control for the specificity of the CD146 antibody used. White arrows indicate the presence of CD146 endothelial staining.

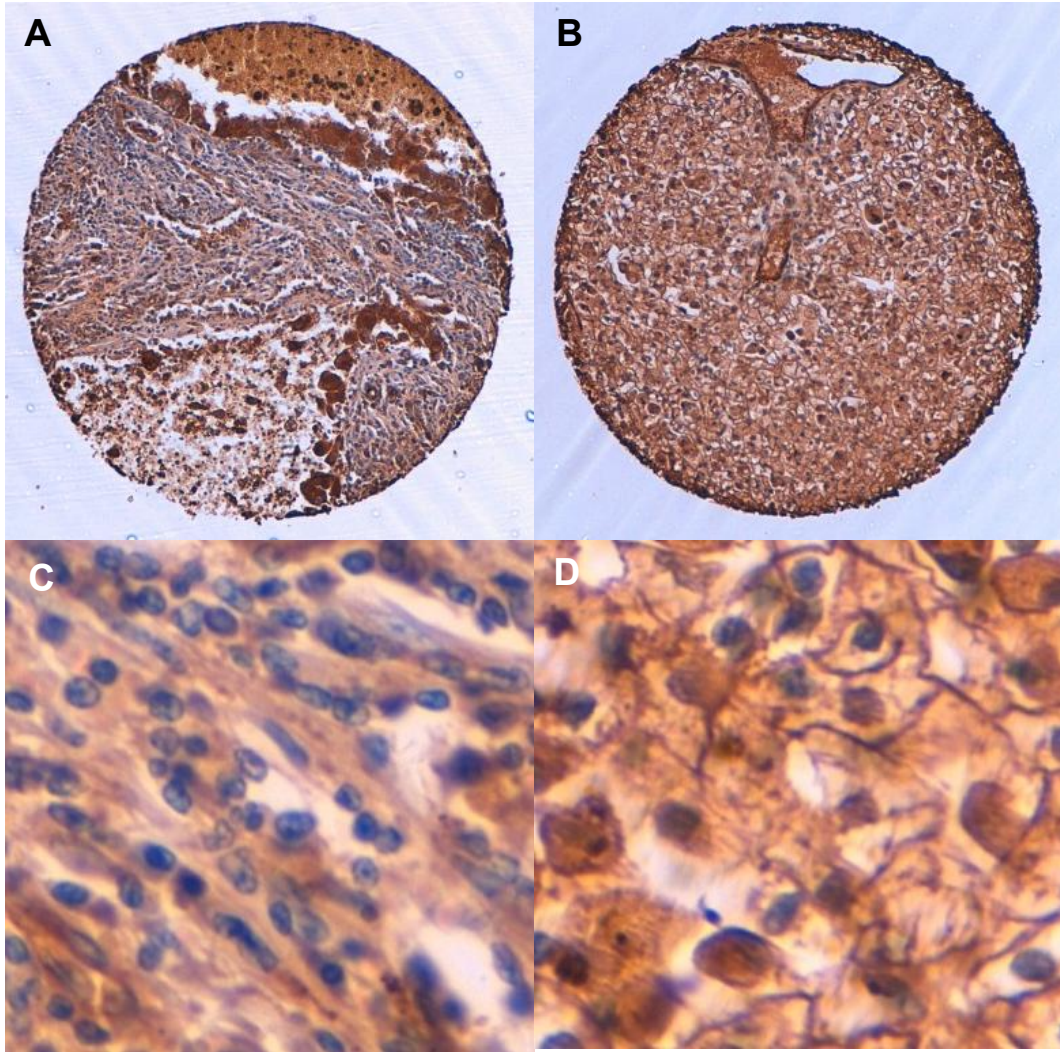
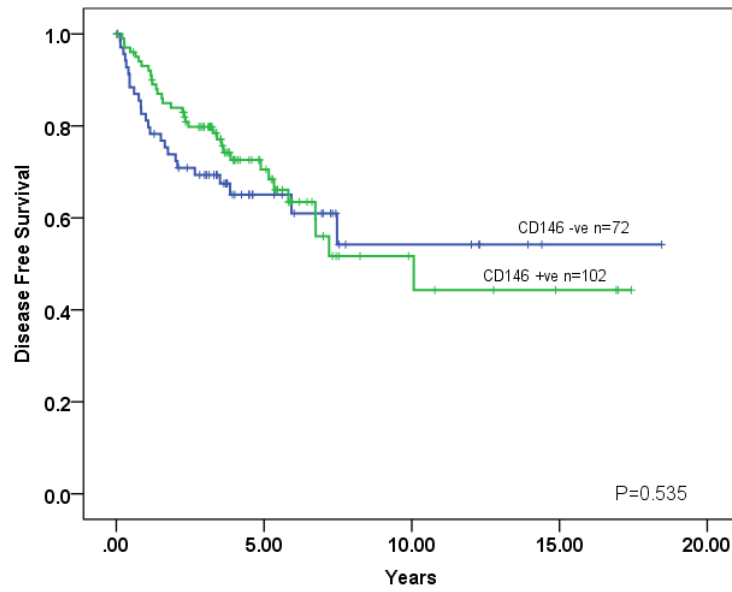


Figure 2.18 Immunohistochemical staining of RCC TMAs for CD146 expression. (A) Representative tumour core scored as CD146 negative. (B) Representative tumour core scored as CD146 positive. (C) x40 magnification of the core shown in A demonstrating negative membrane staining. (D) x40 magnification of the core shown in B demonstrating positive membrane staining.



| Mean DFS | |
|-----------|------|
| CD146 -ve | 11.2 |
| CD146 +ve | 10.3 |
| Overall | 11.0 |

Figure 2.19 Kaplan-Meier DFS curves for CD146 staining CD146-ve n=72 and CD146+ve n=102 with mean disease free survival shown below. P=0.535 as determined by Log-rank comparison.

Table 2.18 Crosstabulation of CD146 with histopathological characteristics of RCC. Significance calculated by Chi-squared or Fisher's exact test as relevant.

| | CD146 negative | CD146 positive |
|----------------------------|----------------|----------------|
| Grade 1 and 2 | 44 | 78 |
| Grade 3 and 4 | 28 | 24 |
| | | P=0.029 |
| Tumour size <7cm | 37 | 64 |
| Tumour size >7cm | 35 | 38 |
| | | P=0.135 |
| Vascular invasion -ve | 42 | 64 |
| Vascular invasion +ve | 30 | 38 |
| | | P=0.557 |
| Microcapsular invasion -ve | 57 | 86 |
| Microcapsular invasion +ve | 15 | 16 |
| | | P=0.382 |
| Micronecrosis -ve | 29 | 58 |
| Micronecrosis +ve | 42 | 43 |
| | | P=0.032 |
| Non-clear cell carcinoma | 24 | 6 |
| Clear cell carcinoma | 48 | 96 |
| | | P=<0.001 |
| Non-Papillary | 52 | 99 |
| Papillary | 20 | 3 |
| | | P=<0.001 |

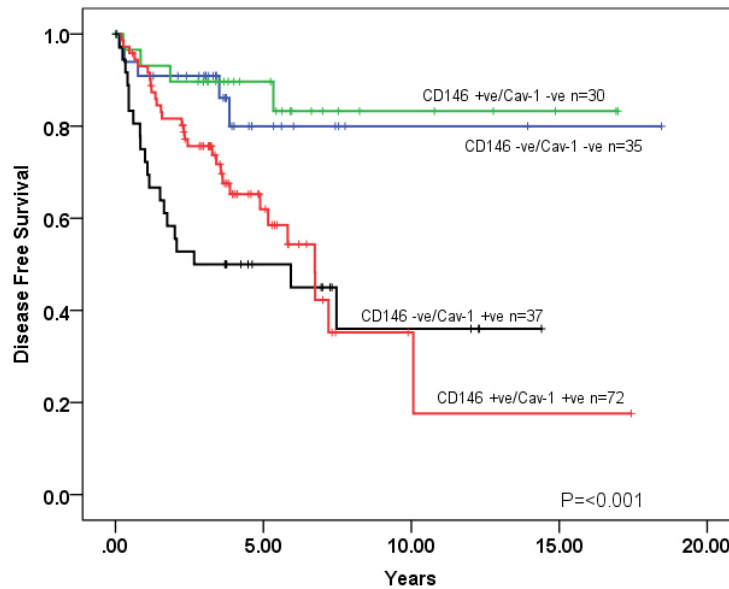
Table 2.19 Cox regression analysis of CD146 expression with histopathological characteristics of RCC. Analysis performed using the 'Enter' method. Both CD146 expression and vascular invasion rejected by the 'Forward Stepwise' (Likelihood ratio) model as not influential. 95% CI=95% Confidence Interval.

| Prognostic indicator | Hazard ratios | 95% CI | P value |
|-----------------------|---------------|-------------|---------|
| CD146 negative | 1 | | |
| CD146 positive | 1.3 | 0.750-2.221 | 0.357 |
| Grade 1 and 2 | 1 | | |
| Grade 3 and 4 | 2.1 | 1.195-3.865 | 0.011 |
| Size <7cm | 1 | | |
| Size >7cm | 2.3 | 1.312-4.134 | 0.004 |
| Vascular invasion -ve | 1 | | |
| Vascular invasion +ve | 1.7 | 0.928-3.249 | 0.084 |
| Capsular invasion -ve | 1 | | |
| Capsular invasion +ve | 2.0 | 1.112-3.622 | 0.021 |
| Micronecrosis -ve | 1 | | |
| Micronecrosis +ve | 3.2 | 1.661-6.102 | <0.001 |

A

| | Cav-1 negative | Cav-1 positive |
|-----------------------|----------------|----------------|
| CD146 negative | 35 | 37 |
| CD146 positive | 30 | 72 |

P=0.010

B

| | Mean DFS |
|---------------------|----------|
| CD146 -ve/Cav-1 -ve | 15.2 |
| CD146 +ve/Cav-1 -ve | 14.6 |
| CD146 -ve/Cav-1 +ve | 6.7 |
| CD146 +ve/Cav-1 +ve | 7.4 |
| Overall | 11.0 |

Figure 2.20 Correlation of CD146 with CAV1 expression and Kaplan-Meier survival analysis. (A) Cross tabulation of CD146 and CAV1 expression in RCC tumour cores. Significant correlation $P < 0.010$ as determined by Chi-squared. (B) Kaplan-Meier DFS curves plotted for CD146 and CAV1 expressed as a composite variable CD146–ve/CAV1–ve $n=35$, CD146+ve/CAV1–ve $n=30$, CD146–ve/CAV1+ve $n=37$, CD146+ve/CAV1+ve $n=72$ mean disease free survival shown below. $P < 0.001$ as determined by Log-rank comparison.

Table 2.20 Crosstabulation of CD146 and CAV1 with histopathological characteristics of RCC. Significance calculated by Chi-squared or Fisher's exact test as relevant.

| | All other tumours | CD146 +ve/Cav-1 +ve |
|----------------------------|-------------------|---------------------|
| Grade 1 and 2 | 71 | 51 |
| Grade 3 and 4 | 32 | 20 |
| | | P=0.681 |
| Tumour size <7cm | 59 | 42 |
| Tumour size >7cm | 44 | 29 |
| | | P=0.806 |
| Vascular invasion -ve | 69 | 37 |
| Vascular invasion +ve | 34 | 34 |
| | | P=0.048 |
| Microcapsular invasion -ve | 86 | 57 |
| Microcapsular invasion +ve | 17 | 14 |
| | | P=0.586 |
| Micronecrosis -ve | 53 | 34 |
| Micronecrosis +ve | 49 | 36 |
| | | P=0.662 |
| Non-clear cell carcinoma | 27 | 3 |
| Clear cell carcinoma | 76 | 68 |
| | | P=<0.001 |
| Non-Papillary | 83 | 68 |
| Papillary | 20 | 3 |
| | | P=0.002 |

Table 2.21 Cox regression analysis of CD146 and CAV1 expression with histopathological characteristics of RCC. Analysis performed using the 'Enter' method. Both CD146 and CAV1 expression and vascular invasion rejected by the 'Forward Stepwise' (Likelihood ratio) model as not influential. 95% CI=95% Confidence Interval.

| Prognostic indicator | Hazard ratios | 95% CI | P value |
|-----------------------|---------------|-------------|---------|
| CD146/Cav-1 negative | 1 | | |
| CD146/Cav-1 positive | 1.4 | 0.825-2.409 | 0.210 |
| Grade 1 and 2 | 1 | | |
| Grade 3 and 4 | 2.1 | 1.186-3.815 | 0.011 |
| Size <7cm | 1 | | |
| Size >7cm | 2.3 | 1.289-4.036 | 0.005 |
| Vascular invasion -ve | 1 | | |
| Vascular invasion +ve | 1.7 | 0.896-3.141 | 0.106 |
| Capsular invasion -ve | 1 | | |
| Capsular invasion +ve | 2.0 | 1.120-3.632 | 0.019 |
| Micronecrosis -ve | 1 | | |
| Micronecrosis +ve | 3.1 | 1.601 | <0.001 |

2.3.6 Vimentin expression in RCC tumours does not identify high risk patients alone or covariate with CAV1

To control for positive immunohistochemical staining of vimentin expression, positive staining localised to the endothelia of normal kidney tissue was used [218] (Figure 2.21). Scorable positive staining for vimentin was found in the cytoplasm of RCC tumour cores (Figure 2.22 B). Vimentin staining was of a uniform intensity, as such, the scoring criteria was defined as positive where staining was observable (vimentin +ve) (Figure 2.22 B) and negative where no staining could be detected (vimentin -ve) (Figure 2.22 A). Scoring in this way resulted in 128 tumours identified as vimentin -ve and 46 tumours identified as vimentin +ve. Kaplan-Meier DFS analysis of this scoring data revealed vimentin +ve tumours have a mean DFS of 8.9 years compared to a mean DFS of 11.5 years in vimentin -ve tumours ($P=0.033$) (Figure 2.22 C).

Crosstabulation of vimentin with the histopathological characteristics of RCC found vimentin to correlate only with increased grade ($P=0.006$), with no correlation between any other of the pathological characteristics or histological subtypes (Table 2.22). Multivariate Cox regression analysis using the enter function showed vimentin positivity to be uninfluential in terms of risk to patients, with a hazard ratio of 1.3 ($P=0.405$), which was weaker than any of the other variables in the model (Table 2.23).

Analysis of the association of vimentin and CAV1 in patient tumours identified a trend toward the co-localisation of the two approaching significance ($P=0.065$) (Figure 2.23 A). Kaplan-Meier DFS analysis of the vimentin/CAV1 covariate showed vimentin +ve/CAV1 +ve tumours to have an associated mean DFS of 7.6 years; however tumours vimentin -ve/CAV1 +ve had a mean DFS of 7.5 years, showing vimentin to have negligible impact on DFS in combination with CAV1 ($P=<0.001$) (Figure 2.23 B).

Crosstabulation of the vimentin/CAV1 covariate with histopathological characteristics of RCC found only a correlation with grade ($P < 0.001$) and microcapsular invasion ($P = 0.014$) and did not select for a specific histological subtype (Table 2.24). Multivariate Cox regression analysis using the enter function of the vimentin/CAV1 covariate found a non-significant hazard ratio to 1.6 ($P = 0.159$), and was not influential in the forward stepwise (likelihood ratio) function (Table 2.25).

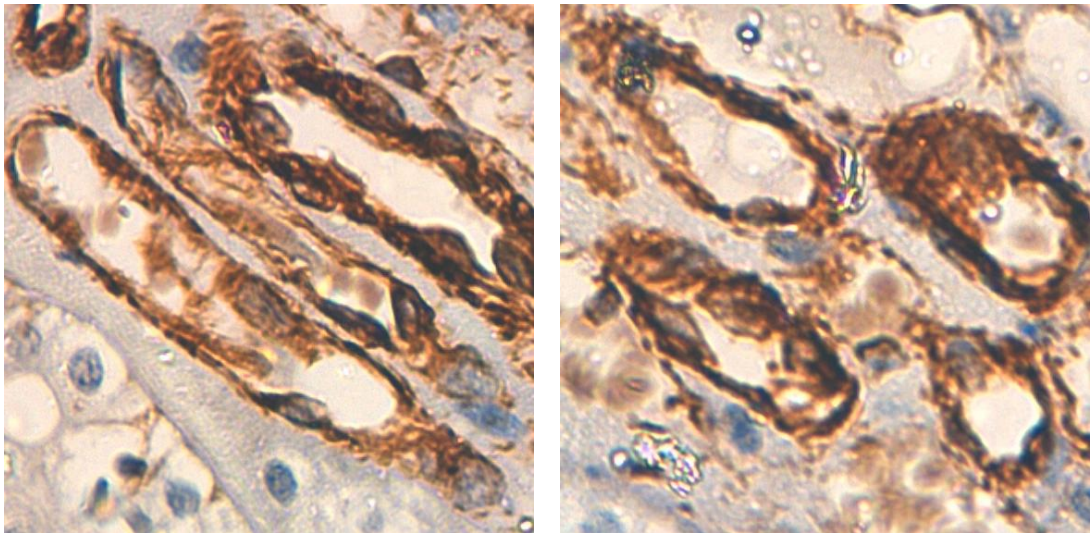
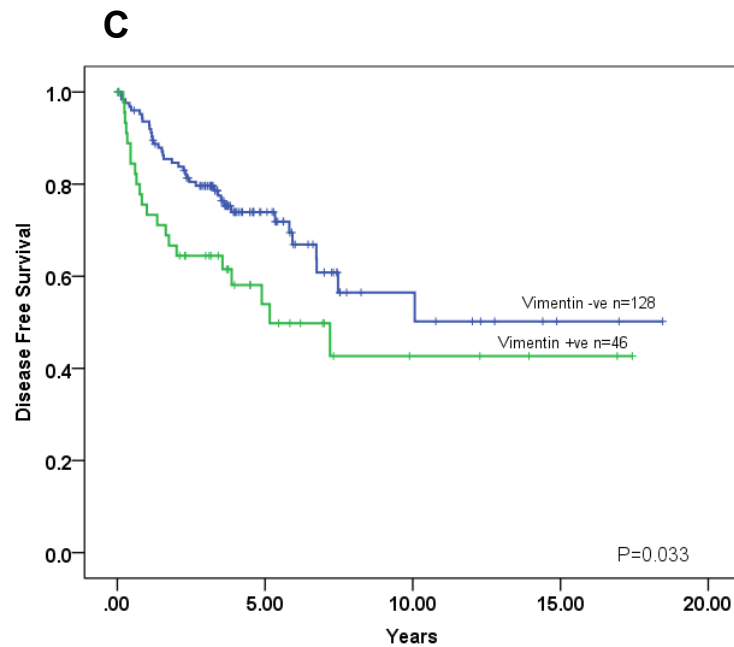
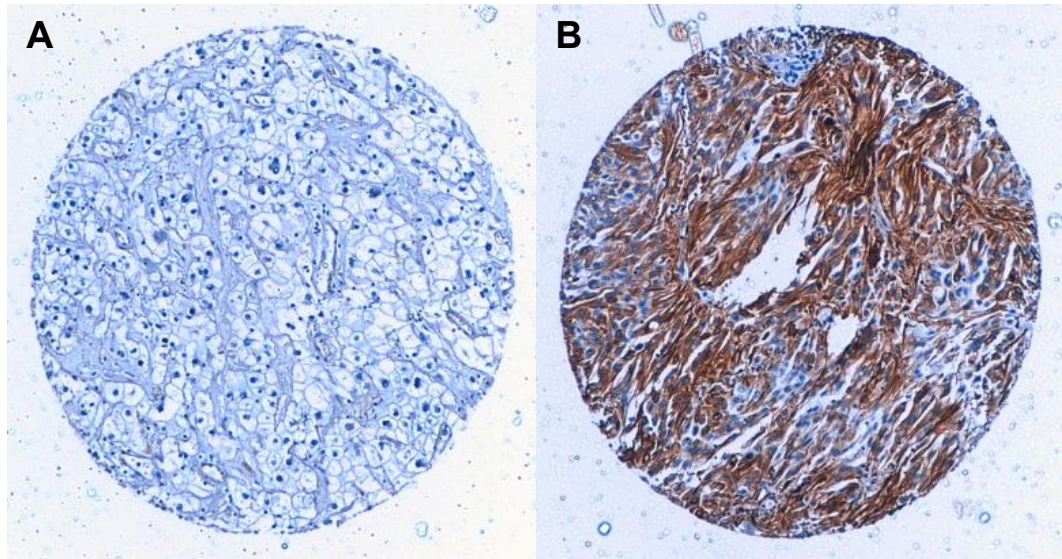


Figure 2.21 Immunohistochemical staining of vimentin in endothelial structures in normal kidney tissue acts as a positive control for specificity of the vimentin antibody used. Images captured at x25 magnification.



| Score | Mean DFS |
|--------------|----------|
| Vimentin -ve | 11.5 |
| Vimentin +ve | 8.9 |
| Overall | 11.0 |

Figure 2.22 Immunohistochemical staining of RCC TMAs for vimentin expression and Kaplan-Meier DFS analysis. (A) Representative tumour core scored as vimentin negative. (B) Representative tumour core scored as vimentin positive. (C) Kaplan-Meier survival curves for vimentin staining vimentin negative n=128 and vimentin positive n=46 with mean disease free survival shown below. P=0.033 as determined by Log-rank comparison.

Table 2.22 Crosstabulation of vimentin with histopathological characteristics of RCC. Significance calculated by Chi-squared or Fisher's exact test as relevant.

| | Vimentin negative | Vimentin positive |
|-----------------------------------|-------------------|-------------------|
| Grade 1 and 2 | 97 | 25 |
| Grade 3 and 4 | 31 | 21 |
| | | P=0.006 |
| Tumour size <7cm | 75 | 26 |
| Tumour size >7cm | 53 | 20 |
| | | P=0.807 |
| Vascular invasion -ve | 80 | 26 |
| Vascular invasion +ve | 48 | 20 |
| | | P=0.476 |
| Microcapsular invasion -ve | 109 | 34 |
| Microcapsular invasion +ve | 19 | 12 |
| | | P=0.087 |
| Micronecrosis -ve | 68 | 19 |
| Micronecrosis +ve | 58 | 27 |
| | | P=0.141 |
| Non-clear cell carcinoma | 20 | 10 |
| Clear cell carcinoma | 108 | 36 |
| | | P=0.346 |
| Non-Papillary | 113 | 38 |
| Papillary | 15 | 8 |
| | | P=0.330 |

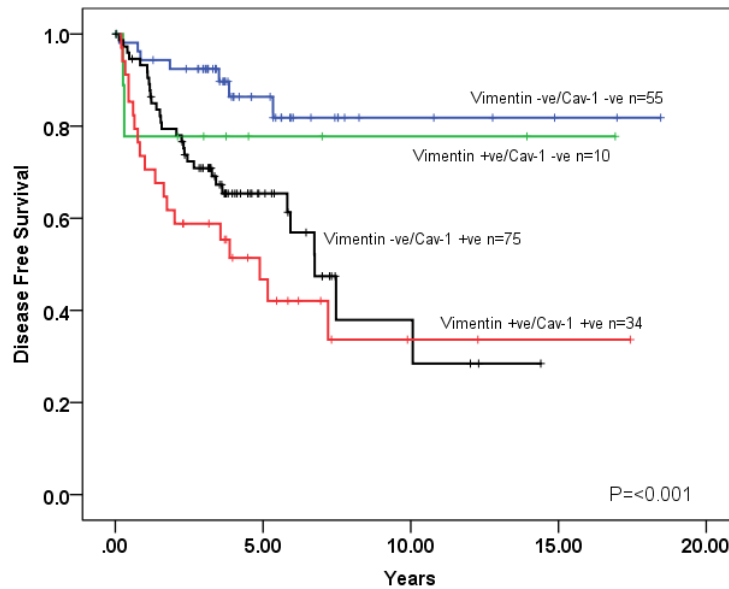
Table 2.23 Cox regression analysis of vimentin expression with histopathological characteristics of RCC. Analysis performed using the 'Enter' method. Both vimentin expression and vascular invasion rejected by the 'Forward Stepwise' (Likelihood ratio) model as not influential. 95% CI=95% Confidence Interval.

| Prognostic indicator | Hazard ratios | 95% CI | P value |
|-----------------------------|----------------------|---------------|----------------|
| Vimentin negative | 1 | | |
| Vimentin positive | 1.3 | 0.716-2.292 | 0.405 |
| Grade 1 and 2 | 1 | | |
| Grade 3 and 4 | 2.0 | 1.094-3.551 | 0.024 |
| Size <7cm | 1 | | |
| Size >7cm | 2.4 | 1.329-4.218 | 0.003 |
| Vascular invasion -ve | 1 | | |
| Vascular invasion +ve | 1.8 | 0.967-3.377 | 0.032 |
| Capsular invasion -ve | 1 | | |
| Capsular invasion +ve | 1.9 | 1.057-3.477 | 0.032 |
| Micronecrosis -ve | 1 | | |
| Micronecrosis +ve | 3.0 | 1.574-5.804 | <0.001 |

A

| | Cav-1 negative | Cav-1 positive |
|-------------------|----------------|----------------|
| Vimentin negative | 53 | 75 |
| Vimentin positive | 12 | 34 |

P=0.065

B

| Score | Mean DFS |
|------------------------|----------|
| Vimentin -ve/Cav-1 -ve | 15.6 |
| Vimentin +ve/Cav-1 -ve | 13.2 |
| Vimentin -ve/Cav-1 +ve | 7.5 |
| Vimentin +ve/Cav-1 +ve | 7.6 |
| Overall | 11.0 |

Figure 2.23 Correlation of vimentin with CAV1 expression and Kaplan-Meier DFS analysis. (A) Cross tabulation of vimentin and CAV1 expression in RCC tumour cores. No significant correlation $P=0.065$ as determined by Chi-squared. (B) Kaplan-Meier survival curves plotted for vimentin and CAV1 expressed as a composite variable (vimentin –ve/CAV1 –ve $n=55$, vimentin +ve/CAV1 –ve $n=10$, vimentin –ve/CAV1 +ve $n=75$, vimentin +ve/CAV1 +ve $n=34$) mean disease free survival shown below. $P < 0.001$ as determined by Log-rank comparison.

Table 2.24 Crosstabulation of vimentin and CAV1 with histopathological characteristics of RCC. Significance calculated by Chi-squared or Fisher's exact test as relevant.

| | All other tumours | Vimentin +ve/Cav-1 +ve |
|----------------------------|-------------------|------------------------|
| Grade 1 and 2 | 106 | 16 |
| Grade 3 and 4 | 34 | 18 |
| | | P=<0.001 |
| Tumour size <7cm | 81 | 20 |
| Tumour size >7cm | 59 | 14 |
| | | P=0.918 |
| Vascular invasion -ve | 89 | 17 |
| Vascular invasion +ve | 51 | 17 |
| | | P=0.146 |
| Microcapsular invasion -ve | 120 | 23 |
| Microcapsular invasion +ve | 20 | 11 |
| | | P=0.014 |
| Micronecrosis -ve | 73 | 14 |
| Micronecrosis +ve | 65 | 20 |
| | | P=0.221 |
| Non-clear cell carcinoma | 25 | 5 |
| Clear cell carcinoma | 115 | 29 |
| | | P=0.663 |
| Non-Papillary | 120 | 31 |
| Papillary | 20 | 3 |
| | | P=0.299 |

Table 2.25 Cox regression analysis of vimentin and CAV1 expression with histopathological characteristics of RCC. Analysis performed using the 'Enter' method. Both vimentin and CAV1 expression and vascular invasion rejected by the 'Forward Stepwise' (Likelihood ratio) model as not influential. 95% CI=95% Confidence Interval.

| Prognostic indicator | Hazard ratios | 95% CI | P value |
|-------------------------|---------------|-------------|---------|
| Vimentin/Cav-1 negative | 1 | | |
| Vimentin/Cav-1 positive | 1.6 | 0.840-2.909 | 0.159 |
| Grade 1 and 2 | 1 | | |
| Grade 3 and 4 | 1.9 | 1.063-3.432 | 0.030 |
| Size <7cm | 1 | | |
| Size >7cm | 2.5 | 1.394-4.484 | 0.002 |
| Vascular invasion -ve | 1 | | |
| Vascular invasion +ve | 1.8 | 0.978-3.357 | 0.059 |
| Capsular invasion -ve | 1 | | |
| Capsular invasion +ve | 1.8 | 0.951-3.257 | 0.072 |
| Micronecrosis -ve | 1 | | |
| Micronecrosis +ve | 3.1 | 1.603-5.901 | <0.001 |

2.3.7 MCT4 expression in RCC tumours does not identify high risk patients alone or as a covariate with CAV1

To control for the specificity of the MCT4 antibody selected, light immunohistochemical staining of tubules in normal kidney tissue samples was used as a positive control for MCT4 staining[238] (Figure 2.24). Immunohistochemical staining of RCC tumour cores with anti-MCT4 found scorable positive membrane staining (Figure 2.25). Positive staining varied in intensity between tumour cores and as such could be scored accordingly. Absence of membrane staining was termed MCT4 score 0 (Figure 2.26 A), light membrane staining was termed MCT4 score 1 (Figure 2.26 B), medium membrane staining was termed MCT4 score 2 (Figure 2.26 C) and strong membrane staining was termed MCT4 score 3 (Figure 2.26 D). Such scoring resulted in 50 tumours identified as MCT4 score 0, 49 tumours identified as MCT4 score 1, 49 tumours identified as MCT4 score 2 and 26 tumours identified as MCT4 score 3. Kaplan-Meier DFS analysis found MCT4 score 3 tumours to have the lowest mean DFS of 4.9 years ($P < 0.001$) (Figure 2.26 A). MCT4 score 1 and MCT4 score 2 produced overlapping survival curves (while MCT2 provides a mean disease free survival of 5.4 years this mean is skewed by rapid censoring after 5 years and the relapse of the last patient in the group). As such, scoring was recoded as: MCT4 0 recoded MCT4 negative, MCT4 score 1 and MCT4 score 2 recoded as MCT4 weak positive and MCT4 3 recoded as MCT4 strong positive. Repeating the Kaplan-Meier DFS analysis with this recoding found MCT4 weak positive to give a mean DFS of 9.9 years, slightly lower than that of overall mean disease free survival ($P < 0.001$) (Figure 2.26 B).

Crostabulation of MCT4 with histological characteristics of RCC found MCT4 to correlate with increased tumour grade ($P < 0.001$), increased vascular invasion ($P < 0.001$) and with micronecrosis ($P = 0.044$) but not with tumour size or microcapsular invasion. MCT4 expression was not specific to either clear cell or

papillary histotypes (Table 2.26). Multivariate Cox regression analysis using the enter function showed MCT4 to have an associated hazard ratio of 1.9 (P=0.049), higher than both vascular and microcapsular invasion (Table 2.27 A). MCT4 also entered into the forward stepwise (likelihood ratio) function with a hazard ratio (2.1 P=0.020) equal to microcapsular invasion and just less than grade (HR=2.2 P=0.008) (Table 2.27 B).

Crosstabulation analysis of MCT4 with CAV1, aimed at examining the association of the two markers in RCC tumours, found no significant correlation between the two (P=0.103) (Figure 2.27 A). Kaplan-Meier DFS analysis of the MCT4/CAV1 covariate found MCT4 +ve/CAV1 +ve tumours to have a mean DFS of 5.1 years, similar to that of MCT4 alone, indicating no real synergistic effect of the marker combination (P=<0.001) (Figure 2.27 B).

Crosstabulation of the MCT4/CAV1 covariate with histopathological characteristics of RCC found the same correlations as with MCT4 univariate, these being between grade (P=<0.001), vascular invasion (P=<0.001) and micronecrosis (P=0.025) (Table 2.28). Again, as with MCT4 alone, no distinction in terms of histological subtype was observed. However, one additional correlation was detected between the covariate and presence of microcapsular invasion (P=0.033) (Table 2.28).

Multivariate Cox regression analysis of the MCT4/CAV1 covariate using the enter function actually found the combination of MCT4 and CAV1 to have a lower hazard ratio non-significant hazard ratio compared to MCT4 or CAV1 alone (HR=1.5 P=0.289). MCT4/CAV1 was rejected by the forward stepwise (likelihood ratio) function as not influential to the analysis (Table 2.29).

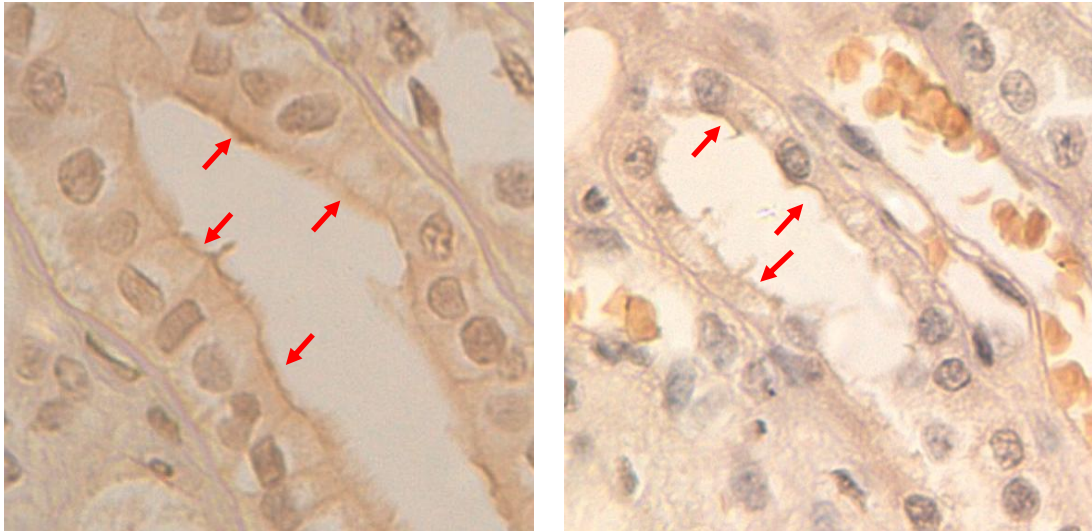


Figure 2.24 Immunohistochemical staining of MCT4 in the epithelial tubule cells in normal kidney acts as a specificity control for the MCT4 antibody selected. Red arrows indicate the presence of specific apical staining for MCT4 in normal kidney epithelial tubule cells.

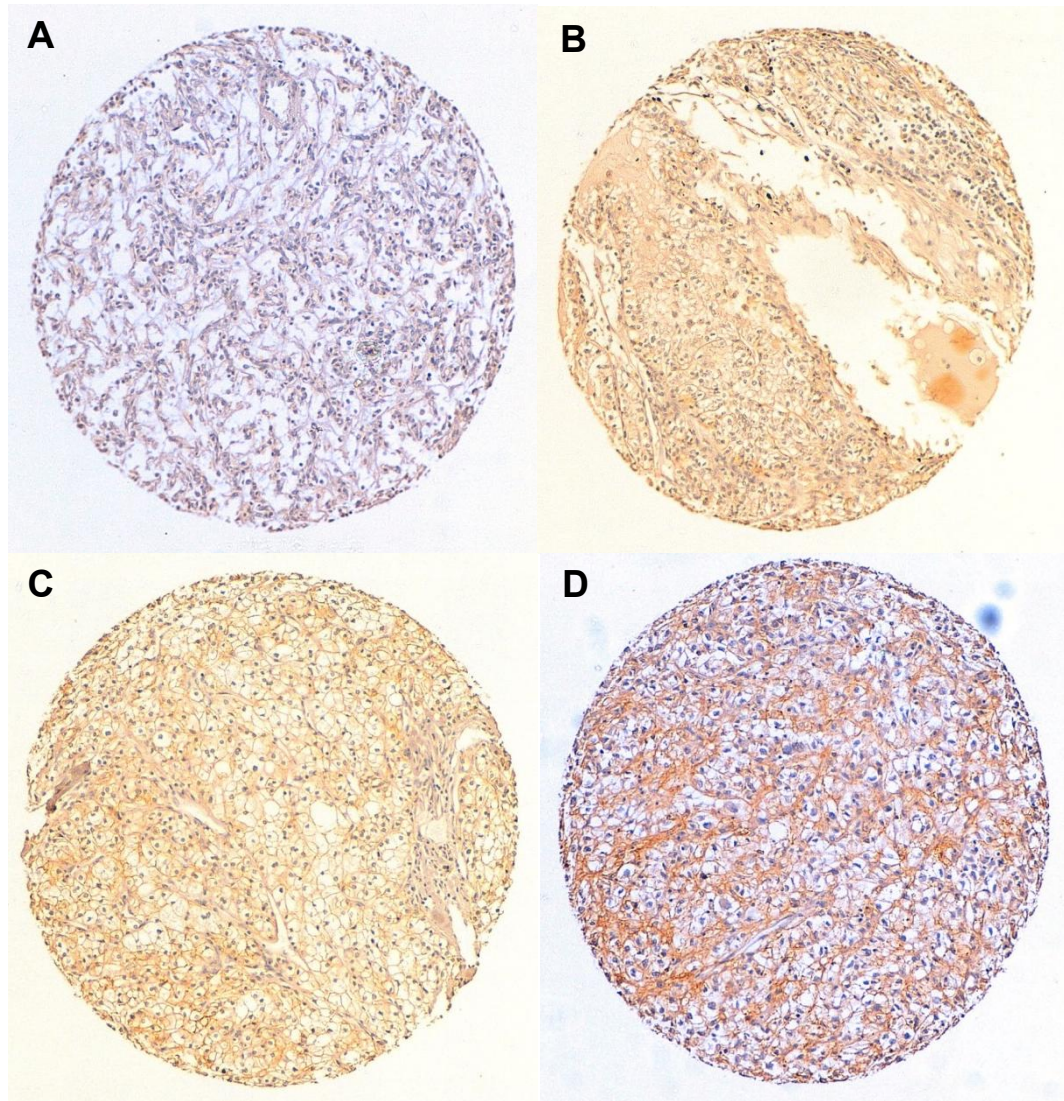


Figure 2.25 Immunohistochemical staining of RCC TMAs for MCT4 expression captured at x10 magnification. Representative tumours of MCT4 scoring criteria (A) MCT4 score 0, (B) MCT4 score 1, (C) MCT4 score 2 and (D) MCT4 score 3.

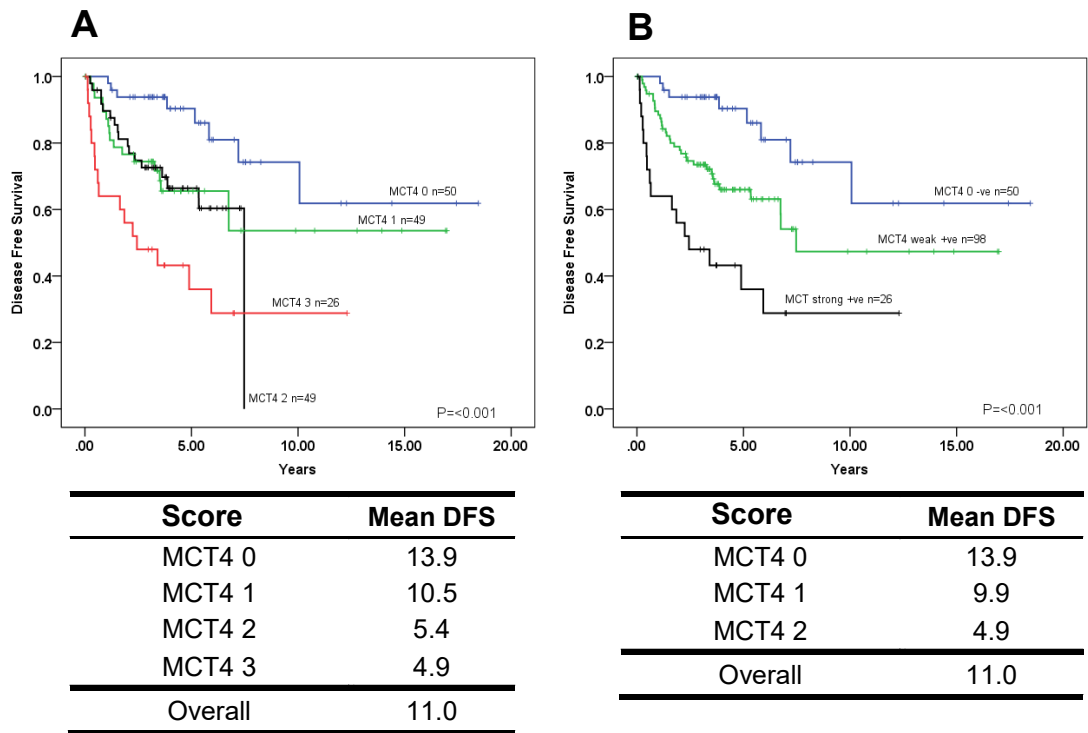


Figure 2.26 Kaplan-Meier DFS curves for MCT4 expression (A) Kaplan-Meier DFS curves for MCT4 plotted using the scoring criteria without recoding (MCT4 0 n=50, MCT4 1 n=49, MCT4 2 n=49 and MCT4 3 n=26) with corresponding mean DFS in years shown below. P=<0.001 as determined by Log-rank comparison. (B) Kaplan-Meier DFS curves for MCT4 staining re-plotted with a score of 0 recoded as MCT4 negative n=50, scores 1 to 2 pooled and recoded as MCT4 weak positive n=98 and a score of 3 recoded as MCT4 strong positive n=26. P=<0.001 as determined by Log-rank comparison.

Table 2.26 Crosstabulation of MCT4 with histopathological characteristics of RCC. Significance calculated by Chi-squared or Fisher's exact test as relevant.

| | MCT4 negative | MCT4 positive |
|-----------------------------------|----------------------|----------------------|
| Grade 1 and 2 | 112 | 10 |
| Grade 3 and 4 | 36 | 16 |
| | | P=<0.001 |
| Tumour size <7cm | 89 | 12 |
| Tumour size >7cm | 59 | 14 |
| | | P=0.183 |
| Vascular invasion -ve | 98 | 8 |
| Vascular invasion +ve | 50 | 18 |
| | | P=<0.001 |
| Microcapsular invasion -ve | 124 | 19 |
| Microcapsular invasion +ve | 24 | 7 |
| | | P=0.188 |
| Micronecrosis -ve | 79 | 8 |
| Micronecrosis +ve | 68 | 17 |
| | | P=0.044 |
| Non-clear cell carcinoma | 29 | 1 |
| Clear cell carcinoma | 119 | 25 |
| | | P=0.036 |
| Non-Papillary | 126 | 25 |
| Papillary | 22 | 1 |
| | | P=0.105 |

Table 2.27 Cox regression analysis of combined MCT4 expression with histopathological characteristics of RCC. (A) Analysis performed using the 'Enter' method. (B) Analysis performed using the 'Forward Stepwise' (Likelihood ratio) vascular invasion rejected by the model as not influential. 95% CI=95% Confidence Interval

A

| Prognostic indicator | Hazard ratios | 95% CI | P value |
|-----------------------------|----------------------|---------------|----------------|
| MCT4 negative | 1 | | |
| MCT4 positive | 1.9 | 1.002-3.580 | 0.049 |
| Grade 1 and 2 | 1 | | |
| Grade 3 and 4 | 2.0 | 1.086-3.502 | 0.025 |
| Size <7cm | 1 | | |
| Size >7cm | 2.5 | 1.338-4.383 | 0.002 |
| Vascular invasion -ve | 1 | | |
| Vascular invasion +ve | 1.6 | 0.822-2.969 | 0.173 |
| Capsular invasion -ve | 1 | | |
| Capsular invasion +ve | 1.9 | 1.035-3.427 | 0.038 |
| Micronecrosis -ve | 1 | | |
| Micronecrosis +ve | 3.2 | 1.701-6.178 | <0.001 |

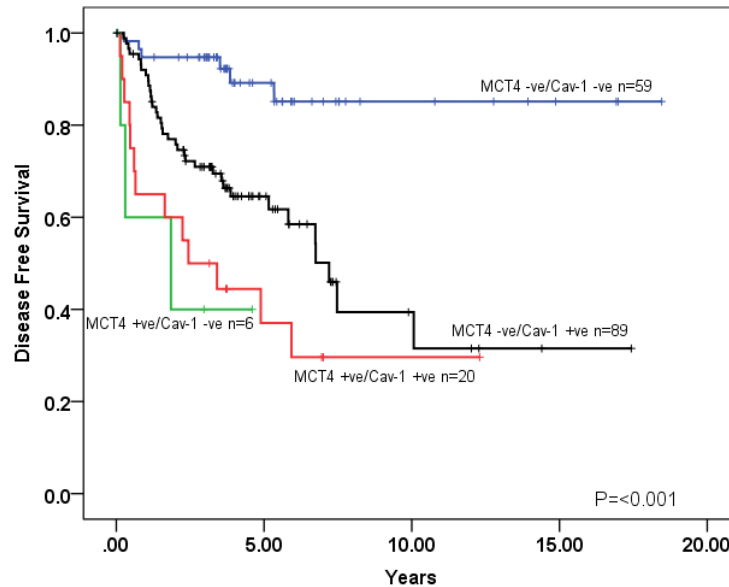
B

| Prognostic indicator | Hazard ratios | 95% CI | P value |
|-----------------------------|----------------------|---------------|----------------|
| MCT4 negative | 1 | | |
| MCT4 positive | 2.1 | 1.125-3.913 | 0.020 |
| Grade 1 and 2 | 1 | | |
| Grade 3 and 4 | 2.2 | 1.219-3.845 | 0.008 |
| Size <7cm | 1 | | |
| Size >7cm | 2.7 | 1.556-4.761 | <0.001 |
| Capsular invasion -ve | 1 | | |
| Capsular invasion +ve | 2.1 | 1.143-3.694 | 0.016 |
| Micronecrosis -ve | 1 | | |
| Micronecrosis +ve | 3.3 | 1.720-6.241 | <0.001 |

A

| | Cav-1 negative | Cav-1 positive |
|---------------|----------------|----------------|
| MCT4 negative | 59 | 89 |
| MCT4 positive | 6 | 20 |

P=0.103

B

| Score | Mean DFS |
|--------------------|----------|
| MCT4 -ve/Cav-1 -ve | 16.2 |
| MCT4 +ve/Cav-1 -ve | 2.3 |
| MCT4 -ve/Cav-1 +ve | 8.6 |
| MCT4 +ve/Cav-1 +ve | 5.1 |
| Overall | 11.0 |

Figure 2.27 Correlation of MCT4 with CAV1 expression and Kaplan-Meier DFS analysis. (A) Cross tabulation of MCT4 and CAV1 expression in RCC tumour cores. No significant correlation $P=0.103$ as determined by Chi-squared. (B) Kaplan-Meier DFS curves plotted for MCT4 and CAV1 expressed as a composite variable (MCT4 -ve/CAV1 -ve $n=59$, MCT +ve/CAV1 -ve $n=6$, MCT4 -ve/CAV1 +ve $n=89$, MCT4 +ve/CAV1 $n=20$) mean disease free survival shown below. $P < 0.001$ as determined by Log-rank comparison.

Table 2.28 Crosstabulation of MCT4 and CAV1 expression with histopathological characteristics of RCC. Significance calculated by Chi-squared or Fisher's exact test as relevant.

| | All other tumours | MCT4 +ve/Cav-1 +ve |
|-----------------------------------|--------------------------|---------------------------|
| Grade 1 and 2 | 116 | 6 |
| Grade 3 and 4 | 38 | 14 |
| | | P=<0.001 |
| Tumour size <7cm | 91 | 10 |
| Tumour size >7cm | 63 | 10 |
| | | P=0.438 |
| Vascular invasion -ve | 101 | 5 |
| Vascular invasion +ve | 53 | 15 |
| | | P=<0.001 |
| Microcapsular invasion -ve | 130 | 13 |
| Microcapsular invasion +ve | 24 | 7 |
| | | P=0.033 |
| Micronecrosis -ve | 82 | 5 |
| Micronecrosis +ve | 71 | 14 |
| | | P=0.025 |
| Non-clear cell carcinoma | 29 | 1 |
| Clear cell carcinoma | 125 | 19 |
| | | P=0.103 |
| Non-Papillary | 132 | 19 |
| Papillary | 22 | 1 |
| | | P=0.220 |

Table 2.29 Cox regression analysis of MCT4 and CAV1 expression with histopathological characteristics of RCC. Analysis performed using the 'Enter' method. Both MCT4 and CAV1 expression and vascular invasion rejected by the 'Forward Stepwise' (Likelihood ratio) model as not influential. 95% CI=95% Confidence Interval.

| Prognostic indicator | Hazard ratios | 95% CI | P value |
|-----------------------------|----------------------|---------------|----------------|
| MCT4/Cav-1 negative | 1 | | |
| MCT4/Cav-1 positive | 1.5 | 0.730-2.886 | 0.289 |
| Grade 1 and 2 | 1 | | |
| Grade 3 and 4 | 2.0 | 1.107-3.567 | 0.021 |
| Size <7cm | 1 | | |
| Size >7cm | 2.4 | 1.337-4.232 | 0.003 |
| Vascular invasion -ve | 1 | | |
| Vascular invasion +ve | 1.7 | 0.876-3.136 | 0.120 |
| Capsular invasion -ve | 1 | | |
| Capsular invasion +ve | 1.9 | 1.058-3.496 | 0.032 |
| Micronecrosis -ve | 1 | | |
| Micronecrosis +ve | 3.2 | 1.655-6.032 | <0.001 |

2.3.8 Cavin-1 expression in RCC tumours does not identify high risk patients as a univariate or covariate with CAV1

To control for the specificity of the Cavin-1 antibody selected, immunohistochemical staining of the endothelium of kidney tissue samples was used as a positive control, as expression of Cavin-1 in the endothelium has been well characterised[74] (Figure 2.28). Immunohistochemical staining of RCC tumour cores with Cavin-1 found scorable positive membrane staining with positive staining to be relatively uniform between tumours (Figure 2.29 A and B). Hence, negative tumours were classified as Cavin-1 negative and positive tumours as Cavin-1 positive. Such scoring identified the majority of tumours (n=133) to be Cavin-1 positive and the remaining tumours (n=41) to be Cavin-1 negative. Kaplan-Meier DFS analysis of scoring found no distinction in terms of disease free survival between the two groups (P=0.598), with a mean DFS for Cavin-1 positive patients of 10.4 years and 11.3 for Cavin-1 negative (Figure 2.29 C).

Crosstabulation of Cavin-1 with histopathological characteristics of RCC found no correlation with any characteristic other than prevalence in clear cell carcinoma (P=0.016) (Table 2.30). Multivariate Cox regression analysis using the enter function indicated Cavin-1 positivity as not influential in predicting patient risk of relapse, resulting in a non-significant hazard ratio of 1.2 (P=0.664) and was rejected from the forward stepwise (likelihood ratio) function (Table 2.29).

Cavin-1 correlated strongly with CAV1 in crosstabulation (P=<0.001) (Figure 2.30 A). Kaplan-Meier DFS analysis found a mean DFS of 8.6 years for Cavin-1 +ve/CAV1 +ve tumours, no greater than that of Cavin -ve/CAV1 +ve tumours which had a mean DFS of 6.3 years (P=<0.001) (Figure 2.30 B). Crosstabulation of the Cavin-1/CAV1 covariate with histopathological characteristics of RCC found correlations with increased grade (P=0.039), vascular invasion (P=<0.001), microcapsular invasion (P=0.011) and micronecrosis (P=0.006) and a prevalence in

clear cell carcinoma ($P=0.010$) (Table 2.32). Multivariate Cox regression analysis of the Cavin-1/CAV1 covariate using the enter function did not increase the associated hazard of Cavin-1 which remained at 1.3 ($P=0.382$). Using the forward stepwise (likelihood ratio) function Cavin-1/CAV1 was rejected as not influential to the analysis (Table 2.33).

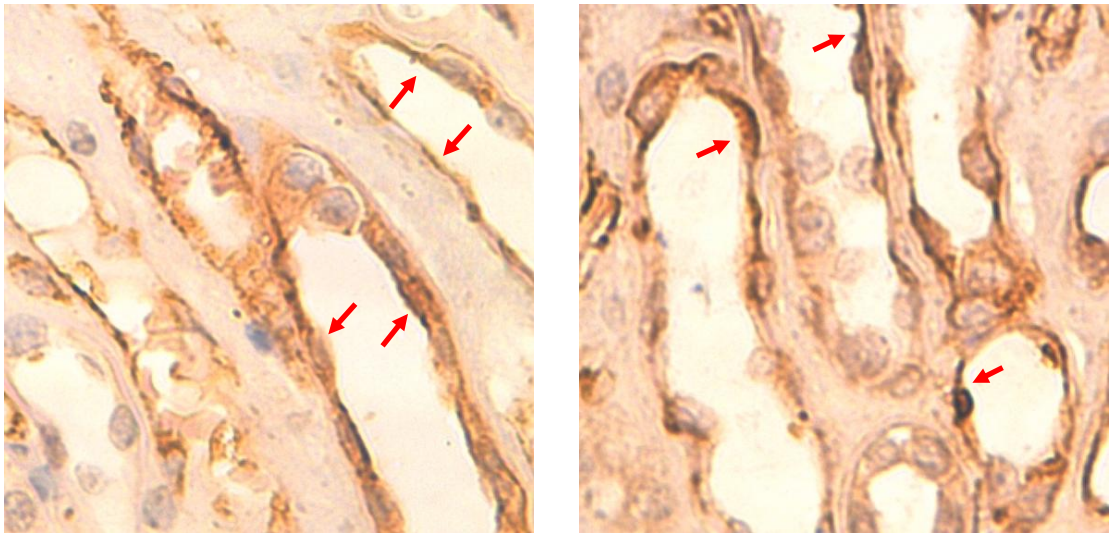
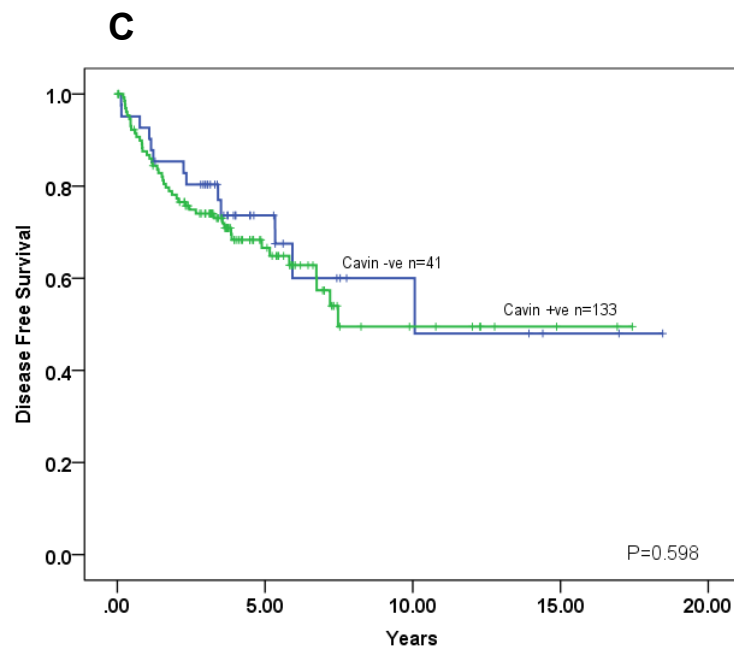
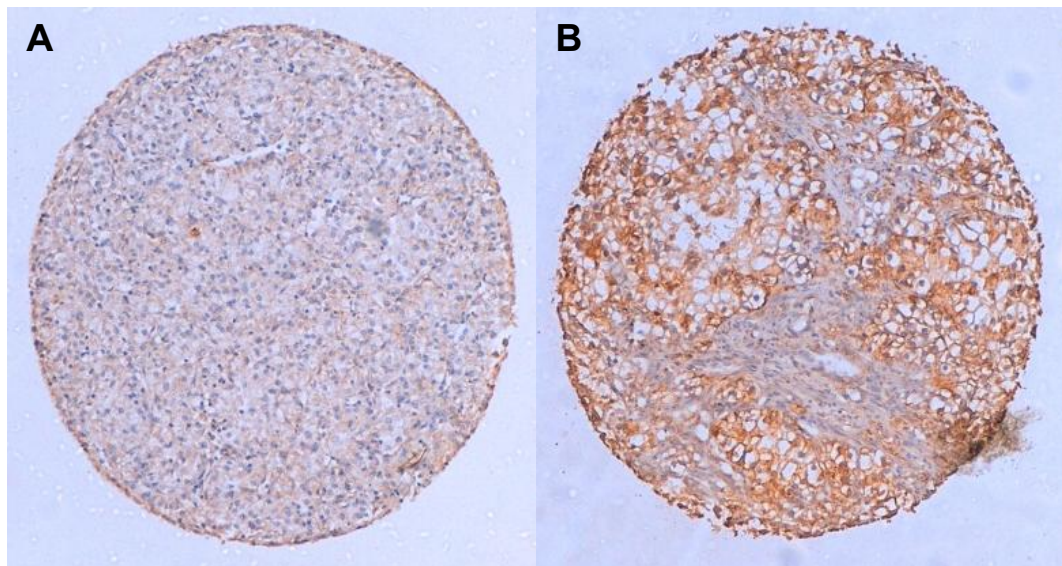


Figure 2.28 Immunohistochemical staining of cavin-1 in endothelial structures in the normal kidney acts as a positive control for the specificity of the cavin-1 antibody used. Red arrows indicate the presence of cavin-1 staining in these endothelial structures. Images captured at x25 magnification.



| Score | Mean DFS |
|-----------|----------|
| Cavin -ve | 11.3 |
| Cavin +ve | 10.4 |
| Overall | 11.0 |

Figure 2.29 Immunohistochemical staining of RCC TMAs for Cavin-1 expression and Kaplan-Meier DFS analysis. (A) Representative Cavin-1 negative tumour core. (B) Representative Cavin-1 positive tumour core. (C) Kaplan-Meier DFS curves for Cavin-1 plotted Cavin-1 negative n=41 and Cavin-1 positive n=133 with corresponding mean disease free survival shown below. P=0.598 as determined by Log-rank comparison.

Table 2.30 Crosstabulation of Cavin-1 expression with histopathological characteristics of RCC. Significance calculated by Chi-squared or Fisher's exact test as relevant.

| | Cavin negative | Cavin positive |
|-----------------------------------|-----------------------|-----------------------|
| Grade 1 and 2 | 29 | 93 |
| Grade 3 and 4 | 12 | 40 |
| | | P=0.921 |
| Tumour size <7cm | 26 | 75 |
| Tumour size >7cm | 15 | 58 |
| | | P=0.426 |
| Vascular invasion -ve | 27 | 79 |
| Vascular invasion +ve | 14 | 54 |
| | | P=0.459 |
| Microcapsular invasion -ve | 36 | 107 |
| Microcapsular invasion +ve | 5 | 26 |
| | | P=0.355 |
| Micronecrosis -ve | 21 | 66 |
| Micronecrosis +ve | 19 | 66 |
| | | P=0.782 |
| Non-clear cell carcinoma | 13 | 17 |
| Clear cell carcinoma | 28 | 116 |
| | | P=0.005 |
| Non-Papillary | 29 | 122 |
| Papillary | 12 | 11 |
| | | P=0.001 |

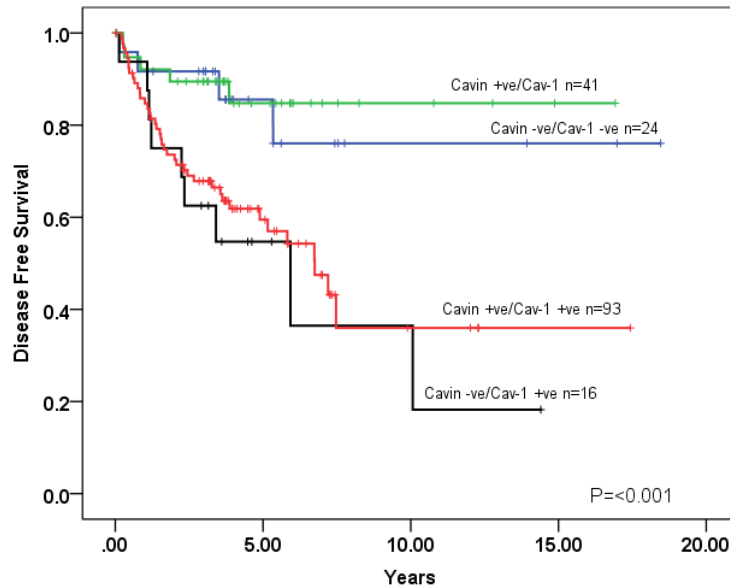
Table 2.31 Cox regression analysis of Cavin-1 expression with histopathological characteristics of RCC. Analysis performed using the 'Enter' method. Both Cavin-1 expression and vascular invasion rejected by the forward likelihood ratio method as not influential. 95% CI=95% Confidence Interval.

| Prognostic indicator | Hazard ratios | 95% CI | P value |
|-----------------------------|----------------------|---------------|----------------|
| Cavin negative | 1 | | |
| Cavin positive | 1.2 | 0.603-2.213 | 0.664 |
| Grade 1 and 2 | 1 | | |
| Grade 3 and 4 | 2.1 | 1.175-3.730 | 0.012 |
| Size <7cm | 1 | | |
| Size >7cm | 2.3 | 1.292-4.047 | 0.005 |
| Vascular invasion -ve | 1 | | |
| Vascular invasion +ve | 1.8 | 0.949-3.284 | 0.073 |
| Capsular invasion -ve | 1 | | |
| Capsular invasion +ve | 2.0 | 1.086-3.573 | 0.026 |
| Micronecrosis -ve | 1 | | |
| Micronecrosis +ve | 3.1 | 1.601-5.892 | 0.001 |

A

| | Cav-1 negative | Cav-1 positive |
|----------------|----------------|----------------|
| Cavin negative | 25 | 16 |
| Cavin positive | 40 | 93 |

P=<0.001

B

| Score | Mean DFS |
|---------------------|----------|
| Cavin -ve/Cav-1 -ve | 14.8 |
| Cavin +ve/Cav-1 -ve | 14.6 |
| Cavin -ve/Cav-1 +ve | 6.3 |
| Cavin +ve/Cav-1 +ve | 8.6 |
| Overall | 11.0 |

Figure 2.30 Correlation of Cavin-1 with CAV1 expression and impact on disease free survival. (A) Cross tabulation of Cavin-1 and CAV1 expression in RCC tumour cores. Significant correlation $P=<0.001$ as determined by Chi-squared. (B) Kaplan-Meier DFS curves plotted for Cavin-1 and CAV1 expressed as a composite variable (Cavin-1 -ve/CAV1 -ve $n=24$, Cavin-1 +ve/CAV1 -ve $n=41$, Cavin-1 -ve/CAV1 +ve $n=16$, Cavin-1 +ve/CAV1 $n=93$) mean disease free survival shown below. $P=<0.001$ as determined by Log-rank comparison.

Table 2.32 Crosstabulation of Cavin-1 and CAV1 expression with histopathological characteristics of RCC. Significance calculated by Chi-squared or Fisher's exact test as relevant.

| | All other tumours | Cavin +ve/Cav-1 +ve |
|----------------------------|-------------------|---------------------|
| Grade 1 and 2 | 63 | 59 |
| Grade 3 and 4 | 18 | 34 |
| | | P=0.039 |
| Tumour size <7cm | 49 | 52 |
| Tumour size >7cm | 32 | 41 |
| | | P=0.541 |
| Vascular invasion -ve | 61 | 45 |
| Vascular invasion +ve | 20 | 48 |
| | | P=<0.001 |
| Microcapsular invasion -ve | 73 | 70 |
| Microcapsular invasion +ve | 8 | 23 |
| | | P=0.011 |
| Micronecrosis -ve | 49 | 38 |
| Micronecrosis +ve | 30 | 55 |
| | | P=0.006 |
| Non-clear cell carcinoma | 21 | 9 |
| Clear cell carcinoma | 60 | 84 |
| | | P=0.005 |
| Non-Papillary | 64 | 87 |
| Papillary | 17 | 6 |
| | | P=0.005 |

Table 2.33 Cox regression analysis of Cavin-1 and CAV1 expression with histopathological characteristics of RCC. Analysis performed using the 'Enter' method. Both Cavin-1 and CAV1 expression and vascular invasion rejected by the forward likelihood ratio method as not influential. 95% CI=95% Confidence Interval.

| Prognostic indicator | Hazard ratios | 95% CI | P value |
|-----------------------|---------------|-------------|---------|
| Cavin/Cav-1 negative | 1 | | |
| Cavin/Cav-1 positive | 1.3 | 0.712-2.430 | 0.382 |
| Grade 1 and 2 | 1 | | |
| Grade 3 and 4 | 2.1 | 1.173-3.688 | 0.012 |
| Size <7cm | 1 | | |
| Size >7cm | 2.3 | 1.306-4.077 | 0.004 |
| Vascular invasion -ve | 1 | | |
| Vascular invasion +ve | 1.7 | 0.910-3.148 | 0.096 |
| Capsular invasion -ve | 1 | | |
| Capsular invasion +ve | 1.9 | 1.062-3.493 | 0.031 |
| Micronecrosis -ve | 1 | | |
| Micronecrosis +ve | 2.9 | 1.512-5.680 | <0.001 |

2.3.9 Regression modeling of all markers conducted as both simple covariate and composite covariates with CAV1 finds CD44+ve/CAV1+ve to be the strongest indicator of poor disease outcome

To understand which marker both alone and in combination with CAV1 is the most informative in terms of prognostic application, a Cox proportional hazard model was used with all covariates used entered as well as all histopathological covariates. This analysis found the CD44/CAV1 covariate to be the most informative marker of disease recurrence ($P < 0.001$), followed by microcapsular invasion ($P < 0.001$), grade ($P = 0.002$), CD105/CAV1 ($P = 0.001$), vascular invasion ($P = 0.010$) and size ($P = 0.031$) (Table 2.34). All other covariates were rejected by the model.

Table 2.34 Cox proportional hazard model of time to disease recurrence using the forward selection function. All histopathological variables and markers alone and in combination with CAV1 expression entered into the model.

| Prognostic indicator | Step | Chi-Square score | P value |
|-----------------------------|-------------|-------------------------|----------------|
| CD44/Cav-1 | 1 | 42.35 | <0.001 |
| Microcapsular Invasion | 2 | 42.32 | <0.001 |
| Grade | 3 | 9.75 | 0.002 |
| CD105/Cav-1 | 4 | 10.79 | 0.001 |
| Vascular Invasion | 5 | 6.71 | 0.010 |
| Size | 6 | 4.63 | 0.031 |

2.4 Discussion

The work presented in this chapter has focused on the investigation of common markers of CSC phenotype as indicators to identify patients at high risk of disease relapse and recurrence. These markers were examined alone and in combination with CAV1.

2.4.1 CAV1 covariate

Expression of CAV1 was found in 109 of the 174 patient tumours analysed with Kaplan-Meier analysis indicating a mean DFS of 8.2 years for patients with CAV1 +ve tumours; expression of CAV1 was revealed as a poor prognostic marker. Furthermore, CAV1 +ve tumours could be stratified during the scoring process into three distinct groups, with the increased intensity of CAV1 staining reflecting a worse outcome (mean DFS of 5.2 years in the most intense CAV1 3 group). In terms of histopathology, expression of CAV1 correlated positively with the presence of both vascular and capsular invasion, tumour grade and micronecrosis. In terms of histological subtyping, CAV1 expression is predominant in clear cell carcinomas, constituting 68% of these tumours. It was also found in the less aggressive papillary carcinomas, a subtype accounting for 34% of all RCC malignancies. The multivariate Cox regression analysis of CAV1 (which used both enter and forward stepwise (likelihood ratio) functions), found CAV1 positive tumours to serve as a significant independent prognostic marker, similar in power to grade. These findings are in agreement with previous studies in which CAV1 expression in RCC is concluded to have a negative effect on patient outcome, with such studies using both overlapping[99], [117], [256] and independent[257], [258] patient cohorts to that described in this current work.

2.4.2 CSC marker covariates

When analysed as simple covariates, only the markers CD44, vimentin and MCT4 had a significant impact upon patient outcome. The markers CD146, EpCAM and Cavin-1 were non-significant as predictors of poor disease outcome, as both simple covariates and in combination with CAV1.

2.4.3 CD44 covariate

Of all the markers examined, CD44 proved to be the most significant in terms of prognostic outcome. Similar to other studies performed on CD44 expression in RCC cohorts, CD44 +ve tumours were associated with a DFS drastically reduced DFS to 3.1 years. CD44 expression also showed a strong correlation with grade and presence of vascular invasion, but not microcapsular invasion, as well as micronecrosis. In the multivariate Cox regression model, CD44 +ve proved to be a potent prognostic marker with a substantial HR (2.9), which presents equivalent, but no greater, indication to that of other histological indices. Nevertheless, the results show CD44 to have potential as an independent variable of disease progression. These findings corroborate similar studies of CD44 expression in smaller RCC patient cohorts[167], [259]–[261].

The crosstabulation of CD44 with CAV1 indicates a strong correlation between the two markers, with 80% of all CD44 positive tumours also positive for CAV1. The composite covariate of CD44 +ve/CAV1 +ve showed such tumours to be associated with a very poor mean DFS of 2.5 years as well as providing a stronger prognostic indication of disease outcome in the Cox regression analysis (HR=3.3 P=0.013 forward stepwise). This composite covariate also proved to be the most significant of all covariates analysed in terms of the prediction of disease recurrence, indicating

its potential use as an independent prognostic marker combination for poor disease outcome in RCC.

As discussed previously, CD44 plays an influential role in the invasion and metastasis of cancer cells[163]. For example, an *in vitro* study investigating the effect of TNF- α on the invasive capacity of RCC cell lines found CD44 upregulation, together with the matrix metalloprotease (MMP-9), in the more invasive TNF- α treated cells[262]. Furthermore, siRNA targeting of CD44 expression in ACHN, 786-O and SN12PM6 cells resulted in a reduction of invasive and migratory capacity in these cells. The CD44 molecule has been reported to co-localise to CAV1 rich lipid rafts in a number of studies[171], [263], [264]. In a non-cancer study, Long et al.[263] investigated the uptake of the microorganism *Cryptococcus neoformans* by human brain microvascular cells. They identified co-localisation of CAV1 and CD44 within lipid rafts, membrane domains found to facilitate the cellular uptake and transport of the organism; siRNA silencing of CAV1 caused a reduction in the *in vitro* transport independent of CD44 spatial expression. The reported mechanism involved the microorganism stimulating the phosphorylation of CAV1 in a CD44-dependant manner. As such, a two-armed mechanism may be proposed by which CAV1 and CD44 interact to facilitate tumour cell vascular invasion and eventual metastatic disease (Figure 2.31). This could consist of stabilisation of CD44 by CAV1 within lipid rafts, enabling the invasive and migratory capacity of CD44 through its regulation of MMP complexes[265] and CD44 direct binding to hyaluronic acid both in the ECM and in the endothelial microenvironment[266]. The interaction of CD44 and CAV1 may lead to subsequent phosphorylation of CAV1 which would transduce pro-invasive cellular signalling to either support anchorage-independent survival through a c-Src/CAV1/Grb7 signalling complex[267] or aid in the rapid turnover of focal adhesion sites[116].

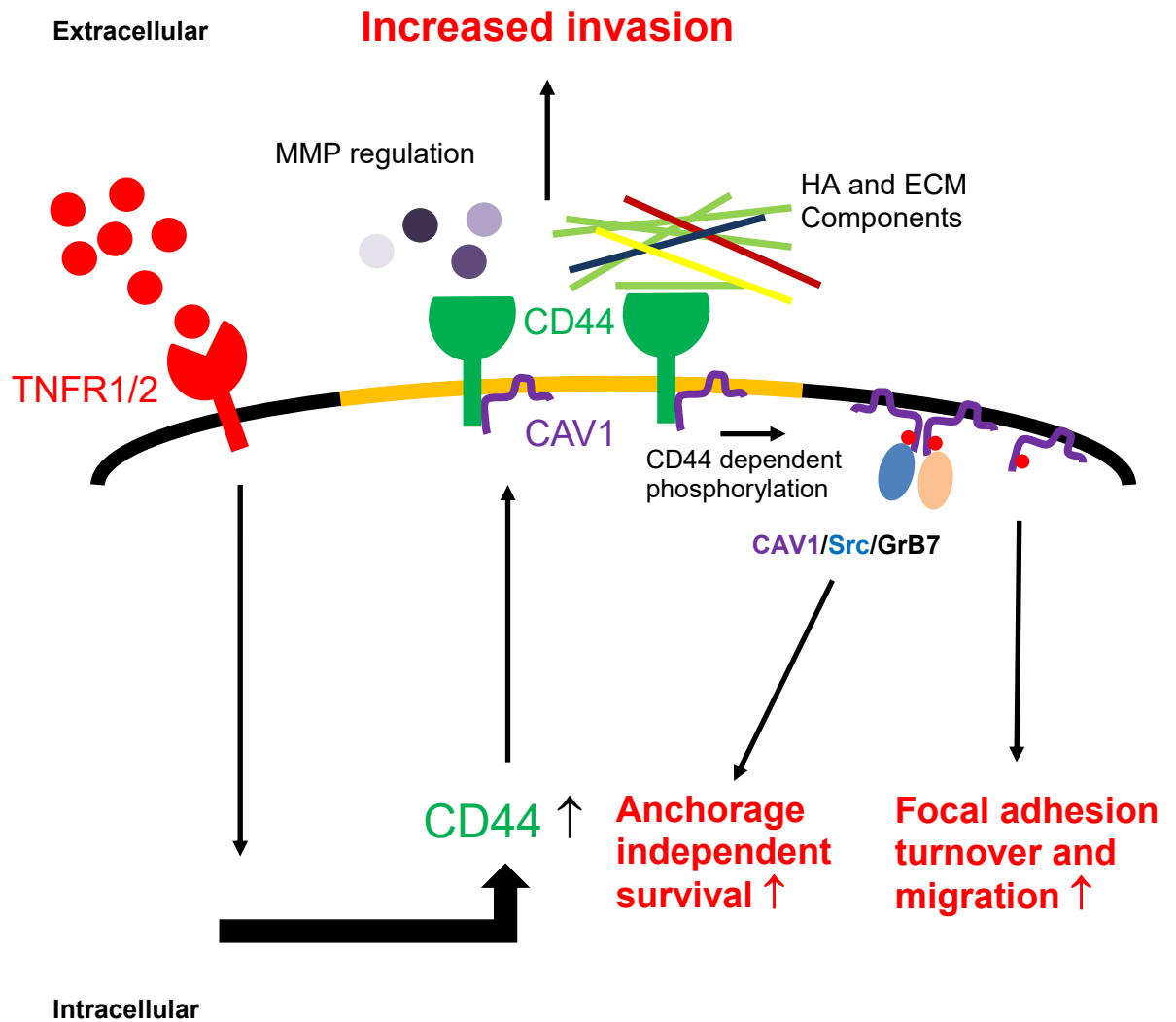


Figure 2.31 Putative model for CD44/CAV1 driven invasion. Co-localisation of CD44 to CAV1 in lipid rafts enables both the activation of CD44 and CD44 phosphorylation of CAV1. Activation of CD44 results in modulation of MMP regulation and interactions with ECM, while CAV1 phosphorylation results in the upregulation of anchorage independent survival through the CAV1/Src/GrB7 complex and increased migration through upregulated focal adhesion turnover.

2.4.4 MCT4 covariate

Immunoprobings of RCC tumour cores for MCT4 expression found distinct patient groups to be negative, weakly positive and strongly positive. MCT4 –ve tumours were associated with an improved prognostic outcome. Patients displaying strong membrane associated staining had the poorest outcome, with mean DFS of 4.2 years. These tumours also correlated strongly with the histopathological parameters

of increased grade, vascular invasion and micronecrosis. Such a correlation with micronecrosis may help to indicate tumours of higher metabolic activity, due to more efficient removal of lactate by MCT4[238]. No correlation was observed between MCT4 expression and the histological subtypes. Cox regression analysis found MCT4 to be an independent prognostic marker capable of identifying poor patient outcome (HR=2.1). No significant correlation was detected between CAV1 and MCT4. The composite covariate MCT4/CAV1 found no synergistic effect on DFS, which remained similar to that of the MCT4 +ve/CAV1 -ve tumours. Cox regression analysis of the MCT4/CAV1 covariate was not significant and failed to identify a poorer prognostic outcome, than that of either of the two markers alone. These findings were in agreement with previous epigenetic[237] and immunohistochemical studies[239], identifying poor disease outcome associated with MCT4 expression in RCC patients. These outcomes further help strengthen the use of MCT4 as a prognostic marker of poor disease outcome and MCT4 as a target for a molecular inhibitor approach for treatment of RCC.

Much of the research regarding MCT4 and CAV1 has been conducted into the relationship of CAV1 and MCT4 in stromal cells of tumours, particularly in malignancies of the breast, in which loss of CAV1 expression and gain in MCT4 expression seems to be important in the progression from an *in situ* to an invasive breast carcinoma[268]. In this work it appears that MCT4 and CAV1 constitute independent non-synergistic risk factors.

2.4.5 Vimentin covariate

The immunoreactivity of the intermediate filament protein vimentin found RCC patient tumours to be either positive or negative for the marker. Patient tumours positive for vimentin displayed a slightly decreased mean DFS of 8.9 years. Expression of vimentin only correlated with grade, and no other histopathological characteristic. Further vimentin was not significant as a prognostic indicator in the

Cox regression analysis. Crosstabulation of vimentin with CAV1 found a trend between the two markers approaching significance ($P=0.065$). Use of the two markers as a compound covariate to explore the effect upon DFS found the vimentin/CAV1 composite covariate not to be indicative of a poorer mean DFS compared to CAV1 expression alone. The covariate did correlate with microcapsular invasion, although this is also evident for CAV1 expression alone, which identified a larger proportion of positive patients (84% of patients showing CAV1 positivity also had evidence of microcapsular invasion). As a covariate in the Cox regression analysis, vimentin/CAV1 was unable to identify patients at greater risk of poor disease outcome ($HR=1.6$). It appeared that while vimentin does indicate a reduced DFS by itself, it did not strongly correlate with any of the pathological characteristics of RCC, such as invasion, the mechanism through which vimentin is thought to have a major structural role[269]. In order to strengthen the prognostic significance of vimentin, it may be of benefit to examine the co-expression of vimentin with other molecules involved in intermediate filament facilitated invasion, such as plectin. Plectin has been found to be upregulated in highly invasive bladder cancer cells, where it interacts with vimentin to generate and anchor to invadopodia[270].

2.4.6 CD105 covariate

CD105 has previously been identified as a putative marker for CSC cells in RCC[61]. In this work CD105 had no impact on DFS, nor did it correlate with any of the histopathological features of the disease or be indicative of a poor disease outcome. However, the majority of CD105 positive tumours were also positive for CAV1 (54% $P=0.075$). Kaplan-Meier analysis of the CD105/CAV1 composite covariate found CD105 +ve/CAV1 -ve tumours to identify a significantly decreased DFS of 5.7 years, and correlating only with the presence of micronecrosis as well as being the fourth most predictive marker of poor disease outcome in the multivariate

analysis. While CD105/CAV1 indicated poor disease outcome, it did not correlate with any of the major pathological features that would indicate a metastatic event has taken place, suggesting that analysis of CD105 and CAV1 composite expression in RCC tumours may have some prognostic value in cases where there is a no observable localised invasion, either vascular or more significantly microcapsular. Tumours carrying the CD105/CAV1 marker combination might indicate progression of the tumour toward increased vascularisation, as both CAV1 and CD105 have been implicated as important to angiogenesis and increased microvessel density[130], [183].

2.4.7 Other markers

The markers EpCAM, CD146 and Cavin-1 failed to demonstrate significance in identifying patients with poor clinical outcome, either alone or in combination with CAV1. Positive staining for EpCAM was found in the majority of patients analysed and was not indicative of patient DFS. Though the expression of Cavin-1 not surprisingly correlated with CAV1, by itself Cavin-1 was not capable of identifying a worse disease outcome either alone or in combination with CAV1, suggesting that the prognostic ability of CAV1 is independent of Cavin-1 expression.

In conclusion, the CSC markers CD44 and CD105 worked in combination with CAV1 expression, to better identify patients at high risk of a poor disease outcome, and could provide additional prognostic indications in the case where common pathological features might not be readily accessible or apparent. In particular CD44, proved to be a potent marker alone in the identification of patient groups at high risk of metastatic disease, a feature only strengthened by combinatorial analysis with CAV1, making it an obvious target for therapeutic intervention. The

presence of MCT4 expression was observed and found to be indicative of poor disease free survival, correlated with features of poor disease outcome and could act as an independent marker of poor prognosis. Such findings supported those of other groups and strengthened the case for therapeutic intervention of lactate efflux by pharmacological targeting of MCT4.

Chapter 3 - Identification and clonogenic evaluation of sub-populations of renal cell carcinoma cells dependant on the expression of cancer stem cell related markers

3 Identification and clonogenic evaluation of sub-populations of renal cell carcinoma cells dependant on the expression of cancer stem cell related markers

3.1 Introduction

3.1.1 Identification and isolation of cancer stem cell populations

Identification and separation of cancer stem cell (CSC) populations from the bulk of a tumour or cell line population can be performed in a number of ways[271]. Many of the methods used to test for the functional ability of CSCs are based on the main hallmarks of CSC activity, such as clonogenicity and resistance to cytotoxic agents. Clonogenicity relates to the ability of CSCs to self-renew giving rise to a CSC and a more differentiated daughter cell. These assays can use a variety of methodologies: generation of colonies when whole cell populations are seeded at low density in adherent culture conditions, formation of tumour spheroids in non-adherent conditions again when seeded at low density or tumour generation when serially transplanted into immunodeficient mouse models (such methodologies are reviewed here[271]).

Identification of CSC populations by resistance to cytotoxic compounds is accomplished through the use of DNA binding dyes which are also the substrates of drug efflux pumps. Such efflux pumps tend to be upregulated in stem cell and CSC populations, therefore cells that have an increased capacity to efflux these drugs can be detected by flow cytometry and sorted from the bulk population[272]. A similar technique can also be used that exploits increased aldehyde dehydrogenase (ALDH) activity, a characteristic of increased resistance to cytotoxicity, in CSC and

stem cell populations[273]. The reliance of these approaches on the functional characteristics of CSCs helps to generate a large population of cells all with generally the same trait, be it upregulated self-renewal or relative chemoresistance. However, cell populations isolated this way may still exhibit a higher degree of heterogeneity. As such CSC identification and isolation often involves the use of specific cell surface markers common to many types of stem cell populations of embryonic, mesenchymal and adult types. This method, generally carried out using multi-colour flow cytometry, allows for the accurate identification of subpopulations within cell lines and tumours based on a panel of surface markers of the experimenter's choosing, typically using around one to three different markers. Once subpopulations have been identified, these cells then can be sorted from the bulk of the population through fluorescence activated cell sorting (FACS) to generate highly pure cell populations with respect to the panel of markers originally selected.

Both of these methods are advantageous when trying to identify CSC populations and as such the decision was made to incorporate both the FACS method of sorting based on cell surface marker expression to identify potential CSC or stem-like subpopulations and the use of colony formation assays to measure the clonogenic capacity of these subpopulations. Subsequently, further investigations were carried out to determine what function CAV1 may fulfil in the clonogenicity of these populations.

3.1.2 Putative CSC surface marker panel

In an effort to isolate the most potent CSC or stem-like cells, it was decided that it would be most advantageous to incorporate as many markers into the antibody panel as possible. Using the FACS Aria III it was possible to assay for eight different surface markers simultaneously. Markers included in the panel were selected based on their ability to identify embryonic, mesenchymal and cancer stem cell populations. Many of the markers explored for their prognostic capabilities were again selected for their physiological *in vitro* activity: CD44, CD105, EpCAM and CD146. Additional markers were selected based on their previous ability to identify and functionally influence MSC activity. The markers selected for analysis are described below.

3.1.3 CD44

As discussed in chapter 2, CD44 defines a large family of transmembrane glycoproteins, which function as a receptor for hyaluronic acid as well as other constituents of the extracellular matrix (ECM). Expression of CD44 has been identified as important in the disease progression of many tumour types. The abundance of hyaluronic present in stem cell niches[274] has led to the use of CD44 as a common marker for CSC populations.

CD44 positive CSC populations have been discovered in tumours from the breast[275], stomach[276], pancreas[277], lung[278] and head and neck[279]. It is important to note that CD44 may not only act as a signpost for a stem-like phenotype but may also play a functional role in the pathology of these tumours. In head and neck squamous cell carcinoma Shigeishi et al.[280] discovered that in CD44⁺ populations CD44 was required for glycogen synthase kinase 3 β (GSK3 β) activation by inhibiting its phosphorylation. Down-regulation of CD44 in these cells resulted in decreased tumourigenicity in severe combined immunodeficient (SCID) mice as well as an up-regulation of an epithelial phenotype and a down-regulation of

self-renewal markers Oct4, Sox2 and nanog. Bourguignon et al.[281] demonstrated an important role for the interaction of CD44 with HA in both breast and ovarian cancer cell lines. Their studies found that binding of HA to CD44 induced the localisation and activation of the stem cell transcription factor Nanog and triggering the expression of Rex1 and Sox2; regulators of stem cell pluripotency. Further to this, they found Nanog capable of binding Stat-3 in the nucleus thereby facilitating the up-regulation of the multidrug transporter MDR1. This demonstrated the ability of CD44 to regulate multiple processes implicit to the CSC phenotype. The ability for CD44 to not only identify CSC populations in a number of tumours but also to act as a crucial factor in the maintenance of such a phenotype made it a clear candidate for inclusion in the putative CSC marker panel.

3.1.4 CD105

In addition to the functions of CD105 in tumour angiogenesis and cellular migration (as discussed in chapter two), CD105 is now frequently used as a marker for the isolation of mesenchymal stem cells (MSCs)[282]. Using CD105, MSCs have been isolated from human bone marrow[283] as well as adipose, liver and cardiac tissues[284].

Such MSCs have also been found to be present in the adult human kidney[285]. This discovery led Bussolati et al.[61] to hypothesise the existence of a CD105⁺ MSC-like population of CSCs within renal carcinomas and indeed tumourigenic CD105⁺ populations were subsequently identified within clinical tumour samples. These CD105⁺ cells demonstrated clonogenic ability, expression of the common stem cell markers nestin, nanog and Oct4 together with a down-regulation in both epithelial markers and the ability to differentiate into epithelial and endothelial lineages. Using this same CD105⁺ CSC population, Azzi et al.[286] were able to

induce epithelial differentiation in these cells which showed a significantly reduced capacity for drug resistance compared to untreated cells. CD105's ability to specifically identify potent CSC populations within RCC led to its inclusion in the putative CSC panel.

3.1.5 CD90

The classical use of CD90 as a marker for HSCs and MSCs[287] has naturally led to its use in the identification of CSCs. Wang et al.[278] identified a potent sub-population of CD90⁺ cells within a population of CD44⁺ cells from small cell lung cancer (SCLC) and large cell carcinoma cell lines. The cells displayed a mesenchymal morphology with increased expression of mesenchymal markers and increased expression of the self-renewal factors Nanog and Oct-4. Similarly, the combinatorial use of CD44 together with CD90 identified in hepatocellular carcinoma a potent CSC population that was capable of forming metastatic lesions in the lung[288]. Similar studies by Yang et al.[289] found CD90⁺ cells within all hepatocellular carcinoma primary samples and 91.6% of paired blood samples all of which were capable of generating tumour nodules in an immunodeficient mouse model. CD90⁺ CSC populations have also been isolated from esophageal cancers in both the primary tumours and derived cell lines[290]. Interestingly, as well as displaying enhanced tumourigenicity and chemoresistance these CD90⁺ cells also displayed increased invasion and migratory ability. The strong evidence for CD90's use as a CSC marker especially when used in combination with CD44 merited its inclusion in the putative CSC panel.

3.1.6 CD146

In addition to the substantial role CD146 appears to play in the aetiology of melanoma (discussed in Chapter 2), CD146 has been used as a potent marker of MSC populations. A study by Baksh et al.[291] identified CD146 as a robust marker for human umbilical cord perivascular cells (HUCPVCs). These cells were much more proliferative with increased pluripotency compared to bone marrow mesenchymal stromal cells (BMSCs). Another study found the CD146⁺ perivascular cells shared a similar gene expression profile and functional biological activity to that of MSCs, further strengthening the case for CD146 as a putative MSC marker[292]. Additional studies went on to establish CD146 as a marker for MSCs capable of tri-lineage differentiation[293] and increased expression of CD146 correlated with a greater capacity for differentiation[294].

In addition to the significance of CD146 in MSC identification, a role for CD146 in embryonic organ development has been suggested. Overall comparison of CD146 expression between embryonic and mature tissues demonstrated much higher expression of CD146 in the embryonic nervous system[295], trachea[296], and kidney[297] which was then lost in the adult tissue[298]. Observations made in chick embryos relating to the involvement of CD146 in kidney development found high levels of CD146 expression and conversely, most cell types of the mature kidney showed active suppression of CD146 expression[297]. These CD146 positive embryonic kidney cells showed a far higher propensity for aggregation in cell-aggregation assays, suggesting a possible role in the structural modelling of the newly forming kidney[299].

Despite the properties mentioned above, CD146 has not been widely adopted as a marker of CSCs in any tumour. It was however found to be expressed on the CD105⁺ population of renal CSCs identified by Bussolati et al.[61] Furthermore, Zeng et al. demonstrated that the up-regulation of CD146 in epithelial breast cancer

cells resulted in the induction of EMT and in pronounced mammosphere formation[300]. The ability for CD146 to identify subpopulations of MSCs with increased proliferative and pluripotent capacity points towards the possibility that CD146 may be a potent and as of yet untapped resource for CSC identification and purification.

3.1.7 EpCAM

While in adult tissues EpCAM expression is restricted to the epithelia, in the embryo expression of EpCAM can be found in embryonic stem cells (ESCs) not yet committed to epithelial differentiation[301]. Indeed, compelling evidence seems to suggest an important role for EpCAM in the maintenance of the ESC phenotype by maintaining the expression of key self-renewal related transcription factors such as Oct-4 and c-Myc[302].

These findings have led to the use of EpCAM in identification of CSC populations. So far EpCAM has been used in combination with CD44⁺ or CD44⁺/CD24⁻ to identify CSCs from breast[275], colorectal[136] and pancreatic carcinomas[60]. Investigations into the mechanism of EpCAM as a potential signalling molecule have revealed interaction with β -catenin and Lef-1. Regulated intra-membrane proteolysis (RIP) of the cytosolic domain of EpCAM generates a peptide termed EpICD, this is then trafficked into the nucleus as a complex with β -catenin and lef-1 which up-regulates proliferative genes[303].

Strong evidence for the role EpCAM plays in embryonic self-renewal, its overexpression in numerous cancers (further discussion in chapter 2) and its successful use as a surface marker able to identify CSCs from multiple tumour types made it a strong candidate for inclusion into the putative CSC marker panel.

3.1.8 CD117

CD117, or c-kit, is a 120 kDa cytokine receptor and member of the type III receptor tyrosine kinase family[304]. CD117 has found use as a marker for haematopoietic progenitor cell lineages in bone marrow, where it has been found to play a critical role in the proliferation, survival and differentiation of these cells[305]. CD117 expression is evident in human primordial germ cells and foetal ovaries[306] and as a potent marker for mouse prostate stem cells[307].

As with many markers selected for this panel, aberrations in CD117 expression have implications in cancer progression. Gain of function mutations have been observed to form tumours in gastrointestinal stromal cells, mast cells and germ cells[308], [309]. Due to the prevalent expression of CD117 in embryonic germ cells the protein has attracted attention in ovarian carcinoma. In this context when used as a single marker, CD117 has previously enriched for a population of tumour cells capable of generating tumours in a third of immunodeficient mouse models[310].

Immunohistochemical analysis of CD117 expression in a range of histological subtypes of RCC revealed that expression is confined almost exclusively to those tumours of a chromophobe or oncocytoma subtype[311]. While no great degree of expression was observed in the clear cell subtype (cell lines of which the following experiments were performed on), it does not preclude the possibility that a small subpopulation of CD117 may exist within RCC cell lines. As such CD117 was included in the marker panel.

3.1.9 CD29 and CD73

CD29 and CD73 comprise the final additions to the panel. CD29, or integrin $\beta 1$ is an integrin subunit capable of binding to a variety of α subunit to generate several different heterogeneous integrin complexes. Together with CD44 the positive expression of CD29 has been used in squamous cell carcinoma to identify CSC populations with increased drug resistance and displaying up-regulation of EMT markers[138]. In the Braca1-associated mouse model of breast cancer, CD29 when used in combination with CD24 and CD49f identified a population of CSCs with enhanced metastatic capacity[312]. CD73, also known as ecto-5'-nucleotidase, is a cell surface nucleotidase which facilitates the conversion of AMP to adenosine. Together they are commonly used for the isolation and purification of MSCs from a variety of different tissue types[313]. CD73 has not been directly used to identify CSC populations but it is widely used to distinguish multiple types of MSCs[313]. Not only this but it appears to play a role in aiding the escape of cancer cells from immune surveillance through the generation of adenosine[314]. This leads to the interesting possibility that CD73 may be able to identify CSC populations not only capable of supporting the growth and resistance of the tumour but also enable escape from the clearance of malignant cells by the immune system.

3.1.10 Aims

This chapter aims to identify putative CSC subpopulations from the RCC cell lines 786-O, A498 and CAKI-1 and evaluate their clonogenic potential by a colony formation assay. To achieve this, a panel of cell surface proteins commonly expressed on mesenchymal, embryonic and cancer stem cells were used. These surface markers were identified and quantified using flow cytometry and a gating hierarchy was generated with the intention of identifying common subpopulations between all three cell lines. Subsequently, cells were sorted and placed into colony

formation assays to establish the clonogenicity of common subpopulations in each cell line.

3.2 Materials and methods

3.2.1 Cell lines

Clear cell renal cell carcinoma cell lines included: 786-O (obtained from the ATCC) cultured in DMEM (Life Technologies) supplemented with 10% FBS and 1% penicillin/streptomycin (Life Technologies); A498 and CAKI-1 cells ATCC cultured in RPMI similarly supplemented. All cell lines were cultured at 37°C with 5% CO₂.

3.2.2 Flow cytometry and sorting

786-O, A498 and CAKI-1 cells grown to ~80% confluence were washed twice in PBS and disaggregated by incubation with Accutase (Life Technologies) for 10 minutes at 37°C. Cells were then resuspended in their respective growth media, counted and resuspended to 1,000,000 cells in 60µL of PBS containing 5% FBS and treated with an antibody cocktail containing 5µL of each of the antibodies corresponding to the marker in the putative CSC panel (Table 3.1) and left to incubate with the cells at 4°C for 30 minutes in the dark to prevent photobleaching. The cell suspension was then washed twice in 1mL of PBS with 5% FBS and adjusted to a final volume of 500µL. Flow cytometry analysis and cell sorting was carried out using a FACSAria III (BD Biosciences). When conducting flow cytometric studies containing multiple different fluorophores it is important to select fluorophores which would demonstrate the least amount of spectral overlap. This was done through both selecting fluorophores with minimal overlap in their emission wavelength range (as illustrated in Figure 3.1 and Figure 3.2) and using the automatic compensation system in the FACSDiva acquisition software to apply a real-time compensation matrix. When selecting fluorophores, where ever possible the brightness of a fluorophore was matched to the predicted expression levels of

the markers selected. Therefore, a marker predicted to have weak expression would be targeted by an antibody conjugated to a bright fluorophore.

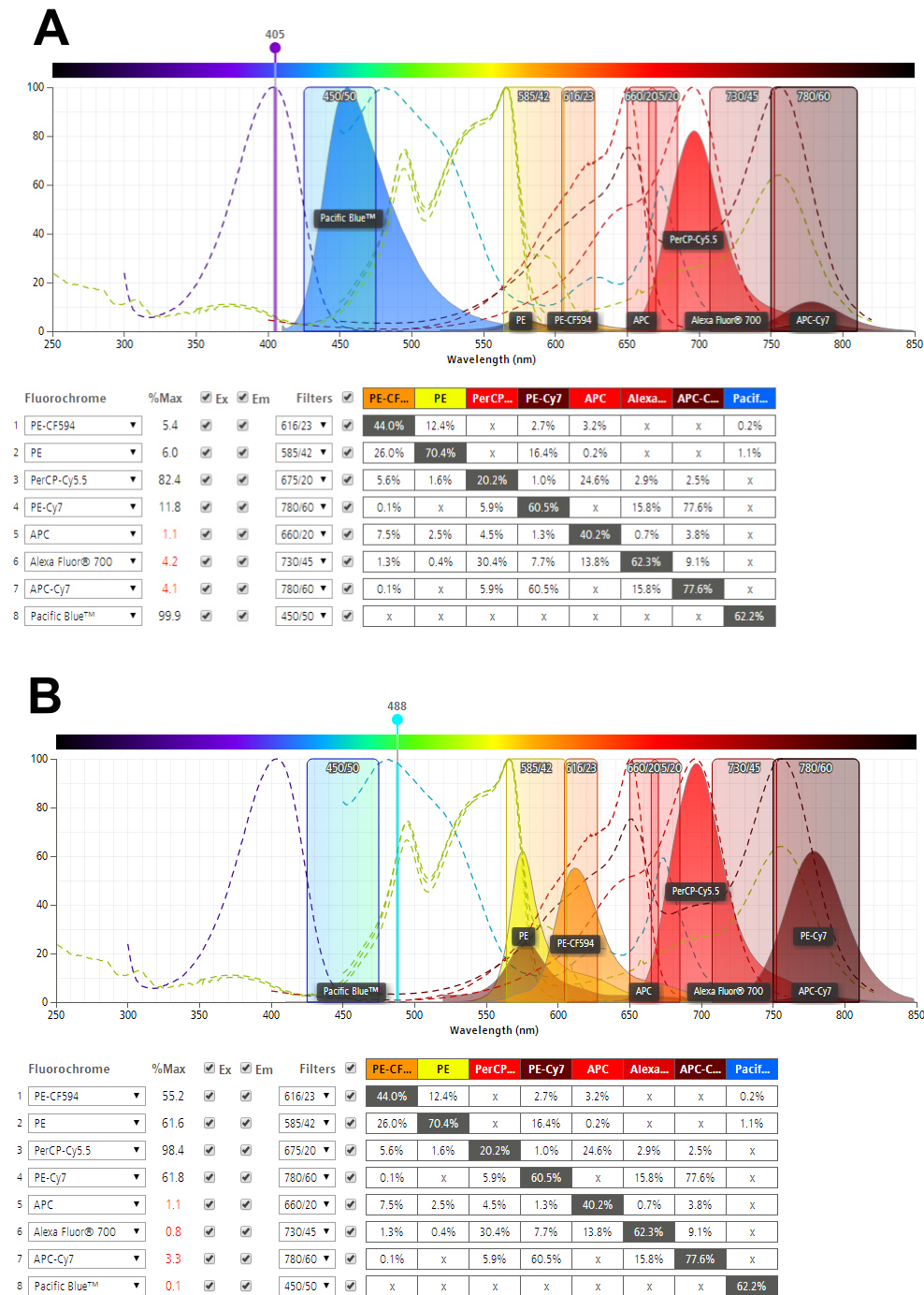


Figure 3.1 Spectral overview of fluorophores selected for flow cytometry analysis. (A) Shows fluorophores excited by the 408nm laser and their subsequent emission range (B) shows the same for the 488nm laser.

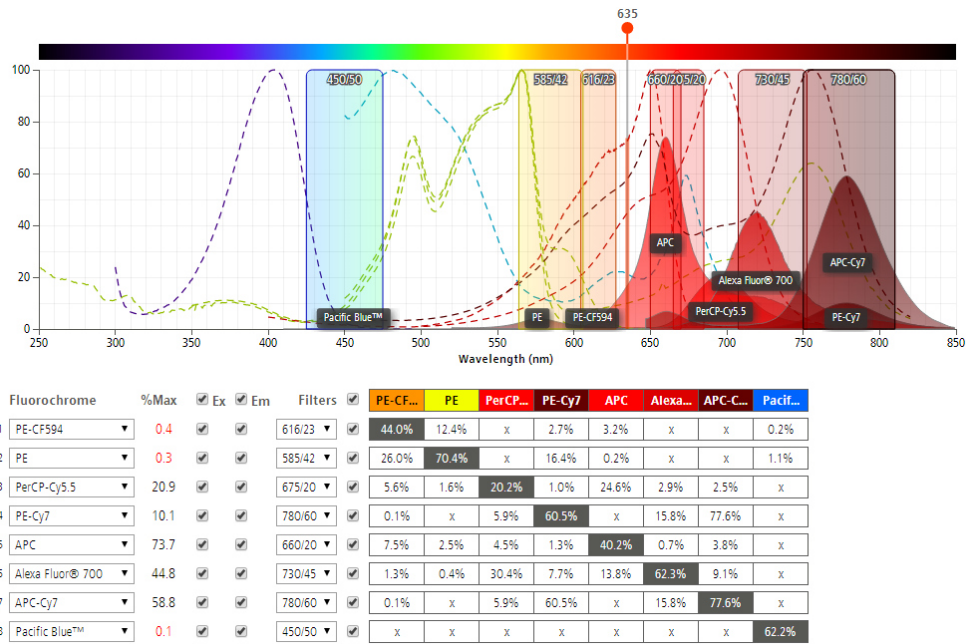


Figure 3.2 Spectral overview for fluorophores excited by the 635nm laser selected for flow cytometry analysis.

To account for spectral overlap of the selected fluorophores each antibody in the panel was incubated with Anti-mouse Ig κ CompBeads (BD Biosciences) for 30 minutes at 4°C. Then each antibody/bead conjugate was analysed individually on the FACS Aria and through the FACSDiva acquisition software a compensation matrix was constructed allowing for real-time compensation to be applied to the stained cell lines during sample preview and acquisition. Flow cytometry data provided represents 500,000 registered events per sample, percentages of subpopulations frequencies are calculated as calculated as number of cells identified by the given marker combination divided by total number of cells after gating for single cells.

Table 3.1 Fluorophore conjugated antibody panel corresponding to markers selected for flow cytometry analysis. All antibodies selected were isotype IgG1- κ and of mouse origin.

| Marker | Fluorophore | Supplier | Product code |
|--------|---------------------------------------|----------------|--------------|
| CD90 | PE | BD Biosciences | 555596 |
| CD146 | PE-Cy7 | BD Biosciences | 562135 |
| CD44 | Alexa Flour 700 | BD Biosciences | 561289 |
| CD105 | APC | Invitrogen | MHCD10505 |
| EpCAM | PerCP-Cy5.5 | BD Biosciences | 347199 |
| CD117 | PE-CF594 (derivative of PE-Texas red) | BD Biosciences | 562407 |
| CD29 | APC-Cy7 | Biolegend | 303014 |
| CD73 | Pacific Blue | Biolegend | 344012 |

3.2.3 Colony formation assay

All cell populations were sorted into 6-well plates already containing 2mL of their respective growth media at a density of 400 cells per well. After two weeks of incubation growth media was removed and the wells were washed twice with 1mL of PBS. Colonies were then stained for five minutes in a 0.5% solution of crystal violet containing 25% methanol to fix and stain the colonies. The crystal violet solution was then aspirated by pipette and the remaining crystal violet solution washed away by submersion of the plate into multiple changes of water. Colonies were counted macroscopically with a colony being judged to contain more than 30 cells.

3.2.4 Statistical analysis

Analysis of two groups was performed by Student's t-test (unpaired) and analysis of multiple groups carried out by one-way ANOVA with a Tukey post-hoc analysis (comparison across all pairs of groups). Statistical differences were deemed significant at the $P \leq 0.05$ level.

3.3 Results

3.3.1 Identification of sub-populations within RCC cell lines

In order to generate a gating hierarchy based on the expression of CSC related surface markers, first single marker histograms were obtained to look for any observable subpopulations. Single marker histograms showed heterogeneity of certain CSC-related cell surface markers in 786-O, A498 and CAKI-1 cell lines. In all three cell lines there appeared to be a relatively small CD90^{high} population in all three RCC cell lines CAKI-1 (Figure 3.3). CD146 followed a similar pattern in having both CD146^{low} and CD146^{high} expression. However, while A498 and CAKI-1 revealed a minority CD146^{high} population, the majority of 786-O cells were CD146^{high} (Figure 3.3). Expression of CD44 and CD105 in both 786-O cells and A498 cells appeared to be uniformly high, while CAKI-1 cells appeared to display more of a bimodal distribution with CD44^{high} and CD105^{high} cells representing the bulk of the population. Interestingly, overall expression of CD105 appeared much lower in 786-O and A498 compared to CAKI-1. EpCAM and CD117 showed a uniformly low expression in 786-O and A498 cells (Figure 3.4). In CAKI-1 there was an EpCAM^{high} and CD117^{high} population, though in the case of CD117 this was caused by spectral overlap of EpCAM PerCP-Cy5.5 into the PE-Texas Red channel which could not be completely compensated for. In all three cell lines CD29 was highly expressed (Figure 3.4). CD73 expression was low in 786-O, A498 and CAKI-1. However, CAKI-1 cells had a small proportion of cells with higher CD73 expression. Due to these observations the gating hierarchy for subsequent work was constructed. As both CD90 and CD146 showed substantial subpopulations in all three cell lines, they formed the first tier of the gating hierarchy as CD90/CD146. CD105/CD44 then formed the second tier owing to the subpopulations apparent in the CAKI-1 cells. Following this was the EpCAM/CD117 tier, due to the presence of an EpCAM^{High}

population in CAKI-1 cells. The final tier was CD73/CD29, the most homogeneous markers.

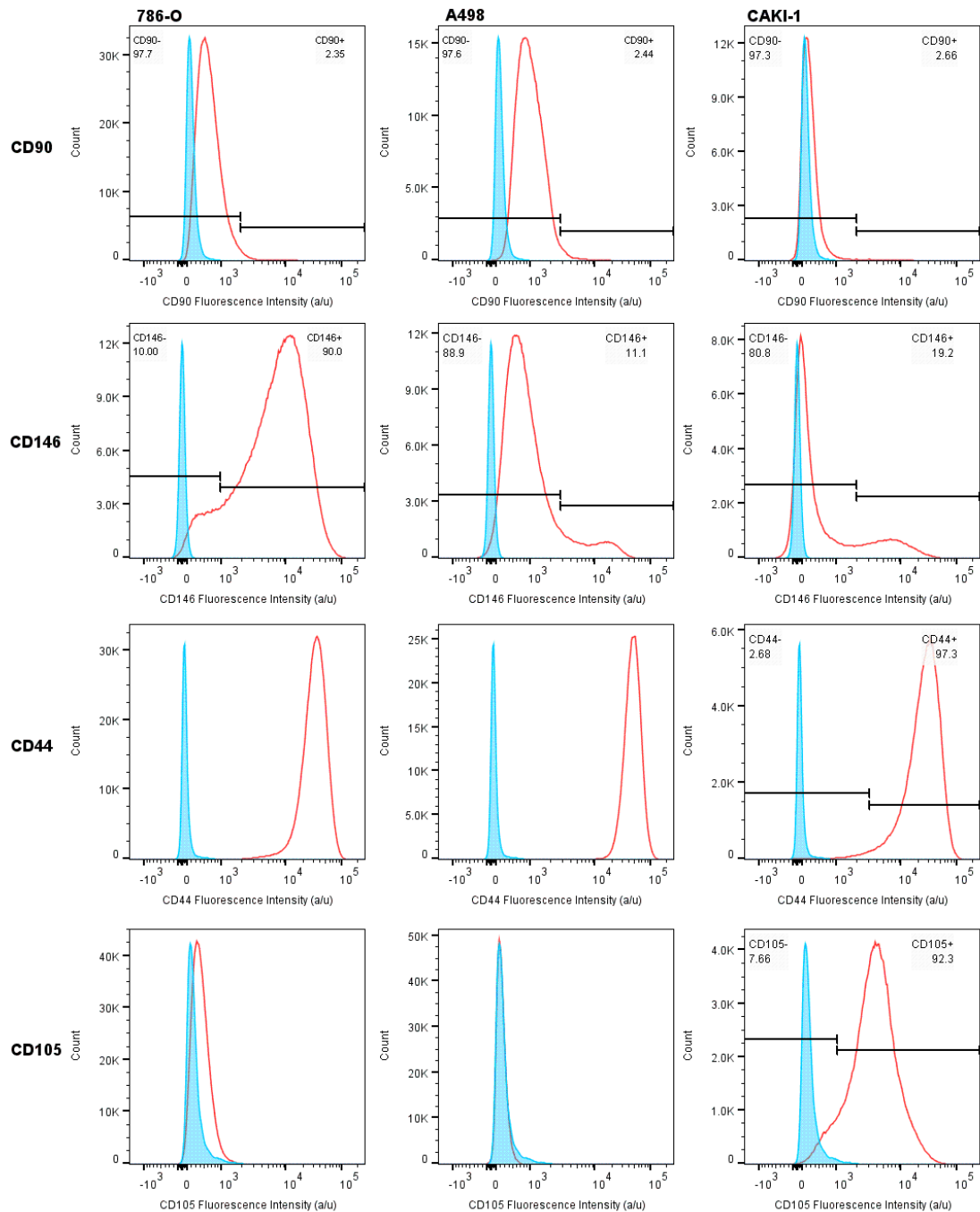


Figure 3.3 Single marker histograms of cell surface CSC markers (red histograms) CD90, CD146, CD44 and CD105 against unstained cells (blue histograms) in 786-O (left), A498 (middle) and CAKI-1 (right). Data acquired from 500,000 events of cells gated in FSC-A/SSC-A for live cells and FSC-A/FSC-H for single cells. Data shown for one of three experiments.

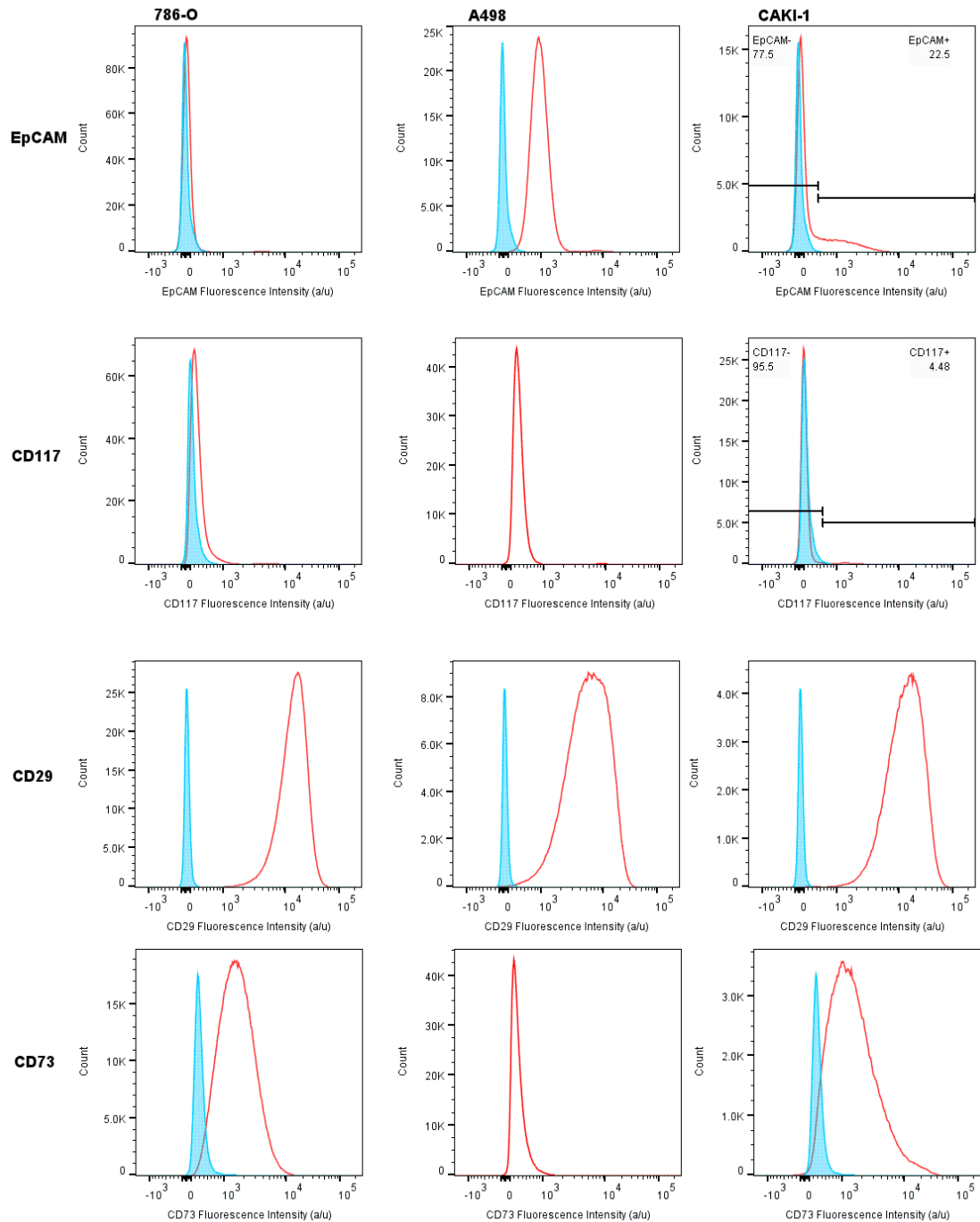


Figure 3.4 Single marker histograms of cell surface CSC markers (red histograms) EpCAM, CD117, CD29 and CD73 against unstained cells (blue histogram) in 786-O (left), A498 (middle) and CAKI-1 (right). Data acquired from 500,000 events of cells gated in FSC-A/SSC-A for live cells and FSC-A/FSC-H for single cells. Data shown for one of three experiments.

3.3.2 Subpopulation heterogeneity in RCC cell lines

Using the data gathered by single marker histogram analysis a gating hierarchy was constructed (Figure 3.5). Cell populations were gated by use of box gates; this allowed for a greater degree of spatial separation between high and low marker expression (as opposed to quadrant gating) and more precise sorting as it enabled the gating of events that were spatially separated by at least 0.25 logs of fluorescence. Such an approach should serve to identify any distinct biological function that may be dependent upon a larger degree of upregulation or downregulation of the marker in question and also facilitates the collection of more pure high and low populations. To ensure only live single cells were analysed and sorted, cells were first gated on forward scatter area (FSC-A) and side scatter area (SSC-A) then forward scatter height (FSC-H) and forward scatter area (FSC-A) to identify single cells (Figure 3.6) and finally forward gated into the surface marker hierarchy (Figure 3.5).

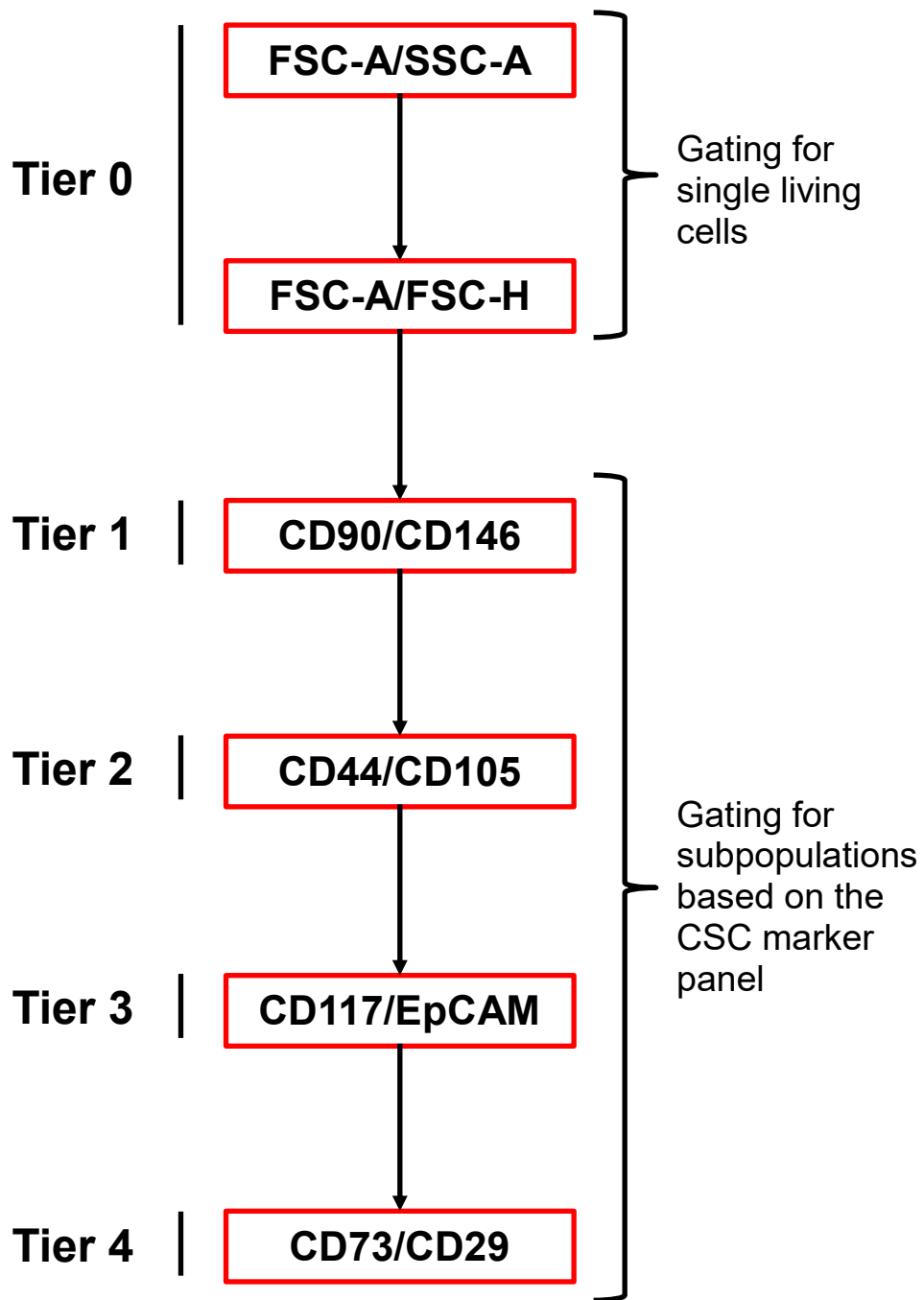


Figure 3.5 Gating hierarchy used for sorting of subpopulations from all three RCC cell lines. Each tier in the hierarchy indicates a forward gating step in the FACSDiva software package.

3.3.2.1 786-O and A498 subpopulation heterogeneity

In all three cell lines the marker combination of CD146/CD90 identified three distinct subpopulations. In the 786-O cells these subpopulations were CD146^{Low}/CD90^{Low} (10.05% ±2.60%), CD146^{High}/CD90^{Low} (69.84% ±5.42%) and CD146^{High}/CD90^{High} (0.98% ±0.22%) (Figure 3.6) (Table 3.2). A498 cells contained the same three subpopulations though the distribution of these subpopulations was altered in terms of CD146; there was a more abundant CD146^{Low}/CD90^{Low} population (65.84% ±7.56%) with a consequential decrease in the proportion of cells in the CD146^{High}/CD90^{Low} population (6.23%) (Figure 3.7). It was also possible to detect a subpopulation of cells CD90^{High}/CD146^{Low} (0.87% ±0.21%). Forward gating of both 786-O and A498 CD146^{Low}/CD90^{Low}, CD146^{High}/CD90^{Low} and CD146^{High}/CD90^{High} revealed no further subpopulations in the remaining marker combinations of the gating hierarchy.

Table 3.2 The frequency of detectable subpopulations in 786-O based on the expression of CSC marker panel. Data represent mean ± standard deviation of three experiments.

| 786-O | |
|---|---------------------------------------|
| Subpopulation | Percentage of single cell gate |
| CD90 ^{High} /CD146 ^{High} | 10.05% ±2.60% |
| CD90 ^{Low} /CD146 ^{High} | 69.84% ±5.42% |
| CD90 ^{Low} /CD90 ^{Low} | 0.98% ±0.22% |

Table 3.3 The frequency of detectable subpopulations in A498 based on the expression of CSC marker panel. Data represent mean ± standard deviation of three experiments.

| A498 | |
|--|---------------------------------------|
| Subpopulations | Percentage of single cell gate |
| CD90 ^{High} /CD146 ^{Low} | 0.87% ±0.21% |
| CD90 ^{Low} /CD146 ^{High} | 6.23% ±0.68% |
| CD90 ^{Low} /CD146 ^{Low} | 65.84% ±7.56% |

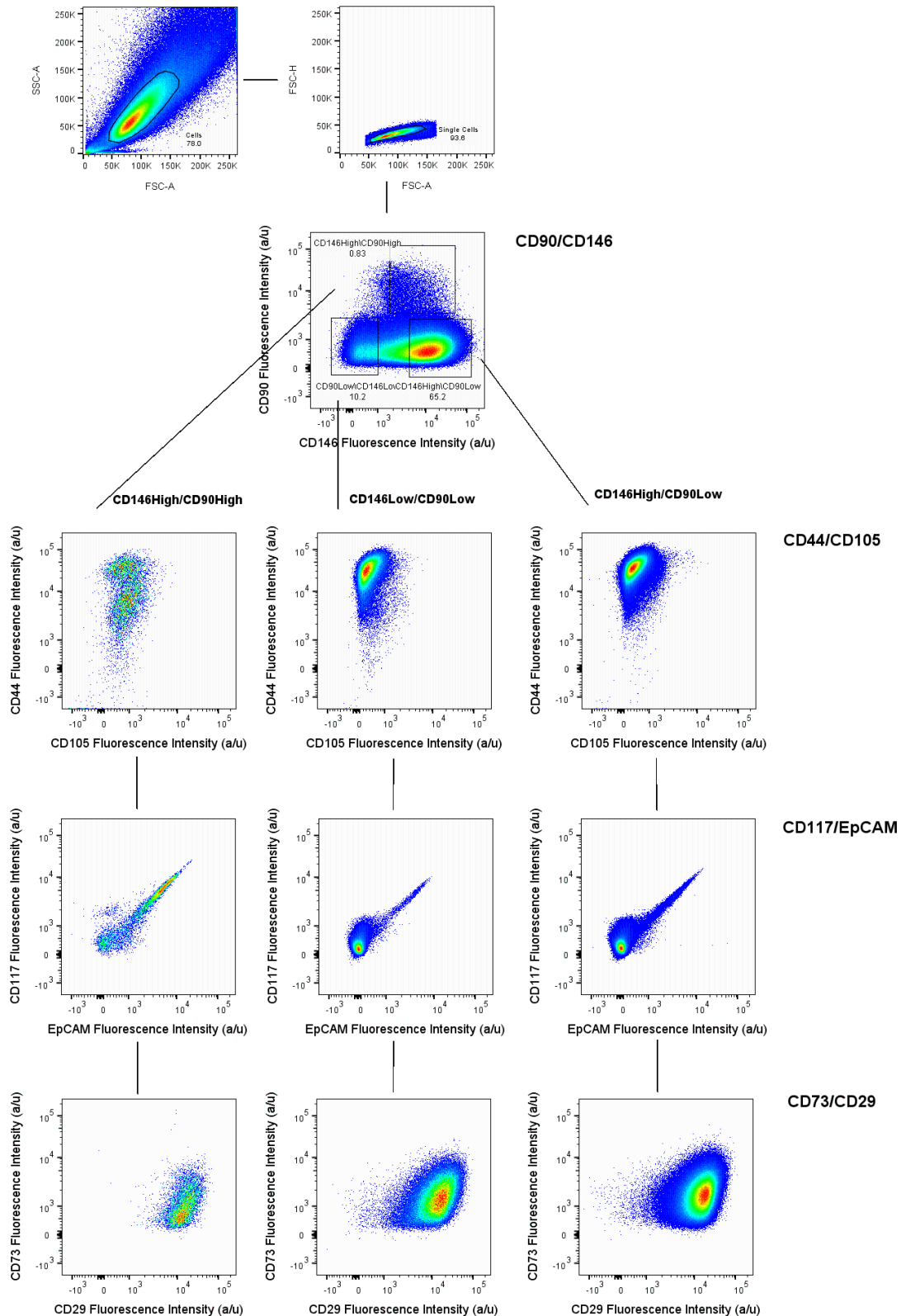


Figure 3.6 Identification of CD90/CD146 subpopulations in 786-O WT cells by flow cytometry. Data represented as bivariate dot-plots of two markers each. Cells were forward gated from CD90/CD146 into CD44/CD105, then CD117/EpCAM, and finally CD73/CD29. Data was acquired from 500,000 events. Data shown for one of three experiments.

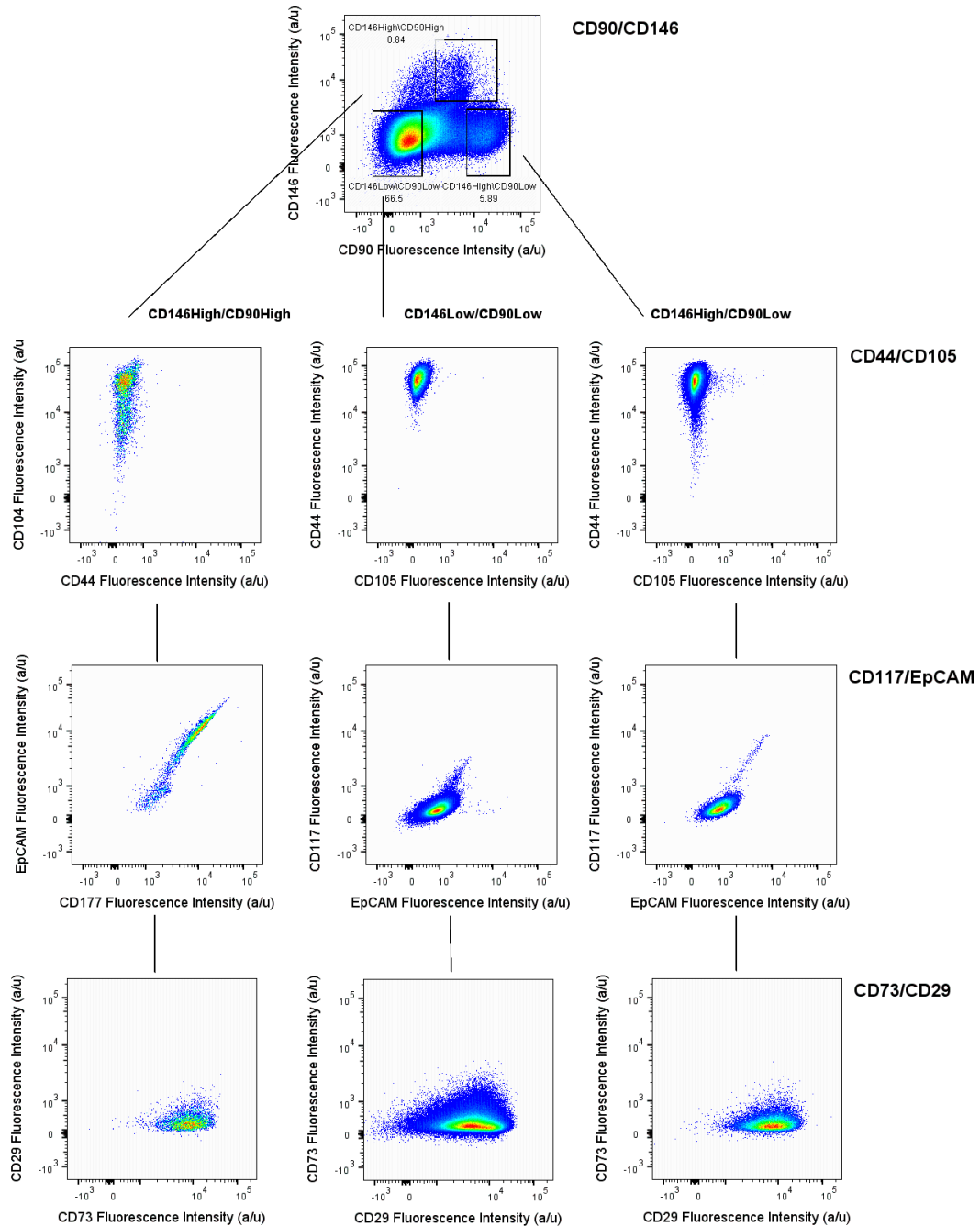


Figure 3.7 Identification of CD90/CD146 subpopulations in A498 WT cells by flow cytometry. Data represented as bivariate dot-plots of two markers each. Cells were forward gated from CD90/CD146 into CD44/CD105, then CD117/EpCAM, and finally CD73/CD29. Data was acquired from 500,000 events. Data shown for one of three experiments.

3.3.2.2 CAKI-1 subpopulation heterogeneity

CAKI-1 also showed the same three distinct CD90/CD146 subpopulations with the majority being CD146^{Low}/CD90^{Low} (71.62% ±4.07%), as found in A498, with the other two populations being a CD146^{High}/CD90^{Low} population (19.73% ±3.83%) and a CD146^{Low}/CD90^{High} (1.43% ±0.62%) subpopulation (Figure 3.8 & Table 3.4 A).

CAKI-1, unlike 786-O and A498, displayed further subpopulation heterogeneity when CD90/CD146 subpopulations were forward gated. Forward gating into a bivariate plot of CD44 and CD105 markers revealed additional CD44^{Low}/CD105^{Low} and CD44^{High}/CD105^{High} populations each of which had different frequencies depending on the CD90/CD146 status of the parent subpopulation (Figure 3.8). Forward gating of the CD146^{Low}/CD90^{High} population resulted in a population of CD44^{Low}/CD105^{Low} (0.13% ±0.09%) and a population of CD44^{High}/CD105^{High} (1.23% ±0.34%). The forward gating of CD146^{Low}/CD90^{Low} population into CD44/CD105 revealed the same CD44^{Low}/CD105^{Low} (61.93 ±5.12%) and CD44^{High}/CD105^{High} (0.16% ±0.42%) subpopulations. In these subpopulations the distributions were skewed more towards the CD44^{High}/CD105^{High} population (84.68% of the cells from the previous gate) with the CD44^{Low}/CD105^{Low} population remaining stable (6.52% of cells from the previous gate). Forward gated CD146^{High}/CD90^{Low} populations showed a near complete loss of the CD44^{Low}/CD105^{Low} population that was present in the other CD146/CD90 subpopulations, resulting in only CD44^{High}/CD105^{High} cells (0.16% ±0.42%) (Figure 3.8 Table 3.4 B).

Further forward gating from the CD44/CD105 tier into the next level of the gating hierarchy, CD117 and EpCAM, revealed no further heterogeneity in the CD146^{Low}/CD90^{High}CD44^{Low}/CD105^{Low} and CD146^{Low}/CD90^{High}CD44^{High}/CD105^{High} as well as the CD146^{Low}/CD90^{Low}/CD44^{Low}/CD105^{Low} population. However the CD146^{Low}/CD90^{Low}/CD44^{High}/CD105^{High} and CD146^{High}/CD90^{Low}/CD44^{High}/CD105^{High} populations contained an EpCAM^{Low} and EpCAM^{High} population, 46.90% ±6.89%

and 6.42% \pm 3.43% respectively. This population was also present in the CD146^{High}/CD90^{Low}/CD44^{High}/CD105^{High} population (0.76% \pm 0.45%) (Figure 3.8 Table 3.4 C).

In the final CD73/CD29 tier the CD90^{High}/CD146^{Low} lineages all resulted in CD73^{Low}/CD29^{High} populations. However, in the CD44^{Low}/CD105^{Low} population of the CD146^{Low}/CD90^{Low} lineage the majority of cells were CD29^{Low}. These three subpopulations displayed relatively little expression of CD73. In contrast, the subpopulations generated from the CD146^{Low}/CD90^{Low} and CD146^{High}/CD90^{Low} all expressed high levels of CD29 and expressed moderate to high amounts of CD73 (Figure 3.8 Table 3.5).

Table 3.4 The frequency of detectable subpopulations in CAKI-1 based on the expression of CSC marker panel. (A) CD90/CD146 tier (B) CD44/CD105 tier (C) EpCAM/CD117 tier. Data represent mean \pm standard deviation of three experiments.

| A – Tier 1 | | CAKI-1 |
|---------------------------|--|---------------------------------------|
| Marker combination | Subpopulation | Percentage of single cell gate |
| CD90/CD146 | CD146 ^{Low} /CD90 ^{High} | 1.43% \pm 0.62% |
| | CD146 ^{Low} /CD90 ^{Low} | 71.62% \pm 4.07% |
| | CD146 ^{High} /CD90 ^{Low} | 19.73% \pm 3.83% |
| B – Tier 2 | | |
| Marker combination | Subpopulation | Percentage of single cell gate |
| CD44/CD105 | CD146 ^{Low} /CD90 ^{High} /CD44 ^{Low} /CD105 ^{Low} | 0.13% \pm 0.09% |
| | CD146 ^{Low} /CD90 ^{High} /CD44 ^{High} /CD105 ^{High} | 1.23% \pm 0.34% |
| | CD146 ^{Low} /CD90 ^{Low} /CD44 ^{Low} /CD105 ^{Low} | 61.93 \pm 5.12% |
| | CD146 ^{Low} /CD90 ^{Low} /CD44 ^{High} /CD105 ^{High} | 0.16% \pm 0.42% |
| | CD146 ^{High} /CD90 ^{Low} /CD44 ^{High} /CD105 ^{High} | 19.73% \pm 3.83% |
| C – Tier 3 | | |
| Marker combination | Subpopulation | Percentage of single cell gate |
| EpCAM/CD117 | CD146 ^{Low} /CD90 ^{High} /CD44 ^{Low} /CD105 ^{Low} /EpCAM ^{Low} /CD117 ^{Low} | No further heterogeneity |
| | CD146 ^{Low} /CD90 ^{High} /CD44 ^{High} /CD105 ^{High} /EpCAM ^{Low} /CD117 ^{Low} | No further heterogeneity |
| | CD146 ^{Low} /CD90 ^{Low} /CD44 ^{Low} /CD105 ^{Low} /EpCAM ^{Low} /CD117 ^{Low} | No further heterogeneity |
| | CD146 ^{Low} /CD90 ^{Low} /CD44 ^{High} /CD105 ^{High} /EpCAM ^{Low} /CD117 ^{Low} | 46.90% \pm 6.89% |
| | CD146 ^{Low} /CD90 ^{Low} /CD44 ^{High} /CD105 ^{High} /EpCAM ^{High} /CD117 ^{Low} | 6.42% \pm 3.43% |
| | CD146 ^{High} /CD90 ^{Low} /CD44 ^{High} /CD105 ^{High} /EpCAM ^{Low} /CD117 ^{Low} | 15.51% \pm 2.74% |
| | CD146 ^{High} /CD90 ^{Low} /CD44 ^{High} /CD105 ^{High} /EpCAM ^{High} /CD117 ^{Low} | 0.76% \pm 0.45% |

Table 3.5 The frequency of detectable subpopulations in CAKI-1 based on the expression of CSC marker panel. (D) CD73/CD29 tier Data represent mean \pm standard deviation of three experiments.

D –Tier 4

| Marker combination | Subpopulation | Percentage of single cell gate |
|--------------------|---|--|
| CD73/CD29 | CD146 ^{Low} /CD90 ^{High} /CD44 ^{Low} /CD105 ^{Low} /EpCAM ^{Low} /CD117 ^{Low} /CD73 ^{Low} /CD29 ^{High} | No further heterogeneity 0.13% \pm 0.09% |
| | CD146 ^{Low} /CD90 ^{High} /CD44 ^{High} /CD105 ^{High} /EpCAM ^{Low} /CD117 ^{Low} /CD73 ^{Low} /CD29 ^{High} | No further heterogeneity 1.23% \pm 0.34% |
| | CD146 ^{Low} /CD90 ^{Low} /CD44 ^{Low} /CD105 ^{Low} /EpCAM ^{Low} /CD117 ^{Low} /CD71 ^{Low} /CD29 ^{Low} | No further heterogeneity 61.93 \pm 5.12% |
| | CD146 ^{Low} /CD90 ^{Low} /CD44 ^{High} /CD105 ^{High} /EpCAM ^{Low} /CD117 ^{Low} /CD73 ^{Low} /CD29 ^{High} | No further heterogeneity 46.90% \pm 6.89% |
| | CD146 ^{Low} /CD90 ^{Low} /CD44 ^{High} /CD105 ^{High} /EpCAM ^{High} /CD117 ^{Low} /CD73 ^{Low} /CD29 ^{High} | No further heterogeneity 6.42% \pm 3.43% |
| | CD146 ^{High} /CD90 ^{Low} /CD44 ^{High} /CD105 ^{High} /EpCAM ^{Low} /CD117 ^{Low} /CD73 ^{Low} /CD29 ^{High} | No further heterogeneity 15.51% \pm 2.74% |
| | CD146 ^{High} /CD90 ^{Low} /CD44 ^{High} /CD105 ^{High} /EpCAM ^{High} /CD117 ^{Low} /CD73 ^{Low} /CD29 ^{High} | No further heterogeneity 0.76% \pm 0.45% |

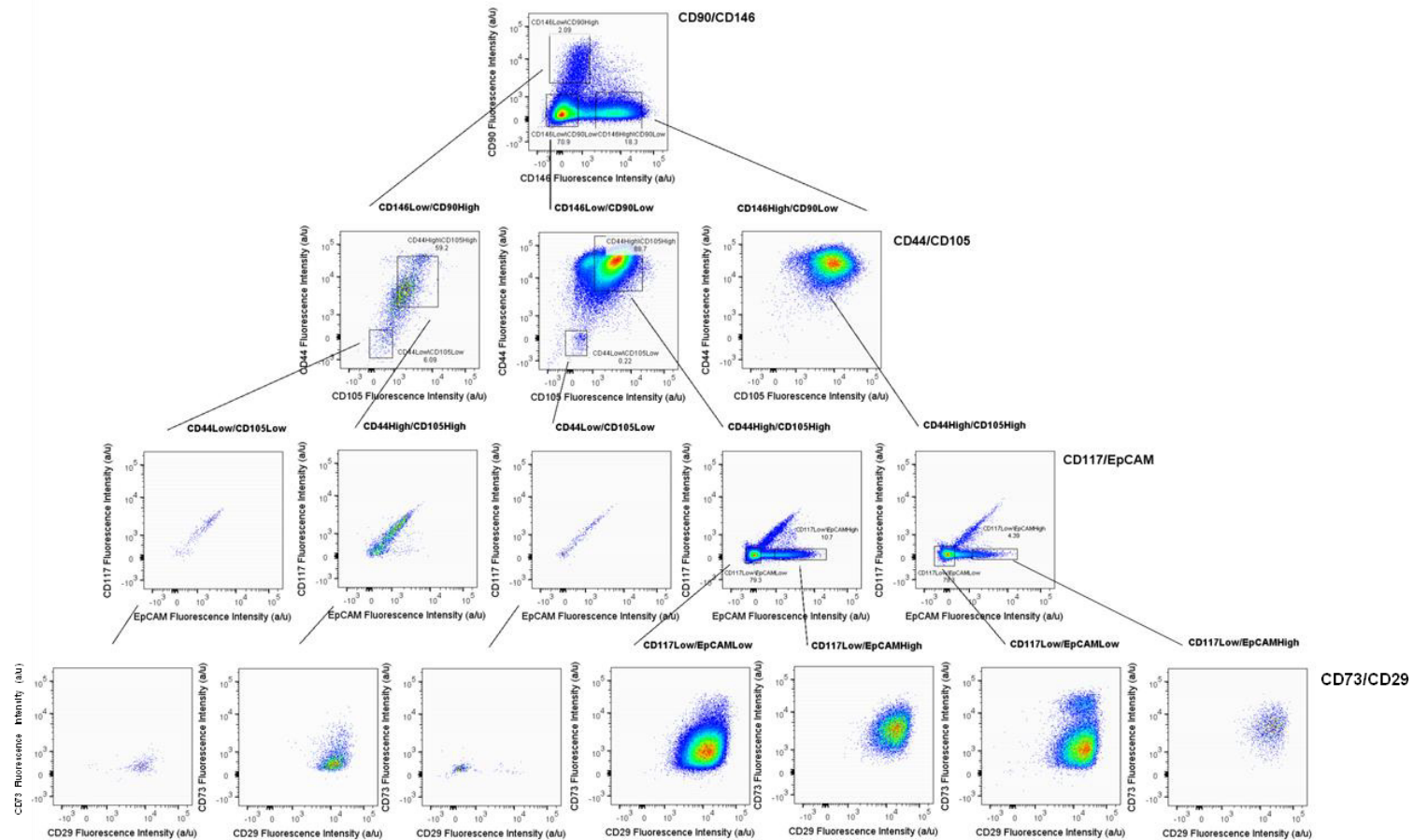


Figure 3.8 Identification of CD90/CD146 subpopulations in CAKI-1 WT cells by flow cytometry, data represented as dot-plots with two channels per plot. Data represented as bivariate dot-plots of two markers each. Cells were forward gated from CD90/CD146 into CD44/CD105, then CD117/EpCAM, and finally CD73/CD29. Data was acquired from 500,000 events. Data shown for one of three experiments.

3.3.3 Colony forming capacity of CD90/CD146 subpopulations from RCC cell lines

In order to identify which, if any, of the subpopulations found within the RCC cell lines were the most clonogenic, and therefore more stem cell-like, colony forming assays were performed on CD90/CD146 subpopulations. CD90/CD146 populations were chosen due to their presence in all three of the cell lines.

786-O appeared to be the most clonogenic of the three cell lines with unsorted cells achieving an average of 40 colonies (Figure 3.9). None of the CD90/CD146 subpopulations isolated from these cells exhibited a colony forming capacity that was significantly different to that of the unsorted (bulk) population. This was also observed when colony formation by CD90/CD146 subpopulations was normalised to the respective unsorted control for each individual experiment (Figure 3.9).

Unlike the 786-O cells, the CD146^{High}/CD90^{High} subpopulation in A498 cells showed a trend towards lower colony formation but this did not reach statistical significance (Figure 3.10). However, when accounting for inter-experimental variation, by normalising each of the CD146/CD90 subpopulations to their respective unsorted population, a 50% reduction in colony formation in the CD146^{High}/CD90^{High} cells when compared with the CD146^{Low}/CD90^{Low} cells was apparent ($P < 0.001$) (Figure 3.10).

Similarly to the A498 cell line, the CD146^{Low}/CD90^{High} population of CAKI-1 also displayed a much lower capacity for colony formation, with an average of 4 colonies formed. This lower colony formation proved to be significantly different from both unsorted cells ($P < 0.01$) and CD146^{Low}/CD90^{Low} ($P < 0.001$). Interestingly cells CD146^{High}/CD90^{Low} also displayed a modest decrease in colony forming capacity, generating an average of 13 colonies. This proved to be significantly lower colony forming capacity than CD146^{Low}/CD90^{Low} cells ($P < 0.05$), which represent the bulk

of the CAKI-1 cell line (Figure 3.11). However, no significant difference was observed when comparing these subpopulations with unsorted cells. When analysed as a percentage of unsorted control, the CD146^{Low}/CD90^{High} population showed a colony forming capacity of 20%, significantly lower than that of the CD146^{Low}/CD90^{Low} population ($P < 0.01$). Percentage colony formation of the CD146^{High}/CD90^{Low} population was decreased compared to the CD146^{Low}/CD90^{Low} cells but this was not statistically significant. (Figure 3.11)

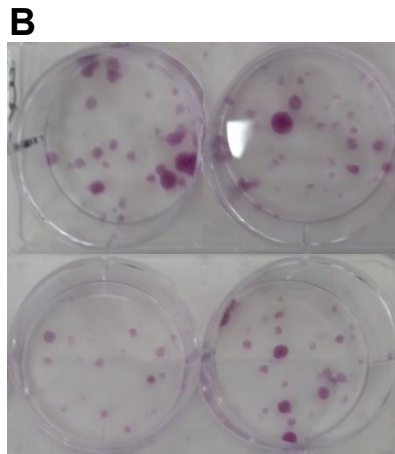
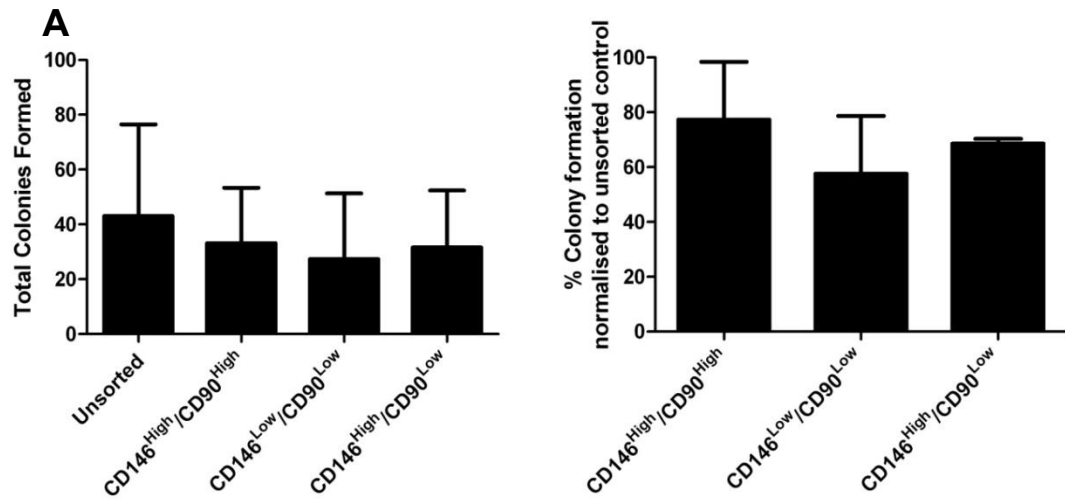


Figure 3.9 Colony formation assays for CD146/CD90 subpopulations in 786-O cells. **A** Total colony formation and percentage colony formation normalised to unsorted control in 786-O WT cells and CD146/CD90 subpopulations. Data represents mean \pm standard deviation $n=6$ wells in 3 separate experiments, each population seeded in duplicate. Significant difference was tested by one-way ANOVA with Tukey post-hoc. **B** Shows representative images of 786-O WT colony formation assays derived from the initial seeding of 400 cells of each of the sorted populations: unsorted (top left), CD146^{High}/CD90^{High} (top right), CD146^{Low}/CD90^{Low} (bottom left) and CD146^{High}/CD90^{Low} (bottom right).

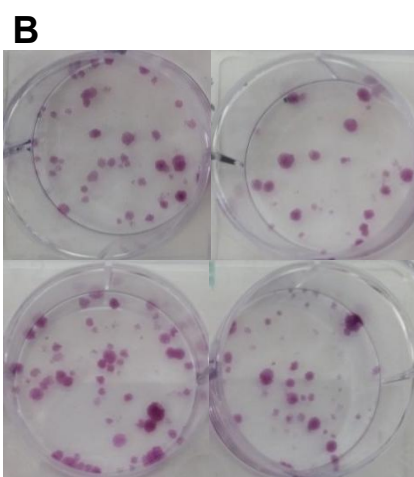
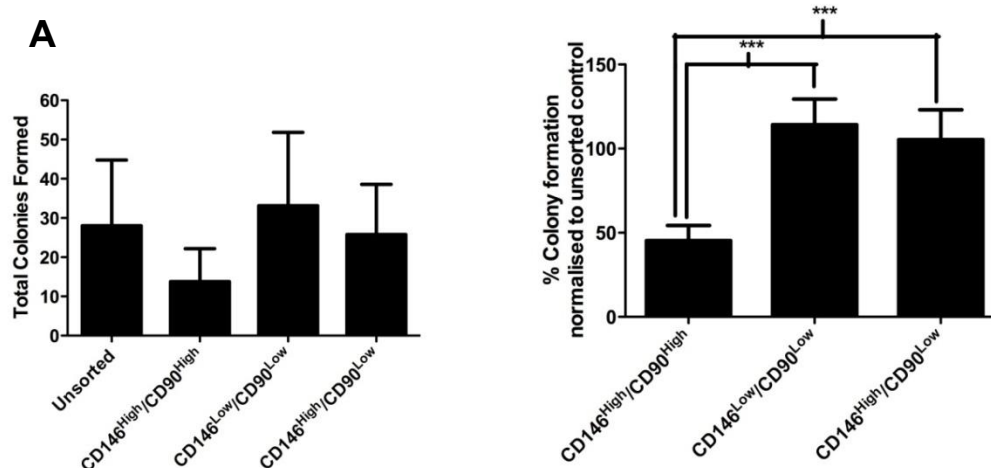
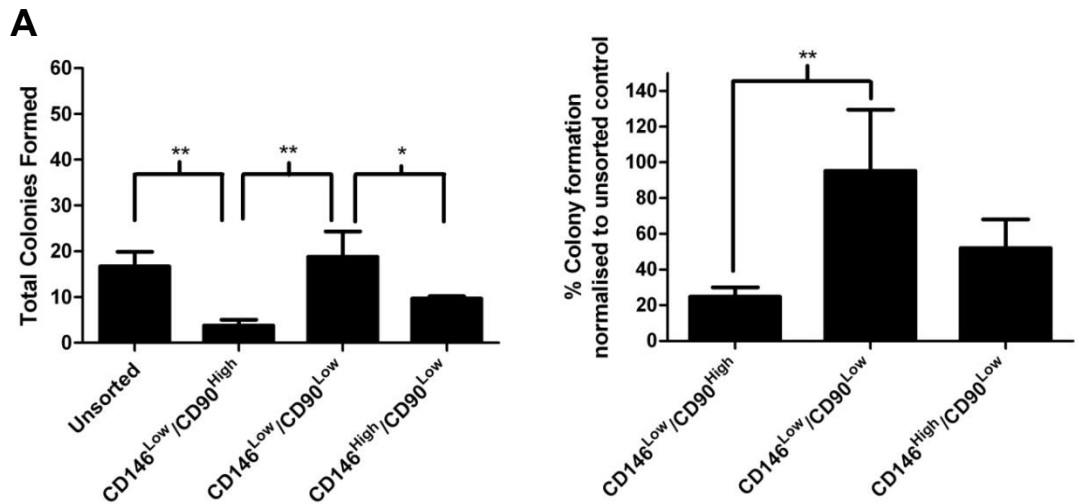


Figure 3.10 Colony formation assays for CD146/CD90 subpopulations in A498 cells (A) Total colony formation and percentage colony formation normalised to unsorted control in A498 WT cells and CD146/CD90 subpopulations. Data represents mean \pm standard deviation $n=8$ wells in 4 separate experiments, each population seeded in duplicate. Statistical difference was tested by one-way ANOVA with Tukey post-hoc *** = $P < 0.001$. (B) Shows representative images of colony formation assays of 400 cells seeded for each of the sorted populations: unsorted (top left), CD146^{High}/CD90^{High} (top right), CD146^{Low}/CD90^{Low} (bottom left) and CD146^{High}/CD90^{Low} (bottom right).



B

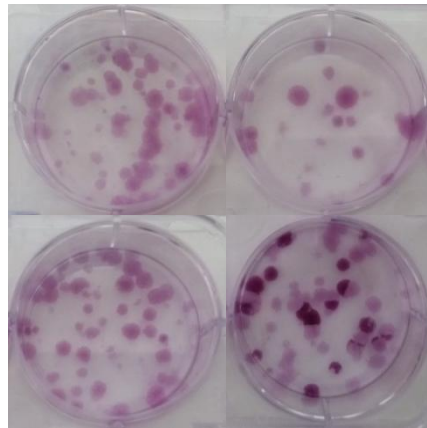


Figure 3.11 Colony formation assays for CD146/CD90 subpopulations in CAKI-1 cells (A) Total colony formation and percentage colony formation normalised to unsorted control in CAKI-1 WT cells and CD146/CD90 subpopulations. Data represents mean \pm standard deviation $n=8$ wells in 4 separate experiments, each population seeded in duplicate. Statistical difference was tested by one-way ANOVA with Tukey post-hoc * = $P<0.05$ ** = $P<0.01$. (B) Shows representative images of colony formation assays of 400 cells seeded for each of the sorted populations: unsorted (top left), CD146^{Low}/CD90^{High} (top right), CD146^{Low}/CD90^{Low} (bottom left) and CD146^{High}/CD90^{Low} (bottom right).

3.4 Discussion

The aim of this chapter has been to identify and evaluate the clonogenicity of putative CSC populations within the RCC cell lines 786-O, A498 and CAKI-1 using the surface markers CD90, CD146, CD44, CD105, EpCAM, CD117, CD29 and CD73.

Of the three cell lines examined, 786-O was the most clonogenic cell line in terms of the total heterogeneous cell line population, with A498 and CAKI-1 having a slightly lower capacity for colony formation. Flow cytometric analysis of the marker panel revealed heterogeneity of expression between all three cell lines with regards to the two markers CD146 and CD90. As such these markers provided the starting tier for the gating hierarchy. Forward gating CD146/CD90 populations in 786-O and A498 cells demonstrated little further sub-population heterogeneity but in CAKI-1 it was possible to identify eight different sub-populations of varying proportions based on the eight markers used.

The bimodal expression of CD146 was detected in all three cell lines with the proportions of cells in the CD146^{Low} and CD146^{High} populations differing between them. The highest proportion of CD146^{High} cells was found in 786-O while A498 and CAKI-1 contained the lowest. Sorting of CD146^{Low} and CD146^{High} populations and evaluation of their clonogenic potential did not yield cells with differing clonogenic potentials in 786-O or A498 but the CD146^{High} population in CAKI-1 had a significantly lower clonogenic potential than the CD146^{Low}/CD90^{Low} population. This data would seem to suggest that while the highest CD146 expression is detected in the more clonogenic 786-O cell line its expression does not necessarily indicate a more clonogenic subpopulation within that cell line, as also evidenced by the decreased clonogenicity of the CAKI-1 CD146^{High}/CD90^{Low} subpopulation. This seems to suggest that if CD146 does play a role in identifying clonogenicity it may be dependent on other, possibly synergistic, markers or biological functionality not

included in this study. Indeed studies by Espagnolle et al[315]. found that in bone marrow MSCs CD146 expression did not significantly influence colony forming capacity but did identify cells committed to vascular smooth muscle differentiation. While CD146 populations did not differ in terms of their colony formation in 786-O it does appear that the CD146^{Low} population formed smaller colonies (Figure 3.6 A) suggesting a possible role for CD146 in identifying the rapidly proliferating bulk of the cell line that are still capable of clonogenicity.

A subpopulation of CD90^{High} cells was found in all three cell lines. This population represented a small percentage of the total cell population in each cell line. In 786-O and A498 CD90^{High} cells were also found to be CD146^{High}, while in CAKI-1 cells the CD90^{High} was associated with CD146^{Low}. In the case of A498 and CAKI-1 the CD90^{High} population formed significantly fewer colonies than the respective unsorted cells and compared to the CD146^{Low}/CD90^{Low} populations, indicating CD90 as a marker for significantly reduced colony formation in these cell lines. Interestingly, in A498 and CAKI-1 cells the CD90^{High} phenotype appeared unaffected by CD146 status, either CD146^{High} or ^{Low}. The CD90^{High} population in A498 and CAKI-1 cells that was associated with decreased colony forming capacity may be the more differentiated daughter lineage of a stem-like population present in either the CD146^{Low}/CD90^{Low} or CD146^{High}/CD90^{Low} population. The inability of CD90 positive cells to enrich for stem like cells has been also found in the identification of CSCs from glioma samples. CD90^{High} populations identified by Woo et al. found did not have a significant advantage in terms of colony formation compared to their CD90^{Low} counterparts[316]. Further to this, rat bone and adipose derived MSCs identified by CD90 and CD29 positivity displayed a decrease in colony forming capacity and decrease in osteogenic and adipogenic capacity compared to the bulk cell population[317].

Surprisingly, CD105 a marker which has been used previously to isolate CSC or tumour initiating populations from primary RCC samples[61], was only highly expressed in the CAKI-1 cell line with relatively little expression detectable in 786-O and A498 cells. Further to this, while unsorted 786-O cells displayed the highest mean total colonies formed it also showed a large degree of variation between experiments. However in CD105 expressing CAKI-1 cells, variation between experiments was greatly reduced. This suggests the possibility that CD105 expression maybe required for stability of clonogenicity or provides protection from the relatively harsh conditions required for flow cytometry and cell sorting. In addition to CD105 expression CAKI-1 is also derived from a lung metastatic kidney tumour[318] ,and therefore may have inherently greater resistance to such conditions.

However, an absence or low levels of CD105 in Caki-1 cells may still affect colony formation. Forward gating of CAKI-1 $CD146^{High}/CD90^{Low}$ and $CD146^{Low}/CD90^{Low}$ populations into a bivariate plots of CD44/CD105 revealed that over 80% of both these populations highly expressed CD44 and CD105. However, in the less clonogenic $CD146^{Low}/CD90^{High}$ population the population displaying $CD44^{High}/CD105^{High}$ expression was reduced to below 60% with an increase in the $CD44^{Low}/CD105^{Low}$ gate. This may indicate that while an increased proportion of $CD105^{High}$ cells does not identify a substantial increase in clonogenic potential, it is still important in maintaining a high degree of clonogenicity.

CD44 has seen widespread use as a marker of CSCs and has been used for multiple tumour types. It is capable of identifying relatively small ($CD44^{High}$) CSC populations through to CSC populations ($CD44^{High}$) that represent the bulk of the tumour[162]. In the case of 786-O, A498 and CAKI-1 a universally high expression of CD44 was observed. CAKI-1 contained a relatively small proportion of $CD44^{Low}$ cells predominantly found associated with the less clonogenic $CD90^{High}$ lineage. The

same uniformly high expression was also true for the marker CD29 which, like CD44, has been used extensively to identify MSCs[287]. While this does rule out the use of a CD29 and CD44 marker combination to identify a more potent CSC population it suggests a strong mesenchymal phenotype for these cell lines.

Table 3.6 Characterisation summary of CSC surface markers used in RCC cell lines

| Marker | Ability to identify subpopulations | Notes |
|---------------|---|--|
| CD90 | Informative | All cell lines contain a CD90 high population |
| CD146 | Informative | All cell lines contain a CD146 high population. |
| C44 | Not informative | All cell lines appear to highly express CD44 |
| CD105 | Not informative | 786-O and A498 low expression of CD105 with no CD105 high population. |
| EPCAM | Not informative | Only CAKI-1 has a EpCAM high population. |
| CD117 | Not informative | All cell lines appear CD117 low. |
| CD73 | Not informative | 786-O and A498 generally low. CAKI-1 cells either High or low depending on subpopulation |
| CD29 | Not informative | 786-O and A498 generally high. CAKI-1 cells either high or low depending on subpopulation. |

In summary, CSC related cell surface marker analysis of the RCC cell lines 786-O, A498 and CAKI-1 revealed subpopulations identified by varying expression levels of the markers CD90, CD146, and in the CAKI-1 cell line CD44 and CD105 (Table 3.6). In particular, expression of CD90 and CD146 was found to be bimodal in all three cell lines and as such this combination was used as the first tier of the gating

hierarchy for cell sorting. Sorting of CD90/CD146 subpopulations into colony formation assays did not enrich for a more clonogenic sub-population in these cells but did identify a population of CD90^{High} cells in the A498 and CAKI-1 lines with decreased clonogenic capacity. Further forward gating of CD90/CD146 subpopulations in 786-O and A498 found homogeneity in the markers EpCAM, CD117, CD29 and CD73. In CAKI-1 forward gating of CD90/CD146 populations found further heterogeneity, especially in regards to CD44/CD105 expression. While the identification of such subpopulations was possible, they were found at extremely low frequencies such that sorting in sufficient numbers would be impractical. Therefore further experimentation focused on the effect of CAV1 upon the clonogenicity of CD90/CD146 subpopulations in these RCC cell lines.

Chapter 4 - Effect of CAV1 knockdown on the subpopulation distribution and clonogenicity of RCC cell lines

4 Effect of CAV1 knockdown on the subpopulation distribution and clonogenicity of RCC cell lines

4.1 Introduction

The balance for stem cells to both drive the formation of healthy tissue through differentiation and maintain themselves as a pool of undifferentiated cells is one of the defining features of stem cells. It governs the ability for embryonic tissue generation and organogenesis as well as homeostasis of healthy adult tissue. The acquisition of such 'stem-like' functional characteristics is now thought to be integral to the progression, metastatic spread and disease recurrence of multiple cancers, though the mechanisms by which this 'stem-like' phenotype is regulated remain elusive and will vary depending on the tissue of origin[319]. CAV1, has been implicated in both normal tissue function and disease progression for a number of cancers through a multitude of cellular physiological processes[103], [320]. Naturally, this has led to the study of CAV1, and caveolae, in relationship to the maintenance and regulation of the stem cell phenotype.

4.1.1 CAV1 as a regulator of stem cell phenotype

The context dependent role of CAV1 in biological processes is also apparent in the functional biology of stem cell populations of embryonic and mesenchymal origin. Several studies using CAV1 knockout mice have found hyperproliferation of intestinal crypt stem cells[107], neural stem cells of the subventricular zone of the brain[321] and mammary stem cells[322]. The same upregulation of proliferation was also observed in mesenchymal stem cell (MSC) populations isolated from the bone marrow of CAV1 knockout mice[323]. In neural progenitor cells of CAV1 knockout mice, CAV1 has been shown to downregulate proliferation through activation of glucocorticoid receptor signalling[324]. In human MSC populations downregulation of CAV1 enhanced proliferation and osteogenic differentiation[325].

Contrasting to this in another study[326] the capacity for adipogenic differentiation of MSCs was found to decrease with overexpression of CAV1. This increase in CAV1 expression became more pronounced as cells approached senescence, suggesting overexpression of CAV1 in MSCs important in stabilising the adipocyte phenotype. Unlike other adult stem cell populations hematopoietic stem cells (HSCs) isolated from CAV1 knockout mice showed a decrease in differentiation of B cell populations. In addition, HSCs displayed reduced self-renewal capacity *in vitro* and an inability to reconstitute haematopoiesis in immune-deficient mouse models[327].

Contrary to the inhibitory role of CAV1 upon proliferation in adult MSCs, CAV1 and caveolae play an important part in the self-renewal of embryonic stem cells (ESCs). For example, ESCs treated with either methyl- β -cyclodextrin (M β C) (a classical method of depleting caveolae through removal of cholesterol from the plasma membrane) or by CAV1 siRNA decreased cell proliferation as well as the expression of cell cycle markers cyclin D1 and E, and several self-renewal transcription factors[328]. Supplementary to this, CAV1 phosphorylation and the presence of caveolae were required for promoting proliferation of mouse ESCs grown upon a fibronectin matrix a major component of the ESC extracellular niche[329]. The signalling regulation involved the FAK/Src/integrin β 1 network inducing the Akt/ERK1/2 pathway. This role was further investigated by Park et al.[330] who found that the pro-proliferative effect of CAV1 in mouse ESCs could be induced by estradiol-17 β mediated phosphorylation of CAV1. They further confirmed CAV1 was required for potentiation of EGF signalling through EGFR driving proliferation and migration[331]. This role for CAV1 as a mediator for intracellular signalling has also been investigated in mouse ESCs. For example reduction of both CAV1 by siRNA and of caveolae by M β C treatment prevented the downstream phosphorylation of Akt and mTOR leading to reduced DNA synthesis and the reduced expression of cyclins[332]. Furthermore localisation of leukemia inhibitory

factor (LIF) to caveolae through glycan LacdiNAc allows the potentiation of STAT3 signalling by LIF. However, CAV1 was not critical to this STAT3 activation; suggesting a CAV1 redundant system of caveolae-based signalling is in place in cells where such signalling is critical for cellular processes such as self-renewal[333].

Regulation of the proliferation of stem cell populations is not the only means by which the propensity for self-renewal can be governed. Alterations to the differentiation potential of stem cells can result in an increase or decrease in self-renewing stem cell populations. CAV1 has been variously implicated in the regulation of these processes. For example, *in vitro* the osteogenic differentiation of human MSCs is associated with upregulation of CAV1[325]. While the neurogenesis of rat bone marrow MSCs is promoted by downregulation of CAV1 inducing downregulation of the Notch signalling pathway, suggesting CAV1 acts to preserve the undifferentiated phenotype[334]. This ability to preserve stem cell populations is also apparent in the bone marrow MSCs of CAV1 knockout mice. These bone marrow MSCs have an increase capacity for osteogenic differentiation compared to their CAV1 expressing counterparts[335]. Such findings have also been established in human MSC where CAV1 knockdown increased adipogenic[326] and osteogenic[325] differentiation. This implies the possibility that CAV1 expression acts to hold these stem cell populations in an undifferentiated multipotent state.

The ability for CAV1 to hold cells in an undifferentiated stem cell phenotype would be likely to occur within caveolae domains through the interaction of CAV1 with cell surface receptors responsible for activation of differentiation, the presence here of CAV1 would hold pro-differentiation molecules in an inactive state. Some studies have provided data in support of this theory. Mouse bone marrow stromal cells (BMSCs) exposed to the cholesterol biosynthesis inhibitor simvastin, cholesterol being a key component of caveolae, acquired increased potential for osteogenic

differentiation and a diminished response to adipogenic differentiation, indicative of reduced multipotency[336]. Similarly MSCs exposed to oxysterols were reported to display increased osteogenic but reduced adipogenic differentiation[337]. The underlying mechanism relating to oxysterol induced downregulation and decoupling of CAV1 from caveolae to the plasma membrane. Considering CAV1's direct involvement in the regulation of a number of signalling pathways thought to be key for potentiation of differentiation such as Wnt/ β -catenin[338], [339], transforming growth factor beta (TGF- β)[340], [341] and bone morphogenetic protein (BMP)[342], [343], it appears caveolae/CAV1 may provide a nexus point of differentiation of stem cell populations.

It appears therefore that CAV1 maybe a key molecule for driving CSC populations from both a perspective of maintaining a balance of self-renewal to that of increased bulk cell differentiation. Indeed, exploiting the differentiation of CSCs has already been investigated in RCC samples. By treating CD105⁺ CSCs with recombinant human interleukin-15 (rhIL-15) the CD105⁺ cells were induced towards epithelial differentiation, and a reduced self-renewal capacity with an increased sensitivity to common cytotoxic agents[73]. However, to a larger extent the role of CAV1 in the biology of CSCs remains largely unexplored, though the handful of discoveries that have been made thus far have once again revealed context-dependent roles for CAV1. In non-small cell lung carcinoma the CSC phenotype can be induced by exposure to nitric oxide (NO). Such treatment mediated CAV1 upregulation which induced resistance to anoikis and spheroid formation as well as increasing the migration and invasion of these cells[344]. Conversely, investigations into the nature of CAV1 expression in the progression of pancreatic cancer Salem et al. found CAV1 expression to actually indicate transition to an epithelial phenotype and decreased tumourgenicity in immunodeficient mice[345].

CAV1 appears to play an important role in many aspects of clonogenicity in stem cell biology, from regulating the proliferative capacity of stem cell populations to acting as a gatekeeper to differentiation. Furthermore, these functions are not only observed in one specific stem cell population but in MSCs from various tissues and those of embryonic origin, in which CAV1 and caveolae expression appears to be of great importance. As such this has led us to suggest a potential role for CAV1 either in directing the proliferation of CSC subpopulations in RCC or in the regulation of differentiation to less clonogenic subtypes.

4.1.2 Aims

This chapter aimed to understand the relationship of CAV1 in the clonogenicity of the RCC cell lines 786-O, A498 and CAKI-1. More specifically, it sought to explore how:

- CAV1 can affect the clonogenic capacity of both the total heterogeneous cell line population and also the subpopulations identified by CD90/CD146 expression in the previous chapter.
- Understand how CAV1 expression affects subpopulation distribution and if such changes in distribution maybe causative in any change in clonogenic capacity observed. For example, would a large increase in CD90^{High} cells result in reduced clonogenicity capacity of the total cell line.
- Effects on clonogenicity were then further confirmed using spheroid formation assays.
- To understand if any effect on clonogenicity is linked to proliferative capacity a series of proliferation assays were conducted together with assessment of cell cycle regulation under clonogenic conditions.

4.2 Materials and Methods

4.2.1 Generation of CAV1 shRNA knockdown cell lines

In order to probe the effect of CAV1 knockdown on assays requiring extended periods of incubation CAV1 stable shRNA knockdowns were generated. Five separate SureSilencing shRNA plasmids (Qiagen), containing four sequences specific to CAV1 and one containing a scrambled negative control shRNA, were transfected by heatshock into competent JM109 *E. coli* (Promega). Subsequently, 100 μ L of the transfected cultures were spread onto LB agar (Fisher Scientific) plates containing 50 μ g/mL ampicillin (Sigma Aldrich) and incubated for 16 hours at 37 $^{\circ}$ C to allow the growth of viable colonies. Single colonies for each plasmid were picked and streaked onto new LB agar/ampicillin plates and incubated for a further 16 hours to allow the formation of single colonies. Single colony were then picked from each plate and inoculated into separate 15mL centrifuge tubes containing 1mL of LB broth (Fisher Scientific) containing 50 μ g/mL ampicillin and incubated for 12 hours on an orbital shaker at 37 $^{\circ}$ C. Following this each 1mL culture was inoculated into 250mL of fresh LB broth/ampicillin and incubated at 37 $^{\circ}$ C for a further 4 hours. After this cultures were collected and plasmids purified using the QIAfilter Plasmid Midi Kit (Qiagen). Plasmid DNA was then quantified by a GeneQuant spectrophotometer at 260nm. Confirmation of successful transfection was carried out by Pst-1 (New England Biolabs) digestion of 10 μ g of plasmid DNA which was then separated by agarose gel electrophoresis producing two bands one of 3209 bp and one of 1402 bp (Appendix 1).

For transfection into RCC cell lines, Cells were seeded into 24-well plates at a higher density of 40,000 cells per cm² (as required for transfection with FuGENE[®] HD) and incubated for 24 hours at 37 $^{\circ}$ C. To help ensure a stable knockdown, prior to transfection plasmid DNA was linearized by Sca-1(New England Biolabs)

digestion and prepared for transfection by using the Wizard® SV Gel and PCR Clean-Up system (Promega). Plasmid DNA was then mixed with FuGENE® HD (Promega) at a ratio of 1µg of plasmid DNA to 1.5µL of FuGENE® HD and allowed to complex at room temperature for 15 minutes. During this incubation cells were washed twice in sterile PBS. After the final change of PBS 500mL of respective full media was added to which 200µL of the plasmid complex was added and incubated for 24 hours. To select for successful transfection of the plasmid, cells were first trypsinised then reseeded into 6-well plates at a density of 1,000 cells per cm² in media containing 1µg/mL puromycin (Appendix 1). Cells remained in this selection media which was changed every 3 days until large colonies were visible. Colonies were then trypsinised and reseeded until enough cells were harvestable for frozen stocks and western blot analysis of CAV1 knockdown.

4.2.2 Western Blot

Cells were lysed on ice directly from 6-well tissue culture plates using 200 µL of ice cold lysis buffer (50 mM Tris (pH 7.5), 5 mM EDTA, 1% Triton-X, 150 mM NaCl all obtained from Fisher Scientific) containing a cocktail of protease inhibitors (leupeptin, aprotinin, leupeptin, sodium fluoride, sodium molybdate, phenylarsine and sodium pervandate all obtained from Fisher Scientific), the surface was then scraped and incubated for 15 minutes. Lysates were then collected and cellular debris centrifuged at 20,000g for 15 minutes at 4°C. Preparation of hypoxic lysates was carried out in the same way after 72 hours of incubation under 1% O₂.

Protein concentration was determined by use of the Pierce™ BCA protein assay kit (Thermo Fisher). 25µL of lysate and a calibration curve of bovine serum albumin (BSA) (Sigma Aldrich) (25µg/mL to 2000µg/mL) was incubated for 40 minutes with 200µL with BCA solution and read at 560nm using a LT-5000MS plate reader (Labtech). Proteins were prepared for separation by electrophoresis by heating

20 μ g of lysate to 95 $^{\circ}$ C for 10 minutes in 4x Lamelli sample buffer (Fisher Scientific). Lysates were then loaded into pre-cast mini-PROTEAN TGX 12% polyacrylamide gels (Bio-Rad) with a well for a molecular weight marker Precision Plus Protein[™] WesternC[™] Protein Standards (Bio-Rad) and separated by electrophoresis at 100V for 90 minutes. Separated proteins were then transferred on to nitrocellulose membranes by semi-dry blotting using the Trans-Blot[®] Turbo[™] Transfer system (Bio-Rad). Gels and the recipient nitrocellulose membranes were allowed to equilibrate in blotting buffer containing 20% methanol for 15 minutes. A 'transfer-sandwich' was then constructed; this consisted of a layer of filter paper, the nitrocellulose membrane, gel and a final layer of filter paper. This was all placed in a transfer cassette and electrophoresed at 25V for 30 minutes. Following transfer membranes were washed twice in distilled water and blocked for 60 minutes in blocking buffer (5% non-fat powdered milk in tris buffered saline containing 0.1% v/v Tween 20 (TBS-T)). For immunoprobng, primary antibodies were diluted in blocking buffer CAV1 1:1000 (Cell Signalling, New-England Biolabs), β -actin 1:1,000 (Sigma Aldrich), Cyclin D1 1:1000 (Cell Signalling, New-England Biolabs) and HIF-2 α 1:500 (Novus-biologicals) and incubated overnight (~16 hours) at 4 $^{\circ}$ C on a rolling mixer. Membranes were then washed in TBS-T three times for 15 minutes each at room temperature on a rolling rocker. After washing membranes were then incubated with either HRP conjugated anti-mouse or anti-rabbit IgG 1:10,000 (Cell Signalling, New-England Biolabs) for 60 minutes at room temperature and were then washed in another 3 changes of TBS-T for 15 minutes. Specific protein bands were then revealed by using the chemiluminescence SuperSignal[®] West Dura Extended Duration Substrate kit with images captured using a ChemiDoc[™] imaging system.

4.2.3 Spheroid formation assays

Cells were first washed twice in sterile PBS rinsed with 2mL of trypsin, which was then removed, and incubated at 37 $^{\circ}$ C. Cells were then resuspended in serum free

stem cell media containing 20ng/mL epidermal growth factor (EGF), 20ng/mL basic fibroblast growth factor (bFGF), 1mL 50x B27 serum replacement supplement and 1% penicillin/streptomycin (all from Life Technologies). To ensure reproducibility in cell seeding, cells were seeded at 400 cells per well in 96-well, using the cell sorting capability of the FACsaria III, into ultralow adherence plates (Corning) containing 150µL of serum free stem cell media per well. Cells were then incubated at 37°C for 2 weeks with 20µL of fresh stem cell media added to each well every 3 days. The number of spheroids formed per well was manually counted after two weeks by phase contrast microscopy. Tumour spheroid formation was accepted as 3D structures generally larger than around 40µm in diameter and showing a relatively smooth but slightly cobbled surface.

For both hypoxic spheroid and colony formation cells were incubated in 1% O₂ with 5% CO₂ at 37°C (using a Leec Touch 50S incubator) all other elements of the methodology for each assay remained the same.

4.2.4 Proliferation assays

CAKI-1 scrambled shRNA control and CAV1 shRNA knockdown cells were seeded at 10,000 cells per cm² in 24-well plates for 72 hours. After which cell growth was accessed by either MTT or total cell counts. For MTT assays 200µL of 2mg/mL MTT (Sigma Aldrich) was spiked into each well of the 24-well plate and incubated for 2 hours at 37°C to allow the formazan reaction product to develop. After this, cells were gently washed once with room temperature PBS and then solubilised in DMSO. 200µL of each well was transferred to a new well in a 96-well plate and absorbance was read at 560nm (using a Labtech ELISA plate reader) with DMSO used as a background control. For total cell counts, cells were washed twice with PBS then 200µL of trypsin was added and quickly aspirated then incubated at 37°C for 5 minutes. Each well was then resuspended with 100µL of PBS and then diluted

into 10mL of isotone buffer and analysed using a Coulter-counter (Beckman-Coulter).

4.2.5 Cell cycle analysis

Analysis of cell cycle distribution of CAKI-1 scrambled shRNA control and CAV1 shRNA knockdown cells was determined using propidium iodide (PI) staining. Cells were first trypsinised as previously described and resuspended in 1mL of 5% FBS in PBS then centrifuged at 200g. The cell pellet was then resuspended in another 1mL of 5% FBS in PBS. Cells were then fixed by drop-wise addition to -20°C 70% ethanol and incubated at -20°C overnight. For cell staining, a solution containing 0.1% Triton X-100, 1 mg of RNase (Sigma Aldrich), and 100 mg/mL PI (Sigma Aldrich) in 4.5mL of 5% FBS in PBS was made fresh for each experiment. Ethanol fixed cells were pelleted at 200g at 4°C for 10 minutes the ethanol supernatant was discarded. The pellet was then resuspended in 1mL of 5% FBS in PBS and washed twice by the same centrifugation steps. The final pellet was then resuspended in 500 μL of the staining solution and incubated at room temperature for 30 minutes. Analysis of IP staining was carried out using the FACSVerse™ where PI was excited by the 488 nm laser and emission detected using a 586/42 nm filter. Cell cycle analysis was carried out using FlowJo Version 10 flow cytometry analysis software.

4.2.6 Statistical analysis

All statistical analysis was carried out using GraphPad Prism 5. All data are presented as mean with \pm standard deviation unless otherwise stated. Statistical difference between single paired groups was carried out by unpaired Student's t-test with statistical significance achieved at $P \leq 0.05$.

4.3 Results

4.3.1 CAV1 differentially affects the distribution of CD146/CD90 subpopulations between RCC cell lines and drives colony formation in CAKI-1 cells

To understand how CAV1 affects the frequency and clonogenicity of subpopulations identified within the 786-O, A498 and CAKI-1 cell lines, CAV1 stable shRNA knockdown approach was employed. Transfection of SureSilencing shRNA plasmid against CAV1 substantially reduced CAV1 expression (Figure 4.1).

Subpopulation flow cytometry analysis of the impact of CAV1 knockdown in 786-O cells by flow cytometry showed a significant increase in the percentage of cells within the CD146^{Low}/CD90^{Low} population with a concomitant decrease in the percentage of cells found in the CD146^{High}/CD90^{Low} population. The knockout of CAV1 also led to a reduction in the CD146^{High}/CD90^{High} population; however this did not reach the level of statistical significant. Forward-gating each of the CD146/CD90 subpopulations revealed no changes in surface marker expression following CAV1 downregulation (Figure 4.2, Figure 4.5 A and Table 4.1). While CAV1 seems to have significant involvement in influencing the proportion of CD146^{High}/CD90^{Low} and CD146^{High}/CD90^{High} populations it did not however reduce colony formation in the total unsorted 786-O cell line or in any of the CD146/CD90 subpopulations (Figure 4.6). The morphology of colonies formed by 786-O seems to be unaffected by CAV1 status with both scrambled shRNA and CAV1 shRNA cells forming colonies of roughly the same size and frequency.

The shift in distribution of CD146 populations induced by CAV1 knockdown found in the 786-O cells was also found in A498 cells. A498 CAV1 shRNA cells showed a significant decrease in the CD146^{High}/CD90^{Low} population from 4% to 0.5%. However, unlike in 786-O, the percentage of A498 cells in the CD146^{Low}/CD90^{High}

population of remained unaffected by reduced CAV1 expression (Figure 4.3, Figure 4.5 B and Table 4.1). Similarly to the 786-O cells, down-regulation of CAV1 in the A498 cells had no effect on the colony forming capacity of the total unsorted population or between the distinct CD146/CD90 subpopulations. In terms of colony morphology reduction of CAV1 expression did not significantly reduce the size or morphology of colonies formed (Figure 4.7).

Interestingly knockdown of CAV1 in CAKI-1 cells did not cause a change in either the CD146^{High}/CD90^{Low} or the CD146^{Low}/CD90^{High} populations (Figure 4.4, Figure 4.5 C Table 4.1). In contrast to 786-O and A498, down-regulation of CAV1 in CAKI-1 caused a significant reduction in colony formation. This reduction in clonogenicity was seen in the total unsorted population and in each of the distinct CD146/CD90 populations. In addition to this, CAV1 shRNA cells that were capable of colony formation formed colonies of reduced size compared to scrambled shRNA control (Figure 4.8).

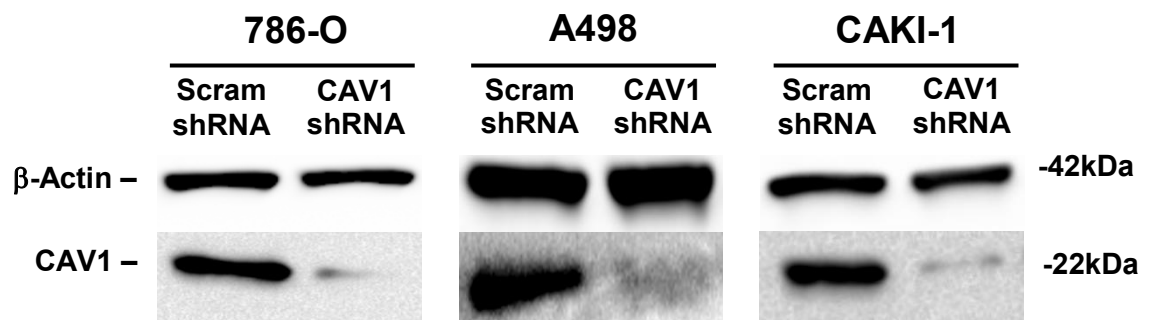


Figure 4.1 Downregulation of CAV1 in 786-O, A498 and CAKI-1 cells by SureSilencing shRNA plasmid. Evaluation of CAV1 knockdown performed by western blot with β -actin used as a loading control.

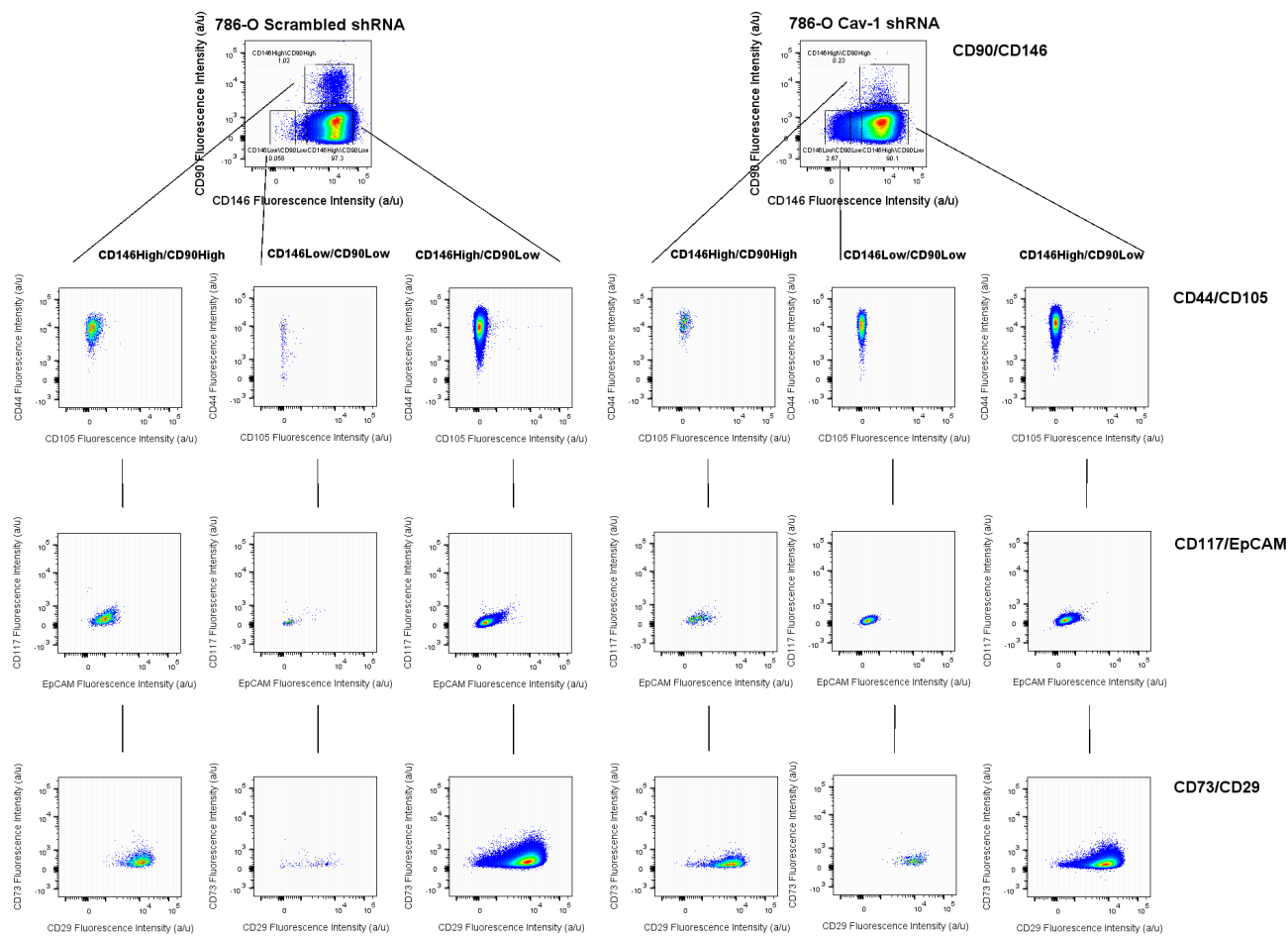


Figure 4.2 Gating hierarchies for both scrambled shRNA control cells and CAV1 shRNA transfected 786-O cells using the 8 marker putative CSC panel. Prior to sorting cells were first gated for live cells by FSC-A/SSC-A then single cells by FSC-H/FSC-A. Cells were then forward gated into each tier of the hierarchy. Data represents 500,000 events analysed for both 786-O scrambled shRNA and 786-O CAV1 shRNA.

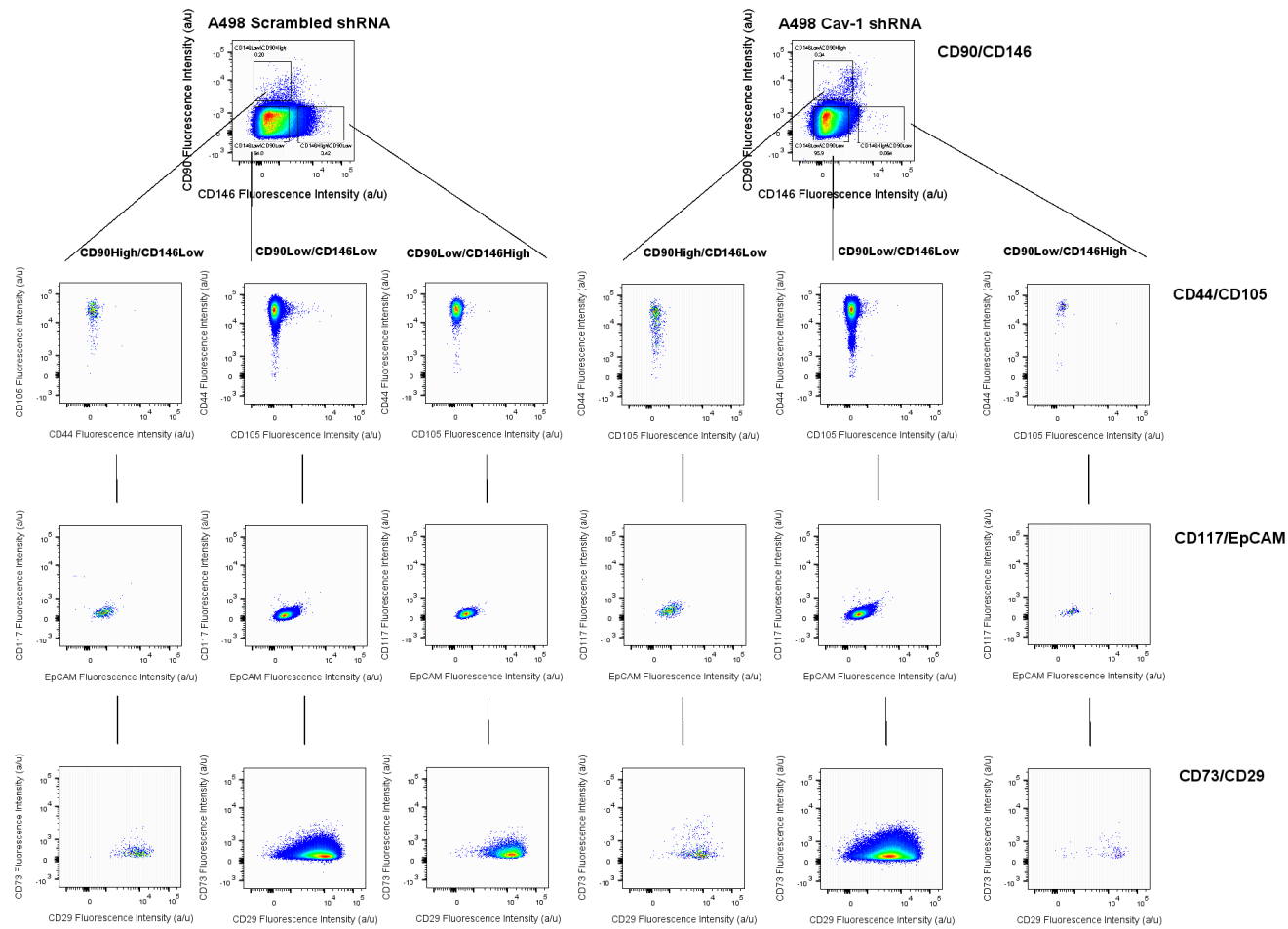


Figure 4.3 Gating hierarchies for both scrambled shRNA control cells and CAV1 shRNA transfected A498 cells using the 8 marker putative CSC panel. Prior to sorting cells were first gated for live cells by FSC-A/SSC-A then single cells by FSC-H/FSC-A. Cells were then forward gated into each tier of the hierarchy. Data represents 500,000 events analysed for both A498 scrambled shRNA and A498 CAV1 shRNA.

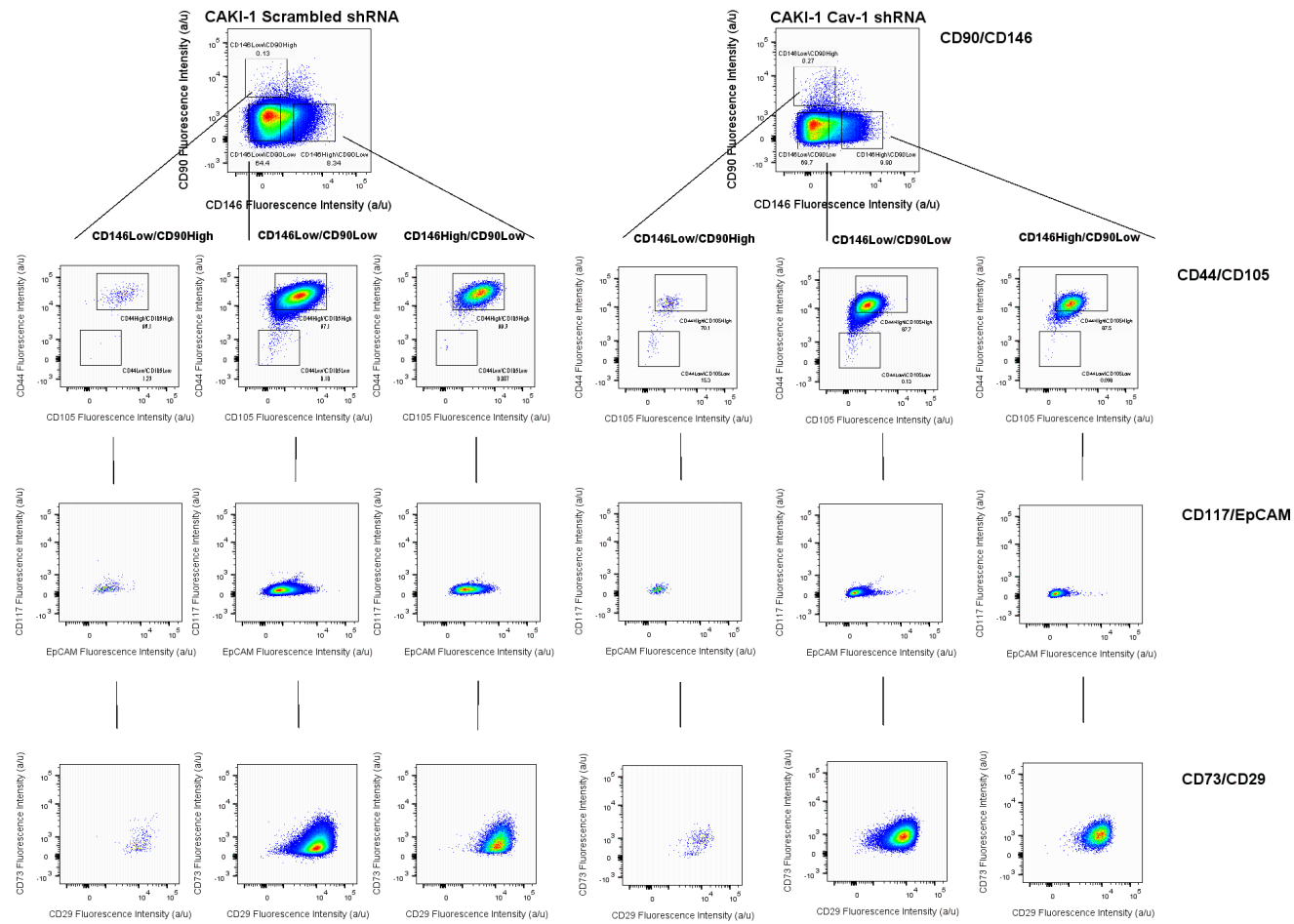


Figure 4.4 Gating hierarchies for both scrambled shRNA control cells and CAV1 shRNA transfected CAKI-1 cells using the 8 marker putative CSC panel. Prior to sorting cells were first gated for live cells by FSC-A/SSC-A then single cells by FSC-H/FSC-A. Cells were then forward gated into each tier of the hierarchy. Data represents 500,000 events analysed for both CAKI-1 scrambled shRNA and CAKI-1 CAV1 shRNA.

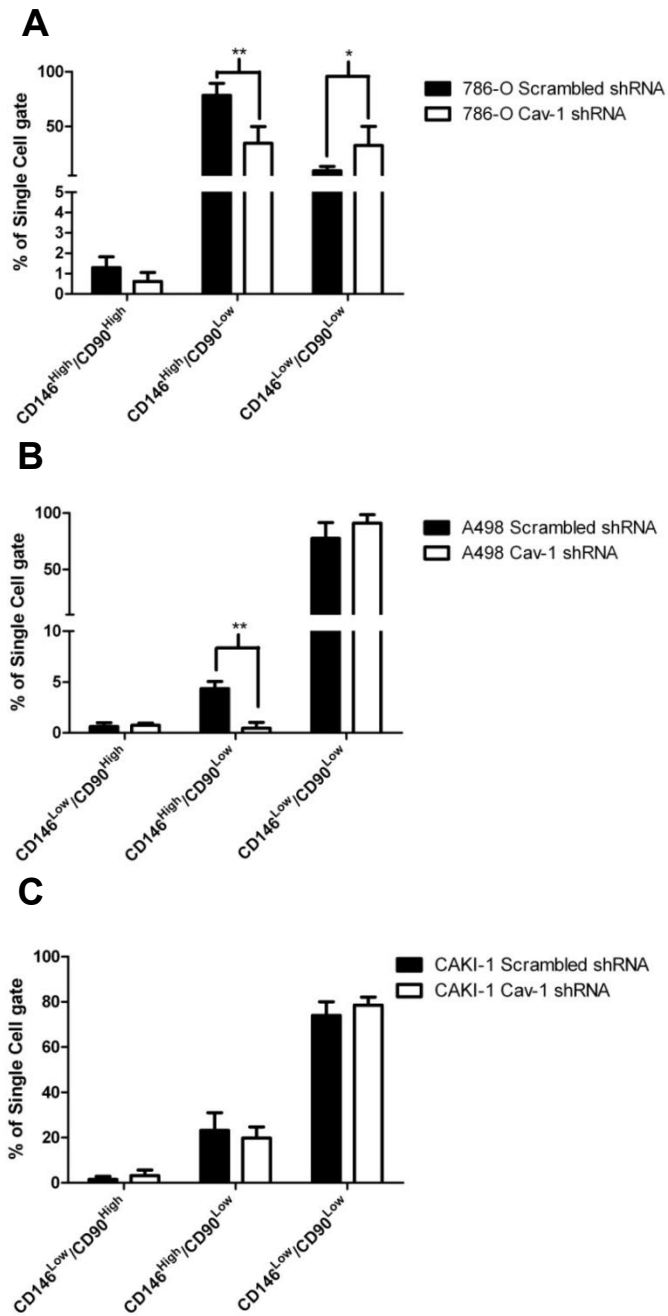
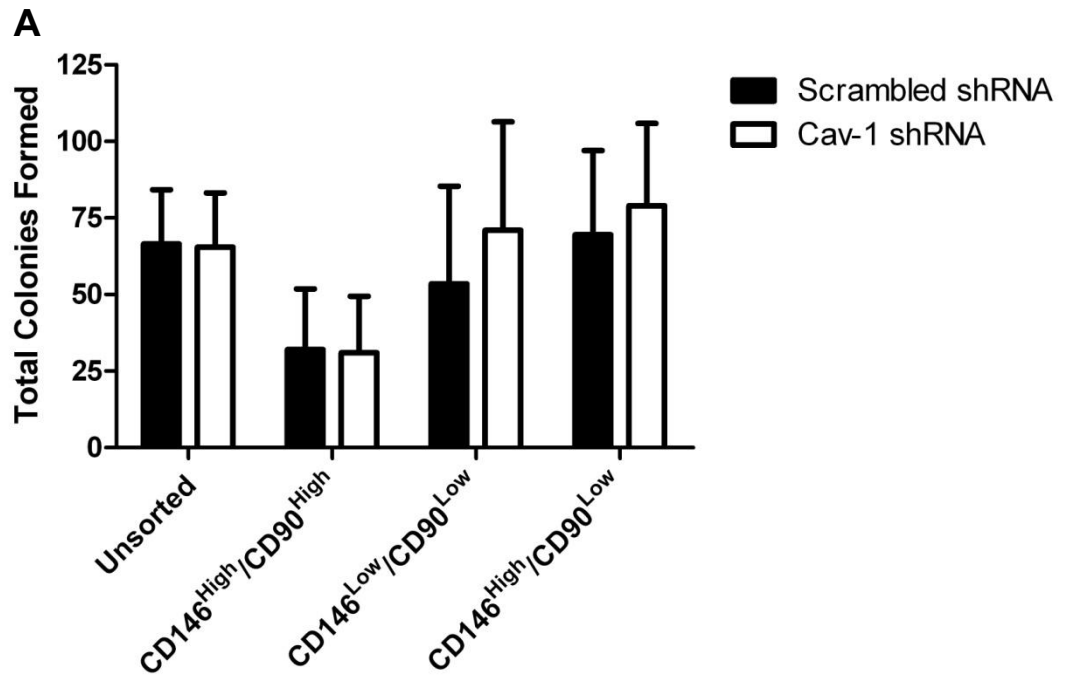


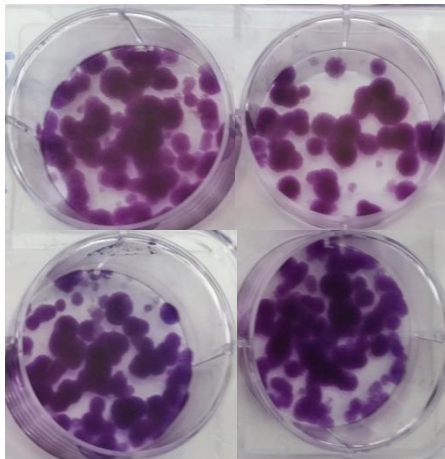
Figure 4.5 Effect of CAV1 knockdown on the mean percentage distribution of CD146/CD90 subpopulations in 786-O (A), A498 (B) and CAKI-1 (C). Data represents mean \pm standard deviation. Significance determined by Student's t test * = $P < 0.05$ ** = $P < 0.01$ n=3-4 separate experiments.

Table 4.1 Proportions of CD90/CD146 subpopulations in the cell lines 786-O, A498 and CAKI-1 in scrambled shRNA control and CAV1 shRNA knockdown cells. Data represents mean \pm standard deviation of 3 to for experiments per cell line, statistical difference was measured by Students T-test.

| 786-O | | | |
|---|------------------------|---------------------|----------------|
| | Scrambled shRNA | CAV1 shRNA | P value |
| CD90 ^{High} /CD146 ^{High} | 1.29% \pm 0.30% | 0.61% \pm 0.25% | 0.164 |
| CD90 ^{Low} /CD146 ^{High} | 78.33% \pm 6.33% | 34.63% \pm 8.73% | 0.015 |
| CD90 ^{Low} /CD90 ^{Low} | 9.38% \pm 2.31% | 32.57% \pm 10.02% | 0.040 |
| A498 | | | |
| | Scrambled shRNA | CAV1 shRNA | P value |
| CD90 ^{High} /CD146 ^{Low} | 0.62% \pm 0.22% | 0.75% \pm 0.12% | 0.626 |
| CD90 ^{Low} /CD146 ^{High} | 4.25% \pm 0.40% | 0.47% \pm 0.32% | 0.002 |
| CD90 ^{Low} /CD146 ^{Low} | 77.47% \pm 8.13% | 91.03% \pm 4.32 | 0.215 |
| CAKI-1 | | | |
| | Scrambled shRNA | CAV1 shRNA | P value |
| CD90 ^{High} /CD146 ^{Low} | 1.55% \pm 0.73% | 3.15% \pm 1.46% | 0.380 |
| CD90 ^{Low} /CD146 ^{High} | 23.17% \pm 4.50% | 19.77% \pm 2.84% | 0.558 |
| CD90 ^{Low} /CD146 ^{Low} | 73.97% \pm 3.47% | 78.50% \pm 2.05% | 0.324 |



B



C

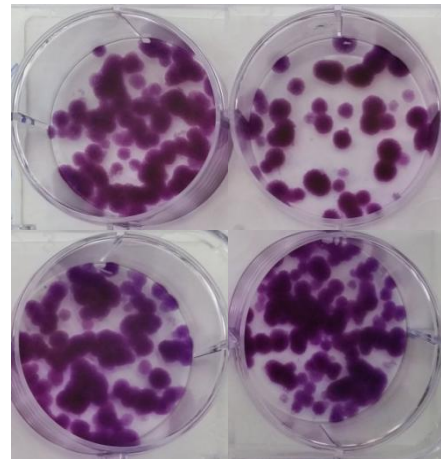
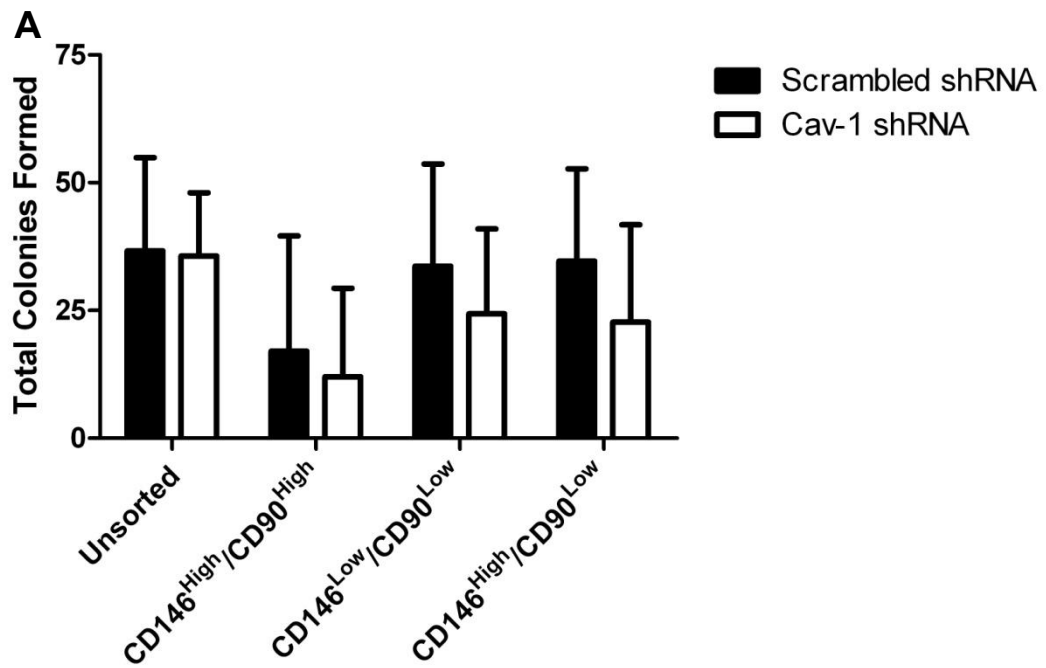
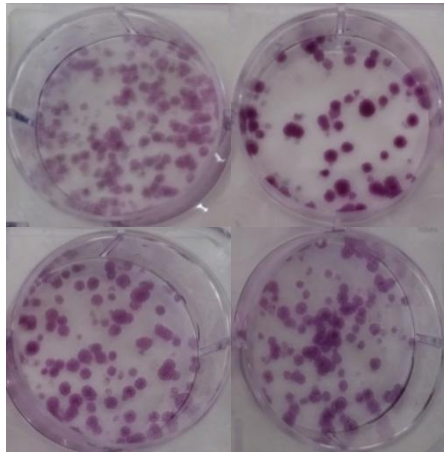


Figure 4.6 Effect of CAV1 downregulation on colony formation of 786-O CD146/CD90 populations (**A**) Graphs showing total colonies formed in CD146/CD90 subpopulations of scrambled shRNA control and CAV1 shRNA knockdown 786-O cells. Data represents mean \pm standard deviation. Analysis by Student's t test found no significant difference when comparing scrambled shRNA to CAV1 shRNA for each subpopulation $n=3$ separate experiments (**B**) Images of colony formation for 786-O scrambled shRNA cells unsorted (top left), CD146^{High}/CD90^{High} (top right), CD146^{Low}/CD90^{Low} (bottom left) and CD146^{High}/CD90^{Low} (bottom right). (**C**) Representative images of colony formation for 786-O CAV1 shRNA (layout the same as **B**)



B



C

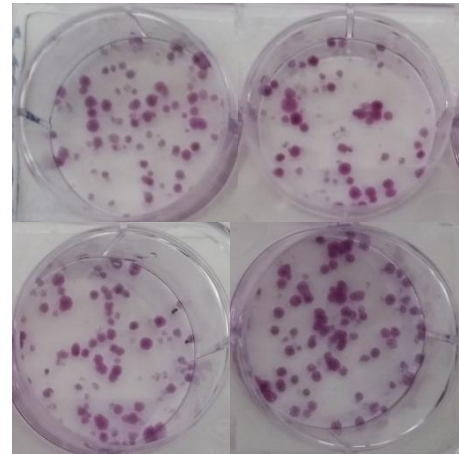
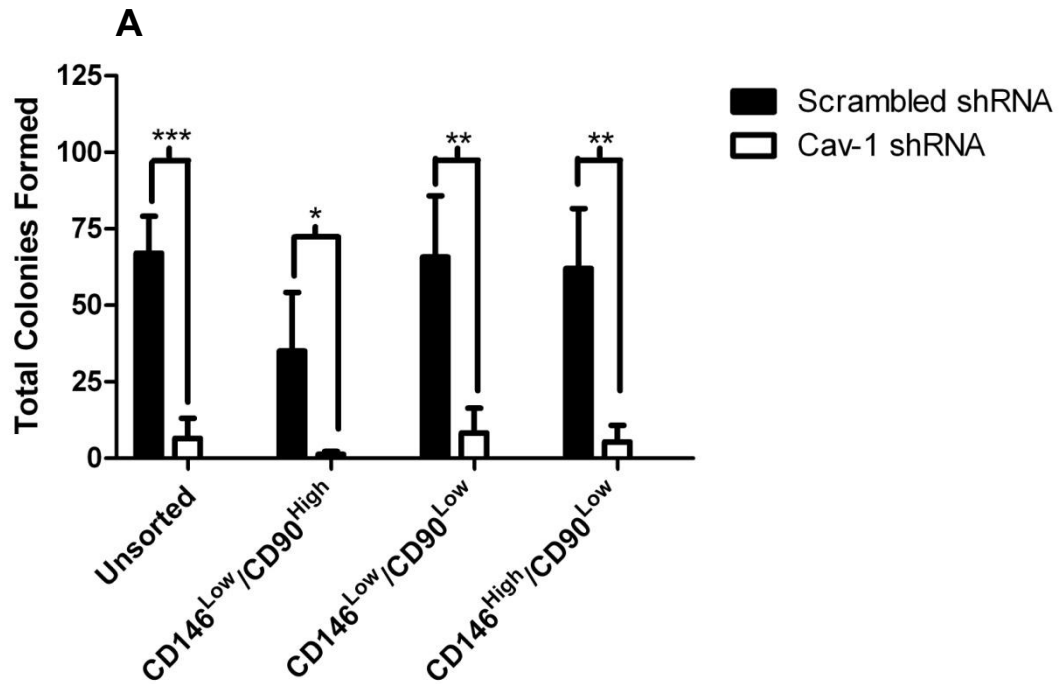
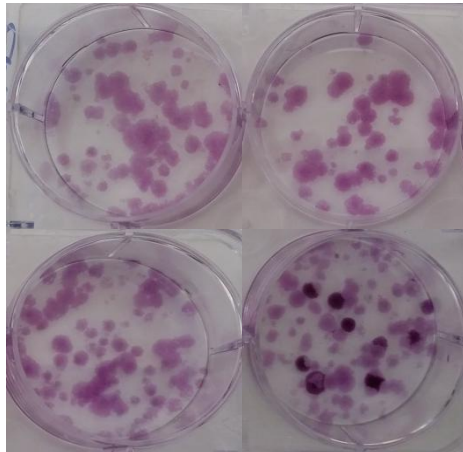


Figure 4.7 Effect of CAV1 downregulation on colony formation of A498 CD146/CD90 populations (**A**) Graphs showing total colonies formed in CD146/CD90 subpopulations of scrambled shRNA control and CAV1 shRNA knockdown A498 cells. Data represents mean \pm standard deviation. Analysis by Student's t test found no significant difference when comparing scrambled shRNA to CAV1 shRNA for each subpopulation $n=3$ separate experiments (**B**) Images of colony formation for A498 scrambled shRNA cells unsorted (top left), CD146^{High}/CD90^{High} (top right), CD146^{Low}/CD90^{Low} (bottom left) and CD146^{High}/CD90^{Low} (bottom right). (**C**) Representative images of colony formation for A498 CAV1 shRNA (layout the same as **B**)



B



C

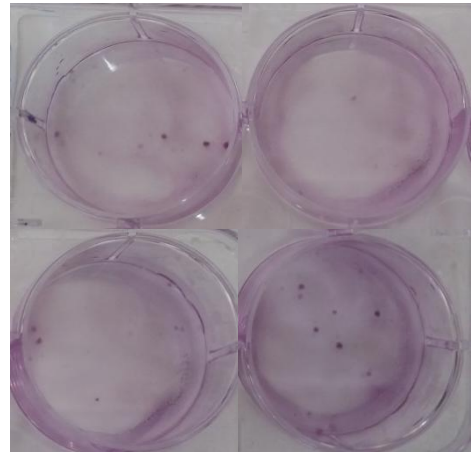


Figure 4.8 Effect of CAV1 downregulation on colony formation of CAKI-1 CD146/CD90 populations (**A**) Graphs showing total colonies formed in CD146/CD90 subpopulations of scrambled shRNA control and CAV1 shRNA knockdown CAKI-1 cells. Data represents mean \pm standard deviation. Significant difference by student's t test was found when comparing scrambled shRNA to CAV1 shRNA for each population * = $P < 0.05$ ** = $P < 0.01$ *** = $P < 0.001$ $n = 4$ separate experiments (**B**) Images of colony formation for CAKI-1 scrambled shRNA cells unsorted (top left), CD146^{Low}/CD90^{High} (top right), CD146^{Low}/CD90^{Low} (bottom left) and CD146^{High}/CD90^{Low} (bottom right). (**C**) Representative images of colony formation for CAKI-1 CAV1 shRNA (positioning the same as **B**)

4.3.2 CAV1 expression drives spheroid formation of CAKI-1 cells but not 786-O or A498

To establish whether CAV1 is capable of driving clonogenicity in more than one form of clonogenic assay spheroid formation assays were carried out to observe the clonogenic capacity of the 786-O, A498 and CAKI-1 cell lines under non-adherent serum deprived conditions. In all experiments 400 cells were seeded per well.

Of the three cell lines 786-O proved to be the most prolific in terms of spheroid formation. Scrambled shRNA control cells produced an average of 34 spheres in 786-O cells, followed by an average of 16 in CAKI-1 and 13 in A498 (Figure 4.9). CAV1 downregulation did not decrease or increase the spheroid forming capacity of 786-O or A498 cells (Figure 4.9 A and B), however, downregulation of CAV1 in CAKI-1 cells caused a significant 75% decrease in spheroid formation, from an average of 16 spheroids to 4 spheroids (Figure 4.9 C).

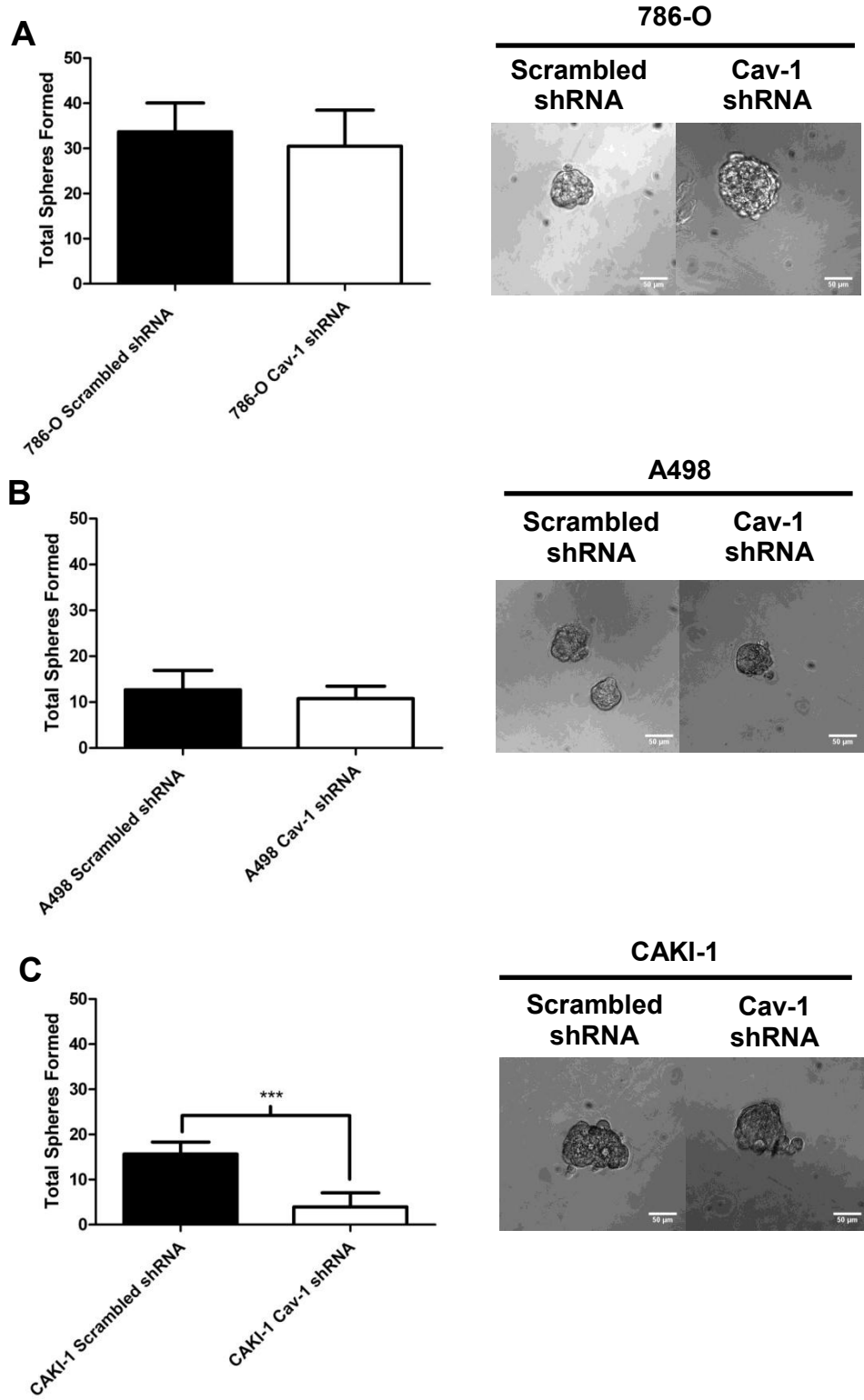


Figure 4.9 Spheroid formation assays of 786-O (A), A498 (B) and CAKI-1 (C) cells bearing scrambled shRNA control or CAV1 shRNA knockdown. Spheroid assays were performed at 400 cells per well. Spheroid formation data presented as mean \pm standard deviation $n=24$ wells from 4 independent experiments. Statistical differences measured by Student's T-test where *** = $P < 0.001$. To the right of each graph are images of spheroids formed for each cell line and treatment. Images captured at $\times 10$ magnification the white scale bar equivalent to $50\mu\text{m}$.

4.3.3 CAV1 expression suppresses proliferation in adherent CAKI-1 cultures and appears to maintain CAKI-1 G2/M phase under non-adherent culture conditions

To understand if CAV1 maintains clonogenicity through upregulating the proliferation and cell cycle progression of CAKI-1 cells, both proliferation and cell cycle analysis of scrambled shRNA control and CAV1 shRNA knockdown cells was carried out.

Under adherent growth conditions downregulation of CAV1 resulted in an increase of CAKI-1 cell proliferation by 55% (measured by direct cell counts Figure 4.10 A) and 43% (by MTT assay Figure 4.10 B). Western blot analysis of the proliferative G1 to S phase cell cycle regulator cyclin D1 found that down-regulation of CAV1 increased the expression of cyclin D1 (Figure 4.10 C). Indicating CAV1 acts as a suppressor of proliferation in CAKI-1 cells under adherent conditions.

Cell cycle analysis of adherent CAKI-1 cells shows that in the scrambled shRNA (CAV1 +ve) cells the majority were found in the G0/G1 phase at 68% with all other cells (32%) committed to cell cycle progression. However, with CAV1 down-regulation these distributions shift with G0/G1 cells accounting for 55% and all other cells committed to cell cycle progression representing 45% (Figure 4.11). This further indicates that CAV1 suppresses proliferation and its down-regulation leads to more cells entering into cell cycle.

The cell cycle of CAKI-1 cells (scrambled shRNA control and CAV1 shRNA knockdown) was then examined under non-adherent spheroid forming conditions. Under these spheroid forming conditions the proportions both Scrambled shRNA control and CAV1 shRNA cells entering into cell cycle was reduced, with in both cases over 80% of cells falling within the G0/G1 phase. Furthermore, under spheroid forming conditions the amount of cells committed to cell cycle progression

was similar for both the scrambled shRNA control cells (12.5%) and the CAV1 shRNA knockdown cells (14%) (Figure 4.11). However, analysis of the spheroid cells committed to cell cycle progression (S and G2/M phases) shows that CAV1 knockdown resulted in an increase in the proportion of cells in S-phase (11% vs 3% for scrambled control) and a decrease in the proportion of G2/M (3.5% vs 9% for scrambled control Figure 4.12).

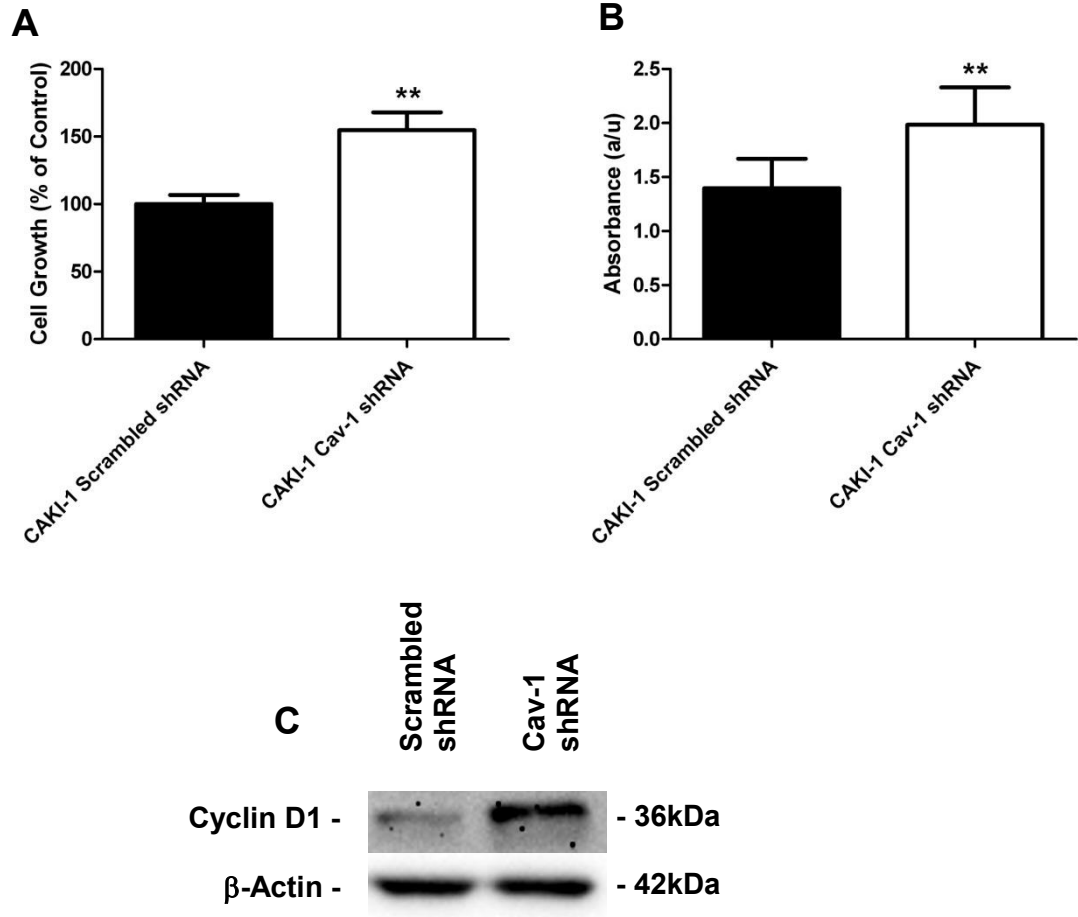


Figure 4.10 Down regulation of CAV1 induces proliferation in CAKI-1 cells (A) Cell growth after 72 hours of CAKI-1 scrambled shRNA and CAV1 shRNA determined by coulter counter n= 16 from 4 separate experiments (B) Cell growth analysed after 72 hours by MTT assay n=12 from 3 separate experiments (C) Western blots showing up-regulation of cyclin D1 in CAV1 shRNA transfected CAKI-1 cells with β -actin used as loading control. Data presented as mean \pm standard deviation. Statistical difference calculated by Student's T-test where ** = $P > 0.01$.

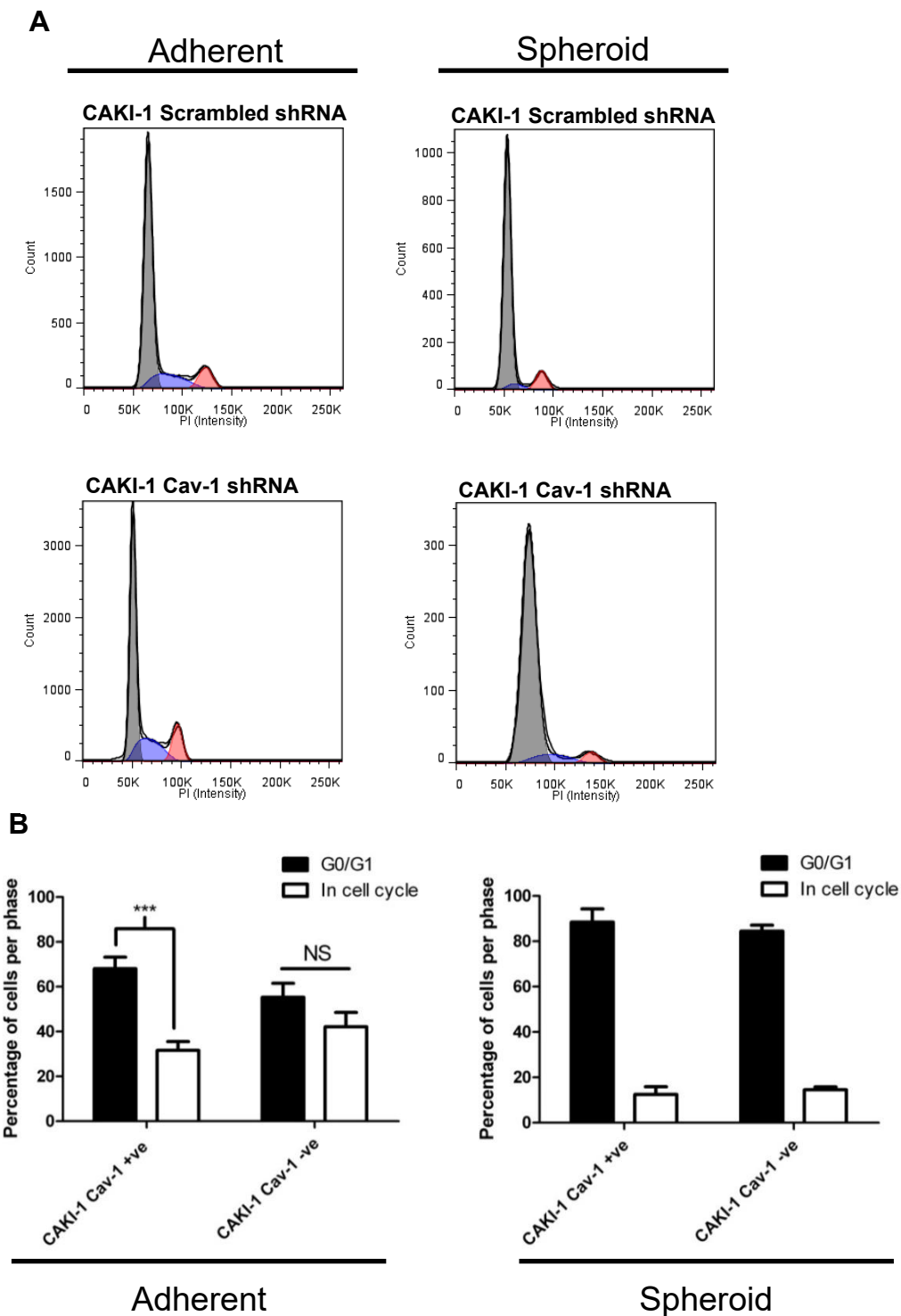


Figure 4.11 Cell cycle analysis of CAKI-1 cells under monolayer adherent conditions and non-adherent spheroid forming conditions in the CAKI-1 Scrambled shRNA control and CAV1 shRNA knockdown cell lines. (A) Histogram data of IP staining, grey shading represents G0/G1, blue shading represents S phase and red shading represents G2/M phase. Data represents a single experiment. (B) Graphed data of three cell cycle experiments where S phase and G2/M have been pooled to show the total proportion of cells in cycle. Data presented as mean \pm standard deviation $n=3$ experiments Statistical difference analysed by Student's t-test *** = $P < 0.001$.

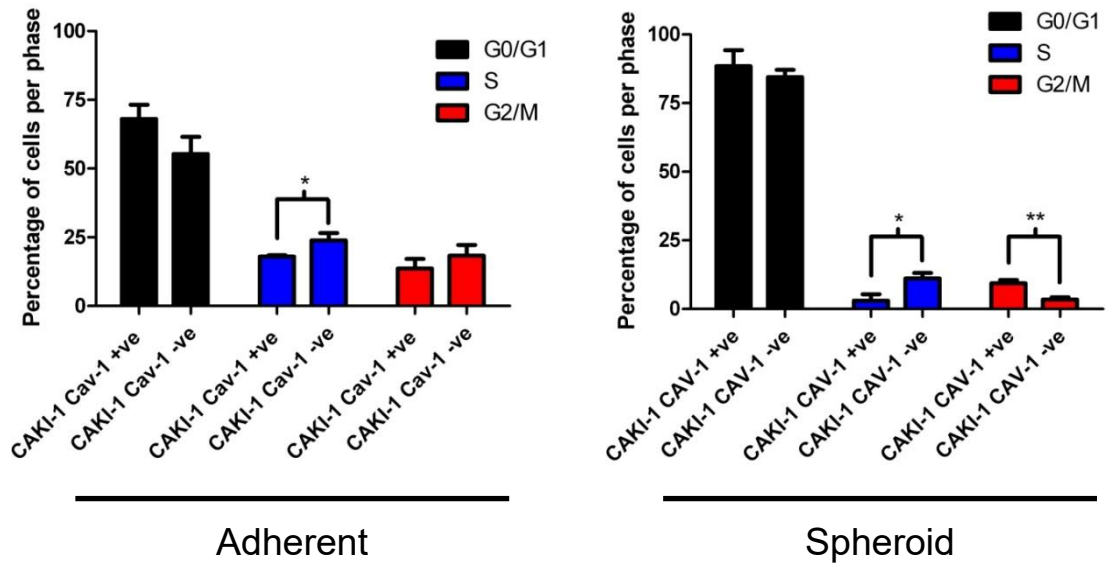


Figure 4.12 Cell cycle analysis of CAKI-1 scrambled shRNA control and CAV1 shRNA cells grown in adherent monolayer and non-adherent spheroid forming conditions now showing both S phase and G2/M phase. Data presented as mean \pm standard deviation n=3 experiments. Statistical difference analysed by student's t-test *** signifies $P < 0.001$.

4.3.4 Activation of hypoxic signalling in CAKI-1 cells helps restore clonogenicity in the absence of CAV1

Of the three cell lines examined CAKI-1 is the only one to express functional wild type VHL. As such we sought to examine how hypoxia would influence the clonogenic capacity of CAKI-1 cells.

Under normoxic (21% O_2) the impact of CAV1 knockout to reduce CAKI-1 clonogenicity was evident in both the adherent colony forming assay and the non-adherent spheroid forming ($P < 0.001$ in both cases) (Figure 4.13 A and Figure 4.13 B). Under hypoxic conditions (1% O_2) the impact of the CAV1 knockout phenotype to drive a reduction in clonogenicity was neutralised in both the colony forming and spheroid forming assays. Specifically in the colony forming assay, while hypoxic increased the control (CAV1 +ve) by 58% it also increased colony formation by 88% in the CAV1 shRNA knockdown (CAV1 -ve) cells (Figure 4.13 A). In spheroid

formation assays under hypoxic conditions no statistical difference between CAKI-1 scrambled shRNA control cells and CAV1 shRNA knockdown was observed (Figure 4.13 B). Here spheroid formation of CAV1 shRNA knockdown cells under hypoxic conditions showed a 62% increase in clonogenicity compared to normoxic conditions

Western blot analysis showed upregulation of HIF-2 α under hypoxic conditions in both CAKI-1 scrambled shRNA control and CAV1 shRNA knockdown cells, indicative of activated hypoxic signalling. HIF-2 α expression was not observable under normoxic conditions indicating functional VHL activity in CAKI-1 cells (Figure 4.14). Analysis of CAV1 expression under hypoxic conditions found CAV1 to be downregulated in scrambled shRNA control cells and further downregulated in CAV1 shRNA knockdown cells (Figure 4.14).

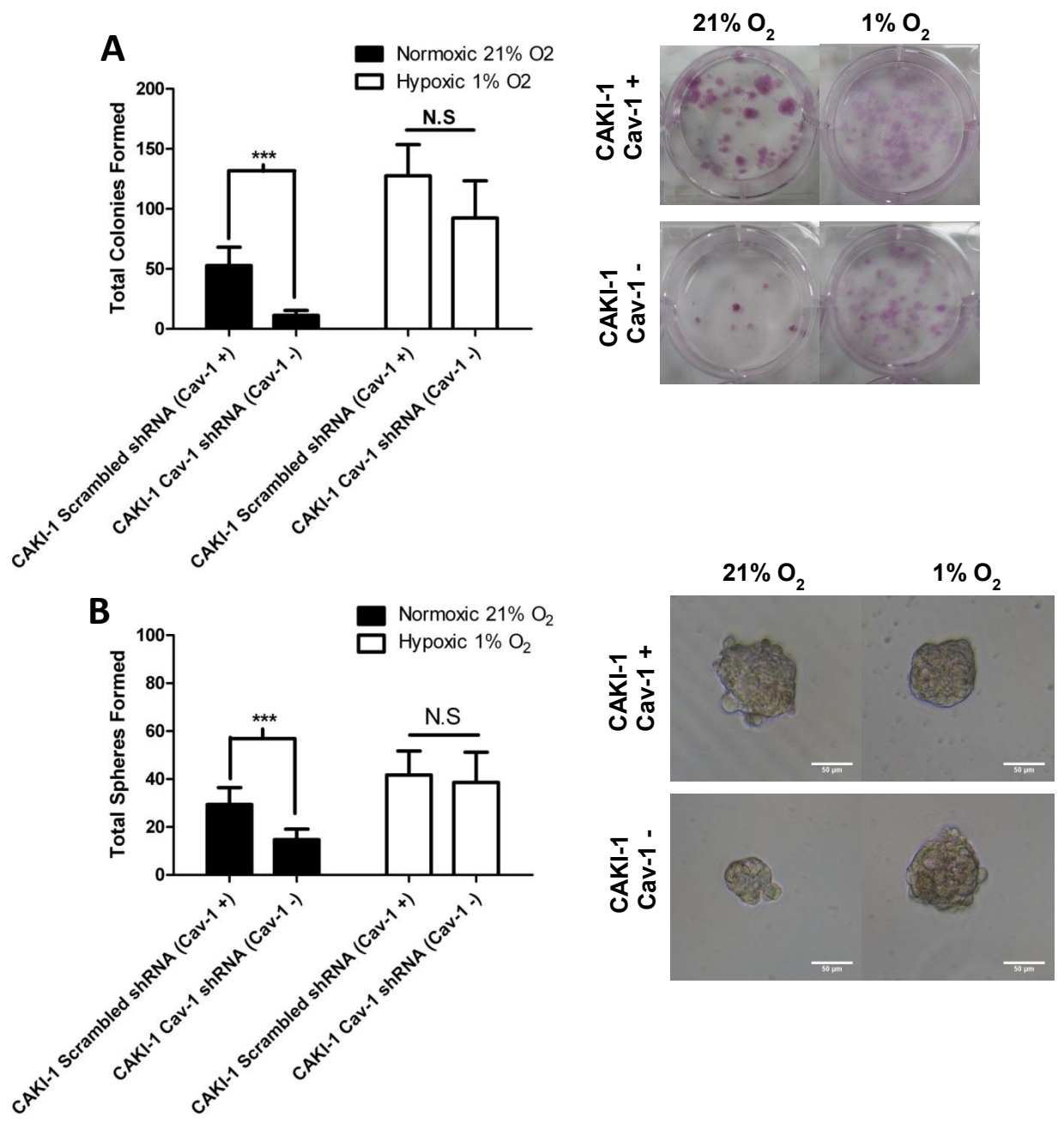


Figure 4.13 Hypoxia drives clonogenicity in the absence of CAV1 in VHL positive CAKI-1. A Total colony formation of scrambled shCAKI-1 cells under hypoxia to the right representative images of colonies stained for counting. B Total spheroid formation of CAKI-1 cells under hypoxia to the right representative images of spheroids formed viewed by phase contrast microscopy. Graphs represent mean \pm SD n=9 from 3 separate experiments for colony formation and n=18 from 3 separate experiments for spheroid formation assays statistical significance calculated by Student's t-test *** signifies P=<0.001

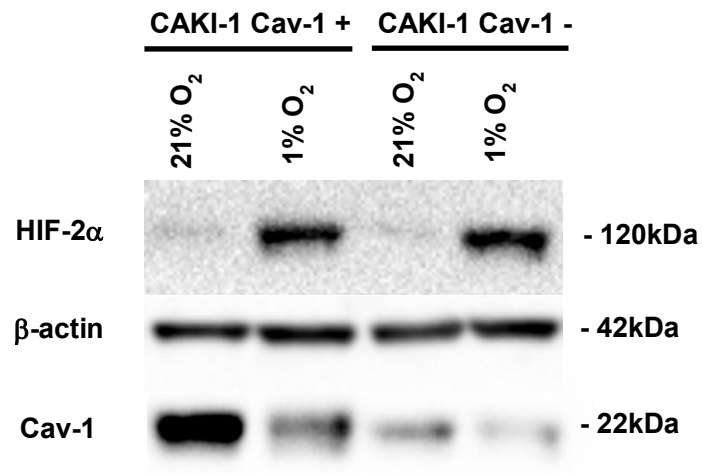


Figure 4.14 Western blots showing activation of hypoxic signalling by expression of HIF-2 α and the effect of hypoxia on CAV1 expression. β -actin used as a loading control.

4.4 Discussion

This chapter has focused on the effect of CAV1 downregulation upon the proportions and clonogenicity of cell subpopulations in the 786-O, A498 and CAKI-1 RCC cell lines. The work went on to analyse how CAV1 may drive clonogenicity and how this may change given the genotypic background of the cell line.

Downregulation of CAV1 in the 786-O and A498 cell lines caused substantial changes in the proportion of CD90/CD146 subpopulations. In 786-O a significant reduction was observed in the CD90^{Low}/CD146^{High} subpopulation and a strong trend was observed toward a decreased proportion of CD90^{Low}/CD146^{High} cells matched by an increased proportion of CD90^{Low}/CD146^{Low} cells. Similar results were observed in the A498 cell line, where CAV1 downregulation caused a decrease in the CD90^{Low}/CD146^{High} population, although appeared not to have any effect on the CD90^{High}/CD146^{Low} population. In both these cell lines there was no difference in their total clonogenicity (colony forming and spheroid forming capacity) or in the colony forming capacity of the sorted CD90/CD146 subpopulations. In both clonogenicity assays the downregulation of CAV1 appeared to have no significant effect on the size or general morphology of colonies or spheroids formed. Taken together while CAV1 may cause changes in the distribution of CD90/CD146 subpopulations this effect has no impact on the clonogenicity of these populations. CD146 has been identified as a marker present on primary RCC CSCs isolated by CD105⁺ populations[61] and RCC CSCs generated through growth of patient-derived xenographs using adult progenitor cell medium[346]. Its upregulation has been demonstrated to drive the invasive capacity of melanoma[347], breast[348] and ovarian cancers[349]. Indeed, in RCC upregulation of CD146 by insulin-like growth factor-binding protein 4(IGFBP-4) induction of Wnt/ β -catenin signalling demonstrated increased migratory and invasive capacity of RCC cells[350]. Further to this CAV1 has been identified as important to the invasive capacity of 786-O,

A498 and CAKI-1 cell lines[131]. Taken together this suggests a possible interaction pro-invasive interaction between CAV1 and CD146 expression in the 786-O and A498 cell lines.

In contrary to the findings in 786-O and A498, downregulation of CAV1 in CAKI-1 cells did not affect the distribution of CD90/CD146 subpopulations or have a profound impact on the expression of surface markers further down the gating hierarchy. However, CAV1 downregulation did have a substantial impact on both the colony forming and spheroid forming capacity of CAKI-1 cells. This downregulation of clonogenicity was found in the whole unsorted cell line as well as the varying CD90/CD146 subpopulations. The ability of CAV1 to drive clonogenicity of CAKI-1 cells is likely to indicate a population of CSC cells not identified by the current marker panel resides within the CAKI-1 cell line that require CAV1 for clonogenicity. Many other potential markers may exist, for example, recently CXCR-4[62] has been used to successfully identify CSC populations from RCC cell lines RCC-26 and RCC-53[62]. Further, subpopulations of CSC like cells have been identified in RCC through the use of less specific methods such as spheroid formation in non-adherent conditions[64], side population assays[63] and aldehyde dehydrogenase (ALDH) activity[351]. Evidence is beginning to accumulate that shows the CSC phenotype in tumours maybe dynamically regulated depending on a host of microenvironmental signals and cellular interactions[352]. For example, NO released from endothelial cells related to the glioblastoma tumour microenvironment can induce CSC phenotype[353]. Indeed, such NO induced CSC phenotypes have been identified in non-small cell lung carcinoma. Moreover such populations were found to upregulate CAV1 which was found to be critical to many key CSC functions[344]. It may be possible that CAV1 plays a role in regulating the response to the conditions used in the clonogenicity assays here to support conversion to a stem-like phenotype.

To understand if CAV1 is driving clonogenicity through upregulation of proliferation and increased progression through the cell cycle proliferative and cell cycle assays were undertaken. Downregulation of CAV1 in CAKI-1 cells caused increased proliferation and resulted in upregulation of cyclin D1. This finding was further confirmed by cell cycle analysis where CAV1 knockdown led to a larger proportion of cells to enter into the cell cycle. Under spheroid forming conditions the proportion of cells in the G2/M phase was greatly reduced by CAV1 knockdown. This data seems to suggest the possibility for a multifunctional or context-dependent role for CAV1 in the biology of CAKI-1. Under adherent growth conditions CAV1 may be suppressing the proliferative capacity of the bulk non-CSC cells and maintaining the self-renewal capacity of more stem cell-like populations. Upregulation of CAV1 may suppress the capacity for differentiation in the CSC cells in the CAKI-1 cell line, favouring a balance of differentiation and self-renewal. Once this inhibitory action of CAV1 is removed this balance may be forced more towards differentiation than preserving self-renewal in much the same way as the previously discussed regulation of CAV1 differentiation in certain MSC populations[334]. As more of the total cell population would be differentiated bulk cells with decreased self-renewal capacity this would be reflected in the clonogenicity assays.

CAKI-1 is the only one of the three cell lines studied to display a decreased capacity for clonogenicity in response to CAV1 knockdown. It is also the only one to have a regulated hypoxia-induced signalling via functional VHL. The work next explored if induction of hypoxic signalling in CAKI-1 cells could restore clonogenic capacity even in the absence of CAV1 expression. Hypoxic incubation of CAKI-1 (CAV1 knockout) cells resulted in an upregulation of HIF-2 α and restoration of clonogenicity measured by both spheroid forming and colony formation (Figure 4.15). Our results appear to indicate that under hypoxic conditions the reduced clonogenicity caused by a lack of CAV1 is compensated for by hypoxia and

activation of hypoxia-inducible pathways. Indeed in a recent study investigating CXCR4 positive RCC CSCs, Micucci et al [354] found HIF-2 α expression important in these cells for upregulation of CXCR4 signalling necessary to stabilise CXCR4 induced self-renewal. Taken together our results seem to suggest CAV1 may be an important driver of self-renewal capacity in RCC tumours which expression functional VHL.

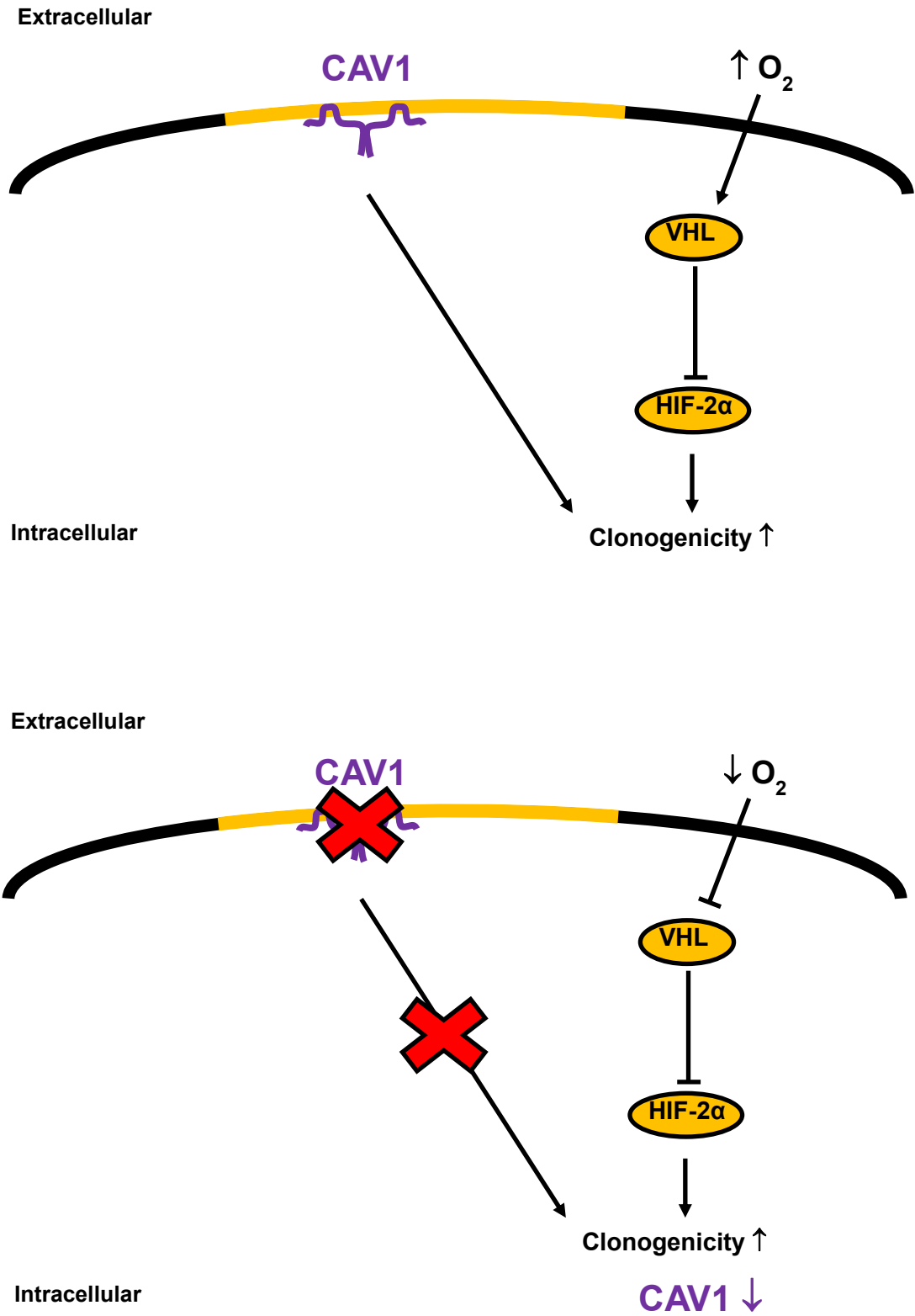


Figure 4.15 The hypoxic response is able to restore clonogenicity in CAKI-1 cells in the absence of CAV1 expression. In CAKI-1 cells knockdown of CAV1 under normoxic conditions significantly reduced colony formation. However, hypoxia was able to restore clonogenicity despite the downregulation of CAV1.

Further, in the control CAKI-1 cells (CAV1 +ve) hypoxia was found to downregulate CAV1 expression. CAV1 is highly expressed in VHL+/+ cell lines as ACHN and CAKI-2 as well as CAKI-1[131]. Aligned to this is an opposite finding. Specifically, a previous study has found that reconstituting functional VHL in the VHL-/- 786-O cell line resulted suppression of CAV1 and exposing these cells to hypoxic conditions then led to an upregulation in CAV1 expression[84]. Further to this other studies have found that under hypoxic conditions CAV1 is upregulated to a maximal expression after around 24 hours then either falls back down to original normoxic levels[355] or actually becomes downregulated after a period of around 72 hours[356], it is noted that in this work cells were incubated under hypoxic conditions for 72 hours.

In conclusion, CAV1 expression modulates the proportion of CD146/CD90 subpopulations in 786-O and A498. However, in these cell lines the level of CAV1 does not affect clonogenicity. In contrast, the VHL+/+ CAKI-1 cell line CAV1 expression failed to change the proportion of CD146/CD90 subpopulations. Here however, the level of CAV1 expression had a significant effect on clonogenicity. Specifically, CAV1 expression was required to drive clonogenicity in both colony formation and spheroid formation assays. Under hypoxic conditions CAV1 knockdown CAKI-1 cells were capable of spheroid and colony formation similar to that of CAV1 expressing CAKI-1 cells. These results indicate an important role for CAV1 in the self-renewal and clonogenicity of VHL competent RCCs.

Chapter 5 - Down-regulation of CAV1 alters various oncogenic signalling pathways in CAKI-1 under clonogenic and hypoxic conditions.

5 Down-regulation of CAV1 alters various oncogenic signalling pathways in CAKI-1 under clonogenic and hypoxic conditions.

5.1 Introduction

Effective targeting of CSC populations in patient tumours will require an in depth understanding of which cell signalling pathways, and associated downstream functional transcription factors, control the stem cell-like phenotype. As such, much research has been invested in identifying which pathways are dysregulated and which aspects of the stem like phenotype they control. Several cell signalling pathways that have been identified thus far, the majority of which are known to be important for normal tissue development/repair, organogenesis and general maintenance of the stem cell phenotype[357]. Of the many molecules involved in these pathways the most widely studied, and promising in terms of therapeutic targeting, are β -catenin and STAT3.

5.1.1 Wnt/ β -catenin signalling in the CSC phenotype and RCC

The Wnt/ β -catenin signalling cascade is driven by a family of secreted glycolipoproteins, termed Wnt's. Wnt's are capable of regulating cell fate determination, cell polarity and proliferation in normal stem cell tissue homeostasis and embryonic development[358]. As such, dysregulation of the Wnt pathway has been implicated as the causative agent of birth defects but also identified as important contributor to the tumorigenesis of a wide range of cancers and other disease[359]. Wnt signalling exerts its physiological effects through the regulation of the transcriptional co-activator β -catenin, this pathway is known as the canonical Wnt signalling pathway. Canonical signalling is the most well-known and reported type of β -catenin regulation, the other being the non-canonical planar-cell polarity pathway which is capable of regulating the cytoskeleton[360]. Activation of β -catenin

through the canonical Wnt signalling pathway requires the interaction of a Wnt protein with the G-protein coupled receptor Frizzled (Fz) and its co-receptor low-density lipoprotein receptor-related protein 5/6 (LRP)[361]. Inhibition of Wnt signalling is achieved through two different ways, either by direct inhibition of Wnt proteins by the secreted antagonists Frizzled-related-proteins (sFRPs) and Wnt inhibitory factor-1 (WIF-1)[358], or inhibition of LRP5/6 signalling through the expression of the secreted Dickkopf-related proteins (DKKs)[362]. Ligand binding and activation of Fz and LRP5/6 complex results in activation of the cytoplasmic polarity protein dishevelled homologue (Dv1)[363]. Activation of DV1 inhibits the Axin-mediated phosphorylation of β -catenin, this results in the cytoplasmic accumulation of β -catenin[364]. An increase in the concentration of cytoplasmic β -catenin results in the translocation of β -catenin to the nucleus. Once within the nucleus β -catenin facilitates the transactivation of target genes together with TCF-LEF transcription factors[365]. In the absence of Wnt signalling, a multiprotein destruction complex consisting of the scaffolding protein axin, adenomatous polyposis coli (APC) and glycogen synthase kinase-3 β (GSK-3 β) facilitates the phosphorylation of β -catenin which targets it for ubiquitination and degradation via the proteasome[366].

Several studies have implicated dysregulation of Wnt signalling as an important contribution to the generation and maintenance of a CSC, or stem cell-like populations, in a number of different malignancies. A population of CSCs identified in non-melanoma cutaneous skin tumours were found to have a profound reliance on the stabilisation of β -catenin for maintenance of their CSC phenotype. Ablation of β -catenin expression in these CSCs resulted in tumour regression *in vivo*[367]. In triple negative breast cancer, shRNA downregulation of β -catenin resulted in reduced tumourigenicity both *in vivo* and *in vitro*. Additionally, significant inhibition of *in vitro* chemoresistance was observed together with the down regulation of self-

renewal related transcription factors Bmi-1 and c-Myc[368]. Similar observations were made by Jang et al.[369], who also found reduction of Wnt signalling and β -catenin activation caused a substantial decrease in the metastatic capability of breast CSCs *in vivo*. In metastatic lung cancer cell lines, downregulation GSK-3 β by miR-544 a was found upregulate β -catenin and maintain the self-renewal capacity of CSCs *in vitro*[370]. Similarly in non-small cell lung cancer CSCs, β -catenin signalling driven by CD44 was capable of driving epithelial to mesenchymal transition (EMT) and was critical to driving metastasis[371]. Furthermore, β -catenin has been identified as a key component of a transcriptional complex including Twist1 and TCF4 which is upregulated in response to EMT. Once activated by Twist1 cleavage this complex was capable of binding to a number of CSC related gene promoter regions[372]. Treatment of hepatocellular carcinoma CSCs with all-trans retinoic acid (ATRA) caused an increase in self-renewal related transcription factors and increased sensitivity to docetaxel[373].

While activating point mutations of β -catenin are rare in RCC[374], several studies have demonstrated that β -catenin may play a significant role in tumorigenesis. It is well reported that induced overexpression of β -catenin by inducible dysregulation of Apc expression in mice is sufficient to cause renal tumours[375], [376]. Indeed, non-clear cell RCCs have been found to display deactivation of the promoter region of the *APC* gene by hypermethylation[377]. Further to this Kojima et al.[378] found homozygous deletion of the gene *CXXC4*, which encodes for the Wnt pathway inhibitor Idax, in aggressive RCCs. In addition to this, promoter hypermethylation has also been detected for an number of other inhibitors of the Wnt signalling pathway such as: sFRP1[379], DKK2[380] and Wnt inhibitory factor 1 (WIF-1)[381]. The tumour suppressor histone deacetylase 10 (HDAC10), often downregulated in primary RCC samples[382], appears to exert regulatory control over β -catenin stabilisation. Downregulation of HDAC10 resulting in decreased phosphorylation of

β -catenin and increase proliferation and invasion[382]. A pro-survival role for β -catenin signalling in RCC has also been detected as small molecule inhibition of β -catenin has been found to induce apoptosis in RCC cell lines[383]. As such the canonical Wnt/ β -catenin signalling pathway seems a likely means by which the CSC phenotype in RCC cells may be propagated.

5.1.2 STAT3 signalling in the CSC phenotype and RCC

The aberrant activation of members of the signal transducer and activator of transcription (STAT) pathway have been identified as important to the regulation of the malignant phenotype[384]. Of all the STAT family members STAT3 has been viewed as one of the most potent in terms of the variety of pro-oncogenic cellular responses it can induce. Additionally, STAT3 has been found to carry out a wider role in the components of the tumour microenvironment such as tumour associated immune and stromal cells[385], [386]. Further to this, STAT3 has been identified as an important factor in the regulation of self-renewal in stem cell populations. In ESC self-renewal, STAT3 is able to preserve stem cell populations in an undifferentiated state by leukemia inhibitory factor (LIF). LIF binding to leukemia inhibitory factor receptor (LIFR) and glycoprotein 130 (gp130) triggers the activation of STAT3 which, through interactions with B-cell lymphoma 3-encoded protein (Bcl3) and octamer-binding transcription factor 4 (Oct-4), is able to maintain pluripotency through upregulation of additional self-renewal related genes such as Nanog and sex determining region y-box 2 (Sox2)[387].

The regulation of STAT3 activity is important for the self-renewal and pluripotent differentiation of embryonic stem cells (ESCs)[388]. This association has led to a number of recent studies examining the role of STAT3 activation in the CSC populations of numerous tumours. In breast cancer cell lines, inhibition of STAT3 together with FAK and Src resulted in a reduction in the total CSC pool, tumourigenicity and metastatic potential[389]. Moon et al. found the proportion,

proliferation and capacity for differentiation of CSC activity of the glioblastoma cell line U87 MG was regulated by PTEN through the control of PI3K/Akt/STAT3 signalling[390]. In prostate cancer the loss or downregulation of the androgen receptor (AR) resulted in: increased activation of STAT3, pronounced expression of CSC associated markers and a more active CSC population in terms of proliferation and tumourigenicity[390]

Regulation of STAT3 activity can be carried out by a number of different upstream signalling pathways such as: the toll-like receptors (TLRs), receptor tyrosine kinases (RTKs), a wide variety of G-protein coupled receptors (GPRs) and cytokine receptors[391]. Of these regulatory signalling pathways the functional activation of STAT3 by interleukin-6 (IL-6) has been the most widely studied in relation to CSC biology. CD44⁺/CD24⁻ breast CSCs have upregulated IL-6 expression which was responsible for activation of STAT3 by Janus kinase 2 (JAK2). This was found to be critical for maintenance of CSC function in these cells[392]. Activation of the IL-6/JAK2/STAT3 pathway has also been observed in spheroid derived CSCs from the lung cancer cell line A549. IL-6 induced activation of STAT3 signalling resulted in the upregulation of the DNA methyltransferase 1 (DNMT1) inhibiting methylation to the promoter regions of p53 and p21, resulting in these lung CSCs[393]. The positive feedback loops characteristic of cytokine signalling pathways have been demonstrated to drive self-renewal of glioblastoma CSCs. Here, the constitutive activation of STAT3/NF- κ B signalling was found to regulate the Notch signalling pathway[394]. Direct activation of STAT3 by IL-6 is not the only means by which STAT3 can be activated to drive CSC phenotype. Activation of STAT3 by Toll-like receptor 2 has been observed in breast CSCs, this resulted in increased secretion of IL-6, thereby setting up constitutive STAT3 activation[395]. Regulation of STAT3 activation by microRNAs has been demonstrated in primary pancreatic cancer

tissue where downregulation of mircoRNA-1181 induced activation of STAT3 and induction of Sox2 expression[396].

In RCC STAT3 has mainly been investigated in terms of its activation by IL-6, which has been demonstrated as an indicator of poor clinical outcome and implicated in disease progression[397]. The high expression of the active form of STAT3, pSTAT3, has been observed in RCC tumour samples by immunohistochemistry, relatively little activation was observed in adjacent non-cancerous kidney tissue[398]. This activation has also been observed in RCC cell lines[399]. Inhibition of STAT3 activation in RCC cell lines 786-O and CAKI-1 has been shown to reduce proliferation and resistance to apoptosis[400]. It is possible that STAT3 may be a key component in driving CSC phenotype in RCC in a CAV1 dependant manner.

5.1.3 Aims

This chapter has aimed to understand how protein expression and phosphorylation was affected by downregulation of CAV1. Once identified, inhibitory studies were carried out to determine what affect direct inhibition of these pathways had on clonogenicity of the CAKI-1 cell line. These studies were carried out by:

- Proteomic array analysis of key regulatory phosphokinases, stem cell related proteins and tumour suppressing and oncogenic proteins. This analysis was carried out under normoxic adherent, normoxic spheroid and hypoxic spheroid forming conditions with CAV1 knockdown.
- Small molecule inhibition of possible pro-clonogenic pathways seen to be downregulated by CAV1 with subsequent colony forming assays to assess the effect on clonogenicity.

5.2 Materials and Methods

5.2.1 Proteomic microarrays

Proteomic analysis of CAKI-1 scrambled shRNA control and CAV1 shRNA knockdown cells were conducted using the human Proteome Profiler™ Antibody arrays kits (R&D Systems): Human Phospho-Kinase Array, Human XL Oncology Array and the Human Pluripotent Stem Cell array. Preparation of the arrays was conducted as instructed by the product protocol, each kit used slightly different buffers and lysis buffers in each case the recommendations of each kit was followed therefore the following is a general summation of array preparation.

Cells were first washed twice with PBS (by centrifugation for spheroid formed cells), lysed in their corresponding lysis buffers, centrifuged at 20,000g for 15 minutes to pellet cellular debris and protein concentration was then quantified as explained in Chapter 4. Before addition of protein lysates, microarray membranes containing immobilised capture antibodies were placed into either 6 or 4 rectangular well multi-dishes and then blocked for 60 minutes in their corresponding blocking buffers. Following this 100µg of total protein was diluted in the corresponding array buffer left to incubate with gentle agitation on a rocking platform shaker for 16 hours at 4°C. Array membranes were then washed three times for 10 minutes each then incubated for 60 minutes at room temperature with a cocktail of detection antibodies followed by another three washes. To enable chemiluminescent detection of bound proteins Streptavidin-HRP was then added to each well and incubated for 30 minutes at room temperature then washed a further three times. For imaging arrays were then placed onto the scanning bed of a ChemiDoc™ imaging system and 1mL of Chemi Reagent Mix was evenly applied to each membrane allowed to incubate for one minute then imaged. Images of developed microarrays were analysed using the ImageJ image analysis software package.

5.2.2 Inhibitor studies

For small molecule inhibition of Wnt and STAT3 activation cells were seeded into 6-well plates as previously described (see Chapter 4). Inhibition of β -catenin activation was performed using IWP-2 which inhibits the N-palmitoyltransferase PORCN, thereby inhibiting the palmitoylation and secretion of Wnt proteins[401]. Inhibition of STAT3 was performed using WP1066. WP1066 inhibits STAT3 activation by inhibition of immediate upstream JAK2-mediated phosphorylation[402]. At 24 hours post-seeding cells were incubated with either 5 μ M IWP-2 (Tocris), 6 μ M WP1066 (Santa Cruz Biotechnology), or DMSO as a vehicle control for a further 24 hours. Following this pre-treatment cells were harvested to assess inhibition of β -catenin (polyclonal antibody obtained from Sigma Aldrich) by western blot (as described in Chapter 4) or phosphorylation of STAT3 at Y705 by flow cytometry (as described in Chapter 3). To assess the effect of STAT3 and Wnt inhibition on clonogenicity, cells were trypsinised and resuspended as previously described and serially diluted to achieve a concentration of 400 cells per well in normal growth media without inhibitor. The remainder of the assay being carried out as previously described.

5.2.3 Statistical analysis

Statistical analysis was carried out using a one-way ANOVA using a Dunnett post-hoc analysis; comparison of all treatments against control group where a P value of less than 0.05 was considered significant.

5.3 Results

5.3.1 Effect of CAV1 knockdown on regulation of phospho-kinase regulated cell signalling under different culture conditions

To assess how CAV1 expression effects the regulation of phospho-kinase signalling networks, many of which have been implicated in the maintenance of CSC function and phenotype, protein microarrays specific to the key regulatory markers in these pathways were used. The regulatory status of these proteins were investigated in normal adherent culture conditions but also in non-adherent spheroid conditions both normoxic and hypoxic.

Under normoxic adherent conditions significant changes in phosphorylation were detected in many proteins in three proteins. Glycogen synthase kinase – $3\alpha/\beta$ (GSK- $3\alpha/\beta$) showed a large 5.5 fold increase in phosphorylation sites serine 21 (S21) and serine 9 (S9) indicating inhibition of GSK- $3\alpha/\beta$ signalling (Table 5.1 labelled 1 Figure 5.1)[403]. Signal transducer and activator of transcription 3 (STAT3) displayed a loss of phosphorylation in both tyrosine 705 (Y705) and serine 727 (S727) of 3 fold and 6.1 fold respectively (Table 5.1 labelled 2 and 3 Figure 5.1) meaning inhibition of STAT3 activity[404]. A 2.6 downregulation of p27 phosphorylation at the threonine 198 site was observed (Figure 5.1 labelled as 5 Table 5.1), this indicates activation of p27[405]. AKT 1/2/3 phosphorylation at site serine 473 (S473) was decreased by 1.8 fold indicating possible inhibition of activation[406] (Table 5.1 labelled 6 Figure 5.1). However, no phosphorylation was detected in the second threonine (T308) phosphorylation site and CAV1 knockdown did not achieve a 2 fold decrease in phosphorylation. A downregulation of p53 phosphorylation was detected at serine 15 (S15) by 1.8 fold (Figure 5.1 labelled as 4 Table 5.1). This suggests an decreased response to DNA damage with CAV1 knockdown[407]. Phosphorylation of p53 at serine 46 and serine 392 remained unaffected.

In cells CAKI-1 cells grown under normoxic spheroid forming conditions showed only one 1.9 fold or greater change in phosphorylation. Phosphorylation of 40kDa proline-rich protein (PRAS40) at threonine 246 displayed a 2.3 fold increase (Figure 5.2 labelled as 1 Table 5.1), indicating PRAS40 activation[408]. Slight downregulation of p53 phosphorylation was observed in the phosphorylation sites serine 15 (S15) (1.6 fold downregulation), serine 46 (S46) (1.8 downregulation) and serine 392 (S392) (1.5 downregulation) (Figure 5.2 labelled together as 2 Table 5.1) compared to only a downregulation of p53 S15 phosphorylation in adherent cells (Figure 5.1). Two components of phosphatidylinositol (3,4,5)-triphosphate (PIP3) signalling pathway experience slight downregulations; Akt 1/2/3 phosphorylation at site threonine 308 exhibited a slight downregulation of 1.6 fold and GSK-3 α/β at S21/S9 a downregulation of 1.6 fold (Figure 5.2 Table 5.1).

CAKI-1 cells grown under hypoxic spheroid conditions had no fold change in phosphorylation greater than 1.9 fold. However, unique to spheroid cells grown under hypoxic conditions HSP27 exhibits a 1.8 fold increase in phosphorylation at the serine 78 and 82 sites (S78 and S82) (Figure 5.3 labelled as 3 Table 5.1), indicating its activation[409]. In addition, reduction of STAT3 phosphorylation of both Y705 and S727 sites was also more pronounced with a 1.7 and 1.8 fold downregulation respectively as well as reduction in p27 phosphorylation of T198 (Figure 5.3 labelled as 4 Table 5.1).

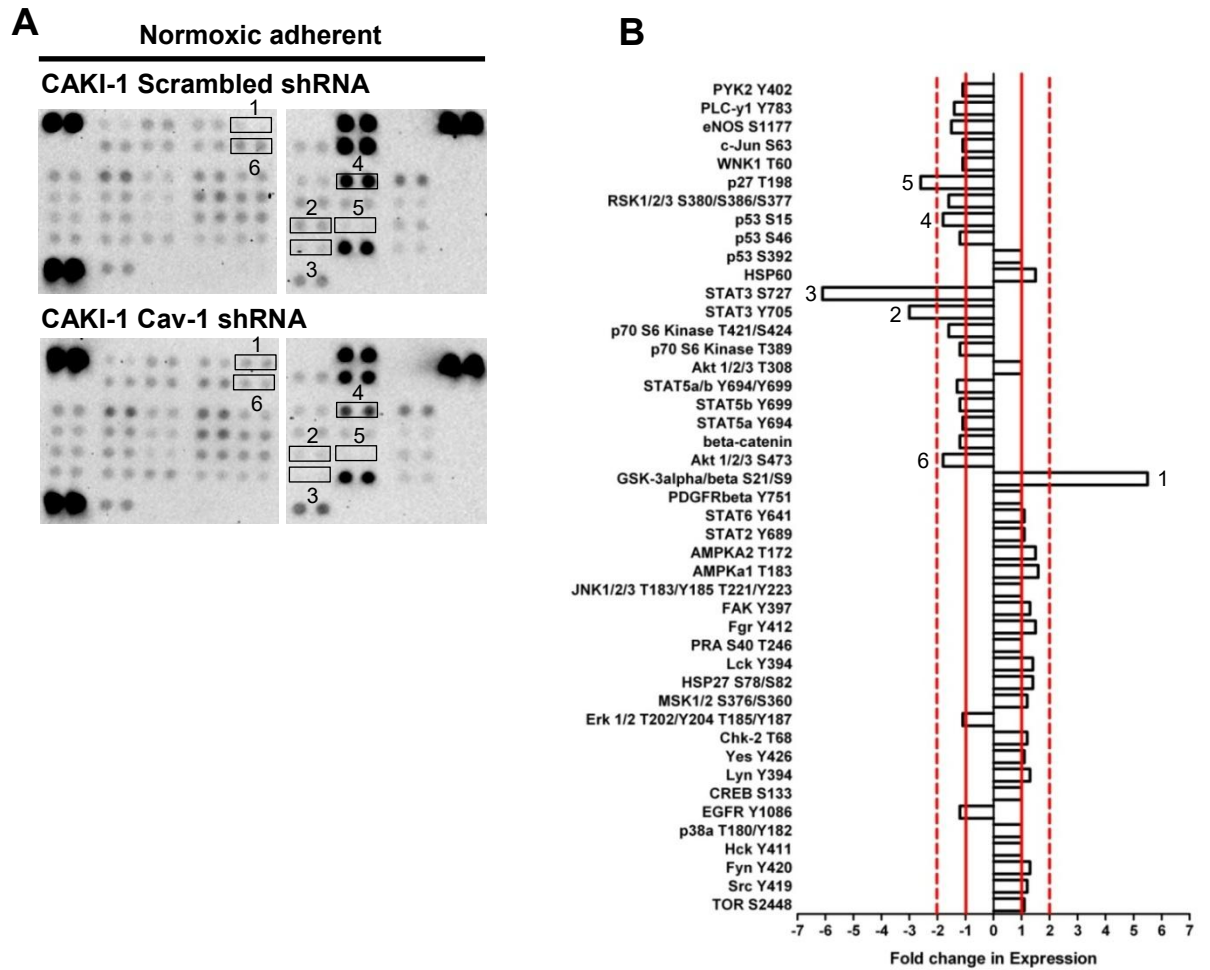


Figure 5.1 Human phospho-kinase array data of CAKI-1 Scrambled shRNA control and CAV1 shRNA knockdown cells grown as an adherent monolayer under normoxic conditions. A Processed arrays phosphor-kinase arrays for both Scrambled shRNA and CAV1 shRNA cells. B Graph showing fold change in expression both positive and negative for each marker with respect to CAV1 down-regulation. Numbers on the graph correspond to the position of a protein on the array.

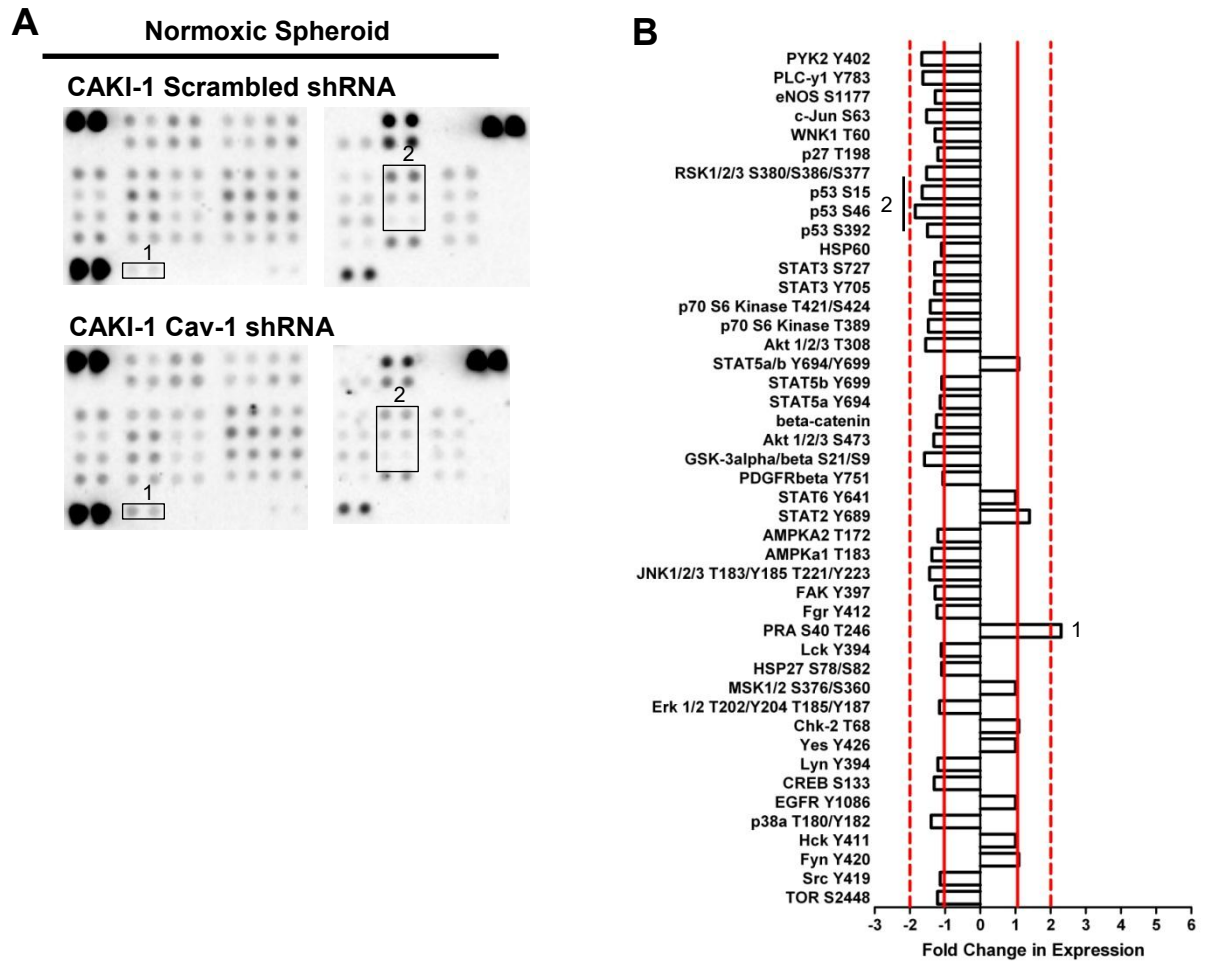


Figure 5.2 Human phospho-kinase array data of CAKI-1 Scrambled shRNA control and CAV1 shRNA knockdown cells grown as spheroids in non-adherent normoxic conditions. A Processed arrays phosphor-kinase arrays for both Scrambled shRNA and CAV1 shRNA cells. B Graph showing fold change in expression both positive and negative for each marker with respect to CAV1 down-regulation. Numbers on the graph correspond to the position of a protein on the array.

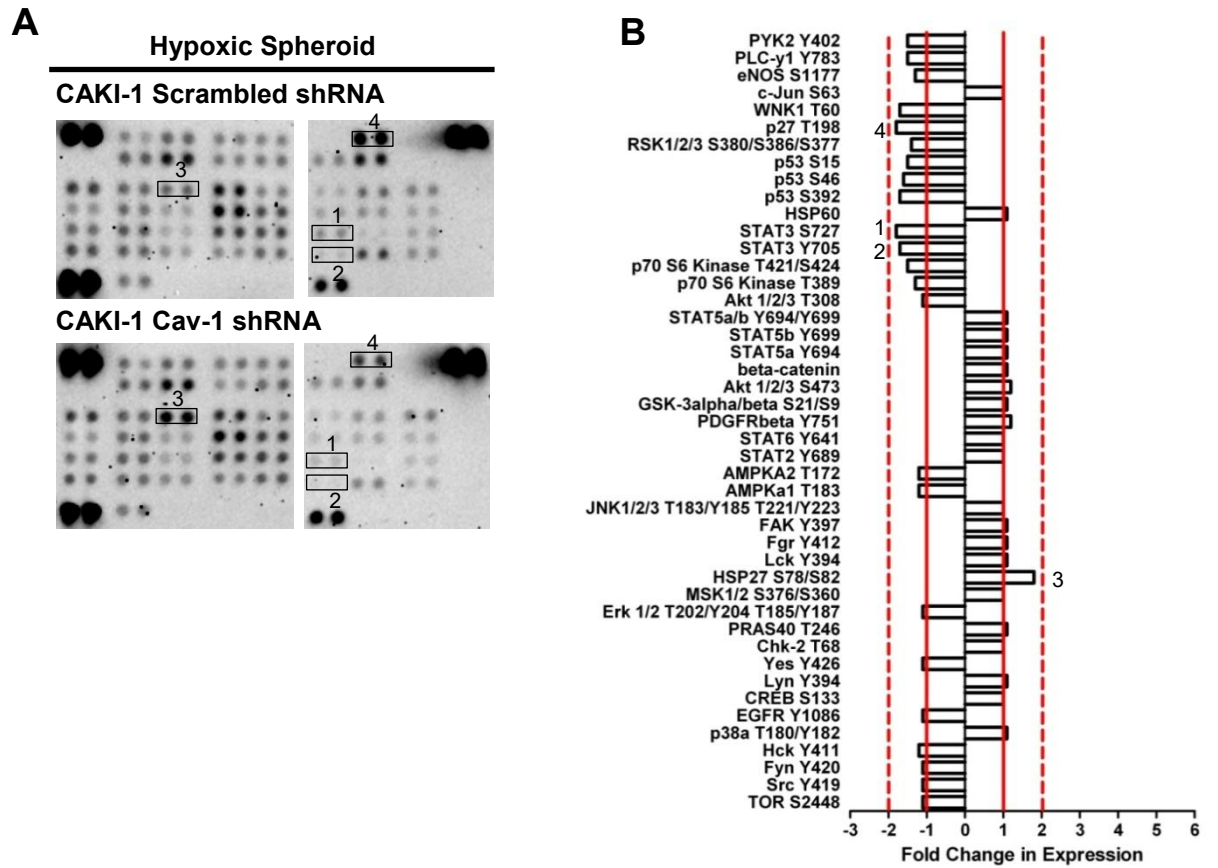




Figure 5.3 Human phospho-kinase array data of CAKI-1 Scrambled shRNA control and CAV1 shRNA knockdown cells grown as spheroids in non-adherent hypoxic conditions. A Processed arrays phosphor-kinase arrays for both Scrambled shRNA and CAV1 shRNA cells. B Graph showing fold change in expression both positive and negative for each marker with respect to CAV1 down-regulation. Numbers on the graph correspond to the position of a protein on the array.

Table 5.1 Heat-map showing the fold changes in phosphorylation induced by CAV1 down-regulation in adherent, spheroid and hypoxic spheroid cells. Only proteins with a fold decrease in at least one condition are shown. ↑ indicates up-regulation ↓ indicates down-regulation.

| Proteins | Normoxic Adherent | Normoxic Spheroid | Hypoxic Spheroid |
|-------------------------|-------------------|-------------------|------------------|
| HSP27 S78/S82 | 1.4 | -1.1 | ↑ 1.8 |
| PRA S40 T246 | 1.0 | ↑ 2.3 | 1.1 |
| Fgr Y412 | ↑ 1.5 | -1.2 | 1.1 |
| AMPKa1 T183 | ↑ 1.6 | -1.4 | -1.2 |
| AMPKA2 T172 | ↑ 1.5 | -1.2 | -1.2 |
| GSK-3alpha/beta S21/S9 | ↑ 5.5 | ↓ -1.6 | 1.1 |
| Akt 1/2/3 S473 | ↓ -1.8 | -1.3 | 1.2 |
| Akt 1/2/3 T308 | 1.0 | ↓ -1.6 | -1.1 |
| p70 S6 Kinase T389 | -1.2 | ↓ -1.5 | -1.3 |
| p70 S6 Kinase T421/S424 | ↓ -1.6 | -1.4 | ↓ -1.5 |
| STAT3 Y705 | ↓ -3.0 | -1.3 | ↓ -1.7 |
| STAT3 S727 | ↓ -6.1 | -1.3 | ↓ -1.8 |
| HSP60 | ↑ 1.5 | -1.1 | 1.1 |
| p53 S392 | 1.0 | ↓ -1.5 | ↓ -1.7 |
| p53 S46 | -1.2 | ↓ -1.8 | ↓ -1.6 |
| p53 S15 | ↓ -1.8 | ↓ -1.6 | ↓ -1.5 |
| RSK1/2/3 S380/S386/S377 | ↓ -1.6 | ↓ -1.5 | -1.4 |
| p27 T198 | ↓ -2.6 | -1.2 | ↓ -1.8 |
| WNK1 T60 | -1.1 | -1.3 | ↓ -1.7 |
| c-Jun S63 | -1.1 | ↓ -1.5 | 1.0 |
| eNOS S1177 | ↓ -1.5 | -1.3 | -1.3 |
| PLC-y1 Y783 | -1.4 | ↓ -1.6 | ↓ -1.5 |
| PYK2 Y402 | -1.1 | -1.7 | ↓ -1.5 |

 >1.9 Fold change in expression
 1.5 – 1.8 Fold change in expression

5.3.2 Effect of CAV1 knockdown on cancer related cell signalling under different culture conditions

To understand how downregulation of CAV1 affects the expression of common oncogenes, tumour suppressors and molecules capable of facilitating progression to malignant disease protein microarrays consisting of such proteins were used (referred to here after as the 'oncology array'). Expression of these proteins were investigated in CAKI-1 scrambled shRNA and CAV1 shRNA knockdown cells under normoxic adherent growth conditions, normoxic non-adherent spheroid forming conditions and under hypoxic non-adherent spheroid forming conditions.

Under normoxic adherent conditions CAV1 knockdown caused a greater than 1.9 fold change in several proteins. Expression of a number of pro-invasive proteins was detected including: urokinase-type plasminogen activator (u-PA) upregulated 2.2 fold, vascular cell adhesion protein (VCAM-1 or CD106) upregulated by 2.3 fold and Cathepsin S upregulated 2.2 fold (Figure 5.4 labelled 1, 2 and 3 respectively Table 5.2 Table 5.3). Hypoxia inducible factor - 1 α (HIF-1 α) shows an upregulation of 4.5 fold in response to CAV1 knockdown (Figure 5.4 labelled 4 Table 5.3). Downregulation of CAV1 also appears to cause significant upregulation of the inhibitor of the Wnt signalling pathway DKK-1[410] with a 4.3 fold increase in expression (Figure 5.4 labelled 5 Table 5.2). The tumour suppressor p53 demonstrated a 2.1 fold decrease in expression with CAV1 knockdown (Figure 5.4 labelled 6 Table 5.3). Several members of the Kallikreins as well as MMP-9 appear to show down regulation however this is due to their extremely low expression similar to that of background resulting in apparent large changes in expression. While several proteins appear to show slight changes in expression the majority were at a level of expression similar to that of background.

Analysis of the same microarrays in normoxic spheroid forming cells also found changes CAV1 dependent downregulation of pro-invasive proteins. VCAM-1/CD106

showed a downregulation of 2.6 fold which was found to be upregulated in normoxic adherent conditions with CAV1 knockdown (Figure 5.5 labelled 1 Table 5.2). In addition to this, intercellular adhesion molecule-1 (ICAM-1) showed downregulation of 2.1 fold with CAV1 knockdown (Figure 5.5 labelled as 3 Table 5.3). Interestingly, under spheroid forming conditions CAV1 shRNA knockdown cells displayed a 2.5 fold decrease in expression of angiopoietin-like 4 which is not observed in normoxic adherent cells (Figure 5.5 labelled 2 Table 5.2). The CAV1 induced downregulation of p53 observed in adherent cells was also present in the spheroid forming cells, albeit to a much lesser extent, with a 1.6 fold change in expression (Figure 5.5 labelled 4 Table 5.3).

Downregulation of CAV1 in hypoxic spheroid forming cells causes changes in the expression of many proteins in the oncology array. In regard to proteins regulator and effector proteins upregulated under hypoxic conditions, upregulation of angiopoietin-like 4 and HIF-1 α by 3 and 3.5 fold respectively (Figure 5.6 labelled 6 and 7 Table 5.2 Table 5.3). In addition, the RCC CSC marker[61] and microvascular density marker[186] CD105 was shown to be upregulated 2 fold with CAV1 downregulation under hypoxic conditions (Figure 5.6 labelled 3 Table 5.2). Interestingly, the pro-invasive proteins u-PA and cathepsin S, which showed no difference in expression in response to CAV1 knockdown in normoxic spheroids, were upregulated by 3.3 fold and 2.8 fold respectively (Figure 5.6 labelled 5 and 1 respectively Table 5.2 Table 5.3). In addition to this, ICAM-1 and VCAM-1/CD106 expression are both downregulated by 2.1 and 1.8 respectively fold in spheroid forming cells under hypoxic conditions, a change in expression which was also observed in normoxic spheroid forming cells (Figure 5.6 labelled 9 and 12 respectively Table 5.3). Of note a 9.5 fold increase in serpin E1[411], an inhibitor of u-PA, with CAV1 downregulation under hypoxic conditions was observed (Figure 5.6 labelled 8 Table 5.3). Significant changes in the regulation of the chemokine

molecules with CXCL8/IL-8 and CLL20/MIP-3a upregulated by 4.1 and 10.9 fold respectively (Figure 5.6 labelled 2 and 4 respectively Table 5.2.). Finally, the downregulation of tumour suppressors p53 and p27 by 1.8 was also detected, showing p53 activity to be downregulated in a CAV1 dependent manner in all three growth conditions (Figure 5.6 labelled 11 and 13 respectively Table 5.3).

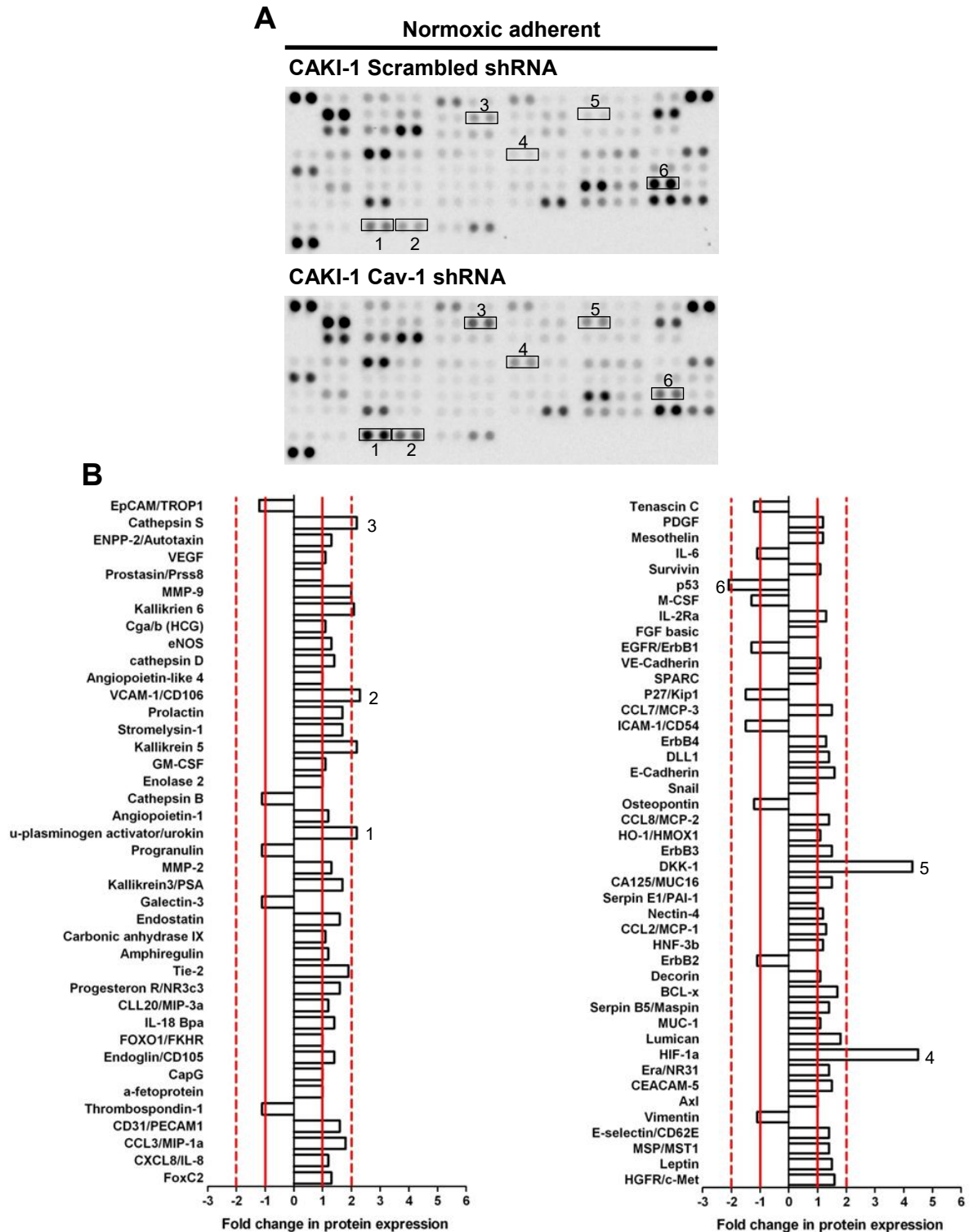


Figure 5.4 Human oncology array data of CAKI-1 Scrambled shRNA control and CAV1 shRNA knockdown cells grown as an adherent monolayer under normoxic conditions. A Processed arrays phosphor-kinase arrays for both Scrambled shRNA and CAV1 shRNA cells. B Graph showing fold change in expression both positive and negative for each marker with respect to CAV1 down-regulation. Numbers on the graph correspond to the position of a protein on the array.

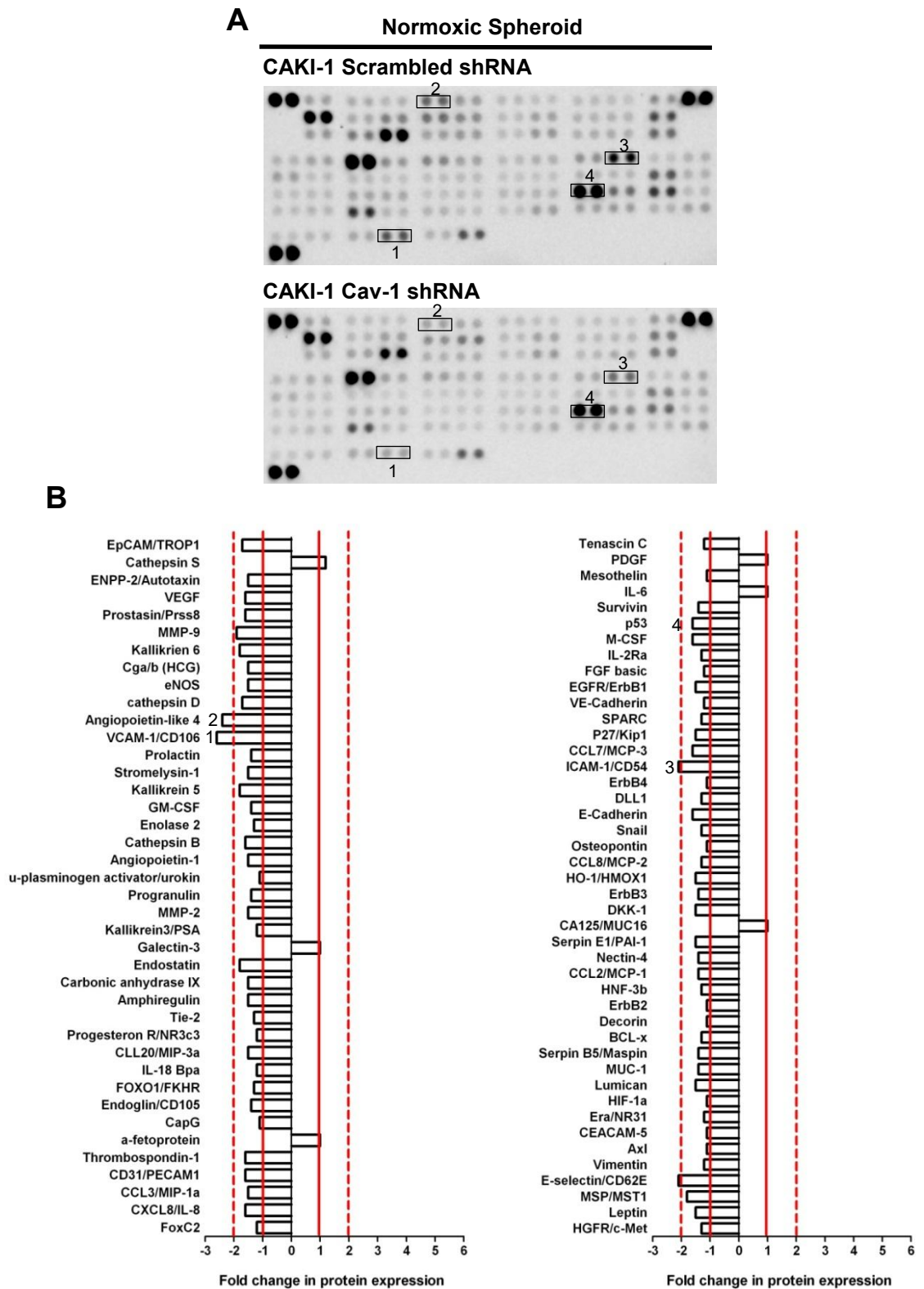


Figure 5.5 Human oncology array data of CAKI-1 Scrambled shRNA control and CAV1 shRNA knockdown cells grown as non-adherent spheroids under normoxic conditions. A Processed arrays phosphor-kinase arrays for both Scrambled shRNA and CAV1 shRNA cells. B Graph showing fold change in expression both positive and negative for each marker with respect to CAV1 down-regulation. Numbers on the graph correspond to the position of a protein on the array.

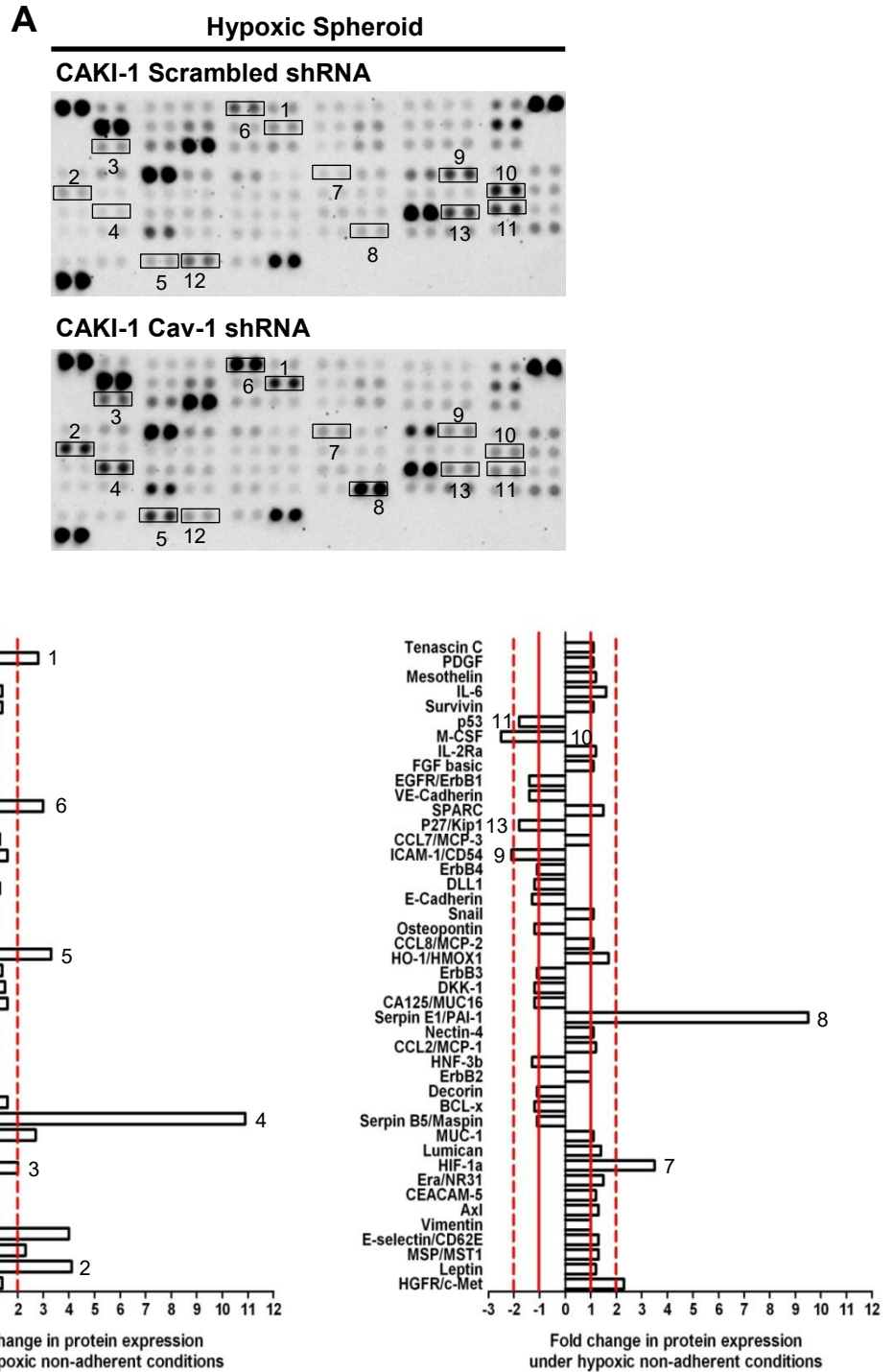



Figure 5.6 Human oncology array data of CAKI-1 Scrambled shRNA control and CAV1 shRNA knockdown cells grown as non-adherent spheroids under hypoxic conditions. A Processed arrays phosphor-kinase arrays for both Scrambled shRNA and CAV1 shRNA cells. B Graph showing fold change in expression both positive and negative for each marker with respect to CAV1 down-regulation. Numbers on the graph correspond to the position of a protein on the array.

Table 5.2 Heat-map showing the fold changes in proteins identified by the oncology array induced by CAV1 down-regulation in adherent, spheroid and hypoxic spheroid cells. ↑ indicates up-regulation ↓ indicates down-regulation.



| Protein | Normoxic Adherent | Normoxic Spheroid | Hypoxic Spheroid |
|-----------------------|-------------------|-------------------|------------------|
| CXCL8/IL-8 | 1.2 | ↓ -1.6 | ↑ 4.1 |
| CCL3/MIP-1a | ↑ 1.8 | ↓ -1.5 | ↑ 2.3 |
| CD31/PECAM1 | ↑ 1.6 | ↓ -1.6 | ↑ 4.0 |
| Thrombospondin-1 | -1.1 | ↓ -1.6 | 1.2 |
| Endoglin/CD105 | 1.4 | -1.4 | ↑ 2.0 |
| IL-18 Bpa | 1.4 | -1.2 | ↑ 2.7 |
| CLL20/MIP-3a | 1.2 | ↓ -1.5 | ↑ 10.9 |
| Progesteron R/NR3c3 | ↑ 1.6 | -1.2 | ↑ 1.6 |
| Tie-2 | ↑ 1.9 | -1.3 | 1.0 |
| Amphiregulin | 1.2 | ↓ -1.5 | -1.1 |
| Carbonic anhydrase IX | 1.1 | ↓ -1.5 | 1.1 |
| Endostatin | ↑ 1.6 | ↓ -1.8 | 1.2 |
| Kallikrein3/PSA | ↑ 1.7 | -1.2 | ↑ 1.6 |
| MMP-2 | 1.3 | ↓ -1.5 | ↑ 1.5 |
| u-PA | ↑ 2.2 | -1.1 | ↑ 3.3 |
| Angiopoietin-1 | 1.2 | ↓ -1.5 | -1.3 |
| Cathepsin B | -1.1 | ↓ -1.6 | 1.1 |
| Kallikrein 5 | ↑ 2.2 | ↓ -1.8 | 1.2 |
| Stromelysin-1 | ↑ 1.7 | ↓ -1.5 | ↑ 1.6 |
| Prolactin | ↑ 1.7 | ↓ -1.4 | 1.3 |
| VCAM-1/CD106 | ↑ 2.3 | ↓ -2.6 | ↓ -1.8 |
| Angiopoietin-like 4 | 1.0 | ↓ -2.4 | ↑ 3.0 |
| Cathepsin D | 1.4 | ↓ -1.7 | 1.2 |
| eNOS | 1.3 | ↓ -1.5 | 1.1 |
| Cga/b (HCG) | 1.1 | ↓ -1.5 | -1.1 |
| Kallikrien 6 | ↑ 2.1 | ↓ -1.8 | 1.2 |

 >1.9 Fold change in expression

 1.5 – 1.8 Fold change in expression

Table 5.3 Heat-map showing the fold changes in proteins identified by the oncology array induced by CAV1 down-regulation in adherent, spheroid and hypoxic spheroid cells. ↑ indicates up-regulation ↓ indicates down-regulation.

| Protein | Normoxic Adherent | Normoxic Spheroid | Hypoxic Spheroid |
|------------------|-------------------|-------------------|------------------|
| MMP-9 | ↑ 2.0 | ↓ -1.9 | 1.2 |
| Prostasin/Prss8 | 1.0 | ↓ -1.6 | 1.4 |
| VEGF | 1.1 | ↓ -1.6 | 1.4 |
| ENPP-2/Autotaxin | 1.3 | ↓ -1.5 | -1.4 |
| Cathepsin S | ↑ 2.2 | 1.2 | ↑ 2.8 |
| EpCAM/TROP1 | -1.2 | ↓ -1.7 | ↓ -1.6 |
| HGFR/c-Met | ↑ 1.6 | -1.3 | ↑ 2.3 |
| Leptin | ↑ 1.5 | ↓ -1.5 | 1.2 |
| MSP/MST1 | 1.4 | ↓ -1.8 | 1.3 |
| E-selectin/CD62E | 1.4 | ↓ -2.1 | 1.3 |
| Vimentin | -1.1 | -1.2 | 1.0 |
| Axl | 1.0 | -1.1 | 1.3 |
| CEACAM-5 | 1.5 | -1.1 | 1.2 |
| Era/NR31 | 1.4 | -1.2 | ↑ 1.5 |
| HIF-1a | ↑ 4.5 | -1.1 | ↑ 3.5 |
| Lumican | ↑ 1.8 | ↓ -1.5 | 1.4 |
| BCL-x | ↑ 1.7 | -1.3 | -1.2 |
| Serpin E1/PAI-1 | 1.0 | ↓ -1.5 | ↑ 9.5 |
| CA125/MUC16 | ↑ 1.5 | 1.0 | -1.2 |
| DKK-1 | ↑ 4.3 | ↓ -1.5 | -1.2 |
| HO-1/HMOX1 | 1.1 | ↓ -1.5 | ↑ 1.7 |
| E-Cadherin | ↑ 1.6 | ↓ -1.6 | -1.3 |
| ICAM-1/CD54 | ↓ -1.5 | ↓ -2.1 | ↓ -2.1 |
| CCL7/MCP-3 | ↑ 1.5 | ↓ -1.6 | 1.0 |
| P27/Kip1 | -1.5 | ↓ -1.5 | ↓ -1.8 |
| SPARC | 1.0 | -1.3 | ↑ 1.5 |
| EGFR/ErbB1 | -1.3 | ↓ -1.5 | -1.4 |
| M-CSF | -1.3 | ↓ -1.6 | ↓ -2.5 |
| p53 | ↓ -2.1 | ↓ -1.6 | ↓ -1.8 |
| IL-6 | -1.1 | 1.0 | 1.6 |

 >1.9 Fold change in expression
 1.5 – 1.8 Fold change in expression

5.3.3 Effect of CAV1 knockdown on the expression of pluripotent stem cell markers under different culture conditions

Downregulation of CAV1 severely disrupted the clonogenic and sphere forming capacity of CAKI-1 cells. As a multitude of phenotypic and functional markers of self-renewal regulation have been identified in CSC populations of various tumours, a human pluripotent stem cell proteomics array was used to identify markers which showed around a 1.5 fold or greater change in expression. Analysis of these stemness markers was carried out under normoxic adherent and spheroid forming cells as well as spheroid forming cells under hypoxia.

Under normoxic adherent conditions CAKI-1 cells showed no significant downregulation or upregulation in any of the stemness markers in the microarray (Figure 5.7 Table 5.4). However in cells capable of spheroid formation CAV1 dependent downregulation was detected in three different proteins. The pro-angiogenic vascular endothelial growth factor receptor 2 (VEGF R2) (1.9 fold) (Figure 5.8 labelled 3 Table 5.4). The self-renewal transcription factor of ESCs Nanog was downregulated 1.7 fold (Figure 5.8 labelled 2 Table 5.4). The marker of foetal development and hepatocellular carcinoma β -fetoprotein (AFP) was downregulated 1.9 fold (Figure 5.8 labelled 1 Table 5.4). These changes observed in stemness markers of spheroid forming cells under normoxic were not apparent in spheroid forming cells under hypoxic conditions (Figure 5.9 Table 5.4).

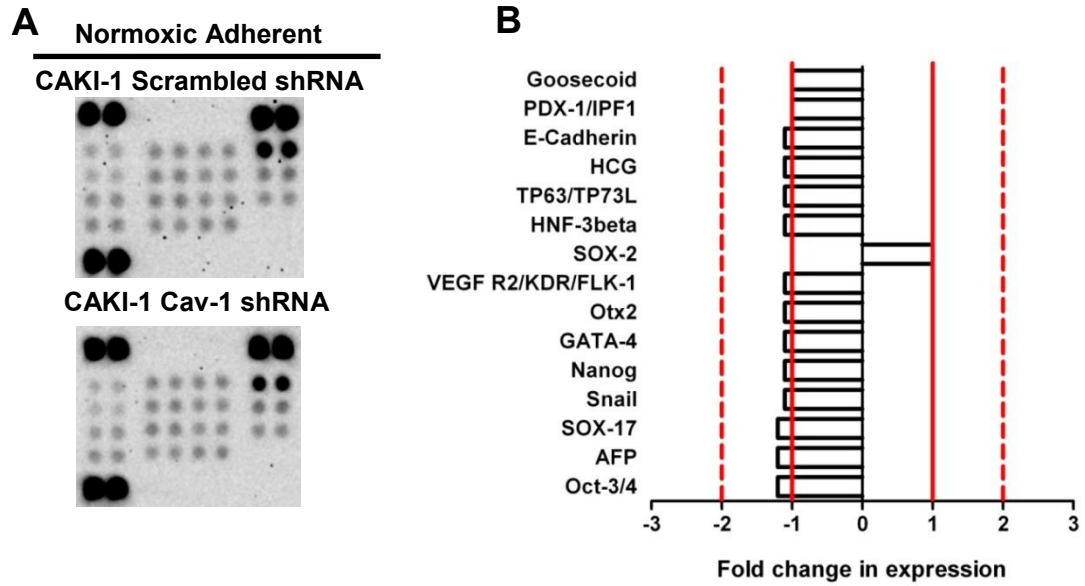


Figure 5.7 Human pluripotent stem cell array data of CAKI-1 Scrambled shRNA control and CAV1 shRNA knockdown cells grown as an adherent monolayer under normoxic conditions. A Processed arrays phosphor-kinase arrays for both Scrambled shRNA and CAV1 shRNA cells. B Graph showing fold change in expression both positive and negative for each marker with respect to CAV1 down-regulation. Numbers on the graph correspond to the position of a protein on the array.

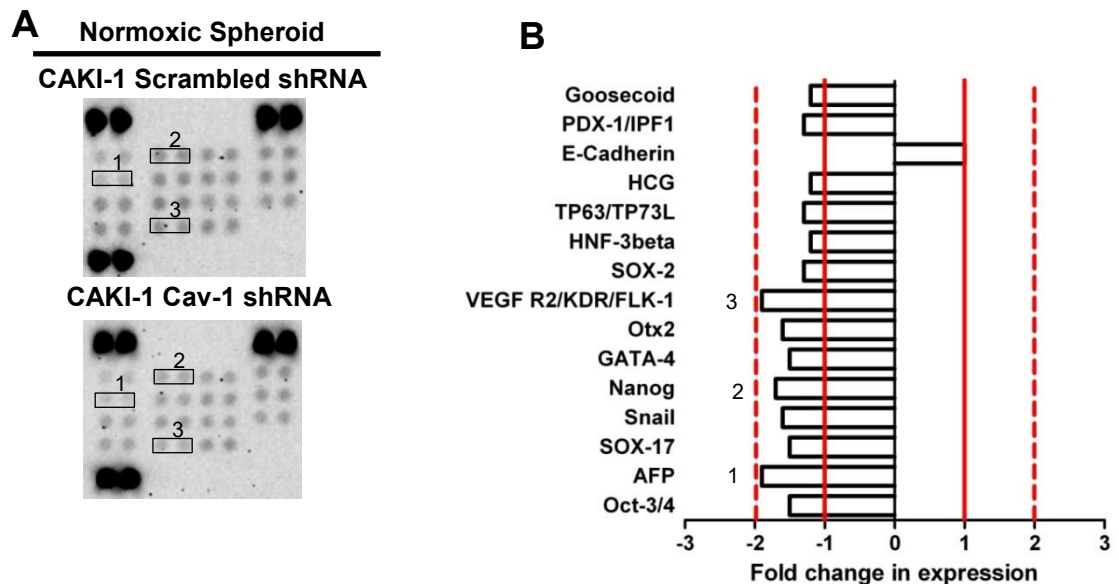


Figure 5.8 Human pluripotent stem cell array data of CAKI-1 Scrambled shRNA control and CAV1 shRNA knockdown cells grown as a non-adherent spheroids under normoxic conditions. A Processed arrays phosphor-kinase arrays for both Scrambled shRNA and CAV1 shRNA cells. B Graph showing fold change in expression both positive and negative for each marker with respect to CAV1 down-regulation. Numbers on the graph correspond to the position of a protein on the array.

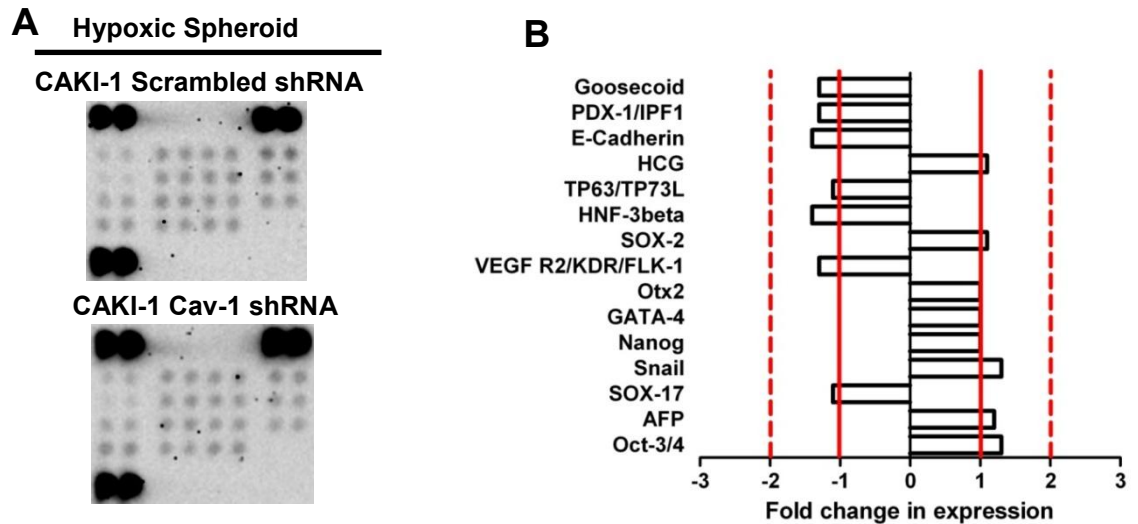


Figure 5.9 Human pluripotent stem cell array data of CAKI-1 Scrambled shRNA control and CAV1 shRNA knockdown cells grown as an non-adherent spheroids under hypoxic conditions. A Processed arrays phosphor-kinase arrays for both Scrambled shRNA and CAV1 shRNA cells. B Graph showing fold change in expression both positive and negative for each marker with respect to CAV1 down-regulation. Numbers on the graph correspond to the position of a protein on the array.

Table 5.4 Heat-map showing the fold changes in proteins identified by the pluripotent stem cell array induced by CAV1 down-regulation under all three conditions.

| Protein | Normoxic Adherent | Normoxic Spheroid | Hypoxic Spheroid |
|------------------|-------------------|-------------------|------------------|
| Oct-3/4 | -1.2 | ↓ -1.5 | 1.3 |
| AFP | -1.2 | ↓ -1.9 | 1.2 |
| SOX-17 | -1.2 | ↓ -1.5 | -1.1 |
| Snail | -1.1 | ↓ -1.6 | 1.3 |
| Nanog | -1.1 | ↓ -1.7 | 1.0 |
| GATA-4 | -1.1 | ↓ -1.5 | 1.0 |
| Otx2 | -1.1 | ↓ -1.6 | 1.0 |
| VEGFR2/KDR/FLK-1 | -1.1 | ↓ -1.9 | -1.3 |

>1.9 Fold change in expression
 1.5 – 1.8 Fold change in expression

5.3.4 Down-regulation of CAV1 causes the downregulation of both STAT3 phosphorylation and β -catenin expression but only STAT3 inhibition affects clonogenicity.

Microarray analysis of the regulation of cell signalling pathways with respect to CAV1 expression found a marked downregulation in the phosphorylation of STAT3 and upregulation of DKK-1 an inhibitor of the Wnt pathway. As such we conducted inhibitor studies to ascertain the ability of each of these pathways to drive clonogenicity in the CAKI-1 cell line.

Western blot analysis suggests that in addition to upregulation of DKK-1 in CAKI-1 CAV1 shRNA knockdown cells β -catenin was also downregulated compared to CAKI-1 scrambled shRNA control cells (Figure 5.10 B). In addition to this, flow cytometric analysis confirmed that CAV1 knockdown to reduce pSTAT3 phosphorylation at its activating Y705 residue (Figure 5.10 A). Treatment of CAKI-1 scrambled shRNA control cells resulted in significant reduction of both pSTAT3 Y705 as determined by flow cytometry and β -catenin expression as determined by Western blot (Figure 5.11 A and B). Colony formation assays with CAKI-1 scrambled shRNA control and CAV1 shRNA knockdown cells pretreated with the either IWP-2 (Wnt pathway inhibitor) or WP1066 (STAT3 inhibitor) caused decreases in colony formation. Inhibition of STAT3 phosphorylation proved to be extremely potent reducing colony formation of scrambled shRNA control cells 98% ($P < 0.001$) (Figure 5.12). Inhibition of the Wnt pathway resulted in a more modest decrease in colony formation of 24% ($P < 0.001$) (Figure 5.12).

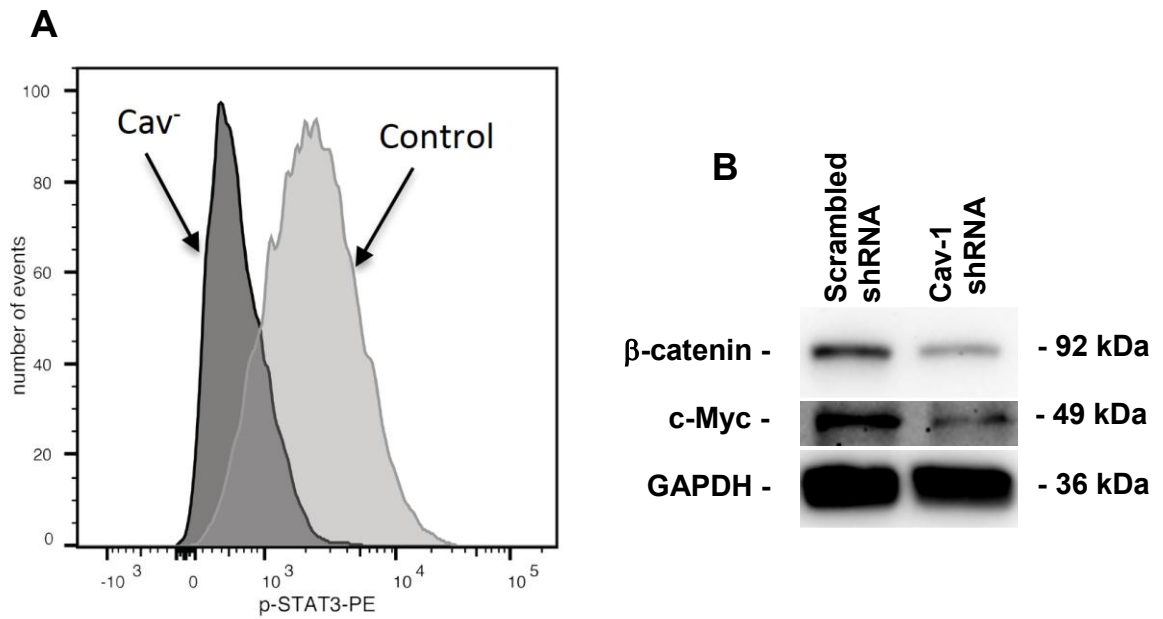


Figure 5.10 CAV1 dependant downregulation of STAT3 and b-catenin in CAKI-1 cells A Flow cytometry of pSTAT3 associated fluorescence taken from 10,000 events. The light grey histogram representing CAKI-1 Scrambled shRNA control cells and the dark grey histogram representing CAKI-1 CAV1 shRNA knockdown cells. B Western blots showing the CAV1 dependent downregulation of β -catenin and c-Myc with GAPDH as a loading control.

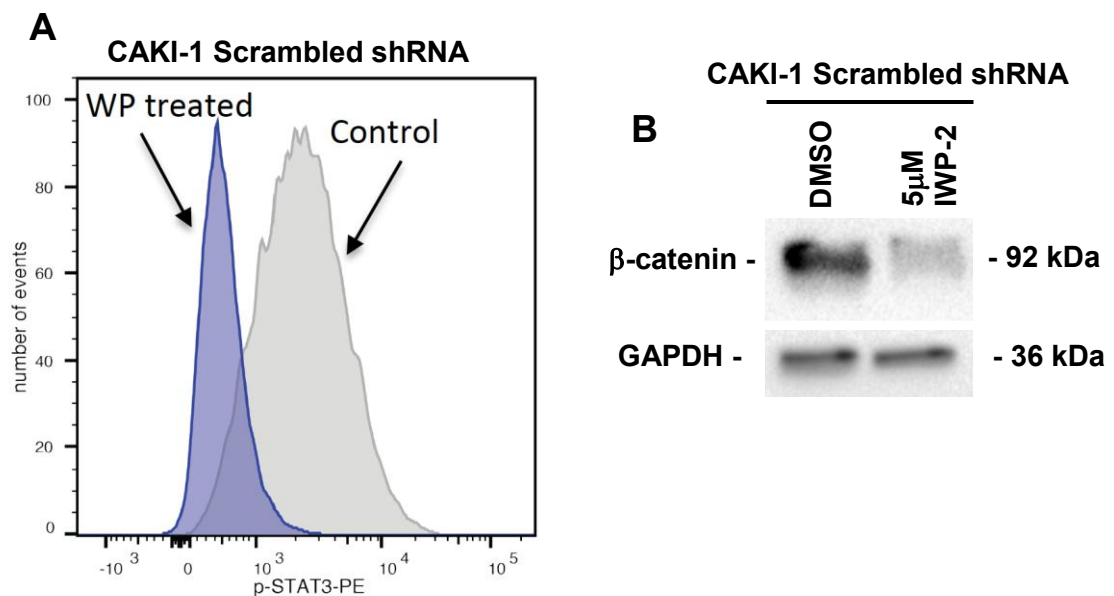


Figure 5.11 Inhibition of STAT3 phosphorylation by WP1066 (A) and β -catenin by IWP-2 (B). A Flow cytometry histograms of fluorescence associated to pSTAT3 in DMSO treated CAKI-1 scrambled shRNA control (light grey histogram labelled Control) and WP1066 6 μ M treated CAKI-1 scrambled shRNA control (blue histogram labelled WP treated). B Western blot showing inhibition of β -catenin by IWP-2 with GAPDH used as a loading control.

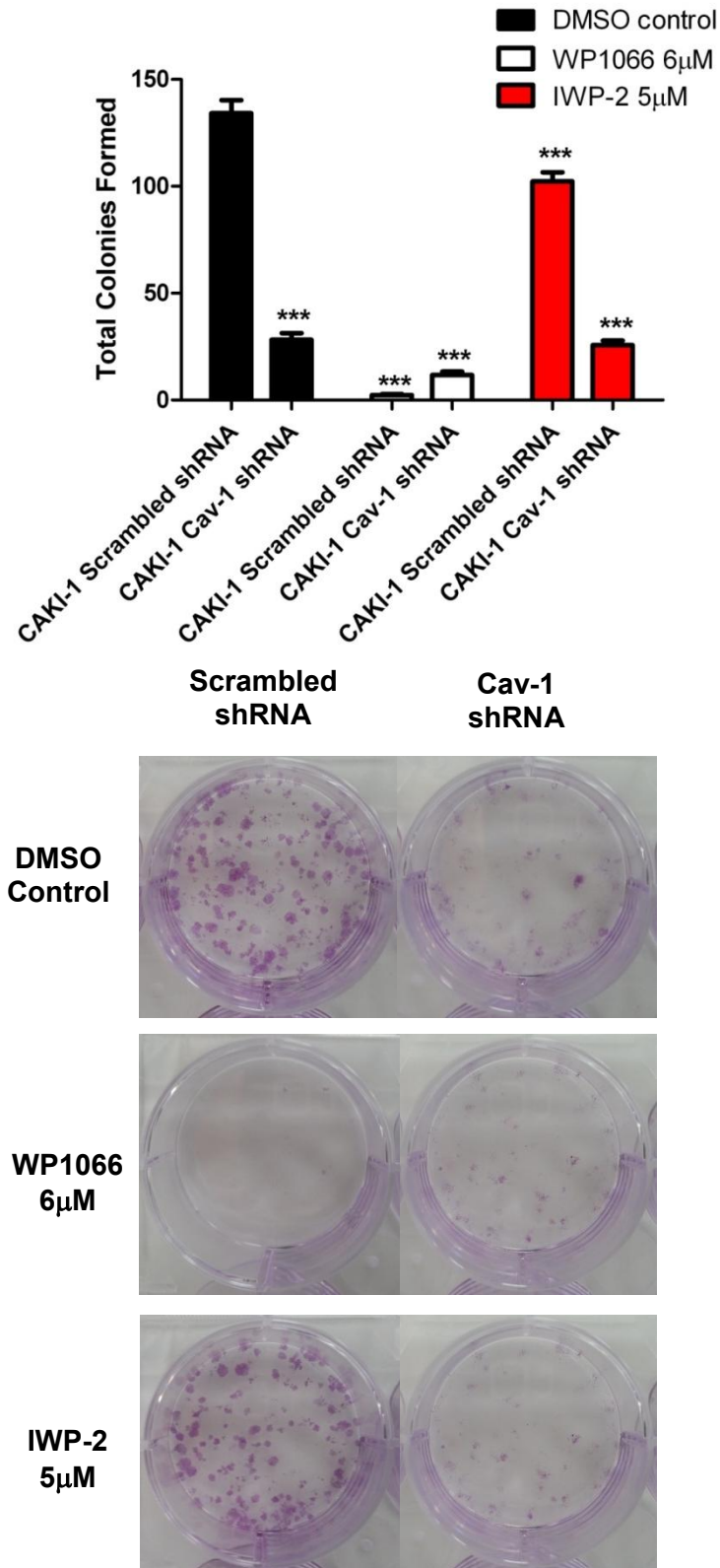


Figure 5.12 Colony formation of CAKI-1 scrambled shRNA control and CAV1 shRNA knockdown cells after small molecule inhibition of STAT3 phosphorylation by WP1066 and Wnt signalling by IWP-2. Data presented as mean \pm standard deviation of 3 experiments. Statistical difference determined by one-way ANOVA with a Dunnett post-hoc. *** = $P < 0.001$

5.4 Discussion

This chapter has used a broad spectrum analysis, in the form of proteomic microarrays, to assess multiple cell signalling pathways in the CAKI-1 cell line to understand which pathways become down or upregulated in response to CAV1 downregulation. This analysis was carried out on normal adherent monolayer cultures as well as in cells capable of spheroid formation, hence increased potency for clonogenicity and self-renewal, under normoxic and hypoxic conditions.

Microarray analysis found CAV1 knockdown under normoxic adherent conditions reduced the amount of STAT3 phosphorylation at both S727 and Y705 residues. In normoxic spheroid forming cells the decrease in STAT3 phosphorylation was far less pronounced. In hypoxic spheroid forming cells however more pronounced downregulation of STAT3 was once again observed in both sites. Inhibition of STAT3 phosphorylation by the small molecule inhibitor WP1066, which we found to significantly reduce the phosphorylation of STAT3, had a profound effect on the colony forming capacity of CAKI-1 cells, nearly completely ablating it.

These results suggest the possibility that CAV1 is driving clonogenicity and spheroid formation through maintaining activation of STAT3. Activation of STAT3 signalling has been demonstrated as integral to driving self-renewal capacity in embryonic stem cells[412] and also implicated in driving the CSC phenotype in a number of cancers[389], [392], [393]. In some of these studies IL-6 stimulation has been shown to be the causative factor in STAT3 activation[393]. However, in microarray analysis, CAV1 knockdown did not alter IL-6 expression in either normoxic adherent or spheroid forming cells (Table 5.3). However the activation of STAT3 by IL-6 signalling appears to be irrelevant for CAKI-1 cells. A previous study by Horiguchi et al. [413] demonstrated CAKI-1 cells to be unresponsive to stimulation by IL-6 and did not express a functional gp130 IL-6 receptor subunit. Indeed some studies have identified STAT3 activation through the phosphatase and tensin homolog

(PTEN)/Akt/mammalian target of rapamycin (mTOR) pathway stimulated by RTK activation[390], [414]. CAV1 downregulation of pSTAT3 has been observed before in metastatic lung cancer cells where siRNA silencing of CAV1 directly reduced the phosphorylation and downstream STAT3 and Erk[120]. CAKI-1 is known to be a PTEN expressing cell line and therefore maintains regulatory control of Akt activity[415]. In microarray analysis we observe that CAV1 knockdown induces a reduction in the activating phosphorylation site S473 of Akt. This poses the interesting possibility that CAV1 drives clonogenicity of CAKI-1 by maintaining Akt directed activation of STAT3. Under CAV1 knockdown PTEN is then able to inhibit Akt activation and thereby reduce the phosphorylation of STAT3 (Figure 5.13). In the PTEN competent A498 cell line such an effect may not be observed due to the VHL deficiency of that cell line which may mask the effect of downregulating CAV1 mediated clonogenicity. Indeed, PTEN has been found to possess a CAV1 binding sequence[86], however interactions of CAV1 with PTEN thus far show increased CAV1 to increase the inhibitory activity of PTEN upon Akt[88]. Interestingly STAT3 activation in RCC has been demonstrated to contribute to HIF-1 α mediated expression of VEGF[416]. However in these studies we find that HIF-1 α expression is actually increased when CAV1 and phosphorylated STAT3 are downregulated under hypoxic conditions. Again further suggesting a possible non synergistic relationship between CAV1 expression and hypoxic signalling.

CAV1 downregulation also caused substantial upregulation of DKK-1 expression, an important inhibitor of Wnt signalling[410]. However, CAV1 downregulation also increase the inhibitory phosphorylation of GSK-3 α/β , a key component of the β -catenin targeting destruction complex. Inhibition of GSK-3 α/β activity would indicate β -catenin stabilisation and accumulation of active β -catenin[417]. While microarray analysis of β -catenin found no substantial downregulation, western blot found β -catenin expression to be downregulated. In addition to this CAV1 knockdown

reduced the expression of the transcription factor c-Myc, understood to be an important factor in self-renewal and the induced pluripotency phenotype[418]. However, inhibition of β -catenin activity in CAKI-1 scrambled shRNA control cells only resulted in a modest reduction in colony forming capacity of these cells. These data appear to suggest a complex role for CAV1 in maintaining the activation of β -catenin.

CAV1 has been found to regulate CSC phenotype through regulation of β -catenin in a previous study. Wang et al.[419] found CAV1 expression to be enriched in breast cancer CSC populations, knockdown of which caused reduced chemoresistance and self-renewal through Akt/GSK3/ β -catenin activation. However, this does not appear to be the only means by which CAV1 expression can regulate β -catenin levels. Previous studies have shown a mechanistic relationship between CAV1, LRP6 and DKK1 in relation to the induction of β -catenin stability and accumulation. Yamamoto et al.[420] found CAV1-dependent internalisation of LRP6 to be critical to the stabilisation of β -catenin activity, by caveolar sequestration and trafficking of the LRP6 associated destruction complex to multivesicular endosomes[421], [422]. In the absence of CAV1 expression DKK1 causes the internalisation of LRP6 through clathrin mediated endocytosis which is incapable of deactivating the destruction complex[420]. As CAV1 downregulation increases DKK1 expression it seems to indicate that as well as maintaining β -catenin levels CAV1 is also suppressing DKK1 expression, potential through sustained activation of β -catenin signalling (Figure 5.13).

Western blotting revealed downregulation of c-Myc with CAV1 knockdown. c-Myc has been demonstrated as a downstream target of both β -catenin[423], [424] and STAT3[425], [426], indicating the possibility of a synergistic interaction between the two. Furthermore, CAV1 knockdown induced slight downregulation of nanog, a

transcription factor implicated as key to the self-renewal capacity of a number CSC populations[427], however this was observed only in the spheroid forming cells and not present in hypoxic spheroid forming cells or normoxic adherent cells. Together, these factors suggest a possible transcriptional basis for the pro-clonogenic activities of CAV1 in CAKI-1.

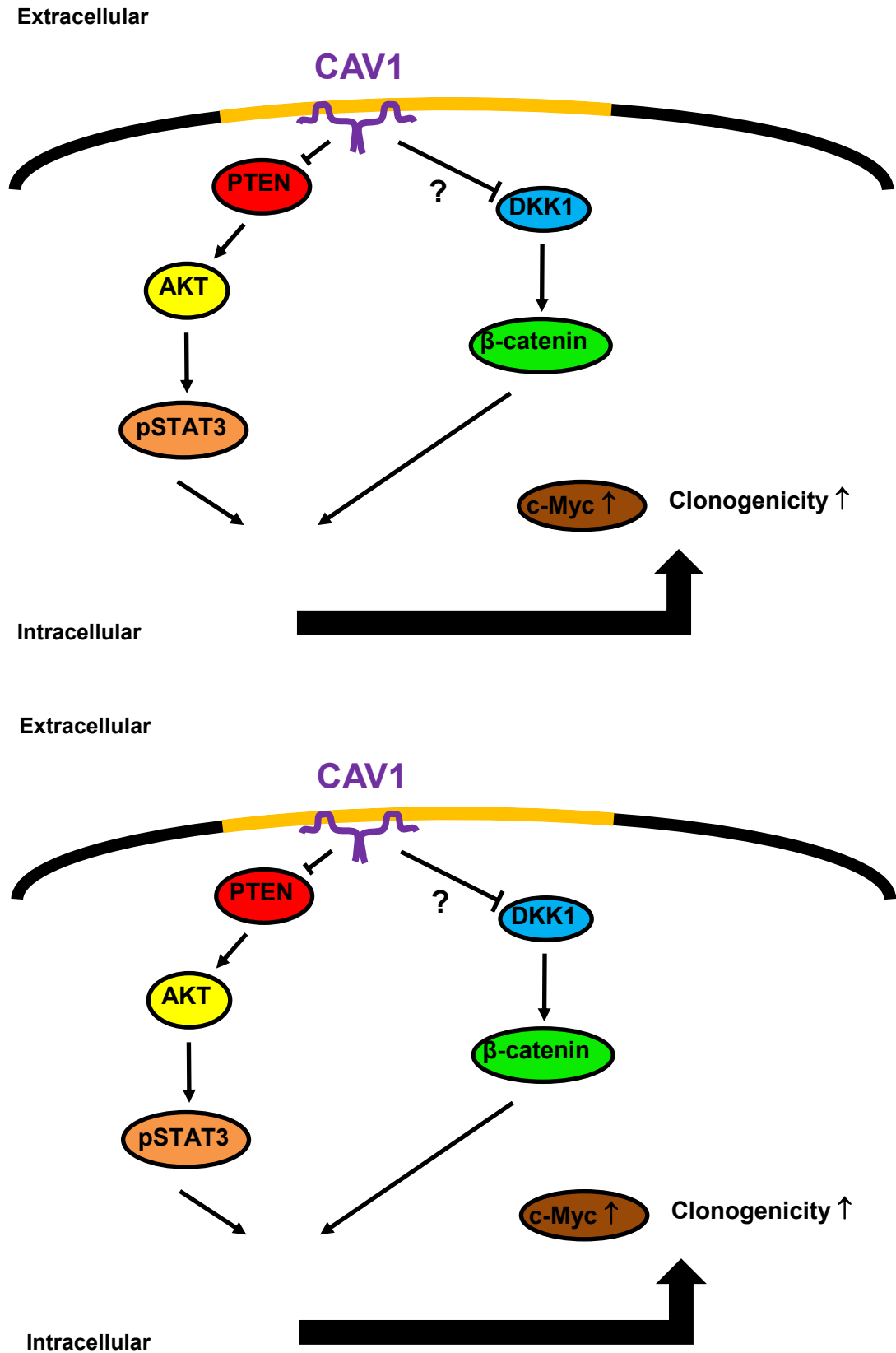


Figure 5.13 Schematic overview of CAV1 regulation of clonogenicity in CAKI-1 cells. CAV1 is capable of maintaining the activation of both pSTAT3, potentially through enabling the activation of Akt, and β -catenin through the inhibition of DKK1.

Downregulation of CAV1 under hypoxic conditions caused upregulation of hypoxia responsive proteins HIF-1 α and angiopoietin-like 4 (ANGPTL4). Interestingly, in normoxic spheroid forming cells, CAV1 downregulation causes a decrease in ANGPTL4 whereas in normoxic adherent cells no effect is observed on ANGPTL4 expression. From this data it appears that expression of ANGPTL4 is being maintained by the presence of CAV1 under normoxic conditions but also inhibited from overexpression under hypoxic conditions. ANGPTL4 has been shown to confer resistance to anoikis[428], [429], cell detachment induced apoptosis, in cancer cells a feature which must be present and induced in CSC populations in order to allow proliferation. This data indicates a possible mechanism by which CSC activity is upregulated under hypoxic CAV1 negative conditions. In addition to alterations in the expression of hypoxia induced proteins, CAV1 downregulation also significantly upregulated the expression of the chemokines IL-8 and CCL20/MIP-3a (here after referred to as CLL20). IL-8 and its receptor CXCR1 have been identified as regulators of CSC phenotype. Pre-treatment of pancreatic cancer cells with IL-8 enhanced: expression of pancreatic CSC associated markers, spheroid formation and invasion[430]. CXCR1/IL-8 signalling has been extensively studied in breast CSCs with ablation of CXCR1 activity resulting in decreased tumourigenicity[431], such targeting was found to increase the effect of treatment with Her2[432]. Together, this data suggests the possibility that under hypoxic conditions CSC phenotype maybe upregulated by a combination of IL-8 stimulation of self-renewal and ANGPLT4 supported anoikis resistance.

Finally, p53 was found to be consistently downregulated, to a greater or lesser extent in all three conditions. p53 has long been known as a major regulator of proliferation of cellular proliferation. Indeed in extensive *in vitro* and *in vivo* models Galbiati et al. [433] showed CAV1 to suppress progression of cells from G0/G1 into

the cell cycle through p53/p21 signalling, thus providing a potential explanation of how CAV1 suppresses proliferation of CAKI-1 cells (Chapter 4).

In summary, CAV1 appears to support clonogenicity of CAKI-1 cells through the activation of STAT3, prevention of β -catenin degradation and allows the upregulation of c-Myc. In addition, under hypoxic conditions CAV1 knockdown resulted in the increased expression of IL-8, a known modulator of CSC phenotype, and ANGPTL4 suggesting a potential means by which hypoxia is able to compensate for loss of CAV1 driven clonogenicity.

Chapter 6 - Concluding discussion

6 Concluding discussion

This work has sought to identify what role CAV1 plays in CSC activity in RCC cell lines and how CAV1 can be used in combination with common markers of CSC phenotype to inform patient prognosis.

A large proportion of RCC tumours were found to be CAV1 positive. As in previous studies[99], [117], [132] CAV1 indicated poor disease free survival, positively correlated with several pathological indices of aggressive disease and acted as an independent prognostic indicator of poor disease outcome. Similarly, positive staining of CD44, a cell surface protein commonly used for the identification and purification of cancer stem cells (CSCs), identified patients with severely reduced disease free survival time and acted as an independent prognostic indicator of poor disease outcome. A strong correlation was found between CD44 and CAV1 expression in RCC tumours which was also indicative of poor disease outcome. Furthermore, a comprehensive multivariate analysis of all marker and histopathological covariates found the combination of CD44 and CAV1 expression to be the most significant in terms of predicting disease outcome. Interestingly, while CD105 expression alone appeared to bare no significance to patient outcome alone, in combination with CAV1 it proved to bare prognostic importance being identified as the fourth most predictive marker of poor disease outcome. MCT4 expression in RCC tumours also identified patients with significantly shorted disease free survival, correlated with indicators of aggressive disease and acted as an independent prognostic indicator of disease relapse. Surprisingly, MCT4 did not correlate with CAV1 expression with the combination of the two markers in RCC tumours actually diminishing its prognostic significance in cox regression analysis.

With a panel of cell surface markers commonly used for the identification and purification of embryonic, mesenchymal and cancer stem cells it was possible to identify subpopulations of cells based on the expression CD146/CD90 in 786-O, A498 and CAKI-1 cells. While CD146/CD90 expression was not capable of identifying more clonogenic population of cells, cells found to be CD90^{High} in the A498 and CAKI-1 cell lines demonstrated a significantly lower capacity for colony formation. While CSCs populations have been identified in primary RCC samples[61] by highly expression of CD105 no such bimodal expression was observed in the 786-O. High a high bimodal of CD105 was observed in the CAKI-1 cells, however the highly expression population represented the majority of the cell line and did not appear to enrich for clonogenicity. Interestingly, in all three cell lines high expression of CD44 was noted and in the CAKI-1 cell line a bimodal expression was observable.

Downregulation of CAV1 in 786-O and A498 cell lines caused changes to the proportion of CD146/CD90 cells; however downregulation of CAV1 expression did not significantly alter the clonogenic capacity of such populations. In the VHL+/+ CAKI-1 cells downregulation of CAV1 did not alter the proportions of CD146/CD90 cells but did cause a substantial reduction in colony forming capacity in these cells as well as the total unsorted cell line. CAV1 downregulation decreased both colony forming capacity and spheroid forming capacity. By inducing activation of hypoxic pathways it was possible to reverse the CAV1 mediated downregulation of clonogenicity, suggesting CAV1 expression to be important in maintaining clonogenicity and self-renewal in tumours with active VHL expression.

Proteomic microarray analysis revealed that downregulation of CAV1 in CAKI-1 cell lines resulted caused a downregulation of STAT3 phosphorylation and increased the expression of the Wnt pathway inhibitor DKK-1. Western blot and flow cytometry found downregulation of β -catenin, pSTAT3 and c-Myc, a self-renewal driving

transcription factor downstream of both STAT3 and β -catenin, dependent on CAV1 knockdown in CAKI-1 cells. Subsequently inhibition of STAT3 and to a lesser extent β -catenin resulted in reduced colony formation, suggesting CAV1 supports clonogenicity mainly through maintaining activation STAT3 signalling.

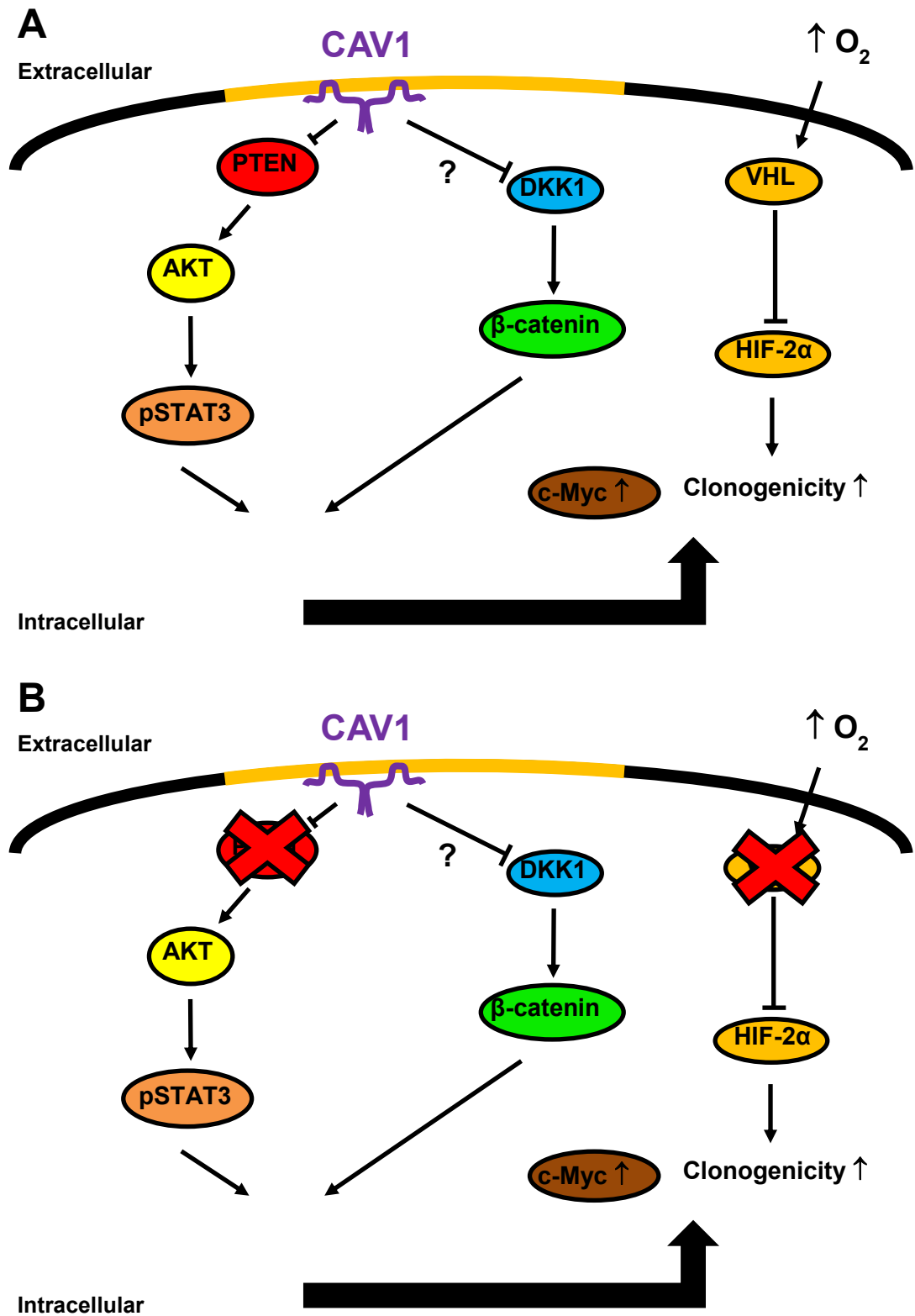


Figure 6.1 Schematic illustrating the role of CAV1 in the VHL +/+ PTEN +/+ CAKI-1 cell line (**A**) and the VHL-/- PTEN -/- 786-O cell line. In CAKI-1 cells (**A**) the presence of CAV1 drives pSTAT3 Y705 phosphorylation and β -catenin while hypoxia driven clonogenicity is inhibited by function VHL. In 786-O cells (**B**) loss of PTEN means CAV1 loses control of pSTAT3 driven clonogenicity and loss of VHL ensures deregulation of hypoxic response resulting in upregulation of clonogenicity.

In conclusion CAV1 in combination with the marker of CSC phenotype CD44 can identify patients with aggressive disease at high risk of relapse after therapy. Additionally, in flow cytometry studies CAV1 downregulation did not appear to affect the amount of expression or cell surface localisation of CD44. This suggests that if a biological relationship exists between the two it may either be driven by CD44 directly or CAV1 may affect the cell surface localisation of CD44. As such, mechanistic investigation into the role of CD44 in the invasive and migratory capacity of RCC cells merits further investigation. In VHL +/- CAKI-1 cells downregulation of CAV1 drastically reduced clonogenicity through what appears to be a STAT3 dependent manner. Further study should be conducted to understand how CAV1 orchestrates STAT3 activation, results here appear to indicate such a mechanism maybe carried out through Akt activation.

7 References

- [1] E. Jonasch, J. Gao, and W. K. Rathmell, "Renal cell carcinoma.," *BMJ*, vol. 349, no. nov10 11, p. g4797, 2014.
- [2] K. Gupta, J. D. Miller, J. Z. Li, M. W. Russell, and C. Charbonneau, "Epidemiologic and socioeconomic burden of metastatic renal cell carcinoma (mRCC): A literature review," *Cancer Treatment Reviews*, vol. 34, no. 3. pp. 193–205, 2008.
- [3] S. C. King, L. A. Pollack, J. Li, J. B. King, and V. A. Master, "Continued increase in incidence of renal cell carcinoma, especially in young patients and high grade disease: United States 2001 to 2010.," *J. Urol.*, vol. 191, no. 6, pp. 1665–70, Jun. 2014.
- [4] S. D. O'Connor, P. J. Pickhardt, D. H. Kim, M. R. Oliva, and S. G. Silverman, "Incidental finding of renal masses at unenhanced CT: prevalence and analysis of features for guiding management.," *AJR. Am. J. Roentgenol.*, vol. 197, no. 1, pp. 139–45, Jul. 2011.
- [5] B. Ljungberg, S. C. Campbell, H. Y. Cho, D. Jacqmin, J. E. Lee, S. Weikert, and L. A. Kiemeny, "The Epidemiology of Renal Cell Carcinoma," *Eur. Urol.*, vol. 60, no. 4, pp. 615–621, 2011.
- [6] B. Escudier, T. Eisen, W. M. Stadler, C. Szczylik, S. Oudard, M. Siebels, S. Negrier, C. Chevreau, E. Solska, A. A. Desai, F. Rolland, T. Demkow, T. E. Hutson, M. Gore, S. Freeman, B. Schwartz, M. Shan, R. Simantov, and R. M. Bukowski, "Sorafenib in advanced clear-cell renal-cell carcinoma.," *N. Engl. J. Med.*, vol. 356, no. 2, pp. 125–34, Jan. 2007.
- [7] R. J. Motzer, B. I. Rini, R. M. Bukowski, B. D. Curti, D. J. George, G. R. Hudes, B. G. Redman, K. A. Margolin, J. R. Merchan, G. Wilding, M. S. Ginsberg, J. Bacik, S. T. Kim, C. M. Baum, and M. D. Michaelson, "Sunitinib in patients with metastatic renal cell carcinoma.," *JAMA*, vol. 295, no. 21, pp. 2516–24, Jun. 2006.
- [8] C. N. Sternberg, I. D. Davis, J. Mardiak, C. Szczylik, E. Lee, J. Wagstaff, C. H. Barrios, P. Salman, O. A. Gladkov, A. Kavina, J. J. Zarbá, M. Chen, L. McCann, L. Pandite, D. F. Roychowdhury, and R. E. Hawkins, "Pazopanib in locally advanced or metastatic renal cell carcinoma: results of a randomized phase III trial.," *J. Clin. Oncol.*, vol. 28, no. 6, pp. 1061–8, Feb. 2010.
- [9] S. A. Rosenberg, J. C. Yang, S. L. Topalian, D. J. Schwartzentruber, J. S. Weber, D. R. Parkinson, C. A. Seipp, J. H. Einhorn, and D. E. White, "Treatment of 283 consecutive patients with metastatic melanoma or renal cell cancer using high-dose bolus interleukin 2.," *JAMA*, vol. 271, no. 12, pp. 907–13.
- [10] S. D. Fossá, "Interferon in metastatic renal cell carcinoma.," *Semin. Oncol.*, vol. 27, no. 2, pp. 187–93, Apr. 2000.
- [11] J. D. Hunt, O. L. Van Der Hel, G. P. McMillan, P. Boffetta, and P. Brennan, "Renal cell carcinoma in relation to cigarette smoking: Meta-analysis of 24 studies," *Int. J. Cancer*, vol. 114, no. 1, pp. 101–108, 2005.
- [12] B. A. C. Van Dijk, L. J. Schouten, L. A. L. M. Kiemeny, R. A. Goldbohm, and P. A. Van Den Brandt, "Relation of height, body mass, energy intake, and physical activity to risk of renal cell carcinoma: Results from the Netherlands Cohort Study," *Am. J. Epidemiol.*, vol. 160, no. 12, pp. 1159–1167, 2004.

- [13] M. Y. Choi, S. H. Jee, J. W. Sull, and C. M. Nam, "The effect of hypertension on the risk for kidney cancer in Korean men," *Kidney Int.*, vol. 67, no. 2, pp. 647–652, 2005.
- [14] W. H. Chow, G. Gridley, J. F. Fraumeni, and B. Järnholm, "Obesity, hypertension, and the risk of kidney cancer in men.," *N. Engl. J. Med.*, vol. 343, no. 18, pp. 1305–1311, 2000.
- [15] I. Ishikawa, Y. Saito, M. Asaka, N. Tomosugi, T. Yuri, M. Watanabe, and R. Honda, "Twenty-year follow-up of acquired renal cystic disease.," *Clin. Nephrol.*, vol. 59, no. 3, pp. 153–159, 2003.
- [16] S. K. Rakowski, E. B. Winterkorn, E. Paul, D. J. R. Steele, E. F. Halpern, and E. A. Thiele, "Renal manifestations of tuberous sclerosis complex: Incidence, prognosis, and predictive factors.," *Kidney Int.*, vol. 70, no. 10, pp. 1777–1782, 2006.
- [17] W. M. Linehan, "Genetic basis of kidney cancer: Role of genomics for the development of disease-based therapeutics," *Genome Research*, vol. 22, no. 11, pp. 2089–2100, 2012.
- [18] M. J. Calzada, "Von Hippel-Lindau syndrome: molecular mechanisms of the disease.," *Clin. Transl. Oncol.*, vol. 12, no. 3, pp. 160–5, Mar. 2010.
- [19] G. Kovacs, R. Erlandsson, F. Boldog, S. Ingvarsson, R. Müller-Brechlin, G. Klein, and J. Sümeji, "Consistent chromosome 3p deletion and loss of heterozygosity in renal cell carcinoma.," *Proc. Natl. Acad. Sci. U. S. A.*, vol. 85, no. 5, pp. 1571–5, Mar. 1988.
- [20] W. M. Linehan, J. S. Rubin, and D. P. Bottaro, "VHL loss of function and its impact on oncogenic signaling networks in clear cell renal cell carcinoma.," *Int. J. Biochem. Cell Biol.*, vol. 41, no. 4, pp. 753–6, Apr. 2009.
- [21] V. E. Moch, H., Humphrey, P.A., Ulbright, T.M., Reuter, *WHO Classification of Tumours of the Urinary System and Male Genital Organs.*, Fourth edi. 2016.
- [22] G. Kovacs, "Molecular cytogenetics of renal cell tumors.," *Adv. Cancer Res.*, vol. 62, pp. 89–124, 1993.
- [23] B. Shuch, A. Amin, A. J. Armstrong, J. N. Eble, V. Ficarra, A. Lopez-Beltran, G. Martignoni, B. I. Rini, and A. Kutikov, "Understanding pathologic variants of renal cell carcinoma: distilling therapeutic opportunities from biologic complexity.," *Eur. Urol.*, vol. 67, no. 1, pp. 85–97, Jan. 2015.
- [24] B. Shuch, G. Bratslavsky, W. M. Linehan, and R. Srinivasan, "Sarcomatoid renal cell carcinoma: a comprehensive review of the biology and current treatment strategies.," *Oncologist*, vol. 17, no. 1, pp. 46–54, 2012.
- [25] D. F. R. Griffiths, A. Verghese, A. Golash, H. G. Kynaston, P. N. Matthews, A. J. L. Hart, and J. B. Court, "Contribution of grade, vascular invasion and age to outcome in clinically localized renal cell carcinoma.," *BJU Int.*, vol. 90, no. 1, pp. 26–31, Jul. 2002.
- [26] R. P. Gibbons, J. E. Monte, R. J. Correa, and J. T. Mason, "Manifestations of renal cell carcinoma.," *Urology*, vol. 8, no. 3, pp. 201–6, Sep. 1976.
- [27] H. J. Fahn, Y. H. Lee, M. T. Chen, J. K. Huang, K. K. Chen, and L. S. Chang, "The incidence and prognostic significance of humoral hypercalcemia in renal cell carcinoma.," *J. Urol.*, vol. 145, no. 2, pp. 248–50, Feb. 1991.

- [28] B. I. Rini, S. C. Campbell, and B. Escudier, "Renal cell carcinoma.," *Lancet*, vol. 373, no. 9669, pp. 1119–32, Mar. 2009.
- [29] V. Margulis, R. F. Sánchez-Ortiz, P. Tamboli, D. D. Cohen, D. A. Swanson, and C. G. Wood, "Renal cell carcinoma clinically involving adjacent organs: experience with aggressive surgical management.," *Cancer*, vol. 109, no. 10, pp. 2025–30, May 2007.
- [30] M. L. Blute, B. C. Leibovich, C. M. Lohse, J. C. Cheville, and H. Zincke, "The Mayo Clinic experience with surgical management, complications and outcome for patients with renal cell carcinoma and venous tumour thrombus.," *BJU Int.*, vol. 94, no. 1, pp. 33–41, Jul. 2004.
- [31] J. Folkman, "Tumor angiogenesis: therapeutic implications.," *N. Engl. J. Med.*, vol. 285, no. 21, pp. 1182–6, Nov. 1971.
- [32] S. C. Clifford, S. Walsh, K. Hewson, E. K. Green, A. Brinke, P. M. Green, F. Gianelli, C. Eng, and E. R. Maher, "Genomic organization and chromosomal localization of the human CUL2 gene and the role of von Hippel-Lindau tumor suppressor-binding protein (CUL2 and VBP1) mutation and loss in renal-cell carcinoma development.," *Genes. Chromosomes Cancer*, vol. 26, no. 1, pp. 20–8, Sep. 1999.
- [33] S. N. Greer, J. L. Metcalf, Y. Wang, and M. Ohh, "The updated biology of hypoxia-inducible factor.," *EMBO J.*, vol. 31, no. 11, pp. 2448–60, May 2012.
- [34] G. L. Semenza, "Defining the role of hypoxia-inducible factor 1 in cancer biology and therapeutics.," *Oncogene*, vol. 29, no. 5, pp. 625–34, Feb. 2010.
- [35] D. B. Mendel, A. D. Laird, X. Xin, S. G. Louie, J. G. Christensen, G. Li, R. E. Schreck, T. J. Abrams, T. J. Ngai, L. B. Lee, L. J. Murray, J. Carver, E. Chan, K. G. Moss, J. O. Haznedar, J. Sukbuntherng, R. A. Blake, L. Sun, C. Tang, T. Miller, S. Shirazian, G. McMahon, and J. M. Cherrington, "In vivo antitumor activity of SU11248, a novel tyrosine kinase inhibitor targeting vascular endothelial growth factor and platelet-derived growth factor receptors: determination of a pharmacokinetic/pharmacodynamic relationship.," *Clin. Cancer Res.*, vol. 9, no. 1, pp. 327–37, Jan. 2003.
- [36] R. J. Motzer, T. E. Hutson, P. Tomczak, M. D. Michaelson, R. M. Bukowski, S. Oudard, S. Negrier, C. Szczylik, R. Pili, G. a Bjarnason, X. Garcia-del-Muro, J. a Sosman, E. Solska, G. Wilding, J. a Thompson, S. T. Kim, I. Chen, X. Huang, and R. a Figlin, "Overall survival and updated results for sunitinib compared with interferon alfa in patients with metastatic renal cell carcinoma.," *J. Clin. Oncol.*, vol. 27, no. 22, pp. 3584–90, Aug. 2009.
- [37] S. M. Wilhelm, C. Carter, L. Tang, D. Wilkie, A. McNabola, H. Rong, C. Chen, X. Zhang, P. Vincent, M. McHugh, Y. Cao, J. Shujath, S. Gawlak, D. Eveleigh, B. Rowley, L. Liu, L. Adnane, M. Lynch, D. Auclair, I. Taylor, R. Gedrich, A. Voznesensky, B. Riedl, L. E. Post, G. Bollag, and P. A. Trail, "BAY 43-9006 exhibits broad spectrum oral antitumor activity and targets the RAF/MEK/ERK pathway and receptor tyrosine kinases involved in tumor progression and angiogenesis.," *Cancer Res.*, vol. 64, no. 19, pp. 7099–109, Oct. 2004.
- [38] B. Escudier, A. Pluzanska, P. Koralewski, A. Ravaud, S. Bracarda, C. Szczylik, C. Chevreau, M. Filipek, B. Melichar, E. Bajetta, V. Gorbunova, J.-O. Bay, I. Bodrogi, A. Jagiello-Gruszfeld, and N. Moore, "Bevacizumab plus interferon alfa-2a for treatment of metastatic renal cell carcinoma: a randomised, double-blind phase III trial.," *Lancet*, vol. 370, no. 9605, pp.

2103–11, Dec. 2007.

- [39] F. Lin, P. L. Zhang, X. J. Yang, J. W. Prichard, M. Lun, and R. E. Brown, "Morphoproteomic and molecular concomitants of an overexpressed and activated mTOR pathway in renal cell carcinomas.," *Ann. Clin. Lab. Sci.*, vol. 36, no. 3, pp. 283–93, Jan. 2006.
- [40] M. Hager, H. Haufe, R. Kemmerling, W. Hitzl, G. Mikuz, P. L. Moser, and C. Kolbitsch, "Increased activated Akt expression in renal cell carcinomas and prognosis.," *J. Cell. Mol. Med.*, vol. 13, no. 8B, pp. 2181–8, Aug. 2009.
- [41] B. Markman, R. Dienstmann, and J. Taberero, "Targeting the PI3K/Akt/mTOR pathway--beyond rapalogs.," *Oncotarget*, vol. 1, no. 7, pp. 530–43, Nov. 2010.
- [42] B. I. Rini, "Temsirolimus, an inhibitor of mammalian target of rapamycin.," *Clin. Cancer Res.*, vol. 14, no. 5, pp. 1286–90, Mar. 2008.
- [43] G. Hudes, M. Carducci, P. Tomczak, J. Dutcher, R. Figlin, A. Kapoor, E. Staroslawska, J. Sosman, D. McDermott, I. Bodrogi, Z. Kovacevic, V. Lesovoy, I. G. H. Schmidt-Wolf, O. Barbarash, E. Gokmen, T. O'Toole, S. Lustgarten, L. Moore, and R. J. Motzer, "Temsirolimus, interferon alfa, or both for advanced renal-cell carcinoma.," *N. Engl. J. Med.*, vol. 356, no. 22, pp. 2271–81, May 2007.
- [44] C. Swanton, "Intratumor heterogeneity: evolution through space and time.," *Cancer Res.*, vol. 72, no. 19, pp. 4875–82, Oct. 2012.
- [45] P. C. Nowell, "The clonal evolution of tumor cell populations.," *Science*, vol. 194, no. 4260, pp. 23–8, Oct. 1976.
- [46] D. Hanahan and R. a Weinberg, "Hallmarks of cancer: the next generation.," *Cell*, vol. 144, no. 5, pp. 646–74, Mar. 2011.
- [47] a. G. Schepers, H. J. Snippert, D. E. Stange, M. van den Born, J. H. van Es, M. van de Wetering, and H. Clevers, "Lineage Tracing Reveals Lgr5+ Stem Cell Activity in Mouse Intestinal Adenomas.," *Science (80-.)*, vol. 730, Aug. 2012.
- [48] G. Driessens, B. Beck, A. Caauwe, B. D. Simons, and C. Blanpain, "Defining the mode of tumour growth by clonal analysis," *Nature*, pp. 1–5, Aug. 2012.
- [49] T. Lapidot, C. Sirard, J. Vormoor, B. Murdoch, T. Hoang, J. Caceres-Cortes, M. Minden, B. Paterson, M. A. Caligiuri, and J. E. Dick, "A cell initiating human acute myeloid leukaemia after transplantation into SCID mice.," *Nature*, vol. 367, no. 6464, pp. 645–8, Feb. 1994.
- [50] D. Bonnet and J. E. Dick, "Human acute myeloid leukemia is organized as a hierarchy that originates from a primitive hematopoietic cell.," *Nat. Med.*, vol. 3, no. 7, pp. 730–7, Jul. 1997.
- [51] M. Al-Hajj, M. S. Wicha, A. Benito-Hernandez, S. J. Morrison, and M. F. Clarke, "Prospective identification of tumorigenic breast cancer cells.," *Proc. Natl. Acad. Sci. U. S. A.*, vol. 100, no. 7, pp. 3983–3988, 2003.
- [52] S. K. Singh, C. Hawkins, I. D. Clarke, J. A. Squire, J. Bayani, T. Hide, R. M. Henkelman, M. D. Cusimano, and P. B. Dirks, "Identification of human brain tumour initiating cells.," *Nature*, vol. 432, no. 7015, pp. 396–401, Nov. 2004.
- [53] L. Patrawala, T. Calhoun, R. Schneider-Broussard, J. Zhou, K. Claypool, and D. G. Tang, "Side population is enriched in tumorigenic, stem-like cancer

cells, whereas ABCG2+ and ABCG2- cancer cells are similarly tumorigenic.," *Cancer Res.*, vol. 65, no. 14, pp. 6207–19, Jul. 2005.

- [54] C. a O'Brien, A. Pollett, S. Gallinger, and J. E. Dick, "A human colon cancer cell capable of initiating tumour growth in immunodeficient mice.," *Nature*, vol. 445, no. 7123, pp. 106–10, Jan. 2007.
- [55] E. H. Huang, M. J. Hynes, T. Zhang, C. Ginestier, G. Dontu, H. Appelman, J. Z. Fields, M. S. Wicha, and B. M. Boman, "Aldehyde dehydrogenase 1 is a marker for normal and malignant human colonic stem cells (SC) and tracks SC overpopulation during colon tumorigenesis.," *Cancer Res.*, vol. 69, no. 8, pp. 3382–9, Apr. 2009.
- [56] C. F. B. Kim, E. L. Jackson, A. E. Woolfenden, S. Lawrence, I. Babar, S. Vogel, D. Crowley, R. T. Bronson, and T. Jacks, "Identification of bronchioalveolar stem cells in normal lung and lung cancer.," *Cell*, vol. 121, no. 6, pp. 823–35, Jun. 2005.
- [57] A. Eramo, F. Lotti, G. Sette, E. Piloizzi, M. Biffoni, A. Di Virgilio, C. Conticello, L. Ruco, C. Peschle, and R. De Maria, "Identification and expansion of the tumorigenic lung cancer stem cell population.," *Cell Death Differ.*, vol. 15, no. 3, pp. 504–14, Mar. 2008.
- [58] A. T. Collins, P. A. Berry, C. Hyde, M. J. Stower, and N. J. Maitland, "Prospective identification of tumorigenic prostate cancer stem cells.," *Cancer Res.*, vol. 65, no. 23, pp. 10946–51, Dec. 2005.
- [59] P. C. Hermann, S. L. Huber, T. Herrler, A. Aicher, J. W. Ellwart, M. Guba, C. J. Bruns, and C. Heeschen, "Distinct populations of cancer stem cells determine tumor growth and metastatic activity in human pancreatic cancer.," *Cell Stem Cell*, vol. 1, no. 3, pp. 313–23, Sep. 2007.
- [60] C. Li, D. G. Heidt, P. Dalerba, C. F. Burant, L. Zhang, V. Adsay, M. Wicha, M. F. Clarke, and D. M. Simeone, "Identification of pancreatic cancer stem cells," *Cancer Res.*, vol. 67, no. 3, pp. 1030–1037, 2007.
- [61] B. Bussolati, S. Bruno, C. Grange, U. Ferrando, and G. Camussi, "Identification of a tumor-initiating stem cell population in human renal carcinomas.," *FASEB J.*, vol. 22, no. 10, pp. 3696–705, Oct. 2008.
- [62] M. Gassenmaier, D. Chen, A. Buchner, L. Henkel, M. Schiemann, B. Mack, D. J. Schendel, W. Zimmermann, and H. Pohla, "CXC chemokine receptor 4 is essential for maintenance of renal cell carcinoma-initiating cells and predicts metastasis.," *Stem Cells*, vol. 31, no. 8, pp. 1467–76, Aug. 2013.
- [63] S. K. Addla, M. D. Brown, C. A. Hart, V. A. C. Ramani, and N. W. Clarke, "Characterization of the Hoechst 33342 side population from normal and malignant human renal epithelial cells.," *Am. J. Physiol. Renal Physiol.*, vol. 295, no. 3, pp. F680–7, Sep. 2008.
- [64] Y. Zhong, K. Guan, S. Guo, C. Zhou, D. Wang, W. Ma, Y. Zhang, C. Li, and S. Zhang, "Spheres derived from the human SK-RC-42 renal cell carcinoma cell line are enriched in cancer stem cells.," *Cancer Lett.*, vol. 299, no. 2, pp. 150–60, Dec. 2010.
- [65] H. Bissig, J. Richter, R. Desper, V. Meier, P. Schraml, A. A. Schäffer, G. Sauter, M. J. Mihatsch, and H. Moch, "Evaluation of the clonal relationship between primary and metastatic renal cell carcinoma by comparative genomic hybridization.," *Am. J. Pathol.*, vol. 155, no. 1, pp. 267–74, Jul. 1999.

- [66] B. Weigelt, A. M. Glas, L. F. A. Wessels, A. T. Witteveen, J. L. Peterse, and L. J. van't Veer, "Gene expression profiles of primary breast tumors maintained in distant metastases.," *Proc. Natl. Acad. Sci. U. S. A.*, vol. 100, no. 26, pp. 15901–5, Dec. 2003.
- [67] B. Weigelt, Z. Hu, X. He, C. Livasy, L. A. Carey, M. G. Ewend, A. M. Glas, C. M. Perou, and L. J. Van't Veer, "Molecular portraits and 70-gene prognosis signature are preserved throughout the metastatic process of breast cancer.," *Cancer Res.*, vol. 65, no. 20, pp. 9155–8, Oct. 2005.
- [68] Z. Mao, M. Bozzella, A. Seluanov, and V. Gorbunova, "DNA repair by nonhomologous end joining and homologous recombination during cell cycle in human cells.," *Cell Cycle*, vol. 7, no. 18, pp. 2902–6, Sep. 2008.
- [69] E. D. Tichy, R. Pillai, L. Deng, L. Liang, J. Tischfield, S. J. Schwemberger, G. F. Babcock, and P. J. Stambrook, "Mouse embryonic stem cells, but not somatic cells, predominantly use homologous recombination to repair double-strand DNA breaks.," *Stem Cells Dev.*, vol. 19, no. 11, pp. 1699–711, Nov. 2010.
- [70] P. M. Chaudhary and I. B. Roninson, "Expression and activity of P-glycoprotein, a multidrug efflux pump, in human hematopoietic stem cells.," *Cell*, vol. 66, no. 1, pp. 85–94, Jul. 1991.
- [71] S. Bao, Q. Wu, R. E. McLendon, Y. Hao, Q. Shi, A. B. Hjelmeland, M. W. Dewhirst, D. D. Bigner, and J. N. Rich, "Glioma stem cells promote radioresistance by preferential activation of the DNA damage response.," *Nature*, vol. 444, no. 7120, pp. 756–60, Dec. 2006.
- [72] M. Todaro, M. P. Alea, A. B. Di Stefano, P. Cammareri, L. Vermeulen, F. Iovino, C. Tripodo, A. Russo, G. Gulotta, J. P. Medema, and G. Stassi, "Colon cancer stem cells dictate tumor growth and resist cell death by production of interleukin-4.," *Cell Stem Cell*, vol. 1, no. 4, pp. 389–402, Oct. 2007.
- [73] S. Azzi, S. Bruno, J. Giron-Michel, D. Clay, A. Devocelle, M. Croce, S. Ferrini, S. Chouaib, A. Vazquez, B. Charpentier, G. Camussi, B. Azzarone, and P. Eid, "Differentiation therapy: targeting human renal cancer stem cells with interleukin 15.," *J. Natl. Cancer Inst.*, vol. 103, no. 24, pp. 1884–98, Dec. 2011.
- [74] G. Sowa, "Caveolae, caveolins, cavins, and endothelial cell function: new insights.," *Front. Physiol.*, vol. 2, no. January, p. 120, Jan. 2012.
- [75] R. G. Parton and K. Simons, "The multiple faces of caveolae.," *Nat. Rev. Mol. Cell Biol.*, vol. 8, no. 3, pp. 185–94, Mar. 2007.
- [76] N. Briand, S. Le Lay, W. C. Sessa, P. Ferré, and I. Dugail, "Distinct roles of endothelial and adipocyte caveolin-1 in macrophage infiltration and adipose tissue metabolic activity.," *Diabetes*, vol. 60, no. 2, pp. 448–53, Feb. 2011.
- [77] T. M. Williams and M. P. Lisanti, "The Caveolin genes: from cell biology to medicine.," *Ann. Med.*, vol. 36, no. 8, pp. 584–95, 2004.
- [78] I. Parolini, M. Sargiacomo, F. Galbiati, G. Rizzo, F. Grignani, J. A. Engelman, T. Okamoto, T. Ikezu, P. E. Scherer, R. Mora, E. Rodriguez-Boulan, C. Peschle, and M. P. Lisanti, "Expression of caveolin-1 is required for the transport of caveolin-2 to the plasma membrane. Retention of caveolin-2 at the level of the golgi complex.," *J. Biol. Chem.*, vol. 274, no. 36, pp. 25718–25, Sep. 1999.

- [79] T. M. Williams and M. P. Lisanti, "The caveolin proteins.," *Genome Biol.*, vol. 5, no. 3, p. 214, Jan. 2004.
- [80] J. Ito, Y. Nagayasu, K. Kato, R. Sato, and S. Yokoyama, "Apolipoprotein A-I induces translocation of cholesterol, phospholipid, and caveolin-1 to cytosol in rat astrocytes.," *J. Biol. Chem.*, vol. 277, no. 10, pp. 7929–35, Mar. 2002.
- [81] A. Schlegel, P. Arvan, and M. P. Lisanti, "Caveolin-1 binding to endoplasmic reticulum membranes and entry into the regulated secretory pathway are regulated by serine phosphorylation. Protein sorting at the level of the endoplasmic reticulum.," *J. Biol. Chem.*, vol. 276, no. 6, pp. 4398–408, Feb. 2001.
- [82] D. J. Dietzen, W. R. Hastings, and D. M. Lublin, "Caveolin is palmitoylated on multiple cysteine residues. Palmitoylation is not necessary for localization of caveolin to caveolae.," *J. Biol. Chem.*, vol. 270, no. 12, pp. 6838–42, Mar. 1995.
- [83] A. Schlegel and M. P. Lisanti, "A molecular dissection of caveolin-1 membrane attachment and oligomerization. Two separate regions of the caveolin-1 C-terminal domain mediate membrane binding and oligomer/oligomer interactions in vivo.," *J. Biol. Chem.*, vol. 275, no. 28, pp. 21605–17, Jul. 2000.
- [84] Y. Wang, O. Roche, C. Xu, E. H. Moriyama, P. Heir, J. Chung, F. C. Roos, Y. Chen, G. Finak, M. Milosevic, B. C. Wilson, B. T. Teh, M. Park, M. S. Irwin, and M. Ohh, "Hypoxia promotes ligand-independent EGF receptor signaling via hypoxia-inducible factor-mediated upregulation of caveolin-1.," *Proc. Natl. Acad. Sci. U. S. A.*, vol. 109, no. 13, pp. 4892–7, Mar. 2012.
- [85] Y. Wei, X. Yang, Q. Liu, J. A. Wilkins, and H. A. Chapman, "A role for caveolin and the urokinase receptor in integrin-mediated adhesion and signaling.," *J. Cell Biol.*, vol. 144, no. 6, pp. 1285–94, Mar. 1999.
- [86] J. Couet, S. Li, T. Okamoto, T. Ikezu, and M. P. Lisanti, "Identification of peptide and protein ligands for the caveolin-scaffolding domain. Implications for the interaction of caveolin with caveolae-associated proteins.," *J. Biol. Chem.*, vol. 272, no. 10, pp. 6525–33, Mar. 1997.
- [87] S. Li, J. Couet, and M. P. Lisanti, "Src tyrosine kinases, Galpha subunits, and H-Ras share a common membrane-anchored scaffolding protein, caveolin. Caveolin binding negatively regulates the auto-activation of Src tyrosine kinases.," *J. Biol. Chem.*, vol. 271, no. 46, pp. 29182–90, Nov. 1996.
- [88] H. Xia, W. Khalil, J. Kahm, J. Jessurun, J. Kleidon, and C. A. Henke, "Pathologic caveolin-1 regulation of PTEN in idiopathic pulmonary fibrosis.," *Am. J. Pathol.*, vol. 176, no. 6, pp. 2626–37, Jun. 2010.
- [89] L. Li, C. H. Ren, S. A. Tahir, C. Ren, and T. C. Thompson, "Caveolin-1 maintains activated Akt in prostate cancer cells through scaffolding domain binding site interactions with and inhibition of serine/threonine protein phosphatases PP1 and PP2A.," *Mol. Cell. Biol.*, vol. 23, no. 24, pp. 9389–404, 2003.
- [90] A. S. Martins, J. L. Ordóñez, A. T. Amaral, F. Prins, G. Floris, M. Debiec-Rychter, P. C. W. Hogendoorn, and E. de Alava, "IGF1R signaling in Ewing sarcoma is shaped by clathrin-/caveolin-dependent endocytosis.," *PLoS One*, vol. 6, no. 5, p. e19846, 2011.
- [91] C. Racine, M. Bélanger, H. Hirabayashi, M. Boucher, J. Chakir, and J. Couet,

- “Reduction of caveolin 1 gene expression in lung carcinoma cell lines.” *Biochem. Biophys. Res. Commun.*, vol. 255, no. 3, pp. 580–6, Feb. 1999.
- [92] S. W. Lee, C. L. Reimer, P. Oh, D. B. Campbell, and J. E. Schnitzer, “Tumor cell growth inhibition by caveolin re-expression in human breast cancer cells.” *Oncogene*, vol. 16, no. 11, pp. 1391–7, Mar. 1998.
- [93] F. C. Bender, M. A. Reymond, C. Bron, and A. F. Quest, “Caveolin-1 levels are down-regulated in human colon tumors, and ectopic expression of caveolin-1 in colon carcinoma cell lines reduces cell tumorigenicity.” *Cancer Res.*, vol. 60, no. 20, pp. 5870–8, Oct. 2000.
- [94] K. Wiechen, L. Diatchenko, A. Agoulnik, K. M. Scharff, H. Schober, K. Arlt, B. Zhumabayeva, P. D. Siebert, M. Dietel, R. Schäfer, and C. Sers, “Caveolin-1 is down-regulated in human ovarian carcinoma and acts as a candidate tumor suppressor gene.” *Am. J. Pathol.*, vol. 159, no. 5, pp. 1635–43, Nov. 2001.
- [95] A. K. Witkiewicz, A. Dasgupta, F. Sotgia, I. Mercier, R. G. Pestell, M. Sabel, C. G. Kleer, J. R. Brody, and M. P. Lisanti, “An absence of stromal caveolin-1 expression predicts early tumor recurrence and poor clinical outcome in human breast cancers.” *Am. J. Pathol.*, vol. 174, no. 6, pp. 2023–34, Jun. 2009.
- [96] F. Galbiati, D. Volonte, J. A. Engelman, G. Watanabe, R. Burk, R. G. Pestell, and M. P. Lisanti, “Targeted downregulation of caveolin-1 is sufficient to drive cell transformation and hyperactivate the p42/44 MAP kinase cascade.” *EMBO J.*, vol. 17, no. 22, pp. 6633–48, Nov. 1998.
- [97] F. Capozza, T. M. Williams, W. Schubert, S. McClain, B. Bouzahzah, F. Sotgia, and M. P. Lisanti, “Absence of caveolin-1 sensitizes mouse skin to carcinogen-induced epidermal hyperplasia and tumor formation.” *Am. J. Pathol.*, vol. 162, no. 6, pp. 2029–39, Jun. 2003.
- [98] G. Yang, L. D. Truong, T. L. Timme, C. Ren, T. M. Wheeler, S. H. Park, Y. Nasu, C. H. Bangma, M. W. Kattan, P. T. Scardino, and T. C. Thompson, “Elevated expression of caveolin is associated with prostate and breast cancer.” *Clin. Cancer Res.*, vol. 4, no. 8, pp. 1873–80, Aug. 1998.
- [99] L. Campbell, M. Gumbleton, and D. F. R. Griffiths, “Caveolin-1 overexpression predicts poor disease-free survival of patients with clinically confined renal cell carcinoma.” *Br. J. Cancer*, vol. 89, no. 10, pp. 1909–13, Nov. 2003.
- [100] T. Ando, H. Ishiguro, M. Kimura, A. Mitsui, Y. Mori, N. Sugito, K. Tomoda, R. Mori, K. Harada, T. Katada, R. Ogawa, Y. Fujii, and Y. Kuwabara, “The overexpression of caveolin-1 and caveolin-2 correlates with a poor prognosis and tumor progression in esophageal squamous cell carcinoma.” *Oncol. Rep.*, vol. 18, no. 3, pp. 601–9, Sep. 2007.
- [101] C. P. Tanase, S. Dima, M. Mihai, E. Raducan, M. I. Nicolescu, L. Albuлесcu, B. Voiculescu, T. Dumitrascu, L. M. Cruceru, M. Leabu, I. Popescu, and M. E. Hinescu, “Caveolin-1 overexpression correlates with tumour progression markers in pancreatic ductal adenocarcinoma.” *J. Mol. Histol.*, vol. 40, no. 1, pp. 23–9, Feb. 2009.
- [102] G. Yang, T. L. Timme, A. Frolov, T. M. Wheeler, and T. C. Thompson, “Combined c-Myc and caveolin-1 expression in human prostate carcinoma predicts prostate carcinoma progression.” *Cancer*, vol. 103, no. 6, pp. 1186–94, Mar. 2005.

- [103] H. H. Patel, F. Murray, and P. a Insel, "Caveolae as organizers of pharmacologically relevant signal transduction molecules.," *Annu. Rev. Pharmacol. Toxicol.*, vol. 48, pp. 359–91, Jan. 2008.
- [104] Y. Lavie, G. Fiucci, and M. Liscovitch, "Up-regulation of caveolae and caveolar constituents in multidrug-resistant cancer cells.," *J. Biol. Chem.*, vol. 273, no. 49, pp. 32380–3, Dec. 1998.
- [105] G. Yuan, I. Regel, F. Lian, T. Friedrich, I. Hitkova, R. D. Hofheinz, P. Ströbel, R. Langer, G. Keller, C. Röcken, W. Zimmermann, R. M. Schmid, M. P. A. Ebert, and E. Burgermeister, "WNT6 is a novel target gene of caveolin-1 promoting chemoresistance to epirubicin in human gastric cancer cells.," *Oncogene*, vol. 32, no. 3, pp. 375–87, Jan. 2013.
- [106] H. Zou, D. Volonte, and F. Galbiati, "Interaction of caveolin-1 with Ku70 inhibits Bax-mediated apoptosis.," *PLoS One*, vol. 7, no. 6, p. e39379, Jan. 2012.
- [107] J. Li, G. S. Hassan, T. M. Williams, C. Minetti, R. G. Pestell, H. B. Tanowitz, P. G. Frank, F. Sotgia, and M. P. Lisanti, "Loss of caveolin-1 causes the hyper-proliferation of intestinal crypt stem cells, with increased sensitivity to whole body gamma-radiation.," *Cell Cycle*, vol. 4, no. 12, pp. 1817–25, Dec. 2005.
- [108] N. Cordes, S. Frick, T. B. Brunner, C. Pilarsky, R. Grützmann, B. Sipos, G. Klöppel, W. G. McKenna, and E. J. Bernhard, "Human pancreatic tumor cells are sensitized to ionizing radiation by knockdown of caveolin-1.," *Oncogene*, vol. 26, no. 48, pp. 6851–62, Oct. 2007.
- [109] Y. Lavie and M. Liscovitch, "Changes in lipid and protein constituents of rafts and caveolae in multidrug resistant cancer cells and their functional consequences.," *Glycoconj. J.*, vol. 17, no. 3–4, pp. 253–9.
- [110] M. Herzog, C. H. Storch, P. Gut, D. Kotlyar, J. Füllekrug, R. Eehalt, W. E. Haefeli, and J. Weiss, "Knockdown of caveolin-1 decreases activity of breast cancer resistance protein (BCRP/ABCG2) and increases chemotherapeutic sensitivity.," *Naunyn. Schmiedebergs. Arch. Pharmacol.*, vol. 383, no. 1, pp. 1–11, Jan. 2011.
- [111] J. Park, E. Bae, C. Lee, S.-S. Yoon, Y. S. Chae, K.-S. Ahn, and N. H. Won, "RNA interference-directed caveolin-1 knockdown sensitizes SN12CPM6 cells to doxorubicin-induced apoptosis and reduces lung metastasis.," *Tumour Biol.*, vol. 31, no. 6, pp. 643–50, Dec. 2010.
- [112] M.-O. Parat, B. Anand-Apte, and P. L. Fox, "Differential caveolin-1 polarization in endothelial cells during migration in two and three dimensions.," *Mol. Biol. Cell*, vol. 14, no. 8, pp. 3156–68, Aug. 2003.
- [113] M. Isshiki, J. Ando, K. Yamamoto, T. Fujita, Y. Ying, and R. G. W. Anderson, "Sites of Ca(2+) wave initiation move with caveolae to the trailing edge of migrating cells.," *J. Cell Sci.*, vol. 115, no. Pt 3, pp. 475–84, Feb. 2002.
- [114] B. D. Riehl, J. S. Lee, L. Ha, and J. Y. Lim, "Fluid-flow-induced mesenchymal stem cell migration: role of focal adhesion kinase and RhoA kinase sensors.," *J. R. Soc. Interface*, vol. 12, no. 104, p. 20141351, Mar. 2015.
- [115] B. Annabi, M. Bouzeghrane, R. Moumdjian, A. Moghrabi, and R. Béliveau, "Probing the infiltrating character of brain tumors: inhibition of RhoA/ROK-mediated CD44 cell surface shedding from glioma cells by the green tea catechin EGCG.," *J. Neurochem.*, vol. 94, no. 4, pp. 906–16, Aug. 2005.

- [116] B. Joshi, S. S. Strugnell, J. G. Goetz, L. D. Kojic, M. E. Cox, O. L. Griffith, S. K. Chan, S. J. Jones, S.-P. Leung, H. Masoudi, S. Leung, S. M. Wiseman, and I. R. Nabi, "Phosphorylated caveolin-1 regulates Rho/ROCK-dependent focal adhesion dynamics and tumor cell migration and invasion.," *Cancer Res.*, vol. 68, no. 20, pp. 8210–20, Oct. 2008.
- [117] L. Campbell, G. Al-Jayyousi, R. Gutteridge, N. Gumbleton, R. Griffiths, S. Gumbleton, M. W. Smith, D. F. R. Griffiths, and M. Gumbleton, "Caveolin-1 in renal cell carcinoma promotes tumour cell invasion, and in co-operation with pERK predicts metastases in patients with clinically confined disease.," *J. Transl. Med.*, vol. 11, no. 1, p. 255, Jan. 2013.
- [118] S. Wang, Q. Kan, Y. Sun, R. Han, G. Zhang, T. Peng, and Y. Jia, "Caveolin-1 regulates neural differentiation of rat bone mesenchymal stem cells into neurons by modulating Notch signaling.," *Int. J. Dev. Neurosci.*, vol. 31, no. 1, pp. 30–5, Feb. 2013.
- [119] H. Mao, A. M. Diehl, and Y.-X. Li, "Sonic hedgehog ligand partners with caveolin-1 for intracellular transport.," *Lab. Invest.*, vol. 89, no. 3, pp. 290–300, Mar. 2009.
- [120] F. Pancotti, L. Roncuzzi, M. Maggiolini, and A. Gasperi-Campani, "Caveolin-1 silencing arrests the proliferation of metastatic lung cancer cells through the inhibition of STAT3 signaling.," *Cell. Signal.*, vol. 24, no. 7, pp. 1390–7, Jul. 2012.
- [121] A. Rodriguez and W. J. Sexton, "Management of locally advanced renal cell carcinoma.," *Cancer Control*, vol. 13, no. 3, pp. 199–210, Jul. 2006.
- [122] M. Sun, S. F. Shariat, C. Cheng, V. Ficarra, M. Murai, S. Oudard, A. J. Pantuck, R. Zigeuner, and P. I. Karakiewicz, "Prognostic factors and predictive models in renal cell carcinoma: a contemporary review.," *Eur. Urol.*, vol. 60, no. 4, pp. 644–61, Oct. 2011.
- [123] S. Thomas, J. B. Overvest, M. D. Nitz, P. D. Williams, C. R. Owens, M. Sanchez-Carbayo, H. F. Frierson, M. A. Schwartz, and D. Theodorescu, "Src and caveolin-1 reciprocally regulate metastasis via a common downstream signaling pathway in bladder cancer.," *Cancer Res.*, vol. 71, no. 3, pp. 832–41, Feb. 2011.
- [124] G. Yang, L. D. Truong, T. M. Wheeler, and T. C. Thompson, "Caveolin-1 expression in clinically confined human prostate cancer: a novel prognostic marker.," *Cancer Res.*, vol. 59, no. 22, pp. 5719–23, Nov. 1999.
- [125] H. A. Alshenawy and M. A. E.-H. A. E.-A. Ali, "Differential caveolin-1 expression in colon carcinoma and its relation to E-cadherin- β -catenin complex.," *Ann. Diagn. Pathol.*, vol. 17, no. 6, pp. 476–82, Dec. 2013.
- [126] S. W. Fine, M. P. Lisanti, F. Galbiati, and M. Li, "Elevated expression of caveolin-1 in adenocarcinoma of the colon.," *Am. J. Clin. Pathol.*, vol. 115, no. 5, pp. 719–24, May 2001.
- [127] H. L. Chen, L. F. Fan, J. Gao, J. P. Ouyang, and Y. X. Zhang, "Differential expression and function of the caveolin-1 gene in non-small cell lung carcinoma.," *Oncol. Rep.*, vol. 25, no. 2, pp. 359–66, Feb. 2011.
- [128] S.-H. Yoo, Y. S. Park, H.-R. Kim, S. W. Sung, J. H. Kim, Y. S. Shim, S. D. Lee, Y.-L. Choi, M.-K. Kim, and D. H. Chung, "Expression of caveolin-1 is associated with poor prognosis of patients with squamous cell carcinoma of the lung.," *Lung Cancer*, vol. 42, no. 2, pp. 195–202, Nov. 2003.

- [129] A. Horiguchi, T. Asano, J. Asakuma, T. Asano, M. Sumitomo, and M. Hayakawa, "Impact of caveolin-1 expression on clinicopathological parameters in renal cell carcinoma.," *J. Urol.*, vol. 172, no. 2, pp. 718–22, Aug. 2004.
- [130] H. J. Joo, D. K. Oh, Y. S. Kim, K. B. Lee, and S. J. Kim, "Increased expression of caveolin-1 and microvessel density correlates with metastasis and poor prognosis in clear cell renal cell carcinoma.," *BJU Int.*, vol. 93, no. 3, pp. 291–6, Feb. 2004.
- [131] L. Campbell, G. Al-Jayyousi, R. Gutteridge, N. Gumbleton, R. Griffiths, S. Gumbleton, M. W. Smith, D. F. R. Griffiths, and M. Gumbleton, "Caveolin-1 in renal cell carcinoma promotes tumour cell invasion, and in co-operation with pERK predicts metastases in patients with clinically confined disease.," *J. Transl. Med.*, vol. 11, p. 255, 2013.
- [132] L. Campbell, B. Jasani, K. Edwards, M. Gumbleton, and D. F. R. Griffiths, "Combined expression of caveolin-1 and an activated AKT/mTOR pathway predicts reduced disease-free survival in clinically confined renal cell carcinoma.," *Br. J. Cancer*, vol. 98, no. 5, pp. 931–40, Mar. 2008.
- [133] W. A. WOODWARD and E. P. SULMAN, "Cancer stem cells□: markers or biomarkers?," *Cancer Metastasis Rev.*, vol. 27, no. 3, pp. 459–470.
- [134] N. Pacini and F. Borziani, "Cancer stem cell theory and the warburg effect, two sides of the same coin?," *Int. J. Mol. Sci.*, vol. 15, no. 5, pp. 8893–930, 2014.
- [135] D. Wang, H. Zhu, Y. Zhu, Y. Liu, H. Shen, R. Yin, Z. Zhang, and Z. Su, "CD133(+)/CD44(+)/Oct4(+)/Nestin(+) stem-like cells isolated from Panc-1 cell line may contribute to multi-resistance and metastasis of pancreatic cancer.," *Acta Histochem.*, pp. 1–8, Oct. 2012.
- [136] P. Dalerba, S. J. Dylla, I.-K. Park, R. Liu, X. Wang, R. W. Cho, T. Hoey, A. Gurney, E. H. Huang, D. M. Simeone, A. A. Shelton, G. Parmiani, C. Castelli, and M. F. Clarke, "Phenotypic characterization of human colorectal cancer stem cells.," *Proc. Natl. Acad. Sci. U. S. A.*, vol. 104, no. 24, pp. 10158–63, Jun. 2007.
- [137] L. La Fleur, A.-C. Johansson, and K. Roberg, "A CD44(high)/EGFR(low) Subpopulation within Head and Neck Cancer Cell Lines Shows an Epithelial-Mesenchymal Transition Phenotype and Resistance to Treatment.," *PLoS One*, vol. 7, no. 9, p. e44071, Jan. 2012.
- [138] S. Geng, Y. Guo, Q. Wang, L. Li, and J. Wang, "Cancer stem-like cells enriched with CD29 and CD44 markers exhibit molecular characteristics with epithelial-mesenchymal transition in squamous cell carcinoma.," *Arch. Dermatol. Res.*, vol. 305, no. 1, pp. 35–47, Jan. 2013.
- [139] Z. Wang and X. Yan, "CD146, a multi-functional molecule beyond adhesion.," *Cancer Lett.*, vol. 330, no. 2, pp. 150–162, 2013.
- [140] M. Munz, P. a Baeuerle, and O. Gires, "The emerging role of EpCAM in cancer and stem cell signaling.," *Cancer Res.*, vol. 69, no. 14, pp. 5627–9, Jul. 2009.
- [141] A. Satelli and S. Li, "Vimentin as a potential molecular target in cancer therapy Or Vimentin, an overview and its potential as a molecular target for cancer therapy," *Cell Mol Life Sci.*, vol. 68, no. 18, pp. 3033–3046, 2011.

- [142] F. Sotgia, U. E. Martinez-Outschoorn, A. Howell, R. G. Pestell, S. Pavlides, and M. P. Lisanti, "Caveolin-1 and cancer metabolism in the tumor microenvironment: markers, models, and mechanisms.," *Annu. Rev. Pathol.*, vol. 7, pp. 423–67, Jan. 2012.
- [143] J. Kang, A. Shakya, and D. Tantin, "Stem cells, stress, metabolism and cancer: a drama in two Acts.," *Trends Biochem. Sci.*, vol. 34, no. 10, pp. 491–9, Oct. 2009.
- [144] L. Liu, H.-X. Xu, W.-Q. Wang, C.-T. Wu, T. Chen, Y. Qin, C. Liu, J. Xu, J. Long, B. Zhang, Y.-F. Xu, Q.-X. Ni, M. Li, and X.-J. Yu, "Cavin-1 is essential for the tumor-promoting effect of caveolin-1 and enhances its prognostic potency in pancreatic cancer.," *Oncogene*, vol. 33, no. 21, pp. 2728–36, May 2014.
- [145] E. Irollo and G. Pirozzi, "CD133: to be or not to be, is this the real question?," *Am. J. Transl. Res.*, vol. 5, no. 6, pp. 563–81, 2013.
- [146] J. Neuzil, M. Stantic, R. Zobalova, J. Chladova, X. Wang, L. Prochazka, L. Dong, L. Andera, and S. J. Ralph, "Tumour-initiating cells vs. cancer 'stem' cells and CD133: what's in the name?," *Biochem. Biophys. Res. Commun.*, vol. 355, no. 4, pp. 855–9, Apr. 2007.
- [147] C. D'Alterio, L. Cindolo, L. Portella, M. Polimeno, C. Consales, A. Riccio, M. Cioffi, R. Franco, P. Chiodini, G. Carteni, V. Mirone, N. Longo, L. Marra, S. Perdonà, L. Claudio, M. Mascolo, S. Staibano, M. Falsaperla, M. Puglisi, G. Martignoni, V. Ficarra, G. Castello, and S. Scala, "Differential role of CD133 and CXCR4 in renal cell carcinoma," *Cell Cycle*, vol. 9, no. 22, pp. 4492–4491, Nov. 2010.
- [148] G. Guler, S. Balci, S. Costinean, C. H. Ussakli, C. Irkkan, D. Suren, E. Sari, K. Altundag, Y. Ozisik, S. Jones, J. Bacher, C. L. Shapiro, and K. Huebner, "Stem cell-related markers in primary breast cancers and associated metastatic lesions.," *Mod. Pathol.*, pp. 1–7, Mar. 2012.
- [149] G. J. Klarmann, E. M. Hurt, L. A. Mathews, X. Zhang, M. A. Duhagon, T. Mistree, S. B. Thomas, and W. L. Farrar, "Invasive prostate cancer cells are tumor initiating cells that have a stem cell-like genomic signature.," *Clin. Exp. Metastasis*, vol. 26, no. 5, pp. 433–46, Jan. 2009.
- [150] O. Gires, "Lessons from common markers of tumor-initiating cells in solid cancers.," *Cell. Mol. Life Sci.*, pp. 4009–4022, Jul. 2011.
- [151] V. Orian-Rousseau, "CD44, a therapeutic target for metastasising tumours," *Eur. J. Cancer*, vol. 46, no. 7, pp. 1271–1277, 2010.
- [152] V. Orian-Rousseau and J. Sleeman, "CD44 is a multidomain signaling platform that integrates extracellular matrix cues with growth factor and cytokine signals," *Adv. Cancer Res.*, vol. 123, pp. 231–254, 2014.
- [153] B. P. Toole, "Hyaluronan in morphogenesis.," *J. Intern. Med.*, vol. 242, no. 1, pp. 35–40, 1997.
- [154] R. F. Thorne, J. W. Legg, and C. M. Isacke, "The role of the CD44 transmembrane and cytoplasmic domains in co-ordinating adhesive and signalling events.," *J. Cell Sci.*, vol. 117, no. Pt 3, pp. 373–380, 2004.
- [155] T. P. Skelton, C. Zeng, A. Nocks, and I. Stamenkovic, "Glycosylation provides both stimulatory and inhibitory effects on cell surface and soluble CD44 binding to hyaluronan," *J. Cell Biol.*, vol. 140, no. 2, pp. 431–446, 1998.

- [156] D. Naor, R. V Sionov, and D. Ish-Shalom, "CD44: structure, function, and association with the malignant process.," *Adv. Cancer Res.*, vol. 71, pp. 241–319, 1997.
- [157] N. Montgomery, A. Hill, S. McFarlane, J. Neisen, A. O'Grady, S. Conlon, K. Jirstrom, E. W. Kay, and D. J. J. Waugh, "CD44 enhances invasion of basal-like breast cancer cells by upregulating serine protease and collagen-degrading enzymatic expression and activity.," *Breast Cancer Res.*, vol. 14, no. 3, p. R84, 2012.
- [158] S. H. Cho, Y. S. Park, H. J. Kim, C. H. Kim, S. W. Lim, J. W. Huh, J. H. Lee, and H. R. Kim, "CD44 enhances the epithelial-mesenchymal transition in association with colon cancer invasion.," *Int. J. Oncol.*, vol. 41, no. 1, pp. 211–8, Jul. 2012.
- [159] Y. Fujita, M. Kitagawa, S. Nakamura, K. Azuma, G. Ishii, M. Higashi, H. Kishi, T. Hiwasa, K. Koda, N. Nakajima, and K. Harigaya, "CD44 signaling through focal adhesion kinase and its anti-apoptotic effect.," *FEBS Lett.*, vol. 528, no. 1–3, pp. 101–8, Sep. 2002.
- [160] C. Echiburú-Chau, D. Roy, and G. M. Calaf, "Metastatic suppressor CD44 is related with oxidative stress in breast cancer cell lines.," *Int. J. Oncol.*, vol. 39, no. 6, pp. 1481–9, Dec. 2011.
- [161] R. C. Bates, N. S. Edwards, G. F. Burns, and D. E. Fisher, "A CD44 survival pathway triggers chemoresistance via lyn kinase and phosphoinositide 3-kinase/Akt in colon carcinoma cells.," *Cancer Res.*, vol. 61, no. 13, pp. 5275–83, Jul. 2001.
- [162] T. Chanmee, P. Ontong, K. Kimata, and N. Itano, "Key Roles of Hyaluronan and Its CD44 Receptor in the Stemness and Survival of Cancer Stem Cells," *Front. Oncol.*, vol. 5, no. August, pp. 1–11, 2015.
- [163] V. Orian-Rousseau, "CD44 Acts as a Signaling Platform Controlling Tumor Progression and Metastasis," *Front. Immunol.*, vol. 6, no. April, pp. 10–13, 2015.
- [164] V. J. Wielenga, K. H. Heider, G. J. Offerhaus, G. R. Adolf, F. M. van den Berg, H. Ponta, P. Herrlich, and S. T. Pals, "Expression of CD44 variant proteins in human colorectal cancer is related to tumor progression.," *Cancer Res.*, vol. 53, no. 20, pp. 4754–6, Oct. 1993.
- [165] Y.-J. Liu, P.-S. Yan, J. Li, and J.-F. Jia, "Expression and significance of CD44s, CD44v6, and nm23 mRNA in human cancer.," *World J. Gastroenterol.*, vol. 11, no. 42, pp. 6601–6, Nov. 2005.
- [166] X.-P. Li, X.-W. Zhang, L.-Z. Zheng, and W.-J. Guo, "Expression of CD44 in pancreatic cancer and its significance.," *Int. J. Clin. Exp. Pathol.*, vol. 8, no. 6, pp. 6724–31, 2015.
- [167] V. Paradis, S. Ferlicot, E. Ghannam, L. Zeimoura, P. Blanchet, P. Eschwege, A. Jardin, G. Benoit, and P. Bedossa, "CD44 is an independent prognostic factor in conventional renal cell carcinomas," *J. Urol.*, vol. 161, no. 6, pp. 1984–1987, Jun. 1999.
- [168] V. Zolota, A. C. Tsamandas, M. Melachrinou, A. Batistatou, and C. Scopa, "Expression of CD44 protein in renal cell carcinomas: association with p53 expression.," *Urol. Oncol.*, vol. 7, no. 1, pp. 13–7.
- [169] B.-J. Jeong, Z. L. Liang, S. M. Huang, J. S. Lim, J. M. Kim, and H. J. Lee,

- “CD44 is associated with tumor recurrence and is an independent poor prognostic factor for patients with localized clear cell renal cell carcinoma after nephrectomy.,” *Exp. Ther. Med.*, vol. 3, no. 5, pp. 811–817, May 2012.
- [170] S. Donatello, I. S. Babina, L. D. Hazelwood, A. D. K. Hill, I. R. Nabi, and A. M. Hopkins, “Lipid raft association restricts CD44-ezrin interaction and promotion of breast cancer cell migration.,” *Am. J. Pathol.*, vol. 181, no. 6, pp. 2172–87, Dec. 2012.
- [171] J.-L. Lee, M.-J. Wang, P.-R. Sudhir, and J.-Y. Chen, “CD44 engagement promotes matrix-derived survival through the CD44-SRC-integrin axis in lipid rafts.,” *Mol. Cell. Biol.*, vol. 28, no. 18, pp. 5710–23, Sep. 2008.
- [172] S. H. Wong, L. Hamel, S. Chevalier, and A. Philip, “Endoglin expression on human microvascular endothelial cells association with betaglycan and formation of higher order complexes with TGF-?? signalling receptors,” *Eur. J. Biochem.*, vol. 267, no. 17, pp. 5550–5560, 2000.
- [173] F. J. Burrows, E. J. Derbyshire, P. L. Tazzari, P. Amlot, A. F. Gazdar, S. W. King, M. Letarte, E. S. Vitetta, and P. E. Thorpe, “Up-regulation of endoglin on vascular endothelial cells in human solid tumors: implications for diagnosis and therapy.,” *Clin. Cancer Res.*, vol. 1, no. 12, pp. 1623–1634, 1995.
- [174] E. Fonsatti, A. P. Jekunen, K. J. A. Kairemo, S. Coral, M. Snellman, M. R. Nicotra, P. G. Natali, M. Altomonte, and M. Maio, “Endoglin is a suitable target for efficient imaging of solid tumors: In vivo evidence in a canine mammary carcinoma model,” *Clin. Cancer Res.*, vol. 6, no. 5, pp. 2037–2043, 2000.
- [175] E. Fonsatti, M. Altomonte, M. R. Nicotra, P. G. Natali, and M. Maio, “Endoglin (CD105): a powerful therapeutic target on tumor-associated angiogenetic blood vessels.,” *Oncogene*, vol. 22, no. 42, pp. 6557–6563, 2003.
- [176] B. Costello, C. Li, S. Duff, D. Butterworth, A. Khan, M. Perkins, S. Owens, A. F. Al-Mowallad, S. O’Dwyer, and S. Kumar, “Perfusion of 99Tcm-labeled CD105 Mab into kidneys from patients with renal carcinoma suggests that CD105 is a promising vascular target.,” *Int. J. Cancer*, vol. 109, no. 3, pp. 436–41, Apr. 2004.
- [177] N. Takahashi, R. Kawanishi-Tabata, A. Haba, M. Tabata, Y. Haruta, H. Tsai, and B. K. Seon, “Association of serum endoglin with metastasis in patients with colorectal, breast, and other solid tumors, and suppressive effect of chemotherapy on the serum endoglin.,” *Clin. Cancer Res.*, vol. 7, no. 3, pp. 524–32, Mar. 2001.
- [178] P. Myśliwiec, K. Pawlak, A. Kukliński, and B. Kedra, “Combined perioperative plasma endoglin and VEGF--a assessment in colorectal cancer patients.,” *Folia Histochem. Cytobiol.*, vol. 47, no. 2, pp. 231–6, 2009.
- [179] R. S. Saad, Y. L. Liu, G. Nathan, J. Celebrezze, D. Medich, and J. F. Silverman, “Endoglin (CD105) and vascular endothelial growth factor as prognostic markers in colorectal cancer.,” *Mod. Pathol.*, vol. 17, no. 2, pp. 197–203, Feb. 2004.
- [180] J.-P. Dales, S. Garcia, P. Bonnier, F. Duffaud, L. Andrac-Meyer, O. Ramuz, M.-N. Lavaut, C. Allasia, and C. Charpin, “CD105 expression is a marker of high metastatic risk and poor outcome in breast carcinomas. Correlations between immunohistochemical analysis and long-term follow-up in a series of 929 patients.,” *Am. J. Clin. Pathol.*, vol. 119, no. 3, pp. 374–80, Mar. 2003.

- [181] R. S. Saad, K. M. Jasnosz, M. Y. Tung, and J. F. Silverman, "Endoglin (CD105) expression in endometrial carcinoma.," *Int. J. Gynecol. Pathol.*, vol. 22, no. 3, pp. 248–53, Jul. 2003.
- [182] T. C. Mineo, V. Ambrogi, A. Baldi, C. Rabitti, P. Bollero, B. Vincenzi, and G. Tonini, "Prognostic impact of VEGF, CD31, CD34, and CD105 expression and tumour vessel invasion after radical surgery for IB-IIA non-small cell lung cancer.," *J. Clin. Pathol.*, vol. 57, no. 6, pp. 591–7, Jun. 2004.
- [183] R. S. Saad, Y. El-Gohary, E. Memari, Y. L. Liu, and J. F. Silverman, "Endoglin (CD105) and vascular endothelial growth factor as prognostic markers in esophageal adenocarcinoma.," *Hum. Pathol.*, vol. 36, no. 9, pp. 955–61, Sep. 2005.
- [184] S. J. Smith, H. Tilly, J. H. Ward, D. C. Macarthur, J. Lowe, B. Coyle, and R. G. Grundy, "CD105 (Endoglin) exerts prognostic effects via its role in the microvascular niche of paediatric high grade glioma.," *Acta Neuropathol.*, vol. 124, no. 1, pp. 99–110, Jul. 2012.
- [185] J. Sandlund, Y. Hedberg, A. Bergh, K. Grankvist, B. Ljungberg, and T. Rasmuson, "Endoglin (CD105) expression in human renal cell carcinoma.," *BJU Int.*, vol. 97, no. 4, pp. 706–10, Apr. 2006.
- [186] W. Dubinski, M. Gabriel, V. V. Iakovlev, A. Scorilas, Y. M. Youssef, H. Faragalla, K. Kovacs, F. Rotondo, S. Metias, A. Arsanious, A. Plotkin, A. H. F. Girgis, C. J. Streutker, and G. M. Yousef, "Assessment of the prognostic significance of endoglin (CD105) in clear cell renal cell carcinoma using automated image analysis.," *Hum. Pathol.*, vol. 43, no. 7, pp. 1037–43, Jul. 2012.
- [187] A. Saroufim, Y. Messai, M. Hasmim, N. Rioux, R. Iacovelli, G. Verhoest, K. Bensalah, J.-J. Patard, L. Albiges, B. Azzarone, B. Escudier, and S. Chouaib, "Tumoral CD105 is a novel independent prognostic marker for prognosis in clear-cell renal cell carcinoma.," *Br. J. Cancer*, vol. 110, no. 7, pp. 1778–84, Apr. 2014.
- [188] J. Moreno-Càceres, L. Caja, J. Mainez, R. Mayoral, P. Martín-Sanz, R. Moreno-Vicente, M. Á. Del Pozo, S. Dooley, G. Egea, and I. Fabregat, "Caveolin-1 is required for TGF- β -induced transactivation of the EGF receptor pathway in hepatocytes through the activation of the metalloprotease TACE/ADAM17.," *Cell Death Dis.*, vol. 5, p. e1326, 2014.
- [189] S. V. Litvinov, M. P. Velders, H. A. M. Bakker, G. J. Fleuren, and S. O. Warnaar, "Ep-CAM: A human epithelial antigen is a homophilic cell-cell adhesion molecule.," *J. Cell Biol.*, vol. 125, no. 2, pp. 437–446, 1994.
- [190] M. Trzpis, P. M. J. McLaughlin, L. M. F. H. de Leij, and M. C. Harmsen, "Epithelial cell adhesion molecule: more than a carcinoma marker and adhesion molecule.," *Am. J. Pathol.*, vol. 171, no. 2, pp. 386–395, 2007.
- [191] W. A. Osta, Y. Chen, K. Mikhitarian, M. Mitas, M. Salem, Y. A. Hannun, D. J. Cole, and W. E. Gillanders, "EpCAM is overexpressed in breast cancer and is a potential target for breast cancer gene therapy," *Cancer Res.*, vol. 64, no. 16, pp. 5818–5824, 2004.
- [192] B. González, S. Denzel, B. Mack, M. Conrad, and O. Gires, "EpCAM is involved in maintenance of the murine embryonic stem cell phenotype," *Stem Cells*, vol. 27, no. 8, pp. 1782–1791, 2009.
- [193] A. Lugli, G. Iezzi, I. Hostettler, M. G. Muraro, V. Mele, L. Tornillo, V. Carafa,

- G. Spagnoli, L. Terracciano, and I. Zlobec, "Prognostic impact of the expression of putative cancer stem cell markers CD133, CD166, CD44s, EpCAM, and ALDH1 in colorectal cancer.," *Br. J. Cancer*, vol. 103, no. 3, pp. 382–90, Jul. 2010.
- [194] G. Spizzo, P. Went, S. Dirnhofer, P. Obrist, R. Simon, H. Spichtin, R. Maurer, U. Metzger, B. von Castelberg, R. Bart, S. Stopatschinskaya, O. R. Köchli, P. Haas, F. Mross, M. Zuber, H. Dietrich, S. Bischoff, M. Mirlacher, G. Sauter, and G. Gastl, "High Ep-CAM expression is associated with poor prognosis in node-positive breast cancer.," *Breast Cancer Res. Treat.*, vol. 86, no. 3, pp. 207–13, Aug. 2004.
- [195] G. Spizzo, P. Went, S. Dirnhofer, P. Obrist, H. Moch, P. A. Baeuerle, E. Mueller-Holzner, C. Marth, G. Gastl, and A. G. Zeimet, "Overexpression of epithelial cell adhesion molecule (Ep-CAM) is an independent prognostic marker for reduced survival of patients with epithelial ovarian cancer.," *Gynecol. Oncol.*, vol. 103, no. 2, pp. 483–8, Nov. 2006.
- [196] H. Kimura, H. Kato, A. Faried, M. Sohda, M. Nakajima, Y. Fukai, T. Miyazaki, N. Masuda, M. Fukuchi, and H. Kuwano, "Prognostic significance of EpCAM expression in human esophageal cancer.," *Int. J. Oncol.*, vol. 30, no. 1, pp. 171–9, Jan. 2007.
- [197] P. Went, S. Dirnhofer, T. Salvisberg, M. B. Amin, S. D. Lim, P.-A. Diener, and H. Moch, "Expression of epithelial cell adhesion molecule (EpCam) in renal epithelial tumors.," *Am. J. Surg. Pathol.*, vol. 29, no. 1, pp. 83–8, Jan. 2005.
- [198] C. Eichelberg, F. K. Chun, J. Bedke, R. Heuer, M. Adam, H. Moch, L. Terracciano, K. Hinrichs, R. Dahlem, M. Fisch, T. Schlomm, G. Sauter, and S. Minner, "Epithelial cell adhesion molecule is an independent prognostic marker in clear cell renal carcinoma.," *Int. J. Cancer*, vol. 132, no. 12, pp. 2948–55, Jun. 2013.
- [199] D. B. Seligson, A. J. Pantuck, X. Liu, Y. Huang, S. Horvath, M. H. T. Bui, K. Han, A. J. L. Correa, M. Eeva, S. Tze, A. S. Beldegrun, and R. A. Figlin, "Epithelial cell adhesion molecule (KSA) expression: pathobiology and its role as an independent predictor of survival in renal cell carcinoma.," *Clin. Cancer Res.*, vol. 10, no. 8, pp. 2659–69, Apr. 2004.
- [200] J. M. Lehmann, B. Holzmann, E. W. Breitbart, P. Schmiegelow, G. Riethmüller, and J. P. Johnson, "Discrimination between benign and malignant cells of melanocytic lineage by two novel antigens, a glycoprotein with a molecular weight of 113,000 and a protein with a molecular weight of 76,000," *Cancer Res.*, vol. 47, no. 3, pp. 841–845, 1987.
- [201] C. Sers, G. Riethmüller, and J. P. Johnson, "MUC18, a melanoma-progression associated molecule, and its potential role in tumor vascularization and hematogenous spread," *Cancer Res.*, vol. 54, no. 21, pp. 5689–5694, 1994.
- [202] W.-F. Liu, S.-R. Ji, J.-J. Sun, Y. Zhang, Z.-Y. Liu, A.-B. Liang, and H.-Z. Zeng, "CD146 Expression Correlates with Epithelial-Mesenchymal Transition Markers and a Poor Prognosis in Gastric Cancer," *International Journal of Molecular Sciences*, vol. 13, no. 5, pp. 6399–6406, 2012.
- [203] W. Li, D. Yang, S. Wang, X. Guo, R. Lang, Y. Fan, F. Gu, X. Zhang, Y. Niu, X. Yan, and L. Fu, "Increased expression of CD146 and microvessel density (MVD) in invasive micropapillary carcinoma of the breast: Comparative study with invasive ductal carcinoma-not otherwise specified," *Pathol. Res. Pract.*,

vol. 207, no. 12, pp. 739–746, 2011.

- [204] G. J. Wu, V. A. Varma, M. W. Wu, S. W. Wang, P. Qu, H. Yang, J. A. Petros, S. D. Lim, and M. B. Amin, “Expression of a human cell adhesion molecule, MUC18, in prostate cancer cell lines and tissues.,” *Prostate*, vol. 48, no. 4, pp. 305–315, 2001.
- [205] G. Kristiansen, Y. Yu, K. Schlüns, C. Sers, M. Dietel, and I. Petersen, “Expression of the cell adhesion molecule CD146/MCAM in non-small cell lung cancer.,” *Anal. Cell. Pathol.*, vol. 25, no. 2, pp. 77–81, 2003.
- [206] G. Feng, F. Fang, C. Liu, F. Zhang, H. Huang, and C. Pu, “CD146 gene expression in clear cell renal cell carcinoma: A potential marker for prediction of early recurrence after nephrectomy,” *Int. Urol. Nephrol.*, vol. 44, no. 6, pp. 1663–1669, 2012.
- [207] J. E. Eriksson, T. Dechat, B. Grin, B. Helfand, M. Mendez, H.-M. Pallari, and R. D. Goldman, “Introducing intermediate filaments: from discovery to disease.,” *J. Clin. Invest.*, vol. 119, no. 7, pp. 1763–71, Jul. 2009.
- [208] T. Katsumoto, A. Mitsushima, and T. Kurimura, “The role of the vimentin intermediate filaments in rat 3Y1 cells elucidated by immunoelectron microscopy and computer-graphic reconstruction.,” *Biol. Cell*, vol. 68, no. 2, pp. 139–46, 1990.
- [209] R. D. Goldman, S. Khuon, Y. H. Chou, P. Opal, and P. M. Steinert, “The function of intermediate filaments in cell shape and cytoskeletal integrity.,” *J. Cell Biol.*, vol. 134, no. 4, pp. 971–83, Aug. 1996.
- [210] M. G. Mendez, S.-I. Kojima, and R. D. Goldman, “Vimentin induces changes in cell shape, motility, and adhesion during the epithelial to mesenchymal transition.,” *FASEB J.*, vol. 24, no. 6, pp. 1838–51, Jun. 2010.
- [211] S. H. Lang, C. Hyde, I. N. Reid, I. S. Hitchcock, C. A. Hart, A. A. G. Bryden, J.-M. Villette, M. J. Stower, and N. J. Maitland, “Enhanced expression of vimentin in motile prostate cell lines and in poorly differentiated and metastatic prostate carcinoma.,” *Prostate*, vol. 52, no. 4, pp. 253–63, Sep. 2002.
- [212] Y. Zhao, Q. Yan, X. Long, X. Chen, and Y. Wang, “Vimentin affects the mobility and invasiveness of prostate cancer cells.,” *Cell Biochem. Funct.*, vol. 26, no. 5, pp. 571–7, 2008.
- [213] Y. Fuyuhiko, M. Yashiro, S. Noda, S. Kashiwagi, J. Matsuoka, Y. Doi, Y. Kato, N. Kubo, M. Ohira, and K. Hirakawa, “Clinical significance of vimentin-positive gastric cancer cells.,” *Anticancer Res.*, vol. 30, no. 12, pp. 5239–43, Dec. 2010.
- [214] H. Jin, S. Morohashi, F. Sato, Y. Kudo, H. Akasaka, S. Tsutsumi, H. Ogasawara, K. Miyamoto, N. Wajima, H. Kawasaki, K. Hakamada, and H. Kijima, “Vimentin expression of esophageal squamous cell carcinoma and its aggressive potential for lymph node metastasis.,” *Biomed. Res.*, vol. 31, no. 2, pp. 105–12, Apr. 2010.
- [215] M. I. Kokkinos, R. Wafai, M. K. Wong, D. F. Newgreen, E. W. Thompson, and M. Waltham, “Vimentin and epithelial-mesenchymal transition in human breast cancer--observations in vitro and in vivo.,” *Cells. Tissues. Organs*, vol. 185, no. 1–3, pp. 191–203, 2007.
- [216] K. Vuoriluoto, H. Haugen, S. Kiviluoto, J.-P. Mpindi, J. Nevo, C. Gjerdrum, C.

- Tiron, J. B. Lorens, and J. Ivaska, "Vimentin regulates EMT induction by Slug and oncogenic H-Ras and migration by governing Axl expression in breast cancer.," *Oncogene*, vol. 30, no. 12, pp. 1436–48, Mar. 2011.
- [217] W. Domagala, J. Lasota, J. Bartkowiak, K. Weber, and M. Osborn, "Vimentin is preferentially expressed in human breast carcinomas with low estrogen receptor and high Ki-67 growth fraction.," *Am. J. Pathol.*, vol. 136, no. 1, pp. 219–27, Jan. 1990.
- [218] S. Pitz, R. Moll, S. Störkel, and W. Thoenes, "Expression of intermediate filament proteins in subtypes of renal cell carcinomas and in renal oncocytomas. Distinction of two classes of renal cell tumors.," *Lab. Invest.*, vol. 56, no. 6, pp. 642–53, Jun. 1987.
- [219] N. A. Abrahams, G. T. MacLennan, J. D. Khoury, A. H. Ormsby, P. Tamboli, C. Doglioni, B. Schumacher, and S. K. Tickoo, "Chromophobe renal cell carcinoma: a comparative study of histological, immunohistochemical and ultrastructural features using high throughput tissue microarray.," *Histopathology*, vol. 45, no. 6, pp. 593–602, Dec. 2004.
- [220] A. A. Williams, J. P. T. Higgins, H. Zhao, B. Ljunberg, and J. D. Brooks, "CD 9 and vimentin distinguish clear cell from chromophobe renal cell carcinoma.," *BMC Clin. Pathol.*, vol. 9, p. 9, 2009.
- [221] J. C. Carvalho, M. J. Wasco, L. P. Kunju, D. G. Thomas, and R. B. Shah, "Cluster analysis of immunohistochemical profiles delineates CK7, vimentin, S100A1 and C-kit (CD117) as an optimal panel in the differential diagnosis of renal oncocytoma from its mimics.," *Histopathology*, vol. 58, no. 2, pp. 169–79, Jan. 2011.
- [222] K. Donhuijsen and S. Schulz, "Prognostic significance of vimentin positivity in formalin-fixed renal cell carcinomas.," *Pathol. Res. Pract.*, vol. 184, no. 3, pp. 287–91, Mar. 1989.
- [223] A. I. Gorelov, Z. N. Narimanian, and D. S. Gorelov, "Prognostic value of ki-67 and vimentin markers in patients with metastatic kidney cancer.," *Urologiia*, no. 3, pp. 54–8, 2014.
- [224] O. Shvarts, D. Seligson, J. Lam, T. Shi, S. Horvath, R. Figlin, A. Beldegrun, and A. J. Pantuck, "p53 is an independent predictor of tumor recurrence and progression after nephrectomy in patients with localized renal cell carcinoma.," *J. Urol.*, vol. 173, no. 3, pp. 725–8, Mar. 2005.
- [225] N. T. Price, V. N. Jackson, and A. P. Halestrap, "Cloning and sequencing of four new mammalian monocarboxylate transporter (MCT) homologues confirms the existence of a transporter family with an ancient past.," *Biochem. J.*, vol. 329 (Pt 2, pp. 321–8, Jan. 1998.
- [226] K. S. Dimmer, B. Friedrich, F. Lang, J. W. Deitmer, and S. Bröer, "The low-affinity monocarboxylate transporter MCT4 is adapted to the export of lactate in highly glycolytic cells.," *Biochem. J.*, vol. 350 Pt 1, pp. 219–27, Aug. 2000.
- [227] D. Meredith, P. Bell, B. McClure, and R. Wilkins, "Functional and molecular characterisation of lactic acid transport in bovine articular chondrocytes.," *Cell. Physiol. Biochem.*, vol. 12, no. 4, pp. 227–34, 2002.
- [228] A. Suzuki, S. A. Stern, O. Bozdagi, G. W. Huntley, R. H. Walker, P. J. Magistretti, and C. M. Alberini, "Astrocyte-neuron lactate transport is required for long-term memory formation.," *Cell*, vol. 144, no. 5, pp. 810–23, Mar. 2011.

- [229] N. Merezhinskaya, S. A. Ogunwuyi, and W. N. Fishbein, "Expression of monocarboxylate transporter 4 in human platelets, leukocytes, and tissues assessed by antibodies raised against terminal versus pre-terminal peptides.," *Mol. Genet. Metab.*, vol. 87, no. 2, pp. 152–61, Feb. 2006.
- [230] O. Warburg, "On the origin of cancer cells.," *Science*, vol. 123, no. 3191, pp. 309–14, Feb. 1956.
- [231] S. P. Mathupala, P. Parajuli, and A. E. Sloan, "Silencing of monocarboxylate transporters via small interfering ribonucleic acid inhibits glycolysis and induces cell death in malignant glioma: an in vitro study.," *Neurosurgery*, vol. 55, no. 6, pp. 1410–9; discussion 1419, Dec. 2004.
- [232] V. Miranda-Gonçalves, M. Honavar, C. Pinheiro, O. Martinho, M. M. Pires, C. Pinheiro, M. Cordeiro, G. Bebian, P. Costa, I. Palmeirim, R. M. Reis, and F. Baltazar, "Monocarboxylate transporters (MCTs) in gliomas: expression and exploitation as therapeutic targets.," *Neuro. Oncol.*, vol. 15, no. 2, pp. 172–88, Feb. 2013.
- [233] "ClinicalTrials.gov [Internet]. Bethesda (MD): National Library of Medicine (US). 2000 Feb 29 - . Identifier NCT00287391, A Phase I Trial of AZD3965 in Patients With Advanced Cancer; September 7, 2015 [cited 2015 Nov 23]; [about 4 screens]. Available from:" .
- [234] C. Pinheiro, A. Longatto-Filho, L. Ferreira, S. M. M. Pereira, D. Etlinger, M. A. R. Moreira, L. F. Jubé, G. S. Queiroz, F. Schmitt, and F. Baltazar, "Increasing expression of monocarboxylate transporters 1 and 4 along progression to invasive cervical carcinoma.," *Int. J. Gynecol. Pathol.*, vol. 27, no. 4, pp. 568–74, Oct. 2008.
- [235] N. Pérttega-Gomes, J. R. Vizcaíno, V. Miranda-Gonçalves, C. Pinheiro, J. Silva, H. Pereira, P. Monteiro, R. M. Henrique, R. M. Reis, C. Lopes, and F. Baltazar, "Monocarboxylate transporter 4 (MCT4) and CD147 overexpression is associated with poor prognosis in prostate cancer.," *BMC Cancer*, vol. 11, p. 312, 2011.
- [236] M. Gerlinger, C. R. Santos, B. Spencer-Dene, P. Martinez, D. Endesfelder, R. A. Burrell, M. Vetter, M. Jiang, R. E. Saunders, G. Kelly, K. Dykema, N. Rioux-Leclercq, G. Stamp, J. J. Patard, J. Larkin, M. Howell, and C. Swanton, "Genome-wide RNA interference analysis of renal carcinoma survival regulators identifies MCT4 as a Warburg effect metabolic target.," *J. Pathol.*, vol. 227, no. 2, pp. 146–56, Jun. 2012.
- [237] P. Fisel, S. Kruck, S. Winter, J. Bedke, J. Hennenlotter, A. T. Nies, M. Scharpf, F. Fend, A. Stenzl, M. Schwab, and E. Schaeffeler, "DNA methylation of the SLC16A3 promoter regulates expression of the human lactate transporter MCT4 in renal cancer with consequences for clinical outcome.," *Clin. Cancer Res.*, vol. 19, no. 18, pp. 5170–81, Sep. 2013.
- [238] Y. Kim, J.-W. Choi, J.-H. Lee, and Y.-S. Kim, "Expression of lactate/H⁺ symporters MCT1 and MCT4 and their chaperone CD147 predicts tumor progression in clear cell renal cell carcinoma: immunohistochemical and The Cancer Genome Atlas data analyses.," *Hum. Pathol.*, vol. 46, no. 1, pp. 104–12, Jan. 2015.
- [239] P. Fisel, V. Stühler, J. Bedke, S. Winter, S. Rausch, J. Hennenlotter, A. T. Nies, A. Stenzl, M. Scharpf, F. Fend, S. Kruck, M. Schwab, and E. Schaeffeler, "MCT4 surpasses the prognostic relevance of the ancillary protein CD147 in clear cell renal cell carcinoma.," *Oncotarget*, vol. 6, no. 31,

pp. 30615–27, Oct. 2015.

- [240] T.-K. Ha, N.-G. Her, M.-G. Lee, B.-K. Ryu, J.-H. Lee, J. Han, S.-I. Jeong, M.-J. Kang, N.-H. Kim, H.-J. Kim, and S.-G. Chi, “Caveolin-1 increases aerobic glycolysis in colorectal cancers by stimulating HMGA1-mediated GLUT3 transcription,” *Cancer Res.*, vol. 72, no. 16, pp. 4097–109, Aug. 2012.
- [241] S. A. Tahir, G. Yang, A. Goltsov, K.-D. Song, C. Ren, J. Wang, W. Chang, and T. C. Thompson, “Caveolin-1-LRP6 signaling module stimulates aerobic glycolysis in prostate cancer,” *Cancer Res.*, vol. 73, no. 6, pp. 1900–11, Mar. 2013.
- [242] A. M. Fra, E. Williamson, K. Simons, and R. G. Parton, “De novo formation of caveolae in lymphocytes by expression of VIP21-caveolin,” *Proc. Natl. Acad. Sci. U. S. A.*, vol. 92, no. 19, pp. 8655–9, Sep. 1995.
- [243] M. M. Hill, M. Bastiani, R. Luetterforst, M. Kirkham, A. Kirkham, S. J. Nixon, P. Walser, D. Abankwa, V. M. J. Oorschot, S. Martin, J. F. Hancock, and R. G. Parton, “PTRF-Cavin, a conserved cytoplasmic protein required for caveola formation and function,” *Cell*, vol. 132, no. 1, pp. 113–24, Jan. 2008.
- [244] A. Hayer, M. Stoeber, C. Bissig, and A. Helenius, “Biogenesis of caveolae: stepwise assembly of large caveolin and cavin complexes,” *Traffic*, vol. 11, no. 3, pp. 361–82, Mar. 2010.
- [245] L. Bai, X. Deng, Q. Li, M. Wang, W. An, A. Deli, Z. Gao, Y. Xie, Y. Dai, and Y.-S. Cong, “Down-regulation of the cavin family proteins in breast cancer,” *J. Cell. Biochem.*, vol. 113, no. 1, pp. 322–8, Jan. 2012.
- [246] C. S. Aung, M. M. Hill, M. Bastiani, R. G. Parton, and M.-O. Parat, “PTRF-cavin-1 expression decreases the migration of PC3 prostate cancer cells: role of matrix metalloprotease 9,” *Eur. J. Cell Biol.*, vol. 90, no. 2–3, pp. 136–42, 2011.
- [247] S. M. Hewitt, D. G. Baskin, C. W. Frevert, W. L. Stahl, and E. Rosa-Molinar, “Controls for immunohistochemistry: the Histochemical Society’s standards of practice for validation of immunohistochemical assays,” *J. Histochem. Cytochem.*, vol. 62, no. 10, pp. 693–7, Oct. 2014.
- [248] C. B. Saper, “A guide to the perplexed on the specificity of antibodies,” *J. Histochem. Cytochem.*, vol. 57, no. 1, pp. 1–5, Jan. 2009.
- [249] S. Holmseth, Y. Zhou, V. V Follin-Arbelet, K. P. Lehre, D. E. Bergles, and N. C. Danbolt, “Specificity controls for immunocytochemistry: the antigen preadsorption test can lead to inaccurate assessment of antibody specificity,” *J. Histochem. Cytochem.*, vol. 60, no. 3, pp. 174–87, Mar. 2012.
- [250] M. Uhlén, L. Fagerberg, B. M. Hallström, C. Lindskog, P. Oksvold, A. Mardinoglu, Å. Sivertsson, C. Kampf, E. Sjöstedt, A. Asplund, I. Olsson, K. Edlund, E. Lundberg, S. Navani, C. A.-K. Szigartyo, J. Odeberg, D. Djureinovic, J. O. Takanen, S. Hober, T. Alm, P.-H. Edqvist, H. Berling, H. Tegel, J. Mulder, J. Rockberg, P. Nilsson, J. M. Schwenk, M. Hamsten, K. von Feilitzen, M. Forsberg, L. Persson, F. Johansson, M. Zwahlen, G. von Heijne, J. Nielsen, and F. Pontén, “Proteomics. Tissue-based map of the human proteome,” *Science*, vol. 347, no. 6220, p. 1260419, Jan. 2015.
- [251] K. M. A. Rouschop, J. J. T. H. Roelofs, M. Sylva, A. T. Rowshani, I. J. M. Ten Berge, J. J. Weening, and S. Florquin, “Renal expression of CD44 correlates with acute renal allograft rejection,” *Kidney Int.*, vol. 70, no. 6, pp. 1127–34, Sep. 2006.

- [252] Y. Katayama, A. Hidalgo, J. Chang, A. Peired, and P. S. Frenette, "CD44 is a physiological E-selectin ligand on neutrophils.," *J. Exp. Med.*, vol. 201, no. 8, pp. 1183–9, Apr. 2005.
- [253] B. J. G. Baaten, C. R. Li, and L. M. Bradley, "Multifaceted regulation of T cells by CD44," *Commun. Integr. Biol.*, vol. 3, no. 6, pp. 508–512, 2010.
- [254] K. S. Hathcock, H. Hirano, S. Murakami, and R. J. Hodes, "CD44 expression on activated B cells. Differential capacity for CD44-dependent binding to hyaluronic acid.," *J. Immunol.*, vol. 151, no. 12, pp. 6712–22, Dec. 1993.
- [255] A. Schrage, C. Loddenkemper, U. Erben, U. Lauer, G. Hausdorf, P. R. Jungblut, J. Johnson, P. A. Knolle, M. Zeitz, A. Hamann, and K. Klugewitz, "Murine CD146 is widely expressed on endothelial cells and is recognized by the monoclonal antibody ME-9F1.," *Histochem. Cell Biol.*, vol. 129, no. 4, pp. 441–51, Apr. 2008.
- [256] L. Campbell, B. Jasani, K. Edwards, M. Gumbleton, and D. F. R. Griffiths, "Combined expression of caveolin-1 and an activated AKT/mTOR pathway predicts reduced disease-free survival in clinically confined renal cell carcinoma.," *Br. J. Cancer*, vol. 98, no. 5, pp. 931–40, Mar. 2008.
- [257] S. Steffens, A. J. Schrader, H. Blasig, G. Vetter, H. Eggers, W. Tränkenschuh, M. A. Kuczyk, and J. Serth, "Caveolin 1 protein expression in renal cell carcinoma predicts survival.," *BMC Urol.*, vol. 11, p. 25, 2011.
- [258] N. B. Phuoc, H. Ehara, T. Gotoh, M. Nakano, S. Yokoi, T. Deguchi, and Y. Hirose, "Immunohistochemical analysis with multiple antibodies in search of prognostic markers for clear cell renal cell carcinoma.," *Urology*, vol. 69, no. 5, pp. 843–8, May 2007.
- [259] X. Li, X. Ma, L. Chen, L. Gu, Y. Zhang, F. Zhang, Y. Ouyang, Y. Gao, Q. Huang, and X. Zhang, "Prognostic value of CD44 expression in renal cell carcinoma: a systematic review and meta-analysis.," *Sci. Rep.*, vol. 5, p. 13157, 2015.
- [260] J. Qin, B. Yang, B.-Q. Xu, A. Smithc, L. Xu, J.-L. Yuan, and L. Li, "Concurrent CD44s and STAT3 expression in human clear cell renal cellular carcinoma and its impact on survival.," *Int. J. Clin. Exp. Pathol.*, vol. 7, no. 6, pp. 3235–44, 2014.
- [261] Y. Zhang, B. Sun, X. Zhao, Z. Liu, X. Wang, X. Yao, X. Dong, and J. Chi, "Clinical significances and prognostic value of cancer stem-like cells markers and vasculogenic mimicry in renal cell carcinoma.," *J. Surg. Oncol.*, vol. 108, no. 6, pp. 414–9, Nov. 2013.
- [262] S. Mikami, R. Mizuno, T. Kosaka, H. Saya, M. Oya, and Y. Okada, "Expression of TNF- α and CD44 is implicated in poor prognosis, cancer cell invasion, metastasis and resistance to the sunitinib treatment in clear cell renal cell carcinomas.," *Int. J. Cancer*, vol. 136, no. 7, pp. 1504–14, Apr. 2015.
- [263] M. Long, S.-H. Huang, C.-H. Wu, G. M. Shackelford, and A. Jong, "Lipid raft/caveolae signaling is required for *Cryptococcus neoformans* invasion into human brain microvascular endothelial cells.," *J. Biomed. Sci.*, vol. 19, p. 19, 2012.
- [264] S. Donatello, I. S. Babina, L. D. Hazelwood, A. D. K. Hill, I. R. Nabi, and A. M. Hopkins, "Lipid Raft Association Restricts CD44-Ezrin Interaction and Promotion of Breast Cancer Cell Migration.," *Am. J. Pathol.*, vol. 181, no. 6,

pp. 2172–2187, Sep. 2012.

- [265] W.-H. Yu, J. F. Woessner, J. D. McNeish, and I. Stamenkovic, “CD44 anchors the assembly of matrilysin/MMP-7 with heparin-binding epidermal growth factor precursor and ErbB4 and regulates female reproductive organ remodeling,” *Genes Dev.*, vol. 16, no. 3, pp. 307–23, Feb. 2002.
- [266] V. Subramaniam, I. R. Vincent, M. Gilakjan, and S. Jothy, “Suppression of human colon cancer tumors in nude mice by siRNA CD44 gene therapy,” *Exp. Mol. Pathol.*, vol. 83, no. 3, pp. 332–40, Dec. 2007.
- [267] H. Lee, D. Volonte, F. Galbiati, P. Iyengar, D. M. Lublin, D. B. Bregman, M. T. Wilson, R. Campos-Gonzalez, B. Bouzahzah, R. G. Pestell, P. E. Scherer, and M. P. Lisanti, “Constitutive and growth factor-regulated phosphorylation of caveolin-1 occurs at the same site (Tyr-14) in vivo: identification of a c-Src/Cav-1/Grb7 signaling cassette,” *Mol. Endocrinol.*, vol. 14, no. 11, pp. 1750–75, Nov. 2000.
- [268] D. Martins, F. F. Beça, B. Sousa, F. Baltazar, J. Paredes, and F. Schmitt, “Loss of caveolin-1 and gain of MCT4 expression in the tumor stroma: key events in the progression from an in situ to an invasive breast carcinoma,” *Cell Cycle*, vol. 12, no. 16, pp. 2684–90, Aug. 2013.
- [269] M. Schoumacher, R. D. Goldman, D. Louvard, and D. M. Vignjevic, “Actin, microtubules, and vimentin intermediate filaments cooperate for elongation of invadopodia,” *J. Cell Biol.*, vol. 189, no. 3, pp. 541–56, May 2010.
- [270] M. Sutoh Yoneyama, S. Hatakeyama, T. Habuchi, T. Inoue, T. Nakamura, T. Funyu, G. Wiche, C. Ohyama, and S. Tsuboi, “Vimentin intermediate filament and plectin provide a scaffold for invadopodia, facilitating cancer cell invasion and extravasation for metastasis,” *Eur. J. Cell Biol.*, vol. 93, no. 4, pp. 157–69, Apr. 2014.
- [271] V. Tirino, V. Desiderio, F. Paino, A. De Rosa, F. Papaccio, M. La Noce, L. Laino, F. De Francesco, and G. Papaccio, “Cancer stem cells in solid tumors: an overview and new approaches for their isolation and characterization,” *FASEB*, vol. 27, no. 1, pp. 13–24, 2013.
- [272] A. Golebiewska, N. H. C. Brons, R. Bjerkvig, and S. P. Niclou, “Critical appraisal of the side population assay in stem cell and cancer stem cell research,” *Cell Stem Cell*, vol. 8, no. 2, pp. 136–47, Feb. 2011.
- [273] P. Marcato, C. A. Dean, C. A. Giacomantonio, and P. W. K. Lee, “Aldehyde dehydrogenase: its role as a cancer stem cell marker comes down to the specific isoform,” *Cell Cycle*, vol. 10, no. 9, pp. 1378–84, May 2011.
- [274] K. Williams, K. Motiani, P. V. Giridhar, and S. Kasper, “CD44 integrates signaling in normal stem cell, cancer stem cell and (pre)metastatic niches,” *Exp. Biol. Med. (Maywood)*, vol. 238, no. 3, pp. 324–38, Mar. 2013.
- [275] M. Al-Hajj, M. S. Wicha, A. Benito-Hernandez, S. J. Morrison, and M. F. Clarke, “Prospective identification of tumorigenic breast cancer cells,” *Proc. Natl. Acad. Sci. U. S. A.*, vol. 100, no. 7, pp. 3983–8, Apr. 2003.
- [276] S. Takaishi, T. Okumura, S. Tu, S. S. W. Wang, W. Shibata, R. Vigneshwaran, S. A. K. Gordon, Y. Shimada, and T. C. Wang, “Identification of gastric cancer stem cells using the cell surface marker CD44,” *Stem Cells*, vol. 27, no. 5, pp. 1006–1020, 2009.
- [277] C. Li, D. G. Heidt, P. Dalerba, C. F. Burant, L. Zhang, V. Adsay, M. Wicha, M.

- F. Clarke, and D. M. Simeone, "Identification of pancreatic cancer stem cells.," *Cancer Res.*, vol. 67, no. 3, pp. 1030–7, Feb. 2007.
- [278] P. Wang, Q. Gao, Z. Suo, E. Munthe, S. Solberg, L. Ma, M. Wang, N. A. C. Westerdaal, G. Kvalheim, and G. Gaudernack, "Identification and Characterization of Cells with Cancer Stem Cell Properties in Human Primary Lung Cancer Cell Lines," *PLoS One*, vol. 8, no. 3, 2013.
- [279] M. E. Prince, R. Sivanandan, A. Kaczorowski, G. T. Wolf, M. J. Kaplan, P. Dalerba, I. L. Weissman, M. F. Clarke, and L. E. Ailles, "Identification of a subpopulation of cells with cancer stem cell properties in head and neck squamous cell carcinoma.," *Proc. Natl. Acad. Sci. U. S. A.*, vol. 104, no. 3, pp. 973–978, 2007.
- [280] H. Shigeishi, A. Biddle, L. Gammon, H. Emich, C. O. Rodini, E. Gemenetzidis, B. Fazil, M. Sugiyama, N. Kamata, and I. C. MacKenzie, "Maintenance of stem cell self-renewal in head and neck cancers requires actions of GSK3b influenced by CD44 and RHAMM," *Stem Cells*, vol. 31, no. 10, pp. 2073–2083, 2013.
- [281] L. Y. W. Bourguignon, K. Peyrollier, W. Xia, and E. Gilad, "Hyaluronan-CD44 interaction activates stem cell marker Nanog, Stat-3-mediated MDR1 gene expression, and ankyrin-regulated multidrug efflux in breast and ovarian tumor cells.," *J. Biol. Chem.*, vol. 283, no. 25, pp. 17635–51, Jun. 2008.
- [282] M. Dominici, K. Le Blanc, I. Mueller, I. Slaper-Cortenbach, F. Marini, D. Krause, R. Deans, A. Keating, D. Prockop, and E. Horwitz, "Minimal criteria for defining multipotent mesenchymal stromal cells. The International Society for Cellular Therapy position statement.," *Cytotherapy*, vol. 8, no. 4, pp. 315–317, 2006.
- [283] C. Muñiz, C. Teodosio, A. Mayado, A. T. Amaral, S. Matarraz, P. Bárcena, M. L. Sanchez, I. Alvarez-Twose, M. Diez-Campelo, A. C. García-Montero, J. F. Blanco, M. C. Del Cañizo, J. Del Pino Montes, and A. Orfao, "Ex vivo identification and characterization of a population of CD13(high) CD105(+) CD45(-) mesenchymal stem cells in human bone marrow.," *Stem Cell Res. Ther.*, vol. 6, no. 1, p. 169, 2015.
- [284] J. Kellner, S. Sivajothi, and I. McNiece, "Differential properties of human stromal cells from bone marrow, adipose, liver and cardiac tissues.," *Cytotherapy*, 2015.
- [285] B. D. Humphreys and J. V Bonventre, "Mesenchymal stem cells in acute kidney injury.," *Annu. Rev. Med.*, vol. 59, pp. 311–325, 2008.
- [286] S. Azzi, S. Bruno, J. Giron-Michel, D. Clay, A. Devocelle, M. Croce, S. Ferrini, S. Chouaib, A. Vazquez, B. Charpentier, G. Camussi, B. Azzarone, and P. Eid, "Differentiation therapy: targeting human renal cancer stem cells with interleukin 15.," *J. Natl. Cancer Inst.*, vol. 103, no. 24, pp. 1884–98, Dec. 2011.
- [287] F.-J. Lv, R. S. Tuan, K. M. C. Cheung, and V. Y. L. Leung, "The surface markers and identity of human mesenchymal stem cells.," *Stem Cells*, pp. 1–18, 2014.
- [288] Z. F. Yang, D. W. Ho, M. N. Ng, C. K. Lau, W. C. Yu, P. Ngai, P. W. K. Chu, C. T. Lam, R. T. P. Poon, and S. T. Fan, "Significance of CD90+ cancer stem cells in human liver cancer.," *Cancer Cell*, vol. 13, no. 2, pp. 153–66, Feb. 2008.

- [289] Z. F. Yang, D. W. Ho, M. N. Ng, C. K. Lau, W. C. Yu, P. Ngai, P. W. K. Chu, C. T. Lam, R. T. P. Poon, and S. T. Fan, "Significance of CD90+ Cancer Stem Cells in Human Liver Cancer," *Cancer Cell*, vol. 13, no. 2, pp. 153–166, 2008.
- [290] K. H. Tang, Y. D. Dai, M. Tong, Y. P. Chan, P. S. Kwan, L. Fu, Y. R. Qin, S. W. Tsao, H. L. Lung, M. L. Lung, D. K. Tong, S. Law, K. W. Chan, S. Ma, and X. Y. Guan, "A CD90(+) tumor-initiating cell population with an aggressive signature and metastatic capacity in esophageal cancer.," *Cancer Res.*, vol. 73, no. 7, pp. 2322–32, Apr. 2013.
- [291] D. Baksh, R. Yao, and R. S. Tuan, "Comparison of proliferative and multilineage differentiation potential of human mesenchymal stem cells derived from umbilical cord and bone marrow.," *Stem Cells*, vol. 25, no. 6, pp. 1384–1392, 2007.
- [292] D. T. Covas, R. A. Panepucci, A. M. Fontes, W. A. Silva, M. D. Orellana, M. C. C. Freitas, L. Neder, A. R. D. Santos, L. C. Peres, M. C. Jamur, and M. A. Zago, "Multipotent mesenchymal stromal cells obtained from diverse human tissues share functional properties and gene-expression profile with CD146 + perivascular cells and fibroblasts," *Exp. Hematol.*, vol. 36, no. 5, pp. 642–654, 2008.
- [293] A. Sorrentino, M. Ferracin, G. Castelli, M. Biffoni, G. Tomaselli, M. Baiocchi, A. Fatica, M. Negrini, C. Peschle, and M. Valtieri, "Isolation and characterization of CD146+ multipotent mesenchymal stromal cells," *Exp. Hematol.*, vol. 36, no. 8, pp. 1035–1046, 2008.
- [294] J. Xu, W. Wang, Y. Kapila, J. Lotz, and S. Kapila, "Multiple differentiation capacity of STRO-1+/CD146+ PDL mesenchymal progenitor cells.," *Stem Cells Dev.*, vol. 18, no. 3, pp. 487–496, 2009.
- [295] E. Taira, K. Kohama, Y. Tsukamoto, S. Okumura, and N. Miki, "Characterization of Gicerin/MUC18/CD146 in the Rat Nervous System," *J. Cell. Physiol.*, vol. 198, no. 3, pp. 377–387, 2004.
- [296] Y. Tsukamoto, E. Taira, T. Kotani, J. Yamate, S. Wada, N. Takaha, N. Miki, and S. Sakuma, "Involvement of gicerin, a cell adhesion molecule, in tracheal development and regeneration.," *Cell Growth Differ.*, vol. 7, no. 12, pp. 1761–1767, 1996.
- [297] N. Takaha, E. Taira, H. Taniura, T. Nagino, Y. Tsukamoto, T. Kotani, T. Matsumoto, S. Sakuma, and N. Miki, "Expression of gicerin in development, oncogenesis and regeneration of the chick kidney," *Differentiation*, vol. 58, no. 5, pp. 313–320, 1995.
- [298] Y. Tsukamoto, E. Taira, N. Miki, and F. Sasaki, "The role of gicerin, a novel cell adhesion molecule, in development, regeneration and neoplasia," *Histology and Histopathology*, vol. 16, no. 2, pp. 563–571, 2001.
- [299] Y. Tsukamoto, T. Matsumoto, E. Taira, T. Kotani, J. Yamate, N. Takaha, R. Tatesaki, T. Namikawa, N. Miki, and S. Sakuma, "Adhesive activity of gicerin, a cell-adhesion molecule, in kidneys and nephroblastomas of chickens," *Cell Tissue Res.*, vol. 292, no. 1, pp. 137–142, 1998.
- [300] Q. Zeng, W. Li, D. Lu, Z. Wu, H. Duan, Y. Luo, J. Feng, D. Yang, L. Fu, and X. Yan, "CD146, an epithelial-mesenchymal transition inducer, is associated with triple-negative breast cancer.," *Proc. Natl. Acad. Sci. U. S. A.*, pp. 1–6, Dec. 2011.

- [301] R. Anderson, K. Schaible, J. Heasman, and C. Wylie, "Expression of the homophilic adhesion molecule, Ep-CAM, in the mammalian germ line.," *J. Reprod. Fertil.*, vol. 116, no. 2, pp. 379–384, 1999.
- [302] B. González, S. Denzel, B. Mack, M. Conrad, and O. Gires, "EpCAM is involved in maintenance of the murine embryonic stem cell phenotype.," *Stem Cells*, vol. 27, no. 8, pp. 1782–91, Aug. 2009.
- [303] D. Maetzel, S. Denzel, B. Mack, M. Canis, P. Went, M. Benk, C. Kieu, P. Papior, P. A. Baeuerle, M. Munz, and O. Gires, "Nuclear signalling by tumour-associated antigen EpCAM.," *Nat. Cell Biol.*, vol. 11, no. 2, pp. 162–171, 2009.
- [304] Y. Yarden, W. J. Kuang, T. Yang-Feng, L. Coussens, S. Munemitsu, T. J. Dull, E. Chen, J. Schlessinger, U. Francke, and A. Ullrich, "Human proto-oncogene c-kit: a new cell surface receptor tyrosine kinase for an unidentified ligand.," *EMBO J.*, vol. 6, no. 11, pp. 3341–3351, 1987.
- [305] C. E. Edling and B. Hallberg, "c-Kit-A hematopoietic cell essential receptor tyrosine kinase," *International Journal of Biochemistry and Cell Biology*, vol. 39, no. 11, pp. 1995–1998, 2007.
- [306] P. E. Høyer, A. G. Byskov, and K. Møllgård, "Stem cell factor and c-Kit in human primordial germ cells and fetal ovaries," in *Molecular and Cellular Endocrinology*, 2005, vol. 234, no. 1–2, pp. 1–10.
- [307] K. G. Leong, B.-E. Wang, L. Johnson, and W.-Q. Gao, "Generation of a prostate from a single adult stem cell.," *Nature*, vol. 456, no. 7223, pp. 804–808, 2008.
- [308] Y. Kitamura and S. Hirota, "Kit as a human oncogenic tyrosine kinase," *Cellular and Molecular Life Sciences*, vol. 61, no. 23, pp. 2924–2931, 2004.
- [309] M. Miettinen and J. Lasota, "Gastrointestinal stromal tumors (GISTs): Definition, occurrence, pathology, differential diagnosis and molecular genetics," *Polish Journal of Pathology*, vol. 54, no. 1, pp. 3–24, 2003.
- [310] L. Luo, J. Zeng, B. Liang, Z. Zhao, L. Sun, D. Cao, J. Yang, and K. Shen, "Ovarian cancer cells with the CD117 phenotype are highly tumorigenic and are related to chemotherapy outcome," *Exp. Mol. Pathol.*, vol. 91, no. 2, pp. 596–602, 2011.
- [311] S. Krüger, K. Sotlar, I. Kausch, and H.-P. Horny, "Expression of KIT (CD117) in renal cell carcinoma and renal oncocytoma.," *Oncology*, vol. 68, no. 2–3, pp. 269–75, 2005.
- [312] A. Vassilopoulos, C. Chisholm, T. Lahusen, H. Zheng, and C.-X. Deng, "A critical role of CD29 and CD49f in mediating metastasis for cancer-initiating cells isolated from a Brca1-associated mouse model of breast cancer.," *Oncogene*, vol. 33, no. 47, pp. 5477–82, Nov. 2014.
- [313] F.-J. Lv, R. S. Tuan, K. M. C. Cheung, and V. Y. L. Leung, "Concise review: the surface markers and identity of human mesenchymal stem cells.," *Stem Cells*, vol. 32, no. 6, pp. 1408–19, Jun. 2014.
- [314] L. Antonioli, P. Pacher, E. S. Vizi, and G. Haskó, "CD39 and CD73 in immunity and inflammation.," *Trends Mol. Med.*, vol. 19, no. 6, pp. 355–67, Jun. 2013.
- [315] N. Espagnolle, F. Guilloton, F. Deschaseaux, M. Gadelorge, L. Sensébé, and P. Bourin, "CD146 expression on mesenchymal stem cells is associated with

- their vascular smooth muscle commitment,” *J. Cell. Mol. Med.*, vol. 18, no. 1, pp. 104–14, Jan. 2014.
- [316] S. R. Woo, Y. T. Oh, J. Y. An, B. G. Kang, D.-H. Nam, and K. M. Joo, “Glioblastoma specific antigens, GD2 and CD90, are not involved in cancer stemness,” *Anat. Cell Biol.*, vol. 48, no. 1, pp. 44–53, Mar. 2015.
- [317] O. G. Davies, P. R. Cooper, R. M. Shelton, A. J. Smith, and B. A. Scheven, “Isolation of adipose and bone marrow mesenchymal stem cells using CD29 and CD90 modifies their capacity for osteogenic and adipogenic differentiation,” *J. Tissue Eng.*, vol. 6, p. 2041731415592356.
- [318] J. Fogh, “Cultivation, characterization, and identification of human tumor cells with emphasis on kidney, testis, and bladder tumors,” *Natl. Cancer Inst. Monogr.*, no. 49, pp. 5–9, 1978.
- [319] F. D. S. E. Melo, L. Vermeulen, E. Fessler, and J. P. Medema, “Cancer heterogeneity—a multifaceted view,” *EMBO Rep.*, vol. 14, no. 8, pp. 686–695, 2013.
- [320] E. Burgermeister, M. Liscovitch, C. Röcken, R. M. Schmid, and M. P. a Ebert, “Caveats of caveolin-1 in cancer progression,” *Cancer Lett.*, vol. 268, no. 2, pp. 187–201, Sep. 2008.
- [321] J.-F. Jasmin, M. Yang, L. Iacovitti, and M. P. Lisanti, “Genetic ablation of caveolin-1 increases neural stem cell proliferation in the subventricular zone (SVZ) of the adult mouse brain,” *Cell Cycle*, vol. 8, no. 23, pp. 3978–83, Dec. 2009.
- [322] F. Sotgia, T. M. Williams, A. W. Cohen, C. Minetti, R. G. Pestell, and M. P. Lisanti, “Caveolin-1-deficient mice have an increased mammary stem cell population with upregulation of Wnt/beta-catenin signaling,” *Cell Cycle*, vol. 4, no. 12, pp. 1808–16, Dec. 2005.
- [323] N. Case, Z. Xie, B. Sen, M. Styner, M. Zou, C. O’Conor, M. Horowitz, and J. Rubin, “Mechanical activation of β -catenin regulates phenotype in adult murine marrow-derived mesenchymal stem cells,” *J. Orthop. Res.*, vol. 28, no. 11, pp. 1531–8, Nov. 2010.
- [324] R. A. Samarasinghe, R. Di Maio, D. Volonte, F. Galbiati, M. Lewis, G. Romero, and D. B. DeFranco, “Nongenomic glucocorticoid receptor action regulates gap junction intercellular communication and neural progenitor cell proliferation,” *Proc. Natl. Acad. Sci. U. S. A.*, vol. 108, no. 40, pp. 16657–62, Oct. 2011.
- [325] N. Baker, G. Zhang, Y. You, and R. S. Tuan, “Caveolin-1 regulates proliferation and osteogenic differentiation of human mesenchymal stem cells,” *J. Cell. Biochem.*, no. July, Jul. 2012.
- [326] J.-S. Park, H.-Y. Kim, H.-W. Kim, G.-N. Chae, H.-T. Oh, J.-Y. Park, H. Shim, M. Seo, E.-Y. Shin, E.-G. Kim, S. C. Park, and S.-J. Kwak, “Increased caveolin-1, a cause for the declined adipogenic potential of senescent human mesenchymal stem cells,” *Mech. Ageing Dev.*, vol. 126, no. 5, pp. 551–9, May 2005.
- [327] L. Bai, G. Shi, L. Zhang, F. Guan, Y. Ma, Q. Li, Y.-S. Cong, and L. Zhang, “Cav-1 deletion impaired hematopoietic stem cell function,” *Cell Death Dis.*, vol. 5, p. e1140, 2014.
- [328] M. Y. Lee, J. M. Ryu, S. H. Lee, J. H. Park, and H. J. Han, “Lipid rafts play an

- important role for maintenance of embryonic stem cell self-renewal.," *J. Lipid Res.*, vol. 51, no. 8, pp. 2082–9, Aug. 2010.
- [329] J. H. Park, J. M. Ryu, and H. J. Han, "Involvement of caveolin-1 in fibronectin-induced mouse embryonic stem cell proliferation: role of FAK, RhoA, PI3K/Akt, and ERK 1/2 pathways.," *J. Cell. Physiol.*, vol. 226, no. 1, pp. 267–75, Jan. 2011.
- [330] J. H. Park, M. Y. Lee, and H. J. Han, "A potential role for caveolin-1 in estradiol-17beta-induced proliferation of mouse embryonic stem cells: involvement of Src, PI3K/Akt, and MAPKs pathways.," *Int. J. Biochem. Cell Biol.*, vol. 41, no. 3, pp. 659–65, Mar. 2009.
- [331] J. H. Park and H. J. Han, "Caveolin-1 plays important role in EGF-induced migration and proliferation of mouse embryonic stem cells: involvement of PI3K/Akt and ERK.," *Am. J. Physiol. Cell Physiol.*, vol. 297, no. 4, pp. C935–44, Oct. 2009.
- [332] M. Y. Lee, S. H. Lee, J. H. Park, and H. J. Han, "Interaction of galectin-1 with caveolae induces mouse embryonic stem cell proliferation through the Src, ERas, Akt and mTOR signaling pathways.," *Cell. Mol. Life Sci.*, vol. 66, no. 8, pp. 1467–78, Apr. 2009.
- [333] N. Sasaki, M. Shinomi, K. Hirano, K. Ui-Tei, and S. Nishihara, "LacdiNac (GalNAc β 1-4GlcNAc) contributes to self-renewal of mouse embryonic stem cells by regulating leukemia inhibitory factor/STAT3 signaling.," *Stem Cells*, vol. 29, no. 4, pp. 641–50, Apr. 2011.
- [334] S. Wang, Q. Kan, Y. Sun, R. Han, G. Zhang, T. Peng, and Y. Jia, "Caveolin-1 regulates neural differentiation of rat bone mesenchymal stem cells into neurons by modulating Notch signaling.," *Int. J. Dev. Neurosci.*, pp. 1–6, Sep. 2012.
- [335] J. Rubin, Z. Schwartz, B. D. Boyan, X. Fan, N. Case, B. Sen, M. Drab, D. Smith, M. Aleman, K. L. Wong, H. Yao, H. Jo, and T. S. Gross, "Caveolin-1 knockout mice have increased bone size and stiffness.," *J. Bone Miner. Res.*, vol. 22, no. 9, pp. 1408–18, Sep. 2007.
- [336] C. Song, Z. Guo, Q. Ma, Z. Chen, Z. Liu, H. Jia, and G. Dang, "Simvastatin induces osteoblastic differentiation and inhibits adipocytic differentiation in mouse bone marrow stromal cells.," *Biochem. Biophys. Res. Commun.*, vol. 308, no. 3, pp. 458–62, Aug. 2003.
- [337] H. T. Kha, B. Basseri, D. Shouhed, J. Richardson, S. Tetradis, T. J. Hahn, and F. Parhami, "Oxysterols regulate differentiation of mesenchymal stem cells: pro-bone and anti-fat.," *J. Bone Miner. Res.*, vol. 19, no. 5, pp. 830–40, May 2004.
- [338] D. A. Rodriguez, J. C. Tapia, J. G. Fernandez, V. A. Torres, N. Muñoz, D. Galleguillos, L. Leyton, and A. F. G. Quest, "Caveolin-1-mediated suppression of cyclooxygenase-2 via a beta-catenin-Tcf/Lef-dependent transcriptional mechanism reduced prostaglandin E2 production and survivin expression.," *Mol. Biol. Cell*, vol. 20, no. 8, pp. 2297–310, Apr. 2009.
- [339] F. Galbiati, D. Volonte, A. M. Brown, D. E. Weinstein, A. Ben-Ze'ev, R. G. Pestell, and M. P. Lisanti, "Caveolin-1 expression inhibits Wnt/beta-catenin/Lef-1 signaling by recruiting beta-catenin to caveolae membrane domains.," *J. Biol. Chem.*, vol. 275, no. 30, pp. 23368–77, Jul. 2000.
- [340] B. Razani, X. L. Zhang, M. Bitzer, G. von Gersdorff, E. P. Böttinger, and M. P.

- Lisanti, "Caveolin-1 regulates transforming growth factor (TGF)-beta/SMAD signaling through an interaction with the TGF-beta type I receptor.," *J. Biol. Chem.*, vol. 276, no. 9, pp. 6727–38, Mar. 2001.
- [341] S. Kim, Y. Lee, J. E. Seo, K. H. Cho, and J. H. Chung, "Caveolin-1 increases basal and TGF-beta1-induced expression of type I procollagen through PI-3 kinase/Akt/mTOR pathway in human dermal fibroblasts.," *Cell. Signal.*, vol. 20, no. 7, pp. 1313–9, Jul. 2008.
- [342] A. Nohe, E. Keating, T. M. Underhill, P. Knaus, and N. O. Petersen, "Dynamics and interaction of caveolin-1 isoforms with BMP-receptors.," *J. Cell Sci.*, vol. 118, no. Pt 3, pp. 643–50, Feb. 2005.
- [343] J. W. Wertz and P. M. Bauer, "Caveolin-1 regulates BMPRII localization and signaling in vascular smooth muscle cells.," *Biochem. Biophys. Res. Commun.*, vol. 375, no. 4, pp. 557–61, Oct. 2008.
- [344] N. Yongsanguanchai, V. Pongrakhananon, A. Mutirangura, Y. Rojanasakul, and P. Chanvorachote, "Nitric oxide induces cancer stem cell-like phenotypes in human lung cancer cells.," *Am. J. Physiol. Cell Physiol.*, vol. 308, no. 2, pp. C89–100, Jan. 2015.
- [345] A. F. Salem, G. Bonuccelli, G. Bevilacqua, H. Arafat, R. G. Pestell, F. Sotgia, and M. P. Lisanti, "Caveolin-1 promotes pancreatic cancer cell differentiation and restores membranous E-cadherin via suppression of the epithelial-mesenchymal transition.," *Cell Cycle*, vol. 10, no. 21, pp. 3692–700, Nov. 2011.
- [346] C. Sagrinati, G. S. Netti, B. Mazzinghi, E. Lazzeri, F. Liotta, F. Frosali, E. Ronconi, C. Meini, M. Gacci, R. Squecco, M. Carini, L. Gesualdo, F. Francini, E. Maggi, F. Annunziato, L. Lasagni, M. Serio, S. Romagnani, and P. Romagnani, "Isolation and characterization of multipotent progenitor cells from the Bowman's capsule of adult human kidneys.," *J. Am. Soc. Nephrol.*, vol. 17, no. 9, pp. 2443–56, Oct. 2006.
- [347] Y. Luo, C. Zheng, J. Zhang, D. Lu, J. Zhuang, S. Xing, J. Feng, D. Yang, and X. Yan, "Recognition of CD146 as an ERM-binding protein offers novel mechanisms for melanoma cell migration.," *Oncogene*, vol. 31, no. 3, pp. 306–21, Jan. 2012.
- [348] G.-F. Zeng, S.-X. Cai, and G.-J. Wu, "Up-regulation of METCAM/MUC18 promotes motility, invasion, and tumorigenesis of human breast cancer cells.," *BMC Cancer*, vol. 11, p. 113, 2011.
- [349] Z. Wu, Z. Wu, J. Li, X. Yang, Y. Wang, Y. Yu, J. Ye, C. Xu, W. Qin, and Z. Zhang, "MCAM is a novel metastasis marker and regulates spreading, apoptosis and invasion of ovarian cancer cells.," *Tumour Biol.*, vol. 33, no. 5, pp. 1619–28, Oct. 2012.
- [350] K. Ueno, H. Hirata, S. Majid, Z. L. Tabatabai, Y. Hinoda, and R. Dahiya, "IGFBP-4 activates the Wnt/beta-catenin signaling pathway and induces M-CAM expression in human renal cell carcinoma.," *Int. J. Cancer*, vol. 129, no. 10, pp. 2360–9, Nov. 2011.
- [351] K. Ueda, S. Ogasawara, J. Akiba, M. Nakayama, K. Todoroki, K. Ueda, S. Sanada, S. Suekane, M. Noguchi, K. Matsuoka, and H. Yano, "Aldehyde dehydrogenase 1 identifies cells with cancer stem cell-like properties in a human renal cell carcinoma cell line.," *PLoS One*, vol. 8, no. 10, p. e75463, 2013.

- [352] M. C. Cabrera, R. E. Hollingsworth, and E. M. Hurt, "Cancer stem cell plasticity and tumor hierarchy.," *World J. Stem Cells*, vol. 7, no. 1, pp. 27–36, Jan. 2015.
- [353] C. Calabrese, H. Poppleton, M. Kocak, T. L. Hogg, C. Fuller, B. Hamner, E. Y. Oh, M. W. Gaber, D. Finklestein, M. Allen, A. Frank, I. T. Bayazitov, S. S. Zakharenko, A. Gajjar, A. Davidoff, and R. J. Gilbertson, "A perivascular niche for brain tumor stem cells.," *Cancer Cell*, vol. 11, no. 1, pp. 69–82, Jan. 2007.
- [354] C. Micucci, G. Matacchione, D. Valli, S. Orciari, and A. Catalano, "HIF2 α is involved in the expansion of CXCR4-positive cancer stem-like cells in renal cell carcinoma.," *Br. J. Cancer*, vol. 113, no. 8, pp. 1178–1185, 2015.
- [355] J. Shen, W. Lee, Y. Li, C. F. Lau, K. M. Ng, M. L. Fung, and K. J. Liu, "Interaction of caveolin-1, nitric oxide, and nitric oxide synthases in hypoxic human SK-N-MC neuroblastoma cells.," *J. Neurochem.*, vol. 107, no. 2, pp. 478–487, Aug. 2008.
- [356] Y. Li, J. Luo, W.-M. Lau, G. Zheng, S. Fu, T.-T. Wang, H.-P. Zeng, K.-F. So, S. K. Chung, Y. Tong, K. Liu, and J. Shen, "Caveolin-1 plays a crucial role in inhibiting neuronal differentiation of neural stem/progenitor cells via VEGF signaling-dependent pathway.," *PLoS One*, vol. 6, no. 8, p. e22901, 2011.
- [357] N. Takebe, L. Miele, P. J. Harris, W. Jeong, H. Bando, M. Kahn, S. X. Yang, and S. P. Ivy, "Targeting Notch, Hedgehog, and Wnt pathways in cancer stem cells: clinical update.," *Nat. Rev. Clin. Oncol.*, vol. 12, no. 8, pp. 445–64, Aug. 2015.
- [358] C. Y. Logan and R. Nusse, "The Wnt signaling pathway in development and disease.," *Annu. Rev. Cell Dev. Biol.*, vol. 20, pp. 781–810, 2004.
- [359] H. Clevers, "Wnt/beta-catenin signaling in development and disease.," *Cell*, vol. 127, no. 3, pp. 469–80, Nov. 2006.
- [360] A. J. Chien, W. H. Conrad, and R. T. Moon, "A Wnt survival guide: from flies to human disease.," *J. Invest. Dermatol.*, vol. 129, no. 7, pp. 1614–27, Jul. 2009.
- [361] X. He, M. Semenov, K. Tamai, and X. Zeng, "LDL receptor-related proteins 5 and 6 in Wnt/beta-catenin signaling: arrows point the way.," *Development*, vol. 131, no. 8, pp. 1663–77, Apr. 2004.
- [362] N. Itasaki, C. M. Jones, S. Mercurio, A. Rowe, P. M. Domingos, J. C. Smith, and R. Krumlauf, "Wise, a context-dependent activator and inhibitor of Wnt signalling.," *Development*, vol. 130, no. 18, pp. 4295–305, Sep. 2003.
- [363] C. Gao and Y.-G. Chen, "Dishevelled: The hub of Wnt signaling.," *Cell. Signal.*, vol. 22, no. 5, pp. 717–27, May 2010.
- [364] R. Habas and I. B. Dawid, "Dishevelled and Wnt signaling: is the nucleus the final frontier?," *J. Biol.*, vol. 4, no. 1, p. 2, 2005.
- [365] L. Arce, N. N. Yokoyama, and M. L. Waterman, "Diversity of LEF/TCF action in development and disease.," *Oncogene*, vol. 25, no. 57, pp. 7492–504, Dec. 2006.
- [366] J. Behrens, "Control of beta-catenin signaling in tumor development.," *Ann. N. Y. Acad. Sci.*, vol. 910, pp. 21–33; discussion 33–5, Jun. 2000.
- [367] I. Malanchi, H. Peinado, D. Kassen, T. Hussenet, D. Metzger, P. Chambon,

- M. Huber, D. Hohl, A. Cano, W. Birchmeier, and J. Huelsken, "Cutaneous cancer stem cell maintenance is dependent on beta-catenin signalling.," *Nature*, vol. 452, no. 7187, pp. 650–3, Apr. 2008.
- [368] J. Xu, J. R. Prosperi, N. Choudhury, O. I. Olopade, and K. H. Goss, "β-Catenin is required for the tumorigenic behavior of triple-negative breast cancer cells.," *PLoS One*, vol. 10, no. 2, p. e0117097, 2015.
- [369] G.-B. Jang, J.-Y. Kim, S.-D. Cho, K.-S. Park, J.-Y. Jung, H.-Y. Lee, I.-S. Hong, and J.-S. Nam, "Blockade of Wnt/β-catenin signaling suppresses breast cancer metastasis by inhibiting CSC-like phenotype.," *Sci. Rep.*, vol. 5, p. 12465, 2015.
- [370] X.-M. Mo, H.-H. Li, M. Liu, and Y.-T. Li, "Downregulation of GSK3β by miR-544a to maintain self-renewal ability of lung cancer stem cells.," *Oncol. Lett.*, vol. 8, no. 4, pp. 1731–1734, Oct. 2014.
- [371] J. Su, S. Wu, H. Wu, L. Li, and T. Guo, "CD44 is functionally crucial for driving lung cancer stem cells metastasis through Wnt/β-catenin-FoxM1-Twist signaling.," *Mol. Carcinog.*, Dec. 2015.
- [372] Y.-W. Chang, Y.-J. Su, M. Hsiao, K.-C. Wei, W.-H. Lin, C.-L. Liang, S.-C. Chen, and J.-L. Lee, "Diverse Targets of β-Catenin during the Epithelial-Mesenchymal Transition Define Cancer Stem Cells and Predict Disease Relapse.," *Cancer Res.*, vol. 75, no. 16, pp. 3398–410, Aug. 2015.
- [373] X. Zhu, W. Wang, X. Zhang, J. Bai, G. Chen, L. Li, and M. Li, "All-Trans Retinoic Acid-Induced Deficiency of the Wnt/β-Catenin Pathway Enhances Hepatic Carcinoma Stem Cell Differentiation.," *PLoS One*, vol. 10, no. 11, p. e0143255, 2015.
- [374] Y. S. Kim, Y. K. Kang, J. B. Kim, S. A. Han, K. I. Kim, and S. R. Paik, "beta-catenin expression and mutational analysis in renal cell carcinomas.," *Pathol. Int.*, vol. 50, no. 9, pp. 725–30, Sep. 2000.
- [375] O. J. Sansom, D. F. R. Griffiths, K. R. Reed, D. J. Winton, and A. R. Clarke, "Apc deficiency predisposes to renal carcinoma in the mouse.," *Oncogene*, vol. 24, no. 55, pp. 8205–10, Dec. 2005.
- [376] C.-N. Qian, J. Knol, P. Igarashi, F. Lin, U. Zylstra, B. T. Teh, and B. O. Williams, "Cystic renal neoplasia following conditional inactivation of apc in mouse renal tubular epithelium.," *J. Biol. Chem.*, vol. 280, no. 5, pp. 3938–45, Feb. 2005.
- [377] C. Battagli, R. G. Uzzo, E. Dulaimi, I. Ibanez de Caceres, R. Krassenstein, T. Al-Saleem, R. E. Greenberg, and P. Cairns, "Promoter hypermethylation of tumor suppressor genes in urine from kidney cancer patients.," *Cancer Res.*, vol. 63, no. 24, pp. 8695–9, Dec. 2003.
- [378] T. Kojima, T. Shimazui, S. Hinotsu, A. Joraku, T. Oikawa, K. Kawai, R. Horie, H. Suzuki, R. Nagashima, K. Yoshikawa, T. Michiue, M. Asashima, H. Akaza, and K. Uchida, "Decreased expression of CXXC4 promotes a malignant phenotype in renal cell carcinoma by activating Wnt signaling.," *Oncogene*, vol. 28, no. 2, pp. 297–305, Jan. 2009.
- [379] Y. Awakura, E. Nakamura, N. Ito, T. Kamoto, and O. Ogawa, "Methylation-associated silencing of SFRP1 in renal cell carcinoma.," *Oncol. Rep.*, vol. 20, no. 5, pp. 1257–63, Nov. 2008.
- [380] H. Hirata, Y. Hinoda, K. Nakajima, K. Kawamoto, N. Kikuno, K. Kawakami, S.

- Yamamura, K. Ueno, S. Majid, S. Saini, N. Ishii, and R. Dahiya, "Wnt antagonist gene DKK2 is epigenetically silenced and inhibits renal cancer progression through apoptotic and cell cycle pathways.," *Clin. Cancer Res.*, vol. 15, no. 18, pp. 5678–87, Sep. 2009.
- [381] K. Kawakami, H. Hirata, S. Yamamura, N. Kikuno, S. Saini, S. Majid, Y. Tanaka, K. Kawamoto, H. Enokida, M. Nakagawa, and R. Dahiya, "Functional significance of Wnt inhibitory factor-1 gene in kidney cancer.," *Cancer Res.*, vol. 69, no. 22, pp. 8603–10, Nov. 2009.
- [382] W. Fan, J. Huang, and H. Xiao, "Histone deacetylase 10 suppresses proliferation and invasion by inhibiting the phosphorylation of β -catenin and serves as an independent prognostic factor for human clear cell renal cell carcinoma.," *Int. J. Clin. Exp. Med.*, vol. 8, no. 3, pp. 3734–42, 2015.
- [383] S. A. VON Schulz-Hausmann, L. C. Schmeel, F. C. Schmeel, and I. G. H. Schmidt-Wolf, "Targeting the Wnt/beta-catenin pathway in renal cell carcinoma.," *Anticancer Res.*, vol. 34, no. 8, pp. 4101–8, Aug. 2014.
- [384] E. B. Haura, J. Turkson, and R. Jove, "Mechanisms of disease: Insights into the emerging role of signal transducers and activators of transcription in cancer.," *Nat. Clin. Pract. Oncol.*, vol. 2, no. 6, pp. 315–24, Jun. 2005.
- [385] A. Herrmann, M. Kortylewski, M. Kujawski, C. Zhang, K. Reckamp, B. Armstrong, L. Wang, C. Kowolik, J. Deng, R. Figlin, and H. Yu, "Targeting Stat3 in the myeloid compartment drastically improves the in vivo antitumor functions of adoptively transferred T cells.," *Cancer Res.*, vol. 70, no. 19, pp. 7455–64, Oct. 2010.
- [386] M. Kortylewski and H. Yu, "Role of Stat3 in suppressing anti-tumor immunity.," *Curr. Opin. Immunol.*, vol. 20, no. 2, pp. 228–33, Apr. 2008.
- [387] C.-Y. Chen, D. S. Lee, Y.-T. Yan, C.-N. Shen, S.-M. Hwang, S. T. Lee, and P. C. H. Hsieh, "Bcl3 Bridges LIF-STAT3 to Oct4 Signaling in the Maintenance of Naïve Pluripotency.," *Stem Cells*, Aug. 2015.
- [388] H. Chen, I. Aksoy, F. Gonnot, P. Osteil, M. Aubry, C. Hamela, C. Rognard, A. Hochard, S. Voisin, E. Fontaine, M. Mure, M. Afanassieff, E. Cleroux, S. Guibert, J. Chen, C. Vallot, H. Acloque, C. Genthon, C. Donnadiou, J. De Vos, D. Sanlaville, J.-F. Guérin, M. Weber, L. W. Stanton, C. Rougeulle, B. Pain, P.-Y. Bourillot, and P. Savatier, "Reinforcement of STAT3 activity reprogrammes human embryonic stem cells to naive-like pluripotency.," *Nat. Commun.*, vol. 6, p. 7095, 2015.
- [389] R. Thakur, R. Trivedi, N. Rastogi, M. Singh, and D. P. Mishra, "Inhibition of STAT3, FAK and Src mediated signaling reduces cancer stem cell load, tumorigenic potential and metastasis in breast cancer.," *Sci. Rep.*, vol. 5, p. 10194, 2015.
- [390] S.-H. Moon, D.-K. Kim, Y. Cha, I. Jeon, J. Song, and K.-S. Park, "PI3K/Akt and Stat3 signaling regulated by PTEN control of the cancer stem cell population, proliferation and senescence in a glioblastoma cell line.," *Int. J. Oncol.*, vol. 42, no. 3, pp. 921–8, Mar. 2013.
- [391] H. Yu, H. Lee, A. Herrmann, R. Buettner, and R. Jove, "Revisiting STAT3 signalling in cancer: new and unexpected biological functions," *Nat. Rev. Cancer*, vol. 14, no. 11, pp. 736–746, 2014.
- [392] L. L. C. Marotta, V. Almendro, A. Marusyk, M. Shipitsin, J. Schemme, S. R. Walker, N. Bloushtain-Qimron, J. J. Kim, S. A. Choudhury, R. Maruyama, Z.

- Wu, M. Gönen, L. A. Mulvey, M. O. Bessarabova, S. J. Huh, S. J. Silver, S. Y. Kim, S. Y. Park, H. E. Lee, K. S. Anderson, A. L. Richardson, T. Nikolskaya, Y. Nikolsky, X. S. Liu, D. E. Root, W. C. Hahn, D. A. Frank, and K. Polyak, "The JAK2/STAT3 signaling pathway is required for growth of CD44+/CD24-stem cell-like breast cancer cells in human tumors.," *J. Clin. Invest.*, vol. 121, no. 7, pp. 2723–35, Jul. 2011.
- [393] C.-C. Liu, J.-H. Lin, T.-W. Hsu, K. Su, A. F.-Y. Li, H.-S. Hsu, and S.-C. Hung, "IL-6 enriched lung cancer stem-like cell population by inhibition of cell cycle regulators via DNMT1 upregulation.," *Int. J. Cancer*, vol. 136, no. 3, pp. 547–59, Feb. 2015.
- [394] J. M. Garner, M. Fan, C. H. Yang, Z. Du, M. Sims, A. M. Davidoff, and L. M. Pfeffer, "Constitutive activation of signal transducer and activator of transcription 3 (STAT3) and nuclear factor κ B signaling in glioblastoma cancer stem cells regulates the Notch pathway.," *J. Biol. Chem.*, vol. 288, no. 36, pp. 26167–76, Sep. 2013.
- [395] L. Conti, S. Lanzardo, M. Arigoni, R. Antonazzo, E. Radaelli, D. Cantarella, R. A. Calogero, and F. Cavallo, "The noninflammatory role of high mobility group box 1/Toll-like receptor 2 axis in the self-renewal of mammary cancer stem cells.," *FASEB J.*, vol. 27, no. 12, pp. 4731–44, Dec. 2013.
- [396] J. Jiang, Z. Li, C. Yu, M. Chen, S. Tian, and C. Sun, "MiR-1181 inhibits stem cell-like phenotypes and suppresses SOX2 and STAT3 in human pancreatic cancer.," *Cancer Lett.*, vol. 356, no. 2 Pt B, pp. 962–70, Jan. 2015.
- [397] K. Kamińska, A. M. Czarnecka, B. Escudier, F. Lian, and C. Szczylik, "Interleukin-6 as an emerging regulator of renal cell cancer.," *Urol. Oncol.*, vol. 33, no. 11, pp. 476–85, Nov. 2015.
- [398] A. Horiguchi, M. Oya, T. Shimada, A. Uchida, K. Marumo, and M. Murai, "Activation of signal transducer and activator of transcription 3 in renal cell carcinoma: a study of incidence and its association with pathological features and clinical outcome.," *J. Urol.*, vol. 168, no. 2, pp. 762–5, Aug. 2002.
- [399] A. Horiguchi, M. Oya, K. Marumo, and M. Murai, "STAT3, but not ERKs, mediates the IL-6-induced proliferation of renal cancer cells, ACHN and 769P.," *Kidney Int.*, vol. 61, no. 3, pp. 926–38, Mar. 2002.
- [400] A. Horiguchi, T. Asano, K. Kuroda, A. Sato, J. Asakuma, K. Ito, M. Hayakawa, M. Sumitomo, and T. Asano, "STAT3 inhibitor WP1066 as a novel therapeutic agent for renal cell carcinoma.," *Br. J. Cancer*, vol. 102, no. 11, pp. 1592–9, May 2010.
- [401] B. Chen, M. E. Dodge, W. Tang, J. Lu, Z. Ma, C.-W. Fan, S. Wei, W. Hao, J. Kilgore, N. S. Williams, M. G. Roth, J. F. Amatruda, C. Chen, and L. Lum, "Small molecule-mediated disruption of Wnt-dependent signaling in tissue regeneration and cancer.," *Nat. Chem. Biol.*, vol. 5, no. 2, pp. 100–7, Feb. 2009.
- [402] A. Ferrajoli, S. Faderl, Q. Van, P. Koch, D. Harris, Z. Liu, I. Hazan-Halevy, Y. Wang, H. M. Kantarjian, W. Priebe, and Z. Estrov, "WP1066 disrupts Janus kinase-2 and induces caspase-dependent apoptosis in acute myelogenous leukemia cells.," *Cancer Res.*, vol. 67, no. 23, pp. 11291–9, Dec. 2007.
- [403] J. R. Woodgett, "Molecular cloning and expression of glycogen synthase kinase-3/factor A.," *EMBO J.*, vol. 9, no. 8, pp. 2431–8, Aug. 1990.
- [404] M. Sakaguchi, M. Oka, T. Iwasaki, Y. Fukami, and C. Nishigori, "Role and

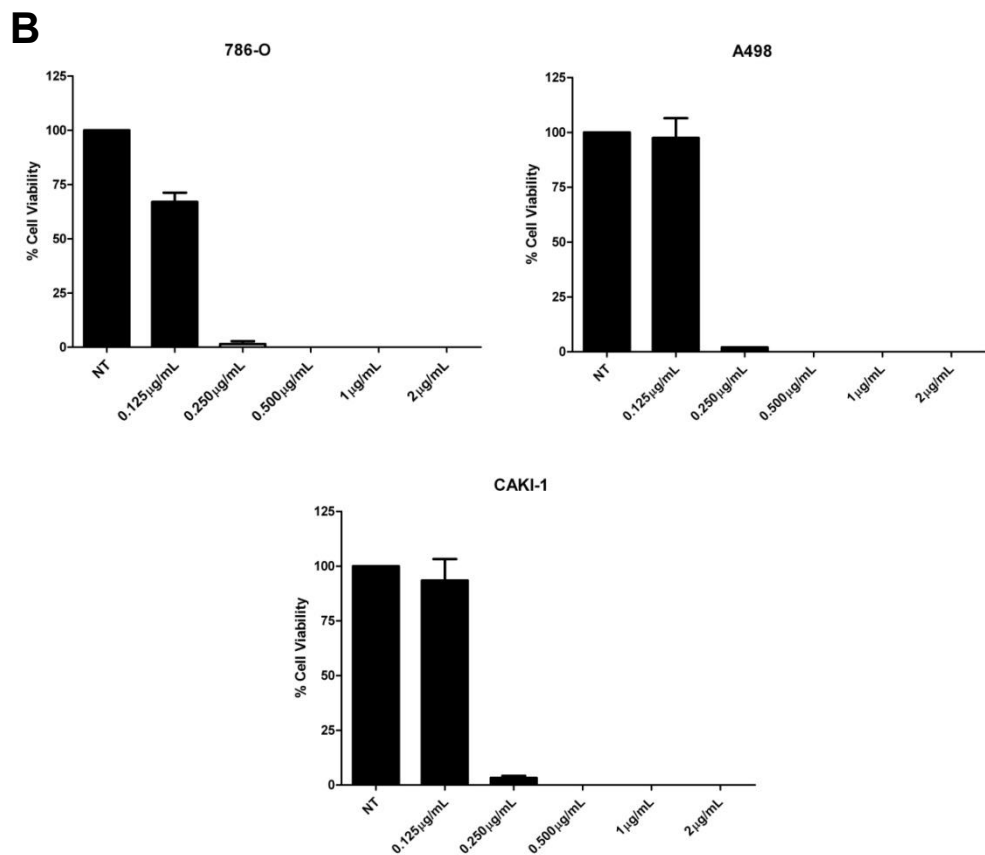
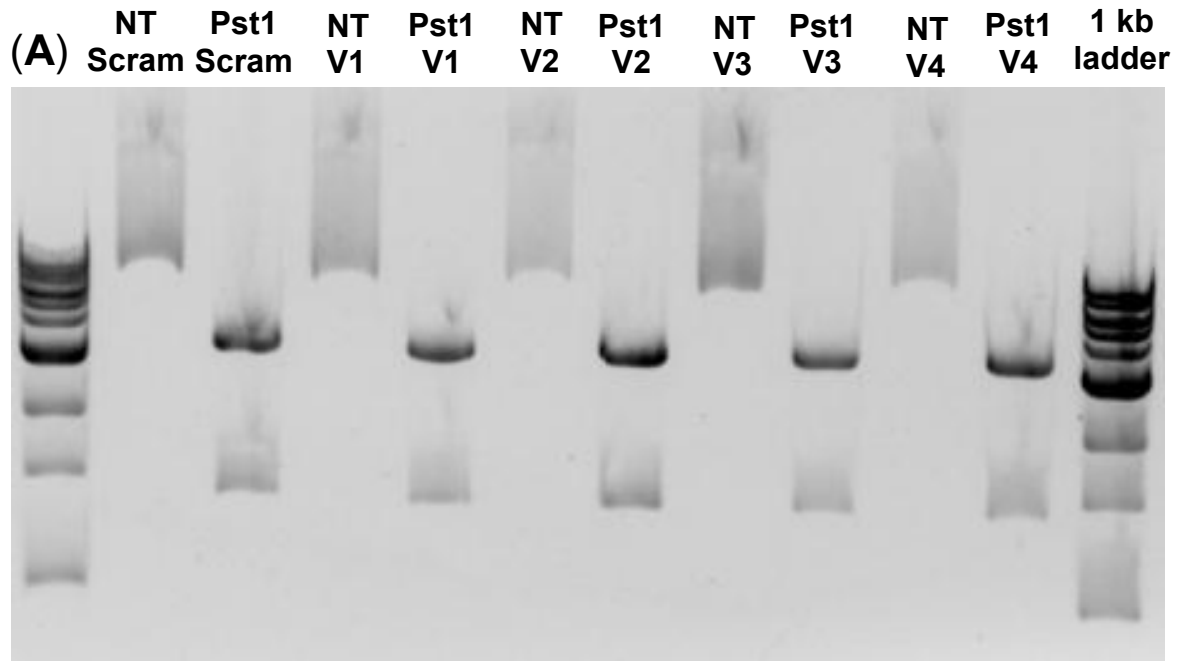
regulation of STAT3 phosphorylation at Ser727 in melanocytes and melanoma cells.," *J. Invest. Dermatol.*, vol. 132, no. 7, pp. 1877–85, Jul. 2012.

- [405] M. Pagano, S. W. Tam, A. M. Theodoras, P. Beer-Romero, G. Del Sal, V. Chau, P. R. Yew, G. F. Draetta, and M. Rolfe, "Role of the ubiquitin-proteasome pathway in regulating abundance of the cyclin-dependent kinase inhibitor p27.," *Science*, vol. 269, no. 5224, pp. 682–5, Aug. 1995.
- [406] D. D. Sarbassov, D. a Guertin, S. M. Ali, and D. M. Sabatini, "Phosphorylation and regulation of Akt/PKB by the rictor-mTOR complex.," *Science*, vol. 307, no. 5712, pp. 1098–101, Feb. 2005.
- [407] S. Y. Shieh, M. Ikeda, Y. Taya, and C. Prives, "DNA damage-induced phosphorylation of p53 alleviates inhibition by MDM2.," *Cell*, vol. 91, no. 3, pp. 325–34, Oct. 1997.
- [408] E. Vander Haar, S.-I. Lee, S. Bandhakavi, T. J. Griffin, and D.-H. Kim, "Insulin signalling to mTOR mediated by the Akt/PKB substrate PRAS40.," *Nat. Cell Biol.*, vol. 9, no. 3, pp. 316–23, Mar. 2007.
- [409] J. R. Thériault, H. Lambert, A. T. Chávez-Zobel, G. Charest, P. Lavigne, and J. Landry, "Essential role of the NH2-terminal WD/EPF motif in the phosphorylation-activated protective function of mammalian Hsp27.," *J. Biol. Chem.*, vol. 279, no. 22, pp. 23463–71, May 2004.
- [410] C. Niehrs, "Function and biological roles of the Dickkopf family of Wnt modulators.," *Oncogene*, vol. 25, no. 57, pp. 7469–81, Dec. 2006.
- [411] B. R. Binder, G. Christ, F. Gruber, N. Grubic, P. Hufnagl, M. Krebs, J. Mihaly, and G. W. Prager, "Plasminogen activator inhibitor 1: physiological and pathophysiological roles.," *News Physiol. Sci.*, vol. 17, pp. 56–61, Apr. 2002.
- [412] T. Matsuda, T. Nakamura, K. Nakao, T. Arai, M. Katsuki, T. Heike, and T. Yokota, "STAT3 activation is sufficient to maintain an undifferentiated state of mouse embryonic stem cells.," *EMBO J.*, vol. 18, no. 15, pp. 4261–9, Aug. 1999.
- [413] A. Horiguchi, M. Oya, K. Marumo, and M. Murai, "STAT3, but not ERKs, mediates the IL-6-induced proliferation of renal cancer cells, ACHN and 769P.," *Kidney Int.*, vol. 61, no. 3, pp. 926–38, Mar. 2002.
- [414] J. Zhou, J. Wulfkühle, H. Zhang, P. Gu, Y. Yang, J. Deng, J. B. Margolick, L. A. Liotta, E. Petricoin, and Y. Zhang, "Activation of the PTEN/mTOR/STAT3 pathway in breast cancer stem-like cells is required for viability and maintenance.," *Proc. Natl. Acad. Sci. U. S. A.*, vol. 104, no. 41, pp. 16158–63, Oct. 2007.
- [415] S. Hara, M. Oya, R. Mizuno, A. Horiguchi, K. Marumo, and M. Murai, "Akt activation in renal cell carcinoma: contribution of a decreased PTEN expression and the induction of apoptosis by an Akt inhibitor.," *Ann. Oncol.*, vol. 16, no. 6, pp. 928–33, Jun. 2005.
- [416] J. E. Jung, H. G. Lee, I. H. Cho, D. H. Chung, S.-H. Yoon, Y. M. Yang, J. W. Lee, S. Choi, J.-W. Park, S.-K. Ye, and M.-H. Chung, "STAT3 is a potential modulator of HIF-1-mediated VEGF expression in human renal carcinoma cells.," *FASEB J.*, vol. 19, no. 10, pp. 1296–8, Aug. 2005.
- [417] D. Wu and W. Pan, "GSK3: a multifaceted kinase in Wnt signaling.," *Trends Biochem. Sci.*, vol. 35, no. 3, pp. 161–8, Mar. 2010.

- [418] N. V. Varlakhanova, R. F. Cotterman, W. N. DeVries, J. Morgan, L. R. Donahue, S. Murray, B. B. Knowles, and P. S. Knoepfler, "myc maintains embryonic stem cell pluripotency and self-renewal.," *Differentiation.*, vol. 80, no. 1, pp. 9–19, Jul. 2010.
- [419] Z. Wang, N. Wang, W. Li, P. Liu, Q. Chen, H. Situ, S. Zhong, L. Guo, Y. Lin, J. Shen, and J. Chen, "Caveolin-1 mediates chemoresistance in breast cancer stem cells via β -catenin/ABCG2 signaling pathway.," *Carcinogenesis*, vol. 35, no. 10, pp. 2346–56, Oct. 2014.
- [420] H. Yamamoto, H. Sakane, H. Yamamoto, T. Michiue, and A. Kikuchi, "Wnt3a and Dkk1 regulate distinct internalization pathways of LRP6 to tune the activation of beta-catenin signaling.," *Dev. Cell*, vol. 15, no. 1, pp. 37–48, Jul. 2008.
- [421] H. Yamamoto, H. Komekado, and A. Kikuchi, "Caveolin is necessary for Wnt-3a-dependent internalization of LRP6 and accumulation of beta-catenin.," *Dev. Cell*, vol. 11, no. 2, pp. 213–23, Aug. 2006.
- [422] V. F. Taelman, R. Dobrowolski, J.-L. Plouhinec, L. C. Fuentealba, P. P. Vorwald, I. Gumper, D. D. Sabatini, and E. M. De Robertis, "Wnt signaling requires sequestration of glycogen synthase kinase 3 inside multivesicular endosomes.," *Cell*, vol. 143, no. 7, pp. 1136–48, Dec. 2010.
- [423] S. Zhang, Y. Li, Y. Wu, K. Shi, L. Bing, and J. Hao, "Wnt/ β -catenin signaling pathway upregulates c-Myc expression to promote cell proliferation of P19 teratocarcinoma cells.," *Anat. Rec. (Hoboken).*, vol. 295, no. 12, pp. 2104–13, Dec. 2012.
- [424] Y. Li, Q. Gao, G. Yin, X. Ding, and J. Hao, "WNT/ β -catenin-signaling pathway stimulates the proliferation of cultured adult human Sertoli cells via upregulation of C-myc expression.," *Reprod. Sci.*, vol. 19, no. 11, pp. 1232–40, Nov. 2012.
- [425] X. Ling and R. B. Arlinghaus, "Knockdown of STAT3 expression by RNA interference inhibits the induction of breast tumors in immunocompetent mice.," *Cancer Res.*, vol. 65, no. 7, pp. 2532–6, Apr. 2005.
- [426] N. Kiuchi, K. Nakajima, M. Ichiba, T. Fukada, M. Narimatsu, K. Mizuno, M. Hibi, and T. Hirano, "STAT3 is required for the gp130-mediated full activation of the c-myc gene.," *J. Exp. Med.*, vol. 189, no. 1, pp. 63–73, Jan. 1999.
- [427] M.-L. Wang, S.-H. Chiou, and C.-W. Wu, "Targeting cancer stem cells: emerging role of Nanog transcription factor.," *Onco. Targets. Ther.*, vol. 6, pp. 1207–20, 2013.
- [428] P. Zhu, M. J. Tan, R.-L. Huang, C. K. Tan, H. C. Chong, M. Pal, C. R. I. Lam, P. Boukamp, J. Y. Pan, S. H. Tan, S. Kersten, H. Y. Li, J. L. Ding, and N. S. Tan, "Angiopoietin-like 4 protein elevates the prosurvival intracellular O₂(-):H₂O₂ ratio and confers anoikis resistance to tumors.," *Cancer Cell*, vol. 19, no. 3, pp. 401–15, Mar. 2011.
- [429] L. S. Terada and F. E. Nwariaku, "Escaping Anoikis through ROS: ANGPTL4 controls integrin signaling through Nox1.," *Cancer Cell*, vol. 19, no. 3, pp. 297–9, Mar. 2011.
- [430] L. Chen, J. Fan, H. Chen, Z. Meng, Z. Chen, P. Wang, and L. Liu, "The IL-8/CXCR1 axis is associated with cancer stem cell-like properties and correlates with clinical prognosis in human pancreatic cancer cases.," *Sci. Rep.*, vol. 4, p. 5911, 2014.

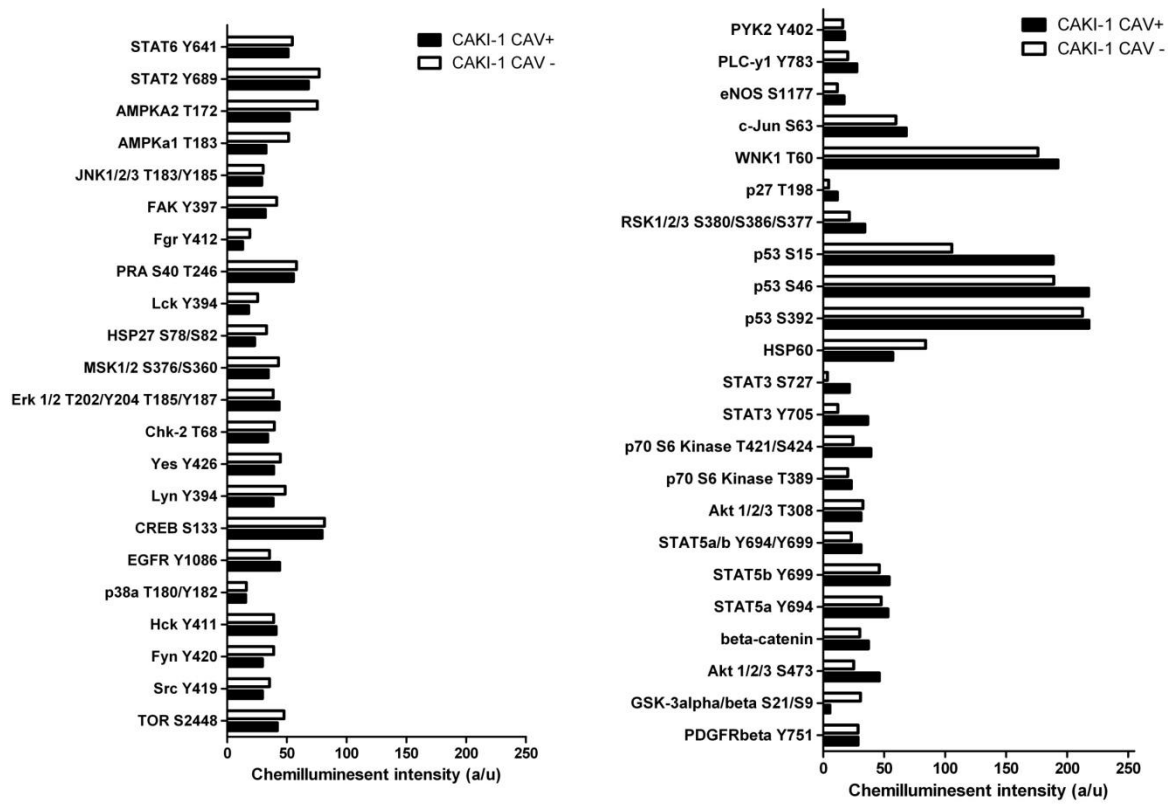
- [431] C. Ginestier, S. Liu, M. E. Diebel, H. Korkaya, M. Luo, M. Brown, J. Wicinski, O. Cabaud, E. Charafe-Jauffret, D. Birnbaum, J.-L. Guan, G. Dontu, and M. S. Wicha, "CXCR1 blockade selectively targets human breast cancer stem cells in vitro and in xenografts.," *J. Clin. Invest.*, vol. 120, no. 2, pp. 485–97, Feb. 2010.
- [432] J. K. Singh, G. Farnie, N. J. Bundred, B. M. Simões, A. Shergill, G. Landberg, S. J. Howell, and R. B. Clarke, "Targeting CXCR1/2 significantly reduces breast cancer stem cell activity and increases the efficacy of inhibiting HER2 via HER2-dependent and -independent mechanisms.," *Clin. Cancer Res.*, vol. 19, no. 3, pp. 643–56, Feb. 2013.
- [433] F. Galbiati, D. Volonté, J. Liu, F. Capozza, P. G. Frank, L. Zhu, R. G. Pestell, and M. P. Lisanti, "Caveolin-1 expression negatively regulates cell cycle progression by inducing G(0)/G(1) arrest via a p53/p21(WAF1/Cip1)-dependent mechanism.," *Mol. Biol. Cell*, vol. 12, no. 8, pp. 2229–44, Aug. 2001.

8 Appendix

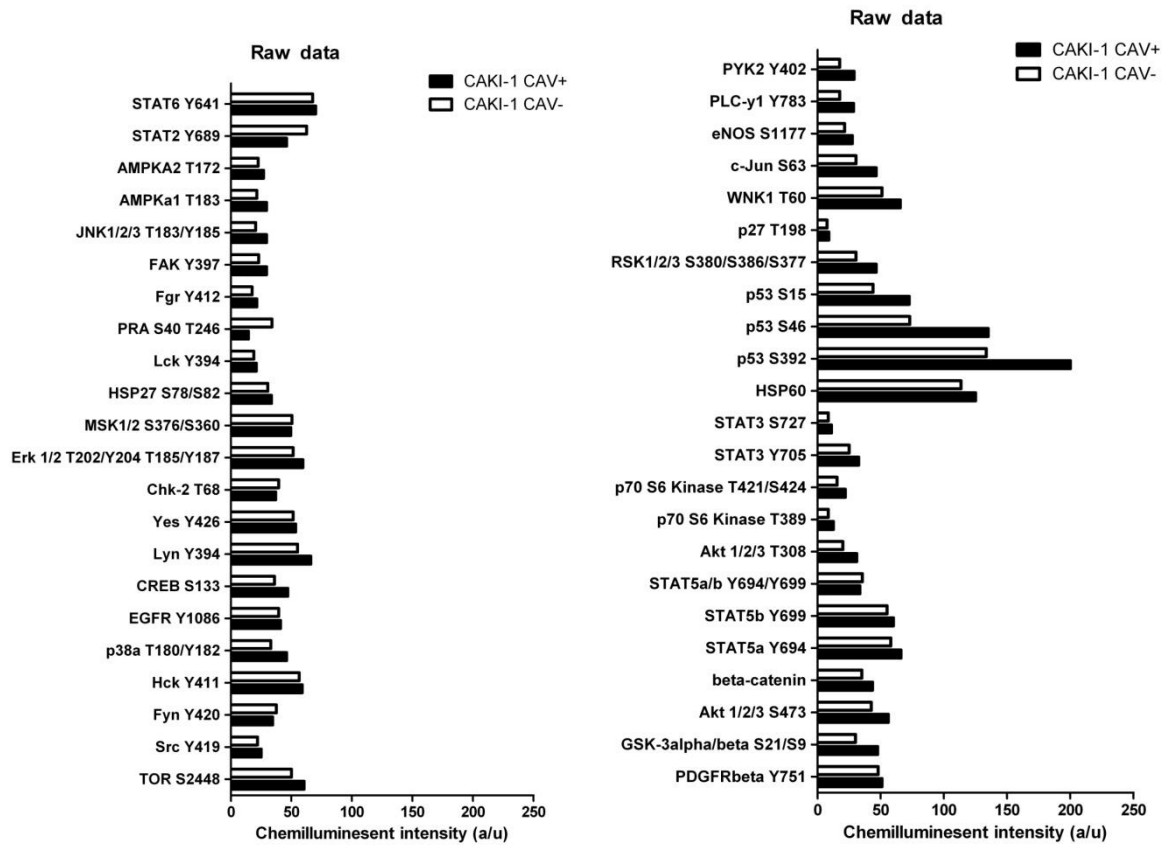


Appendix 1 (A) Agarose gel electrophoresis of Pst1 digest of purified SureSilencing shRNA plasmids. Pst1 digestion of plasmid generates a large 3209 bp fragment and a smaller 1402 bp fragment confirming successful amplification of SureSilencing shRNA plasmids. (B) Minimum inhibitory concentration graphs of 786-O, A498 and CAKI-1 exposed to a concentration

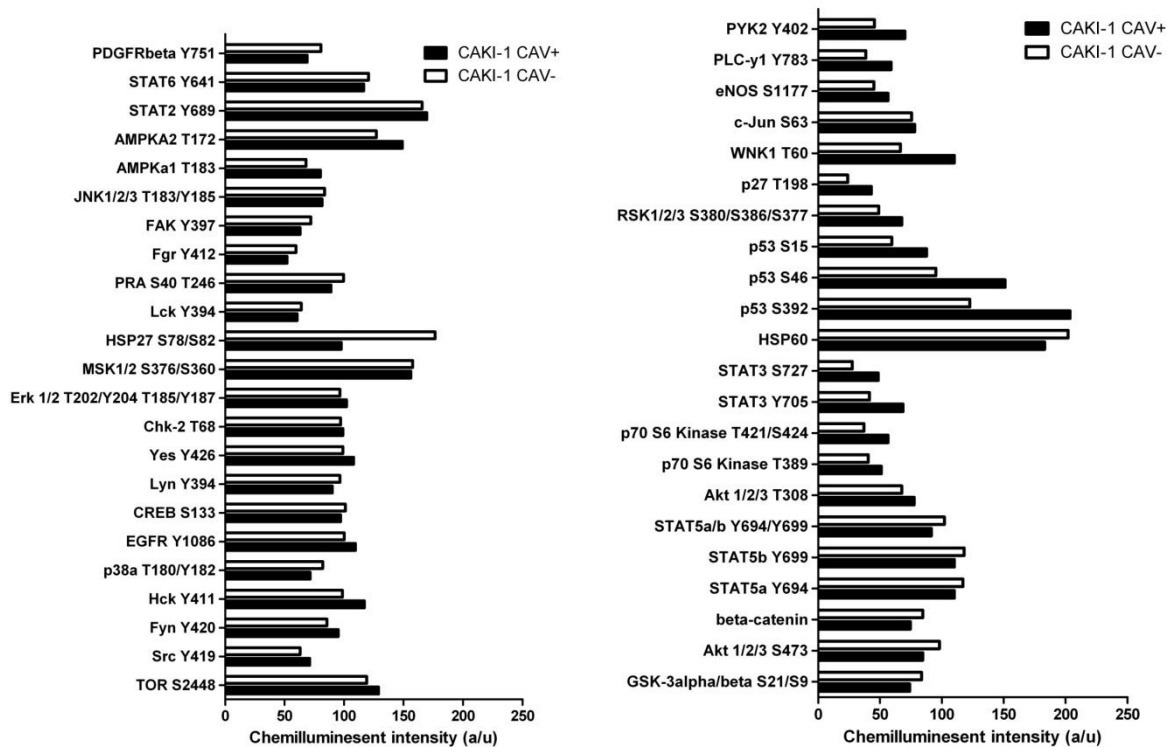
gradient of puromycin from 2 μ g/mL down to 0.125 μ g/mL. Data represents mean \pm standard deviation from eight wells across two experiments.



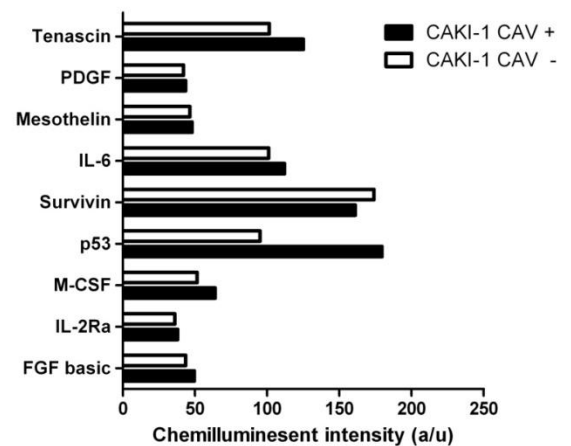
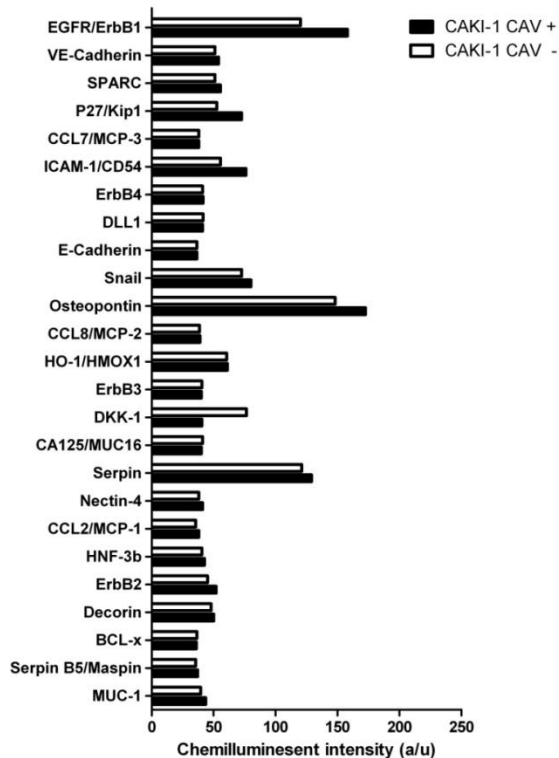
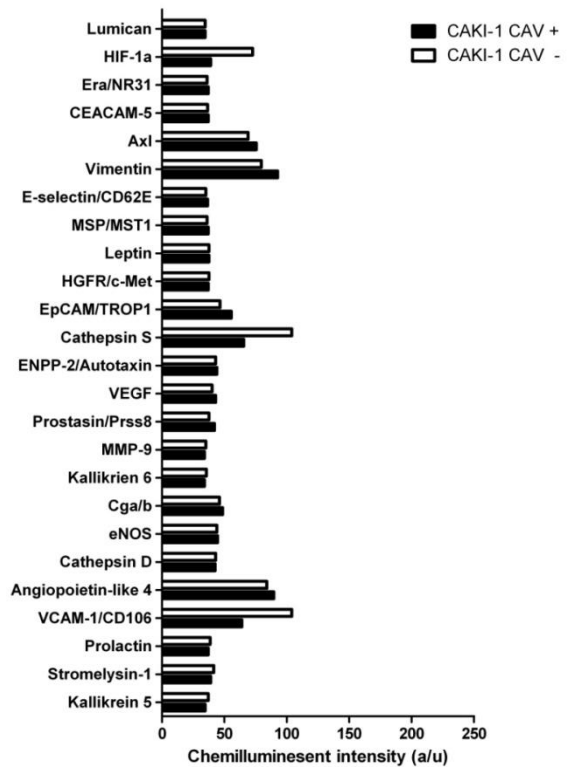
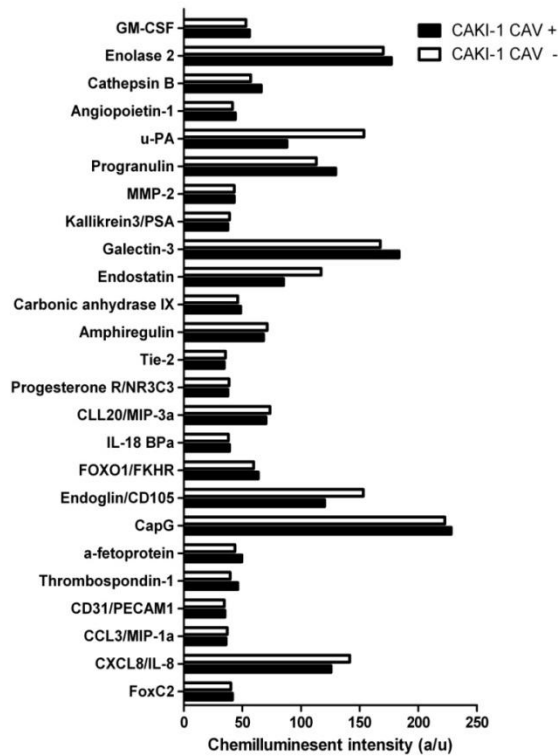
Appendix 2 Raw data from phosphokinase proteomics array for normoxic adherent in CAKI-1 scrambled shRNA control (CAKI-1 CAV+) and CAV1 shRNA knockdown cells (CAKI-1 CAV-)



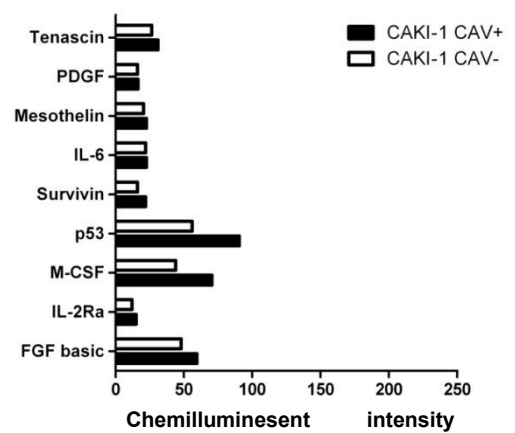
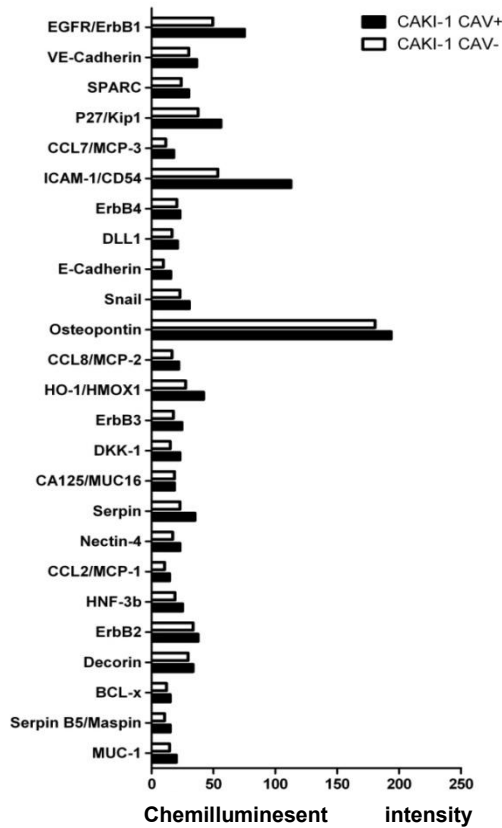
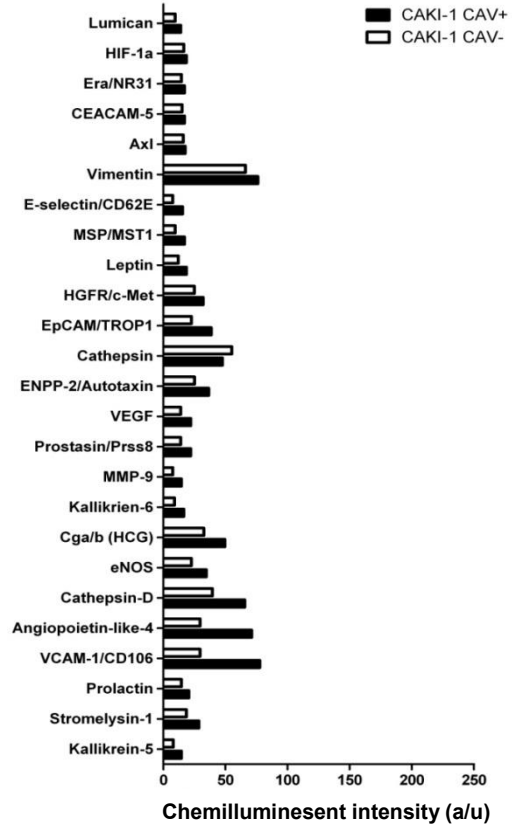
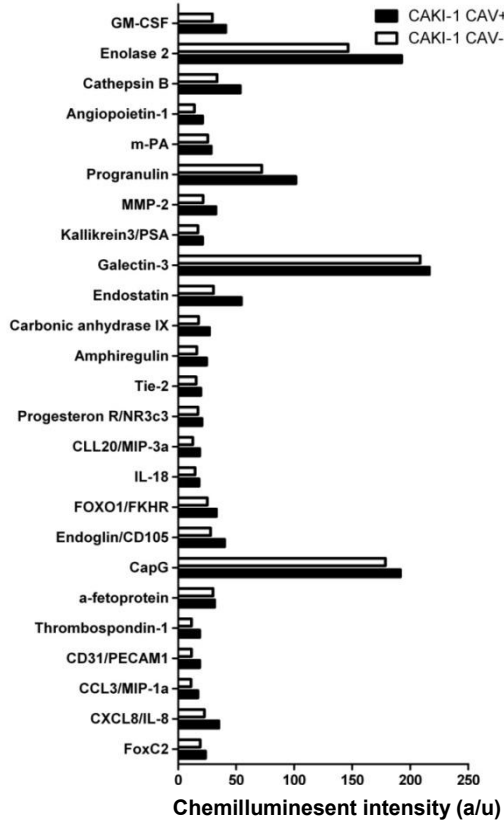
Appendix 3 Raw data from phosphokinase proteomics array for normoxic spheroid conditions in CAKI-1 scrambled shRNA control (CAKI-1 CAV+) and CAV1 shRNA knockdown cells (CAKI-1 CAV-)



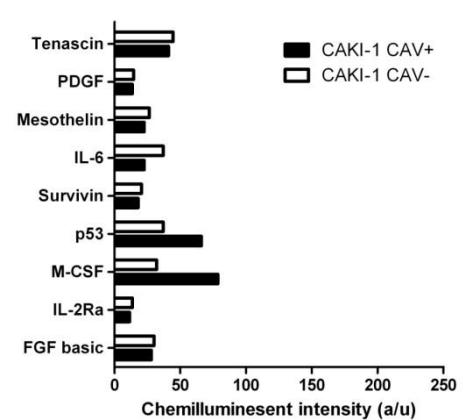
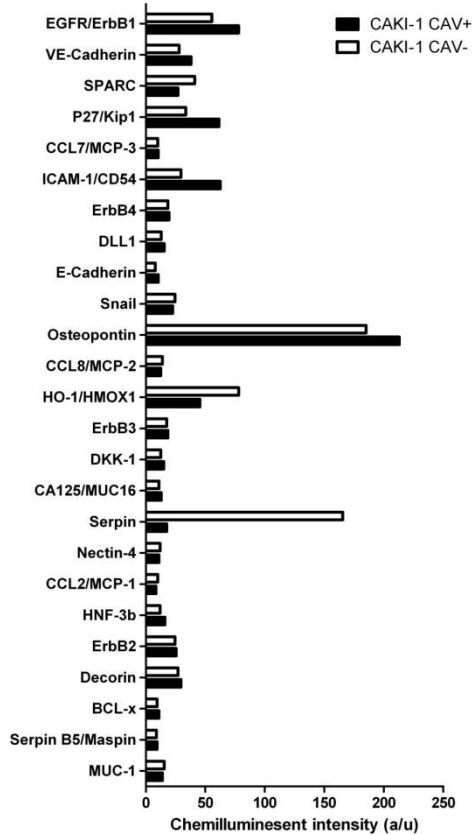
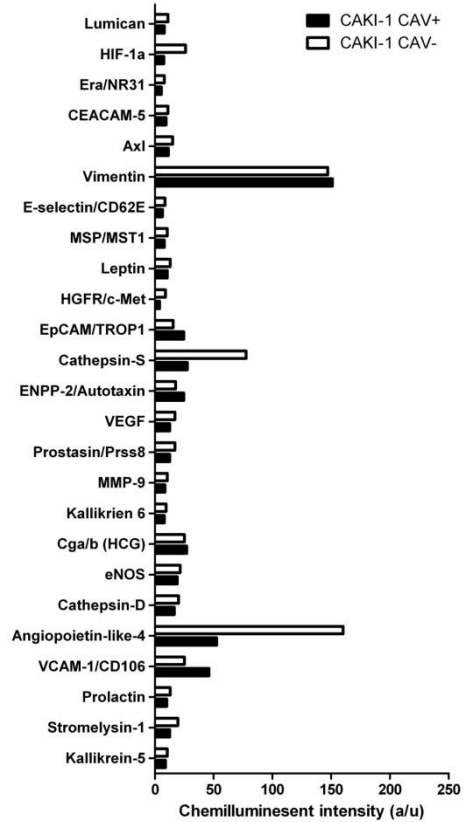
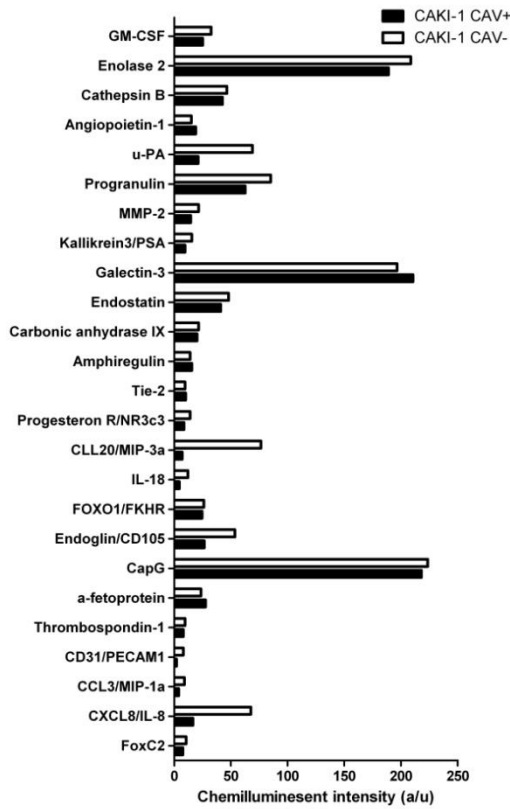
Appendix 4 Raw data from phosphokinase proteomics array for hypoxic spheroid conditions in CAKI-1 scrambled shRNA control (CAKI-1 CAV+) and CAV1 shRNA knockdown cells (CAKI-1 CAV-)



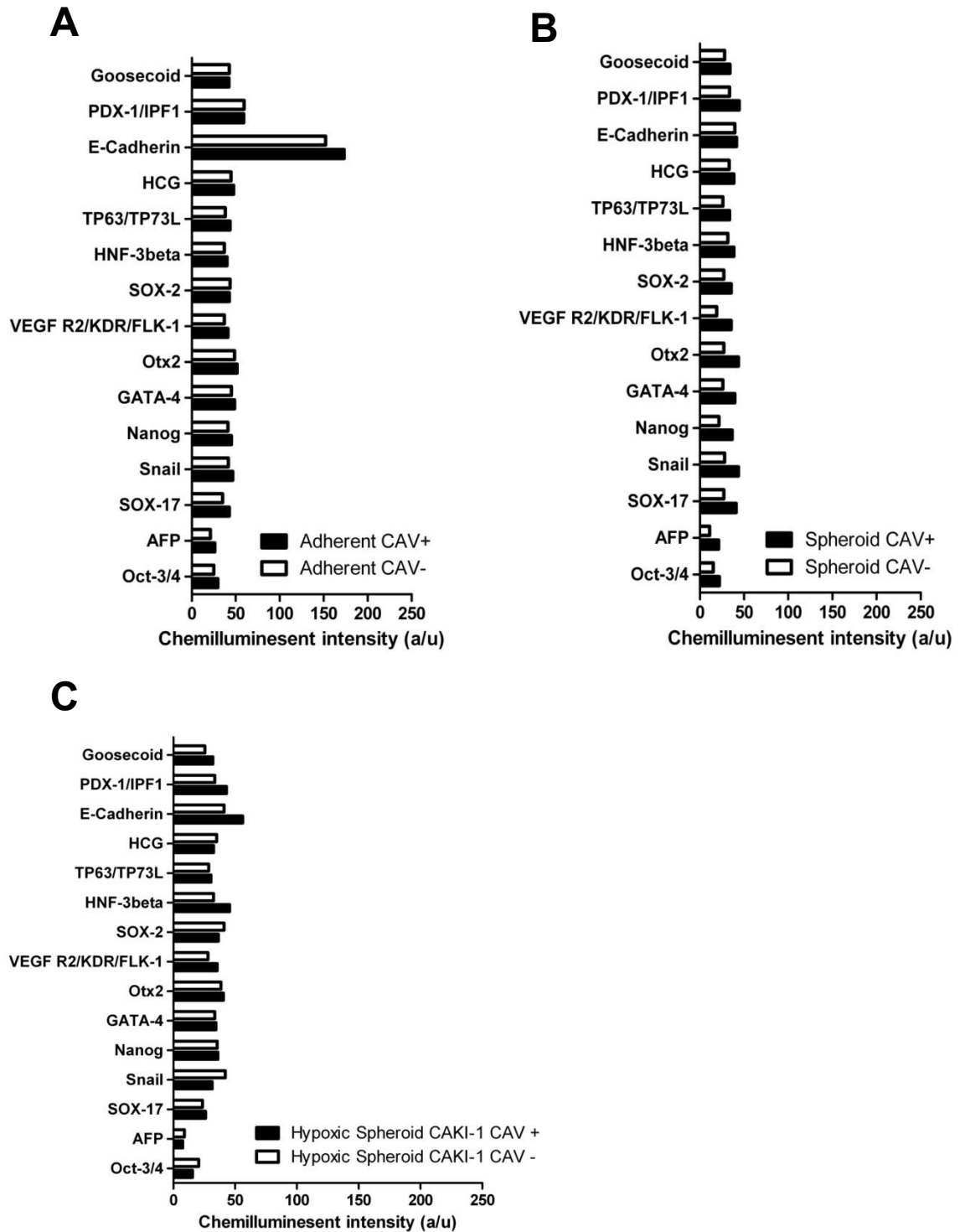
Appendix 5 Raw data from human oncology proteomics array for normoxic adherent conditions in CAKI-1 scrambled shRNA control (CAKI-1 CAV+) and CAV1 shRNA knockdown cells (CAKI-1 CAV-)



Appendix 6 Raw data from human oncology proteomics array for normoxic spheroid forming conditions in CAKI-1 scrambled shRNA control (CAKI-1 CAV+) and CAV1 shRNA knockdown cells (CAKI-1 CAV-)



Appendix 7 Raw data from human oncology proteomics array for hypoxic spheroid forming conditions in CAKI-1 scrambled shRNA control (CAKI-1 CAV+) and CAV1 shRNA knockdown cells (CAKI-1 CAV-)



Appendix 8 Raw data from human pluripotent stem cell proteomics array for (A) normoxic adherent, (B) normoxic spheroid and (C) hypoxic spheroid CAKI-1 scrambled shRNA control (CAKI-1 CAV+) and CAV1 shRNA knockdown cells (CAKI-1 CAV-).